ULTRAFINE PARTICLES IN THE URBAN ATMOSPHERE

by

SENY DAMAYANTI

A thesis submitted to the University of Birmingham for the degree of DOCTOR OF PHILOSOPHY

School of Geography, Earth and Environmental Science

College of Life & Environmental Sciences

University of Birmingham

June 2025

ABSTRACT

Ultrafine particles (UFPs, Dp < 100 nm) are recognised as having a more detrimental effect on human health and climate compared to larger particles. However, critical gaps persist concerning this unregulated pollutant, particularly regarding their control strategies, personal exposure assessment, and new particle formation (NPF) in real-world urban settings. This thesis addresses these gaps through a combination of data analysis obtained from long-term monitoring and short field campaign data and personal exposure campaigns in urban areas in the UK. The research aims to (i) quantify long-term trends (2010-2021) in UFPs particle number and size distribution along with other pollutants at an urban traffic site (London Marylebone Road), (ii) assess personal exposure to important UFPs metrics, specifically particle number concentration (PNC), average diameter, and lung deposit surface area (LDSA) by mobile measurement, (iii) evaluate methods for normalising short-term personal exposure to UFPs and other pollutants with the aim of reflecting an annual mean exposure, and (iv) investigate NPF using an observational dataset collected during a 1-month summer campaign at an urban background site in Manchester.

The results show a statistically significant reduction in all examined air pollutants ranging from 4.7%/yr to 8.3%/yr, with the most rapid decline reported in Black Carbon (BC) and accumulation mode particle concentrations. Nevertheless, there has been little change in the concentration of the nucleation mode (Dp < 30 nm). The implementation of the Diesel Particulate Filter (DPF) was associated with a significant reduction in BC, confirming its efficacy under real-world conditions. Personal exposure assessments revealed that exposure to PNC and LDSA with a smaller average diameter was higher during bus journeys compared to walking, particularly on major

roads compared to residential roads. A method to eliminate spikes in PNC concentrations during walking trips enables source estimation, specifically distinguishing hyperlocal sources from local background contribution (19%) and general local increments (9%). Moreover, new techniques for normalising personal exposure data, which incorporate a correction factor for two distinct timeframes (during the campaign and over a yearly period), have effectively diminished the non-normalised concentration for the majority of examined pollutants, thereby enhancing their comparability to the annual average concentration recorded at a local air monitoring station. NPF substantially contributes to total PNC under favourable conditions such as higher solar radiation and sulphuric acid levels, less polluted atmospheric conditions, and higher wind speed. This study suggests that sulfuric acid is the main driver of nucleation, while ULVOC may play a more important role in particle growth.

The findings demonstrated that while regulatory intervention has significantly decreased solid particles, its impact on the nucleation mode remains limited. Therefore, a more effective control technology is required to mitigate UFP emissions in urban areas. Employing spike removal and normalisation techniques for personal exposure data enhances the distinction between episodic peaks and the actual background exposure, as well as weather-independent trend estimations. Consequently, it improves the understanding of personal exposure evaluation to improve air quality regulations in urban areas. Furthermore, NPF events as a non-traffic UFP source play an important role in urban areas, underscoring the necessity to control gaseous precursors to effectively mitigate personal exposure to UFPs.

ACKNOWLEDGMENT

I would like to express my deepest gratitude to Prof. Roy M. Harrison, who entrusted me with the opportunity to work under his supervision and gain a lot of knowledge throughout this research. My sincere thanks also go to Prof. Francis Pope for his insightful feedback, valuable suggestions, and continuous support throughout my PhD.

I am very grateful to Mary Harding for her kind assistance with the administrative process, even from the time I was still in Indonesia. I would like to express my appreciation to James for his invaluable assistance with the NPF study, and to Dimitrios and Arunik for their support with the Selly Oak project. I also appreciate the help of Siqi Hou and David Beddows for providing essential BAQS data.

To the Indonesian community in Birmingham, thank you for warmly welcoming me and making me feel at home in a foreign country.

I would also like to thank LPDP for their financial support that made it possible for me to pursue my studies at the University of Birmingham.

Finally, I would like to express my heartfelt appreciation to my beloved husband, Novrian, and my children, Shafiyyah and Khalid, for their patience and sacrifices throughout this journey. I am also deeply thankful to my parents and family in Indonesia, whose prayers and unwavering support have been a constant source of strength.

List of Publications and Conferences

Papers published or submitted from this doctoral research

1. **Damayanti, S**., Harrison, R. M., Pope, F., & Beddows, D. C. (2023). Limited impact of diesel particle filters on road traffic emissions of ultrafine particles. *Environment International*, *174*, 107888. https://doi.org/10.1016/j.envint.2023.107888

2. **Damayanti, S**., Bousiotis, D., Baruah, A., Pope, F., & Harrison, R. M. (2025). Analysing Multiple Metrics of Ultrafine Particles from Personal Exposure Campaigns with Source Quantification.

   Submitted to: Environment International

3. **Damayanti, S**., Bousiotis, D., Baruah, A., Pope, F., & Harrison, R. M. (2025). An Evaluation of Methods for Normalising Short Campaign Outdoor Personal Exposure Data to Reflect an Annual Mean.

   Submitted to: Atmospheric Environment

Papers arising from research associated with this doctoral research

1. Harrison, R. M., Beddows, D. C., Tong, C., **& Damayanti, S**. (2022). Non-linearity of secondary pollutant formation estimated from emissions data and measured precursor-secondary pollutant relationships. *npj Climate and Atmospheric Science*, *5*(1), 71.

2. Baruah, A., Bousiotis, D., **Damayanti, S.,** Bigi, A., Ghermandi, G., Ghaffarpasand, O., Harrison, R.M. & Pope, F. D. (2024). A novel spatiotemporal prediction approach to fill air pollution data gaps using mobile sensors, machine learning and citizen science techniques. *npj Climate and Atmospheric Science*, *7*(1), 310.

3. Bousiotis, D., **Damayanti, S**., Baruah, A., Bigi, A., Beddows, D. C., Harrison, R. M., & Pope, F. D. (2024). Pinpointing sources of pollution using citizen science and hyperlocal low-cost mobile source apportionment. *Environment international*, *193*, 109069.

Conference Presentations

1. **Damayanti, S**., Harrison, R. M., Pope, F., Beddows, D.C. and Hou, S. (2022). Interpretation of Particle Number Concentration and Size Distribution at Multiple Sites in the UK. In: 11th International Aerosol Conference 2022. Athens, 4-9 September 2022. **(Virtual Poster Presentation)**
2. **Damayanti, S**., Harrison, R. M., Pope, F., Beddows, D.C. and Hou, S. (2022). Long-term trends of Total Number Count and Black Carbon at Rural, Urban Background, and Urban Traffic Sites in the UK. In: The iCACGP-IGAC 2022 Conference. Manchester, 10-15 September 2022. **(Poster Presentation)**
3. **Damayanti, S**., Harrison, R. M., Pope, F., Bousiotis, D. and Baruah, A. (2023). Assessment of Personal Exposure to Ultrafine Particles in an Urban Neighbourhood in Birmingham. In: Annual Aerosol Science Conference 2023. Teddington, 16th-17th November 2023. **(Oral Presentation).**
4. **Damayanti, S**., Harrison, R. M., Pope, F., Bousiotis, D. and Baruah, A. (2024). Identifying Local Sources of Particulate Matter in An Urban Neighbourhood in Birmingham. In: GEES PGR Conference. Birmingham, 23rd May 2024. **(Oral Presentation)**
5. **Damayanti, S**., Pope, F. and Harrison, R. M. (2024). Ultrafine Particles (UFPs) and Black Carbon (BC) Trends at Multiple Sites in the UK. In: Atmospheric Chemistry Symposium. Birmingham, 26th July 2024. **(Oral Presentation).**
6. **Damayanti, S**., Bousiotis, D., Baruah, A., Pope, F., and Harrison, R. M. (2024). Assessing Multiple Ultrafine Particle Metrics from a Personal Exposure Campaign in Birmingham. In: UKRI/MET 2024 Clean Air Conference. Birmingham, 2nd -3rd October 2024. **(Poster Presentation)**

Contents

List of Figures

List of Tables

Chapter 1: Introduction

1.1 Air Pollution in Urban Areas

Air pollution is considered as a significant contributor to the global burden of disease (Fuller et al., 2022; Murray et al., 2020; Vos et al., 2020), leading to approximately 6.7 million deaths in rural and urban regions in 2019. This is the highest number compared to that caused by other types of pollution (e.g., water pollution, occupational pollution, and lead pollution). Among that total, ambient (outdoor) air pollution accounted for a higher number of deaths (4.5 million) compared to indoor air pollution (Fuller et al., 2022).

It is estimated that over 50% of the world's population resides in urban areas, with this figure expected to rise to approximately 68% by 2050 (UN, 2019). Urbanization has impacted upon air pollutants, specifically $PM_{2.5}$ concentration (Han et al., 2014). This is supported by research indicating that air quality has deteriorated with the increase of population size and density (Borck & Schrauth, 2021, 2024). Air pollution in urban areas is also affected by urban structure, with elevated concentrations of pollutants (NO_x and PM_{10}) found in the scattered and densely constructed regions of European cities (Rodríguez et al., 2016). The scattered city layout potentially reduces connectivity, making people more dependent on vehicles to commute and hence increasing emissions from the transport sector.

Compared to many decades ago, the concentration of air pollutants emitted from fossil fuels, specifically coal combustion, is significantly lower. This improvement was achieved from the adaptation of better and cleaner technologies. However, the rapid growth of motor vehicles in urban areas globally, and hence their exhaust emissions,

has resulted in elevated concentrations of various pollutants (e.g., fine and ultrafine particles or UFPs) (Valavanidis et al., 2008). Analysis of air pollution trends between 2000-2019 in over 13,000 cities shows that $PM_{2.5}$ levels have increased in more than 65% of urban areas worldwide. Despite a notable reduction in emissions of some pollutants in European cities, the urban population's exposure to air pollutants, including $PM_{2.5}$ and O_3, continues to be above the WHO limit for human health protection (Guerreiro et al., 2014; Sicard et al., 2021). In India and China, a significant reduction in pollutant emissions has been recorded, yet persistent high levels of population exposure to particulate matter (PM) during recent decades have also been observed (Gurjar et al., 2016; Zeng et al., 2019).

The decrease in black smoke emissions due to control strategies in developed countries alters both the PM concentration and its composition. This is reflected in a study that found $PM_{2.5}$ composition in London, Beijing, and New Delhi was predominantly comprised of carbonaceous particles emitted from road transport and secondary pollutants, ammonium salts, and secondary organic carbon (Harrison, 2020b). The complexity of PM pollutants, which vary in size, chemical composition, and concentration both temporally and spatially, make them more difficult to study than gaseous pollutants (Harrison & Yin, 2000; Moreno-Ríos et al., 2022); hence, formulating control strategies is more challenging.

1.2 Particulate matter

Particulate matter (PM) is a solid and/or liquid suspended in the air. Among air pollutants, PM is the most reliably linked to human health (Anderson et al., 2012) and is commonly utilised as a proxy indicator for air pollution (WHO, 2024). PM can

originate directly from primary sources (e.g., coal burning, vehicular emission exhaust, and wood burning, etc.) or can be formed via chemical reactions of gaseous components in the atmosphere, referred to as secondary sources (Hinds & Zhu, 2022).

Generally, PM is classified based on its size, a significant property that impacts human health. Different sizes of PM result in particles depositing in various regions of the human respiratory tract, leading to diverse health outcomes (Peters et al., 1997; Schraufnagel, 2020b).

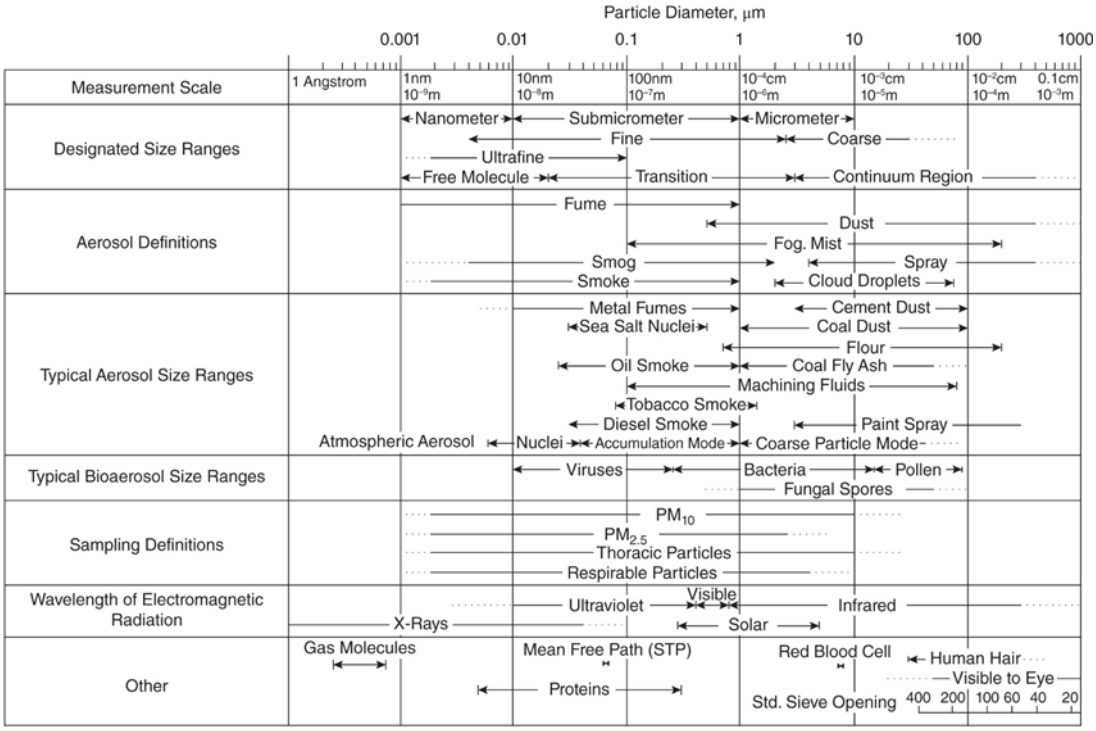

Figure 1 .Range of particle size and aerosol definition (Hinds & Zhu, 2022).

Fig. 1 illustrates the range of particle sizes and other phenomena by various nomenclature, categorising particles into nanometre range (less than 0.01 µm), sub micrometre range (less than 1 µm), micrometre size range (1-10 µm), and those larger

than 10 μm. The largest gas molecule size approaches the smallest particle size (Hinds & Zhu, 2022), indicating a particle formation mechanism from gaseous precursors.

Aerodynamic diameter is a widely used metric for describing particle size, which also reflects their generation and where the particle will deposit in the human body (Anderson et al., 2012). This is defined as the diameter of spherical particles having a density of 1000 kg/m³ that has a similar settling velocity to the particles under study (Hinds & Zhu, 2022).

1.3 Ultrafine Particles (UFPs)

As shown in Fig. 1, PM in air pollution research is broadly classified into PM_{10} (Dp < 10 μm), $PM_{2.5}$ or fine particles (Dp < 2.5 μm), and ultrafine particles (UFPs, Dp < 100 nm). This size affects the particle mass, particle number, and surface area. Fig. 2 shows a typical particle size distribution in the ambient air. An important characteristic of this figure is the particles with a diameter less than 0.1 μm predominantly contribute to the total particle number, whereas those with a diameter larger than 0.1 μm largely contribute to the total particle mass. Consequently, the concentration of UFPs is typically expressed by the number concentration per unit volume of air, whereas the larger particles (Dp > 1μm) are generally measured by their mass concentration.

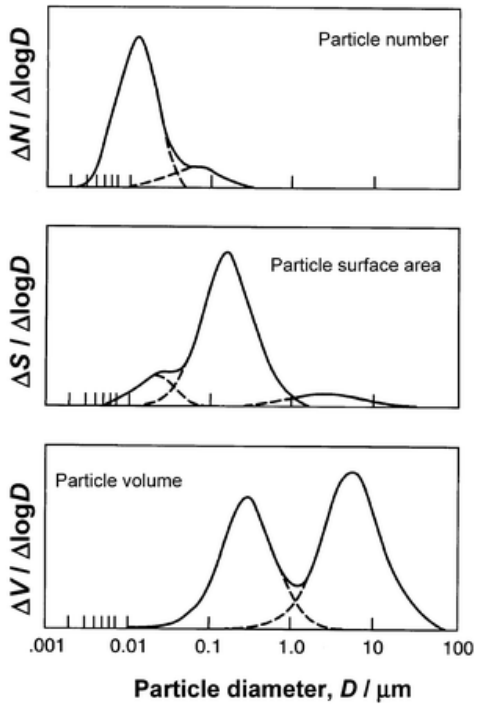

Figure 2. Particle number, particle surface area, and particle volume (equivalent to particle mass) as a function of particle size (Heal et al., 2012).

In terms of particle number size distribution, UFPs are typically expressed in three different modes that reflect their sources and formation processes (Lewis et al., 2018), i.e., nucleation mode, Aitken mode, and accumulation mode. Many literatures define the size range of each mode differently, as summarised by Kumar et al. (2010), which show the particle size ranges are typically classified as those with diameters of 1–30 nm for nucleation, 20–100 nm for Aitken, and 30–300 nm for accumulation. Nonetheless, the first two modes predominantly contribute to the total particle number concentration measured at the urban background or urban traffic monitoring sites (Kumar et al., 2011).

1.3.1 Health effect of UFPs

There is a growing body of knowledge concerning UFPs' effect on human health, particularly on the respiratory system. Compared to larger particles with the identical chemistry, UFPs possess a greater surface area per unit mass, leading to increased biological activity (Günter Oberdörster et al., 2005). This larger surface area also allows UFPs to uptake a greater number of toxic metals and organic compounds, thereby inducing oxidative stress (H. S. Kwon et al., 2020). Owing to their smaller size and larger surface area, UFPs can reach the alveolar region of the human lungs, subsequently translocating to other organs, including the brain or the heart via lymphatic and blood circulation and the nervous system, potentially affecting the neurological system (Buzea et al., 2007; Peters et al., 2006; Samet et al., 2009; Terzano et al., 2010). Furthermore, a study has demonstrated that UFPs are associated with oxidative DNA damage (Vinzents et al., 2005).

Exposure to UFPs, both in the short term (i.e., hours to 1 month) and long term (i.e., 1 month to years), has been associated with more severe effects (Franchini & Manucci, 2007), particularly among vulnerable populations, including the elderly and individuals with cardio-respiratory diseases (Lee et al., 2014). A study revealed that individuals with asthma exhibited a greater cumulative respiratory intake of UFPs for a certain exposure, which may exacerbate their susceptibility to the air pollution health effect (Chalupa et al., 2004). Research indicates that exposure to this tiny particle during commuting may cause acute effects for both healthy individuals and those with compromised health (Knibbs et al., 2011). A recent systematic review study on the health effects of UFP, which analysed 85 studies published between 2011 and 2017,

suggests that short-term exposure to UFPs has been linked to inflammatory and cardiovascular diseases (S. Ohlwein et al., 2019).

Nevertheless, unlike other PM types (i.e., $PM_{2.5}$ and PM_{10}), the guideline level of UFPs has not been formulated by WHO in their latest Air Quality Guideline or AQG (WHO, 2021b). The reason for this is insufficient evidence from epidemiological studies on UFP exposure to set the AQG level (USEPA, 2019; WHO, 2021b). Indeed, the quantity of such studies is increasing, however, the inconsistent use of metrics to assess the exposure makes the results across studies difficult to compare thoroughly. On the other hand, sufficient evidence from extensive epidemiological studies supports the establishment of a good practice statement to address concerns regarding the effect of UFP on human health and the environment. The principal good practice statements include measuring the particle number concentration (PNC) of UFP with Dp ≤ 10 nm, integrating UFP monitoring into the existing station for air quality monitoring, prioritising control strategy for UFP emission sources by categorising them into low (PNC < 1000 #/cm³ of daily average) and high (PNC > 10000 #/cm³ for daily average or > 20000 #/cm³ for hourly average) classifications, and leveraging emerging knowledge and technology for personal exposure assessment.

1.3.2 UFPs in Urban Environments

In urban environments, road vehicles have been identified as the primary source of UFPs (Brines et al., 2015; Chatain et al., 2021; Klompmakera et al., 2015; Rönkkö et al., 2017), especially diesel-powered vehicles (HEI, 2013b), resulting in elevated UFP levels in urban traffic compared to other urban environments (Kittelson et al., 2004; Shi et al., 1999). Prior studies indicated that the concentration of UFP in proximity to the

road was significantly higher and substantially influenced by traffic emissions (Belkacem et al., 2020; Hagler et al., 2009)et al., 2020; Hagler et al., 2009; (Padró-Martínez et al., 2012; Shi et al., 1999; Vu et al., 2015), which account for approximately ~90% of total PNC at heavily trafficked locations (Kumar et al., 2010).

In addition to traffic emissions, nucleation serves as an additional mechanism generating UFPs in urban atmospheres, as extensively studied globally (Alam et al., 2003; Brean et al., 2020a; Cai et al., 2021; Guo et al., 2020; Qian et al., 2007; Siakavaras et al., 2016; Yu et al., 2016). Nucleation particle formation (NPF) events are recognised as important sources of secondary UFPs in urban environments (Kumar et al., 2014; Saha et al., 2018; Sowlat et al., 2016), especially in regions with high insolation, as recorded in several European cities (Brines et al., 2015). Particles generated from this mechanism also potentially act as cloud condensation nuclei (CCN) and hence affect the radiation balance of the Earth (Kerminen et al., 2012).

Nucleation particle formation involves two mechanisms, including the formation of molecular clusters and its subsequent growth (Lehtipalo, 2025; Kulmala et al., 2014), from a diameter of a few nanometres to nucleation and Aitken mode, and possibly toward a size at which they can serve as cloud condensation nuclei (CCN), i.e., more than 50 nm (Kirkby et al., 2011). The former mechanism constantly occurs globally, while the latter requires a particular atmospheric circumstance (Kulmala et al., 2014; Kerminen et al., 2018).

The fundamental process governing NPF remains incompletely understood due to the complex interaction of chemical and physical processes involved (Lehtipalo et al., 2025). Nonetheless, it has been thought that the initial process in the new particle

formation is started by photochemical reactions of key gas precursors, mainly sulfuric acid (Kuang et al., 2008; Kulmala et al., 2007; Wang et al., 2011), which will generate thermodynamically stable clusters (Zhang et al., 2004) in diameter close to 2 nm (Kulmala et al., 2007). Due to its low vapour pressure under a typical atmospheric environment and the capability to form hydrogen bonding with important compounds in the atmosphere, e.g., water, basic species, and organic acids, sulfuric acid is an ideal precursor to those involved in nucleation (Lee et al., 2019). Iodine oxoacids (HIO_x), including iodic acid (HIO_3) and iodous acid (HIO2), are efficient nucleators in coastal marine environments. A chamber study indicated that the nucleation rate of these molecules was faster than sulfuric acid-ammonia under the same condition (He et al., 2021). The follow-up investigation indicated that iodine oxoacid substantially enhances the sulfuric acid-ammonia nucleation formation rate in marine and polar environments by a factor of 10 to 10000 (He et al., 2023). Nevertheless, in polluted urban areas, the role of iodine oxoacids as stabilizer is particularly pronounced, as they enhance growth rates of sub-3 nm particles (Zhang et al., 2024).

Once the clusters are formed, it will subsequently grow mainly by condensation involving low-volatility gaseous molecules, leading to an increase in particle size without a decrease in particle number. This process will compete with the removal mechanism due to the existence of preexisting particles (Harrison et al., 2000; Lee et al., 2019). Alternatively, newly formed particles can grow through a coagulation process due to the motion among them (Holmes, 2007), causing the collision of particles that increase diameter and decrease particle number (Hinds & Zhu, 2022). Apart from sulfuric acid, the condensation of oxygenated organic molecules (OOMs) has been postulated to have an important role, particularly for the growth of newly

formed particles (Brean et al., 2024). Numerous OOMs are present in the atmosphere, and they are commonly classified by their saturation mass concentration (C*, expressed in μg/m^3) as the equivalent of saturation vapour (Stolzenburg et al., 2022) proposed by Schervish & Donahue (2020). The classification is shown in Table 1.

Table 1. **Classification of Organic Compound based on Saturation Mass Concentration (C*)**

	Classes of Organic	**C* (μg/m³)**
ULVOC	Ultra Low Volatility Organic Compound	$C^* < 3 \times 10^{-9}$
ELVOC	Extremely Low Volatility Organic Compound	$3 \times 10^{-9} < C^* < 3 \times 10^{-4}$
LVOC	Low Volatility Organic Compound	$3 \times 10^{-4} < C^* < 0.3$
SVOC	Semi Volatility Organic Compound	$0.3 < C^* < 300$
IVOC	Intermediate Volatility Organic Compound	$300 < C^* < 3 \times 10^6$
VOC	Volatility Organic Compound	$C^* > 3 \times 10^6$

The low volatility of ULVOC facilitates them to efficiently nucleate under typical circumstances, where supersaturation is an essential factor driving this phenomenon (Schervish & Donahue, 2020). ELVOC and LVOC predominantly exist in the particle phase in any ambient conditions and will condense onto pre-existing particle upon collision, however, due to the high curvature of smallest pre-existing particle, LVOC may not condense onto them and instead stick onto a larger particle (Bianchi et al., 2019). SVOC, under equilibrium conditions in the atmosphere, exist in substantial quantities in both gaseous and condensed phase. IVOC, these are molecules with abundance fraction and relatively low vapor pressure, mostly exist in the gas phase

under atmospheric circumstances. The final classes are VOC, which are notably volatile in any circumstances (Bianchi et al., 2019; Donahue et al., 2012).

A comprehensive study on NPF analyses utilising data from 13 sites, including urban background, urban traffic, and rural areas in 5 European countries, revealed that the frequency of NPF occurrence at urban traffic was lower than that observed at urban background and rural areas (Bousiotis et al., 2021b), however, higher growth and formation rates were noted in these areas. The infrequency of NPF was linked to higher pollutant concentration and condensation sink (Bousiotis et al., 2021a), which has been considered as one of the key determinant factors in NPF events across various environments.

Another study examined meteorological parameter effects on NPF using a long-term data set of 85 years (cumulative across the sites) from 16 locations with different land usage across Europe. It demonstrated the NPF event is strongly correlated ($R^2 > 0.94$) to the solar radiation, air temperature, and atmospheric pressure, while revealing a negative association with relative humidity at the majority of study sites (Bousiotis et al., 2021b).

As mentioned earlier, sulfuric acid has been recognised as a crucial precursor of NPF. Nonetheless, owing to a lack of direct observation of sulfuric acid, studies investigating nucleation particle formation in urban environments predominantly employ gaseous pollutants, i.e., SO_2, as a proxy for sulfuric acid (Ali et al., 2025; Németh et al., 2018). Limited studies have performed direct measurements of this molecule (Brean et al., 2019), and there has been no prior study in the UK. Using sulfuric acid proxy instead of direct measurement is subject to significant uncertainty due to insufficient research

on the validity of this proxy in various environments (Kerminen et al., 2018). Additional factors contributing to the regional NPF occurrence include elevated solar radiation intensity, low relative humidity, and pre-existing particle concentration (Kerminen et al., 2018). Highly oxygenated molecules (HOMs) have been regarded as another crucial factor in NPF, particularly during the growth phase of newly formed particles, as evidenced by an observational study in a polluted environment of Beijing (Brean et al., 2019). A study in a mountainous environment in China highlighted that NPF in that area is primarily influenced by HOMs, potentially aided by low levels of sulfuric acid. Furthermore, they have detected more than 1500 of ultralow-volatility HOMs, and ~700 extremely low-volatility promoting nucleation, and particle growth, respectively (Liu et al., 2024).

A study conducted in three European cities employing long-term data on particle number size distribution (PNSD), air pollutant concentration, and sulfuric acid proxy found that the origin of air masses was not a significant factor in the area studied (Németh et al., 2018). They investigated NPF events across three central European cities, i.e., Budapest, Vienna, and Prague, which have a continental climate, a predominant north-westerly wind, and comparable urban features, e.g., area and population size. Their findings indicated that although NPF varied in frequency among all study sites, no significant influence was observed from the air mass origin and back-trajectory analysis, indicating that local conditions play a more important role in these study areas. In contrast, Bousiotis et al., (2021b) studied NPF across 13 European monitoring sites, covering a variety of urban, rural, and roadside settings. Their findings highlighted that the incoming air masses significantly influenced the characteristic of NPF, with cleaner air masses facilitating nucleation, while polluted air masses

supported particle growth. This suggests that various urban areas may possess different atmospheric compositions, contributing to heterogeneity in factors that promote or hinder the nucleation event.

A review study on NPF from field measurements underscores the necessity for more observational data analysis to explore NPF, hence improving understanding of such phenomena across various urban environments and facilitating the generalisation of NPF-related findings from one urban area to another (Kerminen et al., 2018).

1.4 UFPs Abatement Strategy

Policy interventions have been introduced for the road vehicles to improve the air quality globally, including in the UK. This is achieved by imposing the emission standards of pollutants (e.g., EURO standard) and regulating vehicles access to specific areas based on emission standards (e.g., low emission zone and ultra-low emission zone). The enforcement of Euro Standard regulations restricts road vehicle emissions, with higher standards requiring stricter emission limits. Consequently, the implementation of control technology for both new and in-use vehicles become unavoidable. Fig. 3 shows an example of regulation on road vehicles throughout the past decades in London, which ranks as one of the most congested cities in Europe.

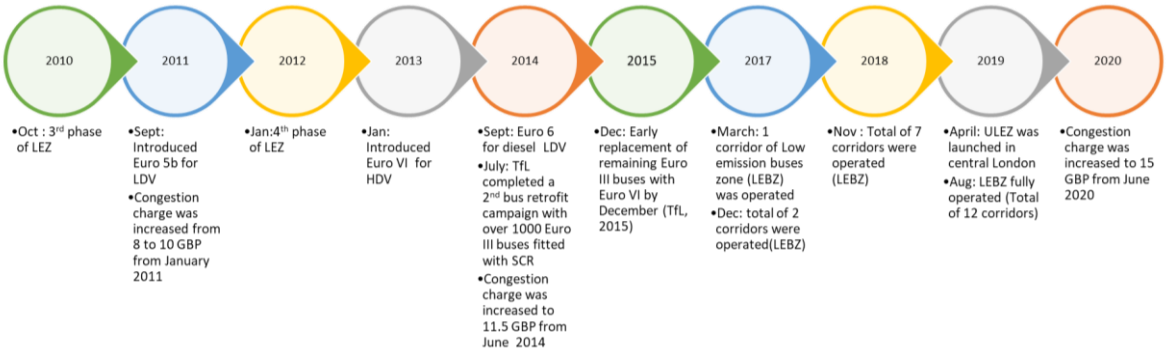

Figure 3. Policy Intervention in the Road Transport Sector Over 2010-2021 in London, UK.

Euro standards are enforced for new vehicles registered in the UK. The initial Euro standards were implemented in 1992, and they have progressively tightened, evolving from Euro 1 to Euro 6 for light-duty vehicles (LDVs) and Euro I to Euro VI for heavy-duty vehicles (HDVs). The limit of particle number (PN), for the first time, was regulated in Euro 5b for diesel LDVs and Euro 6 for petrol LDVs, which were introduced in September 2011 and January 2014, respectively. The PN limit for HDVs was set out in Euro VI, which was implemented in early 2014. The achievement of these additional PN standards requires the fitting of a Diesel Particulate Filter (DPF) (Lewis et al., 2018) on road vehicles. This after-treatment technology has been considered to have efficiency of nearly 100% (Bergmann et al., 2009; Fiebig et al., 2014). A study conducted on-road and in a laboratory measuring PNC and PNSD, specifically for non-volatile particles, from different types of diesel vehicles' exhaust emissions suggested that DPF equipped to the vehicles effectively reduced particle number concentrations across the entire size range examined (9.8 nm-565.7 nm) (Lee et al., 2015). Another study evaluated a DPF fitted to a typical European diesel passenger car found that this

technology reduced 99.5% of particle number and 99.3% of particle mass concentrations (Bergmann et al., 2009).

The congestion charge (CC) was implemented in 2003 to reduce congestion. The impact of this scheme on ambient air pollutants in London was (Atkinson et al., 2009; Beevers & Carslaw, 2005) and found evidence of a relative reduction in PM_{10} and CO. A recent study utilising air pollution data from 2000-2007 has shown that the London Congestion Charge has significantly decreased certain pollutants (CO, NO, and PM_{10}) while increasing NO_x concentrations, which are directly linked to diesel vehicles. This is due to a transition in transportation mode from private car to public transport, which has led to an increase in diesel vehicle mileage, and hence the emissions (Green et al., 2020). Furthermore, following two decades of implementation, the London Congestion Charge has resulted in a 30% decrease in congestion (TfL, 2023).

The low emission zone (LEZ) implemented in London and other European cities, was initially operated to mitigate regulated air pollutants, e.g., PM_{10} and NO_2, to comply with the EU limits (Holman et al., 2015). LEZ in London was enforced in multiple phases from 2008 to 2012, covering most of the Greater London area. Only vehicles that comply with specific PM emission limits are permitted to operate within the zone. Holman et al. (2015) examined the efficacy of LEZ in European countries (i.e., UK, Italy, Germany, Netherlands, and Denmark) and found that LEZ implementation may lead to a modest reduction in PM_{10} and NO_2 average concentration in Germany, while no significant effect was observed in other study sites. In London, the impact of LEZs has been shown to slightly decrease PM_{10} and NO_x levels after 5 years of implementation (Ellison et al., 2013). However, the design of programmes to monitor

changes in many of the locations may have been inadequate to identify small improvements.

The Ultra-Low Emissions Zone (ULEZ), implemented in London in April 2019, has been operated 24 hours every day with the exception of Christmas Day. Initially, the area covered by ULEZ was smaller than LEZ, however, it has been progressively expanded and now both schemes operate within the same territory. Unlike LEZ, it impacts all vehicle types. Cars, vans, and other specialist vehicles require a minimum of Euro 4 and Euro 6 for petrol and diesel-powered, respectively, while motorcycles are required to comply with Euro 3 standards for NO_x emissions. Lorries, coaches, and larger vehicles over 3.5 tonnes only need to pay a charge if they do not meet the ULEZ standard (TfL, 2025). A prior study showed that the London ULEZ led to a small improvement, lowering NO_2 levels by less than 3% and only slightly reducing O_3 and $PM_{2.5}$ levels (Ma et al., 2021). Another study used a model to measure the effects of ULEZ and LEZ and found a more significant reduction in NO and NO_x in the ULEZ compared to LEZ area (Hajmohammadi & Heydecker, 2022). In contrast, a report from the Greater London Authority or GLA (2025) utilising observational data from air quality monitoring stations over England estimated a much greater drop in NO_2 concentration, ranging from 24% to 54% depending on the region. The disparity in methodology and the definition of the pre-intervention period employed by The GLA and the two preceding studies results in the difference in the effect of ULEZ on NO_2 concentration. The GLA relied on the trend analysis and weather normalisation from the observational dataset, while Ma et al., (2021) analysed further using change point detection (CPD) and regression discontinuity design (RDD) as causal inference methods to strengthen the robustness of their findings ((Ma et al., 2021).

A recent study in Seoul has identified a decrease in pollutant concentration, specifically PM_{10}, NO_2, CO, and SO_2, ranging from ~6% to 17%. However, an approximate 10% reduction in $PM_{2.5}$ concentration was noted in association with the ULEZ implementation, possibly attributed to secondary formation (Park & Lim, 2025).

Overall, there has been an increasing number of studies examining the impact of policy on air pollutants, specifically larger particles (i.e., PM_{10} and $PM_{2.5}$) and gaseous pollutants (i.e., NO_x and SO_x). Nonetheless, there is limited study examining how policy implementation influences emerging pollutants, including UFPs, which have been acknowledged to have more adverse effects on human health.

1.5 Mobile Monitoring for Assessing Personal Exposure to UFPs

The assessment of human exposure to UFPs is crucial for understanding the impact of this pollutant on human health and for formulating strategies to improve air quality. This is also recommended by WHO as stated in their most recent guidelines (WHO, 2021b). Human exposure to air pollutants is traditionally assessed using data derived from fixed air quality monitoring stations (Lin et al., 2023; Watson et al., 1988) where the sophisticated and regulatory-grade instruments are deployed. However, this stationary monitoring site typically required a very expensive cost for both deployment and maintenance of instruments, supplementary infrastructure, and well-trained personnel to run the instruments (Frederickson et al., 2023; Motlagh et al., 2020). While fixed-station network data can provide air quality data regarding temporal trends (Hoek et al., 2024) and are appropriate for defining regional air quality assessments (Frederickson et al., 2022), their limitation leads to low spatial resolution (Kumar et al.,

2015; Motlagh et al., 2020), and thus are not capable of capturing pollution at the hyperlocal level (Kumar et al., 2015; An Wang et al., 2023).

Meanwhile, field monitoring results indicated substantial variation of pollutant levels within short distances, particularly for traffic-related air pollutants (TRAP) in urban environments, attributable to the existence of local emission sources (Apte et al., 2017; Frederickson et al., 2022; C. Li et al., 2019; Shah et al., 2023). Studies found that there was substantially more spatial variability in UFPs compared to larger particles ($PM_{2.5}$) (Saha et al., 2019; Wu et al., 2015). Additionally, by combining long-term monitoring data from both fixed sites and mobile measurement data, a study has highlighted that the spatiotemporal profile of UFPs differs from that of other TRAP due to other important sources, i.e., new particle formation (Gani et al., 2021) and restaurant cooking (Saha et al., 2019; Shah et al., 2023; Ye et al., 2020a).

Local sources of UFPs, such as traffic and cooking activities, exhibit the highest concentration near these sources, potentially contributing up to 3 times (Saha et al., 2019) or ~9x higher when inside a vehicle (Apte et al., 2011) compared to that measured in urban backgrounds. Although UFPs concentration decreases rapidly with increasing distance from local sources (Luengo-Oroz & Reis, 2019; Weichenthal et al., 2008) due to rapid dilution, coagulation or other removal mechanisms, these local sources may significantly affect human exposure (Frederickson et al., 2022). Therefore, there is a need to improve the spatiotemporal resolution of UFP to enhance understanding of individuals' exposure to this particle. In addition, although numerous sources (e.g., local sources and background sources) may influence people's

exposure during commuting, their contribution to the total exposure during travel remains not well understood.

Recently, mobile monitoring has become an important complement to stationary measurement conducted at fixed monitoring stations (A. Wang et al., 2023), enhancing the spatiotemporal resolution of air pollution levels (Bousiotis et al., 2024). This method has been extensively used for evaluating personal exposure to air pollutants, which has been regarded as the best approach for more accurately predicting exposure among smaller populations (Han et al., 2017). On the other hand, massive development of air quality monitoring technologies that are simpler, more affordable, and more portable than the regulatory-grade instruments offer study opportunities to do the measurements that were not previously feasible (Bousiotis et al., 2024; A. Wang et al., 2023). A literature review study found that mobile monitoring studies have increased over the past decades, utilising both high-cost and low-cost (~£100s) instruments (A. Wang et al., 2023). Between 2012 and 2021, almost one-third of the examined research was published in the latter year. Nonetheless, among pollutants, UFPs is one of the less studied pollutants compared to other TRAP i.e., NO_2, BC, and CO, particularly by non-low-cost air quality sensors. One of the reasons may be the scarcity of low-cost sensors for ultrafine particles compared to those for larger particles ($PM_{2.5}$, PM_{10}).

To date, there has been a growing number of studies examining personal exposure to UFP through mobile monitoring (Bergmann et al., 2021; He & Qiu, 2022; Knibbs et al., 2011; Luengo-Oroz & Reis, 2019; Patel et al., 2023; Rivas et al., 2017b; Samad et al., 2022; Tran et al., 2025; Van Ryswyk et al., 2021; Weichenthal et al., 2008). In addition

to particle number, lung deposit surface area (LDSA) and diameter are other important variables that need to be comprehended from personal exposure studies. Most prior studies focusing on human exposure to UFP primarily reported number concentration, while investigations into other metrics, i.e., LDSA, remain limited (Amin et al., 2024; Geiss et al., 2016; Liu et al., 2022; Tran et al., 2025). LDSA is also important to assess the dose-response relationship (Baldauf et al., 2016; Lepistö et al., 2020) and serves as a more accurate indicator of UFP-induced inflammatory and oxidative stress response (G. Oberdörster et al., 2005).

1.6 Weather Normalisation of Personal Exposure Data

Research on individual exposure to UFP has predominantly yielded descriptive data reflecting conditions throughout the campaign. In fact, predicting long-term personal exposure to UFPs is crucial for epidemiological research. Previous studies on personal exposure to UFP primarily focused on temporal variation during data collection, which mainly derived from a short campaign, such as specific times of day, days of the week, and seasons (Liu et al., 2022; Luengo-Oroz & Reis, 2019; Weichenthal et al., 2008). In fact, predicting long-term personal exposure to UFPs is crucial for epidemiological research. Furthermore, the results may differ if it is conducted during different timeframes, particularly for the UFPs, where meteorological factors could serve as an important determinant of exposure (Weichenthal et al., 2008). A technique has been developed to reduce bias in air quality data resulting from meteorological impact, widely known as meteorology normalisation. This approach is typically employed by utilising long-term air quality data to obtain more reliable trends in air pollutant concentrations (Grange et al., 2018; Shi et al., 2021), especially for assessing the efficacy of regulations on air quality. In general, this is usually done using three

methods, including the chemistry transport model, the traditional statistical method, and machine learning (Zheng et al., 2023), with the latter two being the most widely used. Machine learning has been utilised in numerous global studies to analyse long-term regulated air quality pollutant data, including in China, Argentina, Spain, Birmingham, Switzerland, and Italy, London, US and India (Diaz Resquin et al., 2023; Falocchi et al., 2021; Grange & Carslaw, 2019; Yong Guo et al., 2022; B. Liu et al., 2023; Lv et al., 2022; Petetin et al., 2020; Shi et al., 2021).

Although extensive meteorological normalisation studies have been undertaken for regulated pollutants, there is a lack of study on UFP, likely due to their unregulated status and the consequent scarcity of measurement data.

The machine learning method has been considered a robust technique for removing weather effects on air quality data; however, prior studies indicate that this method necessitates extensive long-term air quality data, meteorological factors, and advanced computer resources. Therefore, a new simpler approach by leveraging short-term personal exposure data to UFP is required to be developed. Thus, the bias arising from meteorological effects that likely impacts UFP concentration during data collection can be mitigated, leading to a more accurate evaluation of air quality and spatial distribution.

1.7 Research Motivation and Thesis Structure

- Urban traffic sites have been considered as having higher UFPs concentrations than other urban types. In Europe, source apportionment of PNSD at six monitoring stations (two of which are urban traffic) demonstrated that traffic was

the major source at all study sites, contributing between 71% and 90% on an annual average (Rivas et al., 2020). Various policies, specifically on road vehicles, have been enacted to enhance air quality in this region. A systematic evidence map examined over 300 studies on urban policy interventions concerning traffic-related air pollutants (TRAP) globally, revealing that the effectiveness of regulations in mitigating TRAP pollutants (e.g., PM_{10}, $PM_{2.5}$, and NO_x) has been extensively researched, with PM_{10} being the most analysed pollutant (Khreis et al., 2023). Some of the studies have been explained in the previous section, which mostly analysed the larger particles (PM_{10} and $PM_{2.5}$). Nonetheless, there is a lack of analysis focusing on the impact of policy implementation on UFPs concentration. A deep analysis of this relationship is crucial for evaluating the efficacy of existing policies, such as traffic regulations, LEZ, ULEZ, and emission standards, in mitigating health risks associated with UFPs. This study aims to fill this gap by investigating the trend in UFP levels in association with specific policy measures over the past decade..

- The air quality monitoring station is incapable of estimating exposure at the personal level, which can fluctuate based on various factors (e.g., individual activities, modes of transportation, and proximity to emission sources), especially for UFPs that exhibit high spatial and temporal variability. Therefore, personal exposure to UFPs studies by examining important metrics, i.e., particle number and LDSA, is essential to conduct to obtain a more representative exposure at the individual level, which can be used for further health risk assessment in various settings, e.g., urban spaces, commuting modes, activities, etc. This also serves as the implementation of UFP's Good Practice

Statement set by WHO, specifically by leveraging science and technology to evaluate UFP exposure in epidemiological studies and UFP management. On the other side, there has been an increasing body of research on personal exposure to UFPs, primarily undertaken over short durations and only describing conditions during the sampling period, where meteorological factors might greatly affect the measurements. Meteorological normalisation has been extensively performed on long-term air quality data obtained from stationary monitoring stations. To the best author's knowledge, no approach utilising short-term personal exposure data has been conducted. The representativeness of this assessment for longer durations (e.g., seasonal or annual exposure) remains questionable. Therefore, there is a need for further study to develop and evaluate normalisation methods that can mitigate the impact of meteorological factors on human exposure data. This will provide more reliable exposure estimates that can be adapted for epidemiological studies, policy assessment, and long-term health impact evaluation.

- Despite numerous prior studies examining the NPF phenomena in urban settings, the analysis of NPF-related datasets that include direct observations of its primary precursors, such as sulfuric acid and HOMs, particularly in urban areas of the UK, remains limited. This creates a notable gap, as these precursors are acknowledged for facilitating the initial phases of nucleation and particle growth. Consequently, further observational studies that incorporate precursor measurements and meteorological analysis to understand NPF behaviour in urban settings are necessary. This motivation directly guides the next research objective presented below..

The overarching aim of the thesis is to investigate aspects of UFPs, including control strategies, personal exposure assessments, and a major source of secondary UFP (i.e., NPF) to improve the understanding of the sources and processes affecting UFPs, particularly in urban areas of the UK. The objectives of this thesis include:

- Analyse the long-term trends of particle and other traffic-related air pollutant data and evaluate the association between these pollutants and policy interventions enacted during the study period.
- Assess personal exposure to important metrics of UFPs by different commuting modes and develop a method to estimate source contributions.
- Develop techniques to normalise short-term mobile personal exposure data to represent long-term mean exposures.

Investigate the driving factors and characteristics of NPF at the molecular level in an urban area. The chapters in this thesis attempt to address the aforementioned objectives. **Chapter two** (i.e., methodology) will provide detailed information regarding the study locations and the instruments employed to obtain air pollutant data discussed in this thesis. **Chapter three** presents the long-term (12 years) trend of UFPs data, i.e., PNC and PNSD, alongside certain traffic-related air pollutants at a roadside monitoring station in an urban traffic area in London, UK. Further investigation of PNC and PNSD distinguished by wind direction was reported. Additionally, policy interventions are examined with the efficacy of Diesel Particulate Filter in reducing pollutants in that region. **Chapter four** provides analysis of personal exposure to UFP derived from mobile monitoring conducted during a short campaign in an urban neighbourhood area in Birmingham. The variability of UFP metrics, specifically PNC,

average particle size, and LDSA during walking and bus journeys was analysed. This study also proposes a new method for estimating source contributions to overall exposure. **Chapter five** provides a further study from the preceding chapter, focusing on the evaluation of several methods for normalising personal exposure data to represent annual mean. Alongside UFPs, certain pollutants, i.e., BC, PM_1, $PM_{2.5}$, and PM_{10}, measured by low-cost sensors, were also examined. **Chapter six** provides insight into new particle formation based on an observational dataset, highlighting essential precursors such as sulfuric acid and HOMs in an urban background area in Manchester, UK. The characteristics of NPF event days, burst days, i.e., when nucleation occurs without following particle growth, and non-NPF days are discussed. The influence of HOMs with lower volatility, particularly ULVOC is highlighted. **Chapter seven** presents the overarching conclusions from the thesis findings and recommendations for future research.

Chapter 2: Methodology

2.1 Overview

This thesis examined data from both primary i.e., data collected from field measurements and secondary data i.e., existing data measured by air quality monitoring stations to study ultrafine particles in urban environments. The first type of data was gathered for a personal exposure study in Birmingham (Chapter 5 and Chapter 6), while the second type was used to assess long-term monitoring data of UFPs from a traffic area in London (Chapter 3) and to investigate NPF in a background area in Manchester (Chapter 7). The detailed information of each location, the instruments, and the calculation will be elaborated in the following section.

2.2 Study Locations

2.2.1 London Marylebone Road

London Marylebone Road (LMR) is a congested road surrounded by tall buildings, including educational buildings, shops, residences, and tourist attractions, forming a wide street canyon around 40 meters in width (DEFRA, 2025a). The air quality monitoring station at this site is classified as an urban traffic (UT) station, where air pollution is heavily affected by nearby traffic emissions, as defined by UK Department for Environment, Food & Rural Affairs (DEFRA). The additional criteria for the UT station include:

- The sample of air must reflect the air quality of a street segment with a minimum length of 100 metres.
- The position of the sampling probe at a minimum of 25 metres from the edge of major intersections
- The position of the sampling probe is no more than 10 metres from the kerbside.

The monitoring instruments are installed within a self-cabin, approximately 1 metre from the kerbside, as shown in Fig. 5. This site measures various air pollutants, including hydrocarbons, regulated pollutants (e.g., O_3, NO_2, NO_x, $PM_{2.5}$, PM_{10}, SO_2, CO), heavy metals, particle concentrations and numbers, and Black Carbon (BC). The instruments have an inlet height varying from 3 to 4 meters. The UK DEFRA repository (https://uk-air.defra.gov.uk) provides easily accessible data of measured pollutants.

Substantial traffic and reliable long-term air data monitoring, as well as various traffic-related regulations enforced at this location, make this site such an ideal location for air pollution studies over the past decade.(Campbell et al., 2024; Charron & Harrison, 2003; Fuller & Green, 2006; Harrison et al., 2011a; Harrison et al., 2012; Kamara & Harrison, 2021; von Schneidemesser et al., 2010; Zhang & Stevenson, 2022).

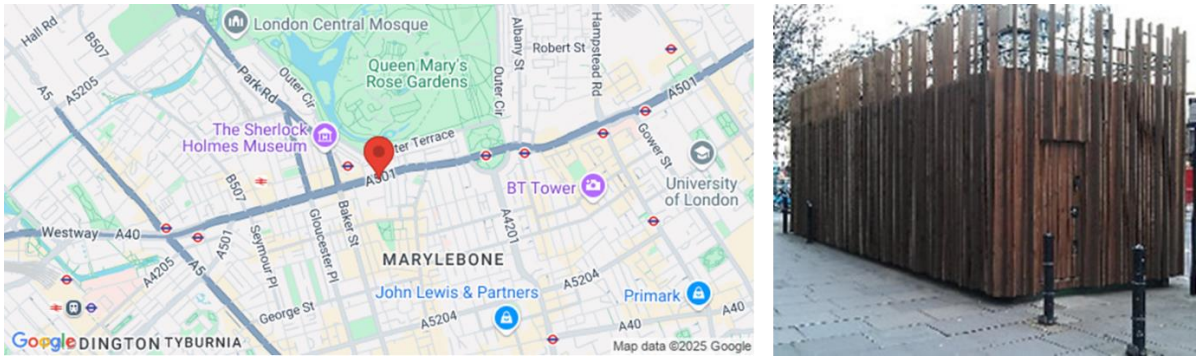

Figure 4. Urban Traffic site located on London Marylebone Road (source: https://uk-air.defra.gov.uk/).

2.2.2 Birmingham

Data on personal exposure to air pollutants was collected by mobile measurements (walking and bus journeys) during a short campaign in spring 2023 in Selly Oak, an urban neighbourhood in Birmingham. Selly Oak is situated on the southern side of the University of Birmingham (Fig. 6) and accommodates a large number of university students. Several potential emission sources exist, particularly those located along a

major road, including a petrol station, shops, and restaurants, which were also passed during the walking and bus measurements.

In addition, data obtained from the Birmingham Air Quality Supersite (BAQS, 52°27'19.9"N 1°55'44.2"W), an air quality monitoring station representing an urban background region, was also utilised. The site is one of the three air quality supersites, along with those in London and Manchester. This site is approximately 1 km on the north side of the Selly Oak area, about 3 km southwest of the city centre, and roughly 100 meters on the east side of the nearest railway line. The BAQS is equipped with reference-grade instruments that measured regulated air pollutants (e.g., O_3, NO_x, SO_2, PM mass concentration), particle number and size distribution, PM composition, and meteorological parameters. The pollutants are measured at 3.2 - 3.4 meters above ground level. Personal exposure devices were also co-located with regulatory-grade instruments at this facility, as described in Chapters 4 and 5.

Figure 5. The location of personal exposure study in Selly Oak Area (left), and Birmingham Air Quality Supersite (right).

2.2.3 Manchester Air Quality Supersite

The Manchester Air Quality Supersite (MAQS) is located on the Fallowfield Campus of the University of Manchester (53°26'39.2"N 2°12'51.9"W), approximately 5 km southeast of the city centre and around 10 km northeast of the Manchester Airport (Fig. 7). Alike BAQS, this site is also classified as an urban background site. This site has various regulatory-grade instruments installed to measure aerosols, gaseous pollutants, and meteorological parameters.

Figure 6. The map shows the location of MAQS (red point) and outside side of The MAQS (right)(CAS, 2025).

During a brief campaign in the summer of 2021 at this site, various pollutants, including PNC, PNSD, sulfuric acid, iodic acid, and HOMs, were quantified for the NPF investigation, with an inlet height approximately of 1 metre. In addition to PNSD and PNC, other pollutants that are regularly monitored, including BC, NO_x, non-refractory pollutants in particulate matter, and meteorological parameters during the campaign period, were obtained from the Centre for Environmental Data Analysis (CEDA) archive, i.e., an atmospheric and earth observation data repository. The inlets for all

the instruments measuring these pollutants are at a height of 6.5 to 7 metres above ground level.

2.3 Instrumentation and Measurement Methods

2.3.1 Instruments used in Field Campaign for Personal Exposure Study

The following personal exposure devices, as well as a GPS, were carried in a backpack, with the inlets positioned within the breathing zone, i.e., the area ~30 cm from the mouth (Int Panis et al., 2010), as seen in Fig. 8.

Figure 7. Sampling setup (a) shows a backpack carried personal exposure devices, (b) shows the position of inlet within the breathing zone of a researcher.

For consistency, the researcher took the same seat on each trip during bus journeys, specifically in the first or second row of the lower deck or stood in the same area when no seat was available. The detail of instruments is explained as follows:

a) DiSCmini

A DiSCmini (Testo SE & Co. KGaA, Germany) was utilised for simultaneously measuring multiple UFPs metrics, including particle number, average diameter, and

LDSA, with a flow rate of 1 L/min at a high-resolution time of 1 second. An inlet tube connector and an impactor supplied by the manufacturer were used, the former was attached to the DiSCmini to allow air sampling within the breathing zone, while the latter was fitted at the end of the inlet tube to remove larger particles (>0.7 microns), following the manufacturer's recommendation. The DiSCmini is capable of measuring particles within the size range of 10-300 nm, with a measured concentration ranging from 10^3 - 10^6 particles/cm^3. This lightweight (0.7 kg), portable, and battery-operated device is appropriate for field measurement, including personal exposure studies.

The working principle of this device is illustrated in Fig. 9.

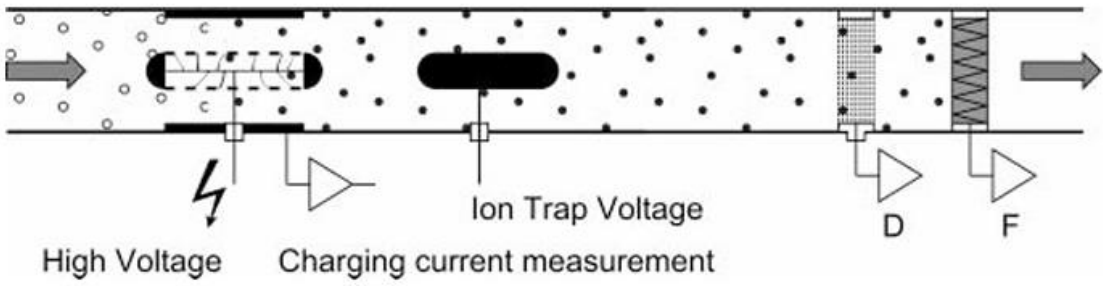

Figure 8. The working principal of a DiSCmini.

The inlet receives the sample air containing particles, which subsequently undergo positive charging in a unipolar diffusion charger. The extra ions will be taken out by an ion trap, while the charged particles will move through and be deposited by a diffusion mechanism in a diffusion stage, generating an electrical current ($I_{diffusion}$). Particles that are not captured during the diffusion stage will enter the filter stage, generating an electrical current (I_{filter}) that will be measured by an electrometer. The smaller particle exhibits larger Brownian motion and will predominantly end up in the diffusion stage.

The ratio of I_{filter} to $I_{diffusion}$ is a function of particle size, as seen in Fig 10, which shows the calculated ratio for monodisperse particles and lognormal size distribution using various widths.

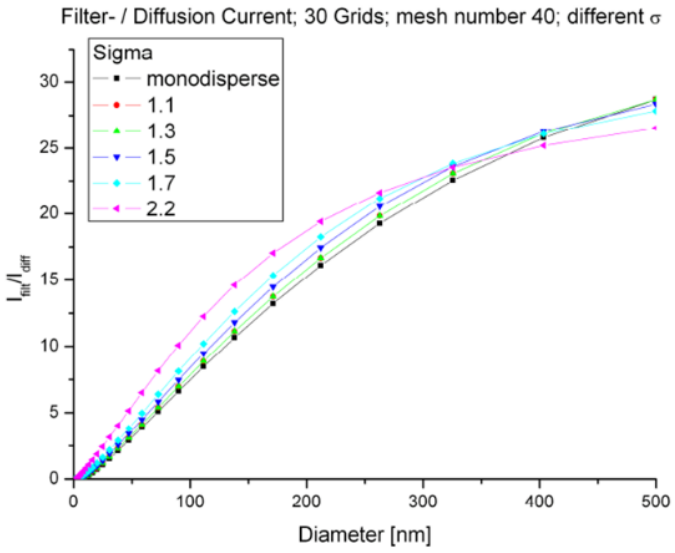

Figure 9. I_{filter} to $I_{diffusion}$ ratio as a function of particle diameter. σ is the geometric standard deviation (Martin Fierz et al., 2008).

This calculation is determined during the calibration process in a laboratory. The resulting calibration curve is stored on the instrument to be used for determining particle size during measurement (Martin Fierz et al., 2008; Fierz et al., 2011). Once particle size is determined, the particle number concentration is then calculated using the power law fit for the particle charge, as indicated in the equation below:

$$N = c\frac{I_{filter} + I_{diffusion}}{d^x}$$ **Equation 1**

where c is a constant established during the instrument calibration, and x = 1.1 (Fierz et al., 2011).

The International Commission on Radiological Protection (ICRP) has developed a model to predict the deposition fraction of particles in various locations of the human respiratory tract (Fig. 11), which shows the fraction as a function of particle diameter (ICRP, 1994a).

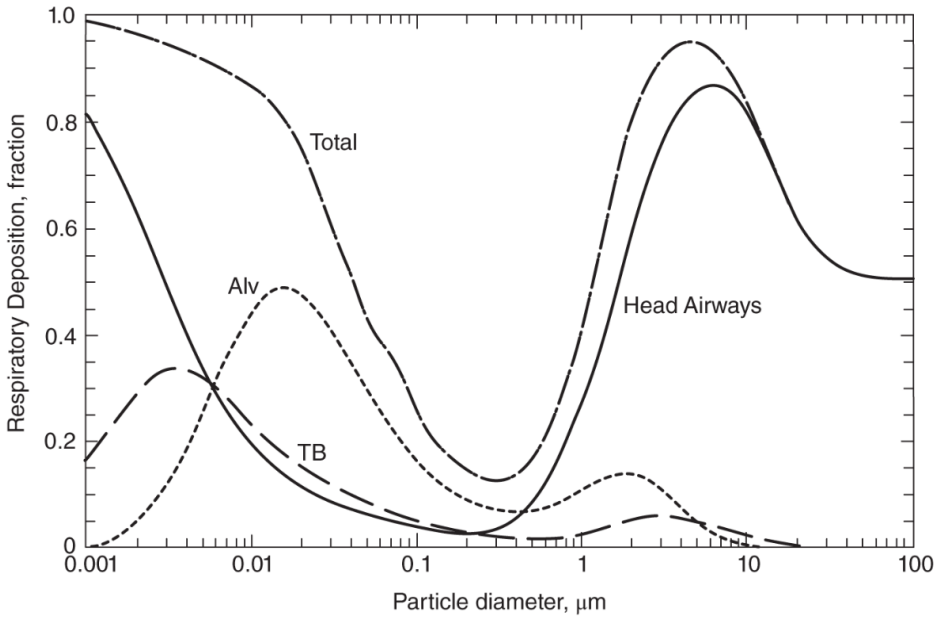

Figure 10. Predicted regional and total deposition for light exercise (nose breathing) based on ICRP model (Hinds & Zhu, 2022; ICRP, 1994a).

LDSA is primarily quantified by utilising the distribution of particle sizes, specifically by the summation of particle surface area in each size bin, weighted by deposition fraction (X. Liu et al., 2023). However, a good association between the LDSA of particles and the signal from a diffusion charger has been found, which is primarily based on the approximately proportionate relationship of LDSA to d1, particularly for particles in the size range of 100–300 nm (Fierz et al., 2011). Therefore, the correlation is applicable to any diffusion charger that does not demonstrate significant losses, including the

DiSCmini, and is achieved by using diffusion charging of particles. A charge *q* imparted to a particle by a diffusion is dependent upon particle size, and can be described as:

$$q \sim = d^{1.1} \qquad \textbf{Equation 2}$$

where d refers to the diameter of particle. The ICRP deposition fraction model demonstrates that as the particle diameter increase in the 20-300 nm range, the fraction of particle deposition decreases, suggesting that the LDSA is roughly comparable to the diffusion charger signal:

LDSA = Particle surface area x deposition probability= d^2 x d^{-1}= d^1 = ~q

By assuming spherical particles, LDSA is subsequently estimated by Eq. 3:

$$S = N\pi d^2 e^{(2\, ln^2 \sigma)} \qquad \textbf{Equation 3}$$

Where d is the geometric mean diameter, and σ denotes the geometric standard deviation of the lognormal particle size distribution (Testo, 2015).

b) Optical Particle Counter

A low-cost sensor was employed to quantify personal exposure to PM (PM_1, $PM_{2.5}$, and PM_{10}) utilising an Optical Particle Counter (OPC) N3 (Alphasense, UK), operating at a flow rate of approximately 1.7 mL/s with a temporal resolution of 10 seconds.

Basically, the OPC-N3 uses a laser beam to detect particle number concentration within a size range of 0.35-40 µm across 24 bins. An inlet draws the particle-containing air sample, which then passes through a laser beam with a wavelength of 658 nm. Individual particles scatter light as they cross the laser beam, which will then be measured by a photodetector. The intensity of scattered light depends upon the particle size, and Mie scattering theory is applied for determining the diameter of the

particle. As particle size is known, particle number counts are then converted into particle mass (PM_1, $PM_{2.5}$, and PM_{10}) based on the assumption of a particle density of 1.65 g mL^{-1} and a refractive index of 1.5+i0. The sensor weight is less than 105 g and can measure up to 2,000 $\mu g/m^3$ for $PM_{2.5}$. The precision of the optical particle counter (OPC), similar to other low-cost sensors measuring particulate matter, is significantly influenced by relative humidity, sometimes leading to overestimation at elevated humidity levels due to the hygroscopic effect (Bousiotis et al., 2024; Crilley et al., 2020), particularly for $PM_{2.5}$ and PM_{10} measurements. Consequently, calibration using relative humidity correction was implemented to enhance the accuracy of particulate matter measurement. The calibration results are presented in Chapter 5, whereas the calibration method of the OPC is elaborated by Bousiotis et al. (2024).

c) Micro Aethalometer

The microAeth AE51 from AethLabs was utilised to measure individual exposure to BC. This instrument is portable and lightweight (approximately of 0.3 g), making it the most commonly used BC monitor in personal exposure studies (Alas et al., 2020; Bista et al., 2022; Rivas et al., 2017b). The operational principle is based on the Aethalometer, a regulatory-grade instrument for monitoring the same pollutant. A sample of air is drawn from the ambient air at a flow rate of 100 mL/min through a filter with a diameter of 3 mm with a temporal resolution of 10 seconds. The tube inlet was attached and positioned within the breathing zone, next to the DiSCmini's inlet. The instrument quantifies BC concentration by measuring light attenuation at a wavelength of 880 nm through a loaded filter, namely a Teflon-coated glass fibre. The obtained light attenuation is then converted to BC mass concentrations using a predefined mass attenuation coefficient (Alas et al., 2020). The microAeth AE51 used in this

investigation was calibrated with the Aethalometer model AE33 from Magee Scientific over a period of five days at BAQS. The outcome of this calibration is detailed in the supplementary information of Chapter 5.

2.3.2 Instruments used in Secondary Data Sources

The study conducted at the London Marylebone Road monitoring station (Chapter 3) employed pre-existing datasets, including PNC and PNSD, and BC measurement, which were downloaded from the UK DEFRA repository, specifically from the “Particle Concentration and Numbers” network, and “UK Black Carbon” network. The regulated pollutants and meteorological parameters were obtained via “Automatic Urban and Rural Network”, and London Heathrow, which were integrated with the OpenAir package (D. C. Carslaw & K. Ropkins, 2012) in R software.

Whereas the NPF study (Chapter 6) employs the dataset from a campaign at the Manchester Air Quality Supersite, with most studied pollutants routinely monitored, and its data can be accessed via the CEDA archive, with the exception of sulfuric acid, iodic acid, and OOMs.

The detailed model of the instruments used in secondary data sources was presented in the respective chapter, while their working principles are briefly explained as follows:

a) SMPS and CPC

Total number concentration and size distribution of aerosols are generally measured by a Condensation Particle Counter (CPC) and a Scanning Mobility Particle Sizer (SMPS), respectively. All of the SMPS and CPC installed at all study locations are TSI Inc. products (TSI, 2014). Generally, the CPC works by generating vapour, typically butanol, isopropyl alcohol, or water, that subsequently condenses onto the particle

surface, resulting in the particle's growth to a size that can be counted optically. The CPC typically sets the diameter at which 50% of the particles can be detected, defined as D_{50}, as a lower limit of detection. The total number concentration of particles per unit volume of air at a certain sample time (e.g., 1 second) and flow rate is then obtained using Eq.4 below:

$$\mathbf{TNC}\left(\frac{particles}{cm^3}\right) = \frac{CPC\ counts\ (particles)}{sample\ time\ (s) x\ flow\ rate\left(\frac{liters}{s}\right) x\ 1000\left(\frac{cm^3}{Liter}\right)} \quad \textbf{Equation 4}$$

The lower limit of CPC varies depend upon the CPC model. However, the CPC installed at the three study locations are capable of measuring particle with size range down to 7 nm up to several µm and detect particles with a concentration of up to 50000 cm^3 at London Marylebone AQMS, and 100000 at MAQS.

The SMPS system comprises of an electrical classifier and a CPC. The former classifies the particles in the sample air, after which the CPC counts them. The particles in the electrical classifier are charged by a bipolar neutralizer so that they have a known charge distribution. They will subsequently be selected based on their electrical mobility, which usually depends on the sizes and the charge state of the particle, by a differential mobility analyser (DMA). The particle size range measured by SMPS is typically between 10 – 1000 nm for a long SMPS or down to 4 nm for a nano SMPS.

b) Aethalometer

The Aethalometer (AE33, Magee Scientific) is used to measure Black Carbon (BC) based on the light transmission through a sample. The measurement of light absorption on a filter-loaded aerosol sample determines the BC concentration. The air

sample is drawn through an area on the filter tape. The aerosol is then analysed by measuring the light transmission through one portion of the filter tape that contains the sample and comparing it with the blank sample as a reference area. The analysis is conducted simultaneously at seven wavelengths, where 880nm is defined as standard use for BC measurement. The BC level is then calculated based on the attenuation of light transmitted through the particle-laden filter using a mass absorption cross section value of 7.77 m^2/g.

c) Chemical Ionisation Mass Spectrometer (CIMS)

Chemical Ionisation Mass Spectrometer (CIMS) is a measurement technique with highly stable tools for measuring some key NPF precursors, including sulfuric acid (Jokinen et al., 2012), VOCs, and HOMs (Zhang et al., 2023).

In this study, a nitrate- based CIMS was installed at Manchester Air quality supersites for approximately 1-month period measurement. The instrument consists of three components: (i) an inlet for chemical ionization at the ambient pressure (CI), (ii) an atmospheric pressure interface (APi), (iii) a time-of-flight mass spectrometer (TOF) (Jokinen et al., 2012). Nitrate ions (NO_3^-), which serve as reagent ions for chemical ionization, are produced within the CI inlet. This is done by introducing nitric acid (HNO_3) vapor into the sheath air, which is subsequently exposed to X-ray radiation, resulting in the nitrate ion formation (Olin et al., 2022). The inlet tube pulls the ambient air sample at a specified flow rate, typically around 8-10 L/min. Sheath flow is subsequently introduced into an ion reaction tube that is concentric with the sample flow. The nitrate ions in this sheath flow are then directed into the sample flow by an electric field, which helps them interact with the analyte molecule. The ionized sample

is then guided into the differentially pumped atmospheric pressure interface (APi) through a critical orifice. The ions thereafter enter the time-of-flight (TOF) mass spectrometer, which measures the duration they need to travel over a specified distance, enabling the calculation of their mass-to-charge ratio (m/z) (Jokinen et al., 2012). The mass and time resolution of this instrument are approximately 3700 $m/\Delta m$ and 1 second, respectively, with a mass spectrum ranging from 7 to 1126 Th (Alage et al., 2024).

d) Chemical Speciation Monitor

Aerosol Chemical Speciation Monitor (ACSM) is capable of quantifying non-refractory components of PM_1 or $PM_{2.5}$ in real time. Non-refractory is defined as a species that is volatile at ~600°C, such as chloride, sulfate, ammonia, nitrate, and organic compounds. The timescale of the vaporisation is extremely short, occurring within a few seconds. The ACSM principally works by collecting a submicron aerosol sample, which will subsequently enter the aerodynamic lens and concentrate into a narrow beam. These concentrated particles then travel through chambers which will eventually reach the final detection chamber where particles collide and immediately vaporize on a heated oven. The resulting vapours are then ionised by electron impact and chemically analysed using a quadrupole mass spectrometer to obtain aerosol mass spectra, which are then used for quantifying chemical species concentration. (Mărmureanu et al., 2025; Ng et al., 2011).

e) Beta Attenuation Mass Monitor

The concentration of particulate mass is automatically measured by a Beta Attenuation Mass Monitor (BAM). The air sample is pulled through a size selective inlet (i.e. $PM_{2.5}$

and PM_{10}) and subsequently passed through a filter tape to collect particulate matter. Carbon-14 emits beta particles, which then pass through the filter tape. The attenuation of beta radiation correlates with the particle mass collected on the filter sample. PM concentration is then obtained by dividing the mass collected with the volume of sample air.

f) Gaseous regulated-pollutant Analyser

Secondary data of some gaseous regulated pollutants, including NO, NO_x, CO, O_3, and SO_2 derived from London Marylebone Road AQMS, were utilised for supporting analysis of data in the UFP study (Chapter 3). The standard methods are applied by the AURN for measuring those pollutants as described below (DEFRA, 2025b):

- **Ozone (O_3)**

Ozone measurement technique is based on UV light absorption at a specific wavelength of 254 nm. The sample of air is passed through a cell tube of length (l), after which the absorption of UV light is quantified by a UV detector. A zero-reference intensity is provided by an ozone-removing scrubber. Ozone concentration (c) is then determined by comparing the UV light intensity between the air path with no ozone (I0) and the air sample (I1), using Eq.5 below (AQEG, 2008):

$$I_1 = I_0 \, e^{-alc} \quad \textbf{Equation 5}$$

Where a is the absorption coefficient at wavelength 254 nm.

- **Nitric Oxide (NO), Nitrogen Dioxide (NO_2), and Nitrogen Oxides (NO_x)**

NO, NO_2, and NO_x concentrations are measured by a chemiluminescent analyser, a widely used instrument for monitoring such pollutants in the UK. The technique of

measurement relies on the detection of light emitted from the reaction between NO and O_3 to generate an excited NO_2 as expressed in Eq. 6-7, with the intensity of the light ($h\upsilon$) is proportional to the NO concentration.

$$NO + O_3 \rightarrow NO_2^* + O_2 \quad \text{Equation 6}$$

$$NO_2^* \rightarrow NO_2 + h\nu \quad \text{Equation 7}$$

This analyser is typically built with dual chamber, with the other chamber used to simultaneously measure NO_x (i.e., $NO+NO_2$) concentration. The total NO_x concentration is obtained by reducing NO_2 concentration in the air sample utilizing an NO_2-to-NO converter. Thus, the concentration of NO_2 is obtained by the subtraction of total NO_x and NO instead of directly measuring such pollutant (AQEG, 2004).

- **Sulfur Dioxide (SO_2)**

The concentration of SO_2 is determined by measuring the UV fluorescence resulted from the absorption of the UV light by SO_2 molecules in the air sample at a wavelength of 214 nm. The intensity of the fluorescence is proportional to SO_2 concentration.

- **Carbon Monoxide (CO)**

The Non-Dispersive Infrared (NDIR) analyser detects carbon monoxide levels in ambient air. This device measures carbon monoxide (CO) by analysing the absorption of infrared (IR) radiation by CO molecules in the ambient air sample. The decrease in infrared radiation after passing the air sample is directly linked to the concentration of CO.

2.4 Data Processing

For data derived from personal exposure monitoring, the clocks of each instrument were aligned before the sampling time. The DiSCmini data was stored on an SD card,

then processed and exported to tab-file format using the Testo DiSCmini data conversion tool software, while data recorded by MicroAeth was downloaded via microAethCOM software by connecting a USB cable to an instrument and a computer. The OPC data measurement was stored on an SD card and can be directly accessed by inserting the SD card into a computer without the need for any software. All the data from each instrument, along with the GPS coordinates, was merged and synchronised in an Excel file. Statistical analysis and data visualization for all studies were mainly done using R software.

2.5 Calculations and NPF Classification

To date, no mathematical definitions determine an NPF event. However, a method proposed by Dal Maso et al. (2005) has been widely used to classify an NPF event (Bousiotis et al., 2021a; Bousiotis et al., 2021b; Brean et al., 2020a; Kerminen et al., 2012; Németh et al., 2018; Siakavaras et al., 2016) that needs to meet the following criteria:

1. The formation of a new mode is clearly observable in the particle size distribution.
2. The mode must start in the nucleation mode (Dp <25 nm).
3. The mode must last for several hours.
4. The mode must show growth.

There are several important parameters describing NPF in the atmosphere. This work uses the parameters listed below.

a) Condensation Sink (CS)

A condensation sink (CS) refers to the rate at which a vapour molecule condenses onto a particle surface. The calculation of this parameter employs particle size distribution data using Eq.8 below. (Kulmala et al., 2012):

$$\boldsymbol{CS = 2\pi D \sum_{d'_p} \beta_{m,d'_p} d'_p N_{d'_p}} \quad \textbf{Equation 8}$$

Where D is the diffusion coefficient of the condensing vapour, which is usually assumed to be sulfuric acid, while dp is the diameter of the particle, Ndp is the particle number at diameter dp, β_m and is a transition-regime (Kulmala et al., 2012)

b) Coagulation Sink (CoagS)

The rate at which a particle (d_p) collides and coagulates into a larger particle (>d_p) is defined as Coagulation sink ($CoagS_{dp}$). This is calculated by the Eq. 9 as follows (Kulmala et al., 2012):

$$\boldsymbol{CoagS_{dp} = \sum_{d'_p=d_p}^{d'_p=max} K(d_p, d'_p) N_{d_p}} \quad \textbf{Equation 9}$$

Where $K(d_p, d'_p)$ refers to the coagulation coefficient between particles sizes d_p and d'_p. The uptake of condensation vapor during the condensation growth potentially serves as a control mechanism and hence inhibits further particle formation (Dal Maso et al., 2005). The rate at which a particle grows defined as the particle growth rate is quantified according to a method by Nieminen et al (2010).

c) Formation Rate

The formation rate at size d_p is calculated using Eq. 10 (Kulmala et al., 2012):

$$\boldsymbol{J_{dp} = \frac{dN_{dp}}{d_t} + CoagS_{dp}.N_{dp} + \frac{GR}{\Delta d_p}.N_{dp}} \quad \textbf{Equation 10}$$

Where $\frac{dN_{dp}}{d_t}$ represents the rate at which particles enter the size $d_{p,}$ and the remaining terms represent the loss mechanisms caused by coagulation sink and particle growth rate.

Chapter 3: Limited impact of diesel particle filters on road traffic emissions of ultrafine particles

Authors: Seny Damayanti, Roy M. Harrison, Francis Pope, David C.S. Beddows

Published in: Environment International, 2023

Author contributions: The study was conceived by RH and FP. DB provided initial scrutiny of the data and SD carried out the data analysis and wrote the first draft of the paper. RH refined the paper, with inputs from FP and DC

Full citation: Damayanti, S., Harrison, R. M., Pope, F., & Beddows, D. C. (2023). Limited impact of diesel particle filters on road traffic emissions of ultrafine particles. Environment International, 174, 107888.

https://doi.org/10.1016/j.envint.2023.107888

Limited Impact of Diesel Particle Filters on Road Traffic Emissions of Ultrafine Particles

Seny Damayanti[1], Roy M. Harrison[1*a], Francis Pope[1] and David C.S. Beddows[2]

[1] School of Geography, Earth & Environmental Sciences University of Birmingham, Birmingham B15 2TT United Kingdom

[2] National Centre for Atmospheric Science School of Geography, Earth and Environmental Sciences University of Birmingham, Edgbaston, Birmingham B15 2TT United Kingdom

[a]Also at: Department of Environmental Sciences, Faculty of Meteorology, Environment and Arid Land Agriculture, King Abdulaziz University, Jeddah, Saudi Arabia

[*] Corresponding author: Roy M. Harrison. Email: r.m.harrison@bham.ac.uk

ORCID ID – Roy M. Harrison: 0000-0002-2684-5226

ORCID ID – Francis Pope: 0000-0001-6583-8347

ABSTRACT

Diesel engines are a major contributor to emissions of both Black Carbon (BC) and ultrafine particles. Analysis of data from the only roadside monitoring site in Europe with a continuous dataset for size-segregated particle number count (Marylebone Road, London) from 2010-2021 reveals that the growing number of vehicles fitted with a Diesel Oxidation Catalyst (DOC) and Diesel Particle Filter (DPF) has been very effective in controlling the emissions of solid particles and hence BC, but that there has been little change in the liquid mode (<30nm) particles, and that concentrations of ultrafine particles (<100nm) still well exceed the threshold for "high" concentrations (>10^4 cm^{-3} /24-hour mean) defined by WHO. BC declined by 81% between 2014 and 2021, but the ultrafine particle (<100nm) count declined by only 26%. Consequently, in locations worldwide with heavy diesel traffic, concentrations of ultrafine particles are likely to remain "high" for the foreseeable future unless more effective abatement technologies are implemented.

Keywords: Ultrafine particles; nanoparticles; policy impact; diesel particle filters (DPF); air pollution

INTRODUCTION

Ultrafine particles (UFPs) are defined as those with a diameter less than 100nm. There are concerns that they may have enhanced toxicity per unit mass and the World Health Organization has recommended enhanced surveillance and precautionary limits on concentration (WHO, 2021). UFPs make a negligible contribution to the PM mass in the ambient air, but they contribute dominantly to the particle number count (PNC) (Harrison et al., 2000; HEI, 2013). Thus, the concentration of UFPs is mainly expressed and quantified by number concentration (particles/cm^3) (Austin et al., 2019; Cassee et al., 2019).

Although there is no strict definition of classification based on size range, particle size distribution are generally classified into three groups which are the Nucleation mode (diameter particle or Dp < 30nm), Aitken mode (Dp 30-100nm), and Accumulation mode (Dp > 100nm), which may reflect their formation process and origin (AQEG, 2018). Many studies have revealed that the PNC in urban traffic-related sites is relatively higher than in other urban environments (Giemsa et al., 2021; Oliveira et al., 2009) because of the emissions from the high volumes of road vehicles. Wahlin et al. (2001) found that petrol and diesel vehicles mainly emit particles with a diameter less than 300nm. Another study in a street canyon found an association between accumulation mode particles and emissions from heavy duty traffic, while a stronger association was found between smaller size range particles (30-60nm) with light duty traffic (Charron and Harrison, 2003).

Globally, policies to improve urban air quality have been implemented in recent decades. For the UK's road transport sector, these involve both requirements for strict emission standards (i.e., Euro standards), and local traffic regulations (e.g., Congestion Charge, Low emission Zone (LEZ), Ultra Low emission Zone (ULEZ)). A policy's effectiveness in improving air quality can be assessed through the trends of pollutant concentration (Gualtieri et al., 2014; Font and Fuller, 2016). Hence, long-term data sets from the air quality measurement site play a crucial role in evaluating and quantifying the impact of those regulation implementations. Studies in the UK to date (Font and Fuller, 2016; Holman et al., 2015; Ma et al., 2021; Harrison and Beddows, 2017) have generally focused on some of the regulated pollutants (e.g., NO_2, $PM_{2.5}$, PM_{10}), and there has been limited study focusing on the UFP, either number concentration (PNC) or number size distribution (PNSD).

In Europe, diesel vehicles are responsible for most of the exhaust particulate matter from road vehicles. Particles emitted in diesel exhaust fall into two main types: solid graphitic (Black Carbon) particles, often comprising a loose aggregate of primary spherules of around 40nm diameter, and a second mode of generally smaller particles, comprising mainly liquid, derived substantially from condensed engine oil (hydrocarbon) vapour (Kittelson et al., 2006; Harrison et al., 2018). The latter particles form in the roadside atmosphere as the hot exhaust gases cool as they mix with cooler ambient air. Some of the first observations of the formation of the semi-volatile particles were made on the heavily trafficked Marylebone Road in London (Charron and Harrison, 2003). Formation of such particles depends upon the presence of condensation nuclei, typically sulfuric acid or tiny ash particles formed from metallic

impurities in the fuel, upon which the semi-volatile hydrocarbons condense. A reduction in the sulphur content of motor fuel in 2007 led to a consequential major reduction in particle number concentrations at Marylebone Road, presumably because of a reduction in sulfuric acid nuclei, causing more vapour to condense on the larger, graphitic particles (Jones et al., 2012).

Our study has analysed 12-years (2010-2021) of particulate matter data derived from Scanning Mobility Particle Sizer (SMPS) and Condensation Particle Counter (CPC) instruments, and other related pollutant data derived from the Automatic Urban and Rural Network (AURN) measured at an urban traffic site in London. This is the only roadside measurement site in Europe with a continuous dataset over this period. Moreover, PNC and PNSD differentiated by wind direction were also further analysed. Some policy interventions implemented during the study period were identified to evaluate any associations between them and the particle number and size distribution.

MATERIALS AND METHODS

***Site Description*:** The London, Marylebone Road (LMR) site has been extensively studied (Harrison and Beddows, 2017; Hicks et al., 2021; Kamara and Harrison, 2021) for air quality research in the UK. Located at 51°31'21.1"N 0°09'16.6"W, the air monitoring equipment is in a large cabin on a sidewalk on the southern side of Marylebone Road. Marylebone Road is a six-lane highway which carries approximately 80000 vehicles/day, and the nearest carriageway is only ~1 metre from the monitoring station. The road is about 32 metres wide, and the buildings

surrounding the site have a maximum height of around 25 metres, forming a street canyon of typical height to width ratio.

***Data Collection*:** Multiple year (2010-2021) datasets of hourly concentration of PNC, PNSD and Black Carbon (BC) were downloaded from the UK-Air data repository. Total number concentrations were derived from a CPC (TSI 3022A to June 2017, then 3772-CEN, both measuring from a lower D_{50} cut point of 7nm) (Tompkins et al., 2021). Particle size distributions were measured using a SMPS. This consists of a CPC (TSI model 3775) combined with an electrostatic classifier (TSI model 3080). The electrostatic classifier consists of a charge neutraliser (incorporating a Kr-85 radioactive source) and a Differential Mobility Analyser (DMA – TSI model 3081) (Tompkins et al., 2021). The range of particle size distribution data derived from the SMPS is 16.55–604.3 nm with 51 size channels. The sum of particles measured by the SMPS (TNCS) is typically substantially less than the total particles counted by the CPC (TNC), mainly due to the different lower measurement cut points. Black carbon is quantified based on light transmission through a filter-based sample using an Aethalometer instrument (model AE22 to November 2019, then AE33) that is operated at several wavelengths, from which the BC concentration is measured at 880nm wavelength using the default mass absorption coefficient built into the instrument (Ciupek et al., 2021). Regulated-pollutants (CO, NO_x, NO_2, NO, $PM_{2.5}$, PM_{10}) concentrations and surface meteorological data were downloaded from the Openair package, which was already integrated with data from Automatic Urban and Rural Network (AURN) and London Heathrow (LHR) Airport. Although the distance between the measurement site and meteorological station at LHR is approximately 22.5 km, the

study by Manning et al. (2000) shows a fair consistency of wind direction up to 40 km from the measurement station. In addition, data from LHR is representative of larger scale air flows and is not influenced by the nearby buildings in London. A wind rose from the entire period (2010-2021) shows a prevailing wind from the south-west direction, as seen in Fig.S1. The pollutant data capture is mostly higher than 90%, apart from TNC and SMPS data (Table S1) which has under 50% data capture in several years due to instrument maintenance.

***Data Analysis*:** Data analysis mainly used the Openair package in R software (Carslaw and Ropkins, 2012) and MS Excel. The Theil-Sen method (Theil, 1950; Sen, 1968) available in the R-Openair package was used to estimate the trend of pollutant concentrations which used the median slope among all lines through the paired sample points. It is very suitable for air quality data analysis because it tends to yield confidence intervals accurately, even for a non-normal dataset, and is also resistant to outliers (Carslaw and Ropkins, 2012). For the slope estimation, the de-seasonalised mode in which any seasonal fluctuation and cyclical variation was removed, was selected to yield a more unambiguous indication of the pollutant trend. This is done using Seasonal Decomposition of Time Series by Loess (STL) i.e a filtering procedure to decompose a time series into seasonal, trend and remainder. The Loess smoother is applied sequentially in STL, allowing for fast computation even for very long time series and significant quantities of trend and seasonal smoothing. This allows analysis of the procedure's properties. It can also decompose time series with missing values (Cleveland et al., 1990).

RESULTS

***Long-term trend of Particle Number and Pollutants Concentrations*:** Data from the roadside Marylebone Road supersite in central London were analysed for trends in particle metrics and other traffic-related pollutants. Table 1 shows the overall Theil-Sen slope of all pollutants in concentration units and per cent per year. It shows many statistically significant downward trends over the given period. The reduction in CO and NO_x is in line with a decline in national emissions from road transport for almost all pollutants in the UK from 2010-2019, based on National Atmospheric Emissions Inventory data (NAEI, 2022).

TNC can be derived from both CPC (TNC) data directly and SMPS (TNCS) data by summing the size bins, as well as for each size-range mode, and all show a downward trend.

Over 2010-2021, the Nucleation mode decreased more slowly (4.9%/year, with confidence interval (CI): 5.52, 4.14%/year) than other modes, while the accumulation mode showed the fastest rate of decline of 7.3%/year (CI: 7.64, 6.99%/year). The Aitken mode decreased at a similar rate to the TNCS. The inventory of total particle number emissions reported by the UK's Air Quality Expert Group (AQEG, 2018) also showed that the transportation sector was the dominant contributor to the TNC emissions in 2005 (as a base year). BC has the most significant decline among other pollutants over the study period, and decreased by 8.3%/year (CI: 8.56, 7.98%/year). BC is primarily released by combustion engines (particularly diesel), wood and coal burning from the residential sector, heavy oil or coal power stations, field burning of agricultural wastes, and forest and vegetation fires (WHO, 2012). In UK urban areas,

194 diesel road traffic is the main source, as revealed by large roadside increments
195 (Harrison and Beddows, 2017). The data for 2014-2021, corresponding to the growing
196 penetration of Euro 6/VI into the vehicle fleet, show an almost level trend in Nucleation
197 particles (+1% per year) and TNC (-0.4% per year). Over this period, Accumulation
198 mode particles fell by 10.2% per year and BC by 12.1% per year.
199 The trends of TNC found in this study are comparable with another recent study by
200 Mikkonen et al (2020) that analysed particle number concentration (Dp 6-1000nm) over
201 2008-2018 in Budapest. They found a decreasing decennial statistical trend (4-5%)
202 that was mainly associated with the decrease in road traffic emissions.
203
204 Due to a vortex in the Marylebone Road street canyon, the emissions from traffic on
205 Marylebone Road are carried directly to the sampler by winds in a southerly sector,
206 while air on northerly sectors is predominantly the background from north London
207 (Harrison et al., 2019), and hence trend analysis differentiated by wind direction was
208 conducted. The summary of the trends of all pollutants is presented in Fig. S2. It shows
209 that the most significant reduction of pollutants mainly occurred when the air came
210 from the southerly sectors, mainly south and south-westerly directions. The very
211 significant reduction observed for BC and Accumulation mode particles over the period
212 2010-2021 was 8.7% (CI: -8.94, -8.34%) and 8% (CI: -8.45, -7.65%) per year,
213 respectively. Smaller reductions of pollutant concentration mainly occurred when the
214 air masses came from the north-easterly wind sector, reflecting a mix of particle
215 sources in the north London area, and a regional background of largely secondary
216 particles.
217

***Time Variation of Pollutants and Particle Size Modes Over 2010-2021*:** Fig. S3 shows the diurnal variation of the traffic-generated pollutants BC and NO_x for each year, while the yearly change is presented in Table S2. Overall, it is observed that concentrations reach a peak during the morning and afternoon rush hour and have a minimum at around 3 am coinciding with the minimum traffic volume, particularly on weekdays (Helfter et al., 2011). Pollutant concentrations, however, remain high during the middle of the day as the traffic volume passing on this road remains high.

The traffic-related pollutants have decreased substantially from 2016 onwards (Fig. S3), which is strongly associated with the rapid growth of the Euro 6/VI vehicle proportion as presented in Fig. S4. Pollutant concentrations were observed sometimes at a lower level in 2020 and 2021, attributable to movement restrictions during Covid-19 which at times led to a dramatic reduction in vehicle numbers in London. However, overall vehicle numbers on Marylebone Road varied little between the years. (Fig. S5). Black Carbon concentrations gradually decreased after 2012 and reduced substantially from 2016 onwards, likely associated with the growing numbers of Euro 6 and VI-compliant vehicles fitted with DPFs, which are reported to remove around 99.9% of all solid, carbonaceous emissions of UFP (Calderón-Garcidueñas and Ayala, 2022). A significant reduction in BC concentration following LEZ implementation and other clean air program policies was also observed at all measurement sites in Leipzig, Germany (Baldauf et al., 2016).

Diurnal variations in particle counts (Fig. S3) over 2010-2021 show a significant reduction of nucleation mode particles from 2013 to 2014, followed by a similar level

from 2014 onward and slightly reduced in 2021. Unlike other pollutants, the concentration level of this mode in 2020 was observed not to be significantly different compared to that in 2014-2016. This trend was reflected in the annual average, particularly in the 225° wind sector with highest concentrations.

A gradual decrease of Aitken mode was observed from 2010-2020, which was very clearly observed during 2016-2020. The Accumulation mode, the solid particles mainly resulting from the combustion of diesel fuel as well as from the growth of Aitken mode (Vu et al., 2015), remains high starting from the morning rush hour and decreases after around 8 PM.

The annual average particle number concentration of each mode and regulated pollutants according wind direction were analysed (Fig. 1, and Fig. S6). As indicated by Fig S3, a sharp decline of Nucleation mode particles was observed from 2013 to 2014, which then stabilises and changes little from 2014 to 2021, seen most clearly in the sectors from 135 to 270 degrees in which the traffic emissions on Marylebone Road are sampled most effectively. An obvious continual decline was observed for the Accumulation mode, particularly in the 135 to 270° wind sectors which are most reflective of the emissions on Marylebone Road. The Aitken mode, also shows a strong decline, but not as substantial as the accumulation mode, presumably because it contains some liquid mode particles which are poorly removed by the DPF. The Nucleation mode proportion of the particles rose from 23% in 2015 to 39% in 2021, and the Accumulation mode shows the opposite trend, decreasing from 22% in 2015

to 12% in 2021. The trend in the proportion of nucleation mode particles out of the total number of particles is shown in Fig. S7.

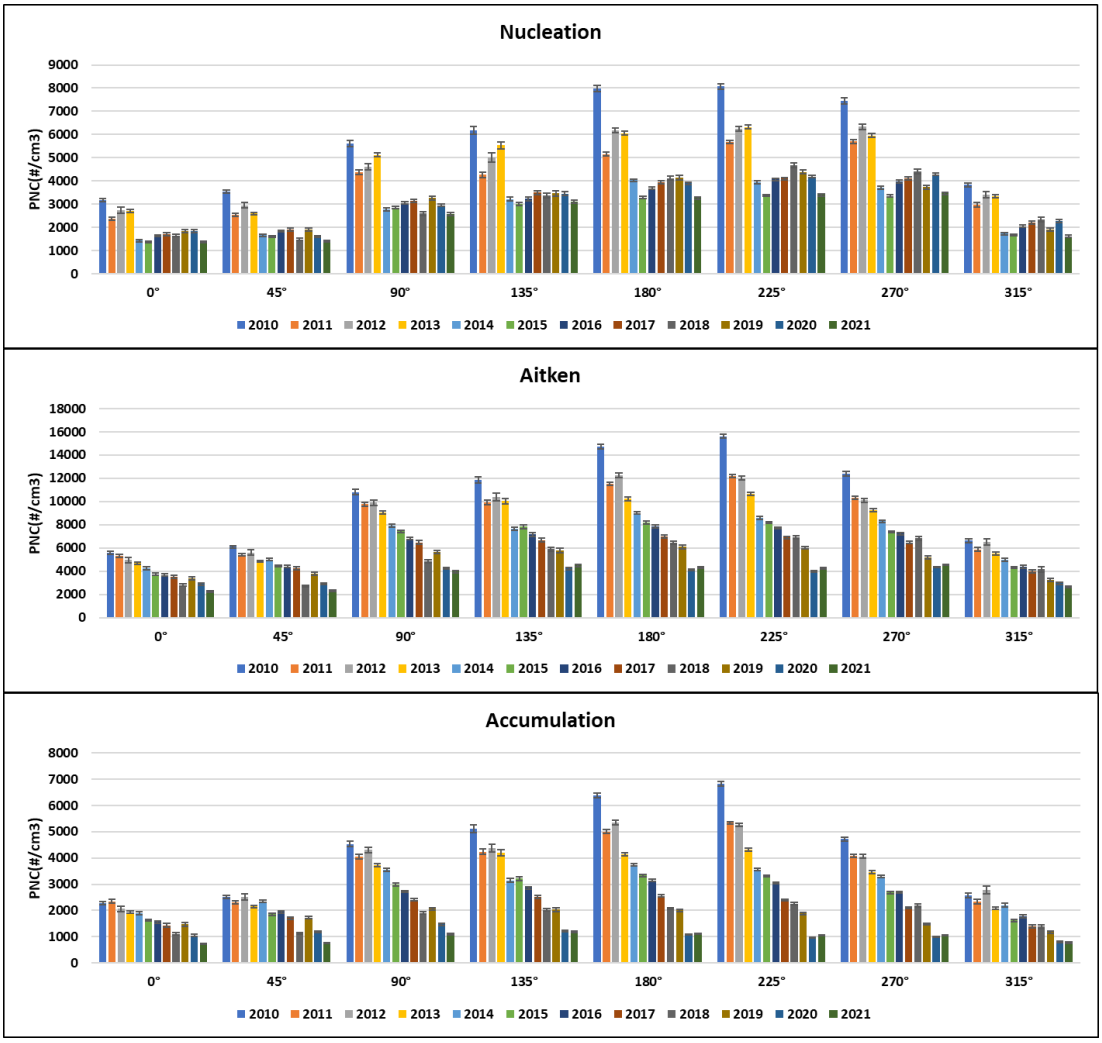

Fig. 1. Annual mean concentration of each particle size mode split by year (2010-2021) and wind direction. Data are filtered according to hourly average wind direction and averaged over one-year intervals. The error bars correspond to one standard error. The Nucleation mode data show a sharp drop from 2013 to 2014, after which there is no clear upward or downward trend. The Aitken and Accumulation mode data show a steady decline. The 180° and 225° data show the greatest contribution of Marylebone Road traffic.

***Continuous Number Size Distribution*:** Annual particle number size distributions are shown in Fig. 2, showing changes over the period 2010-2021. The distribution in 2010

is clearly bimodal, and as time progresses, the contribution of a mode at ca.70nm gradually declines, until it is not visible in the data for 2021. For further investigation, an analysis of PNSD split by wind direction was conducted (Fig. S8). This shows that the change in size distribution affected all wind sectors indicating that the changes seen in the emissions on Marylebone Road also occurred in the air of north London, which dominates the air sampled on winds in the northerly sector.

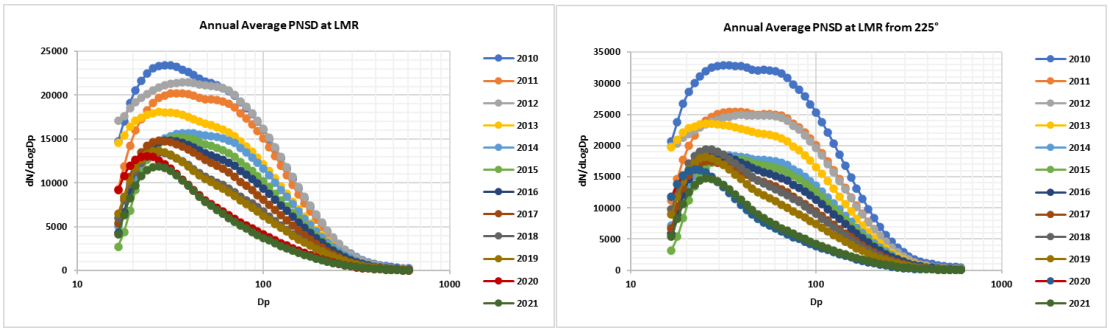

Fig. 2. Annual average particle number size distributions (PNSD) at London, Marylebone Road, 2010-2021. These show all data (left panel), and data only for the 225° wind direction (right panel) which is most affected by Marylebone Road traffic. A mode visible at around 70nm in the earlier years is no longer visible at the end of the time series.

***Emissions Regulation Implementation Over 2010-2021*:** In order to mitigate against the health impacts of fine particle emissions from road traffic, diesel particle filters (DPF) were made mandatory on new light duty diesel vehicles from Euro 5 which was enforced across Europe from January 2011 and continued with the subsequent Euro 6 from September 2015. Particle filters were also required for Gasoline Direct Injection engines by imposition of a similar standard in Euro 6, and for heavy duty vehicles by Euro VI from 2013. The Directive requiring the use of particle filters was framed in terms of a limit on the number of particles emitted per kilometre, and in order to make the test repeatable was limited to particles involatile at 300-400°C and smaller than 23

nm. Due to the natural turnover of the vehicle fleet and the introduction of the London Ultra-Low Emissions Zone requiring diesels to conform to Euro 6 standards from April 2019, a progressively larger proportion of vehicles fitted with DPFs has been using Marylebone Road.

As it takes time for new vehicles which comply with the regulations to penetrate the market, the data on fleet composition, based on vehicle type and Euro standard, was downloaded from the National Atmospheric Emissions Inventory (NAEI, 2022). Data, available from 2013 onward, was filtered so as to use only data from within the Inner London area, as seen in Fig. S4. It shows a steady increase in the aggregate of Euro 5 and Euro 6 in all light duty categories from 2013 to >80% in 3 out of 4 vehicle categories in 2021. A more prominent increase of Euro VI HGVs can be seen from 2015 onwards, from 2% in 2014 and up to 87% in 2021. Buses and coaches were the slowest heavy-duty category to adopt Euro VI but still reached >70% by 2021.
A progressive reduction of vehicle non-compliant with DPFs was observed in all vehicle types during 2013-2021, within the range of 11-26% per year; larger decreases were seen in heavy-duty vehicles (Rigid and Artic, and TfL buses) (see Table S3). These rates of change closely follow the trends of BC and accumulation mode particle reductions during 2014-2021 as seen in Table 1.

The London Low Emission Zone (LEZ) was implemented in four phases from 2008 to 2012, covering initially only parts of central London (Fig. S9), and operates 24h a day. This policy restricts vehicles within the zone based on PM emission standards. The London Ultra-Low Emissions Zone (ULEZ) was introduced in April 2019 and operates

24h every day except Christmas Day. This requires Euro 6 or Euro VI for light and heavy-duty vehicles and has accelerated the uptake of these technologies, and although initially Marylebone Road was on the northern border of the zone and not subject to its regulations, inclusion occurred when the ULEZ was extended in 2021.

The decline in Black Carbon correlated with the increased penetration of vehicles meeting the Euro 5, 6 and VI standards, as exemplified for heavy duty trucks in Fig. 3. The slower decline in Accumulation mode particles than Black carbon is attributable to the large background in secondary Accumulation mode particles which is only indirectly affected by vehicle emissions regulations.

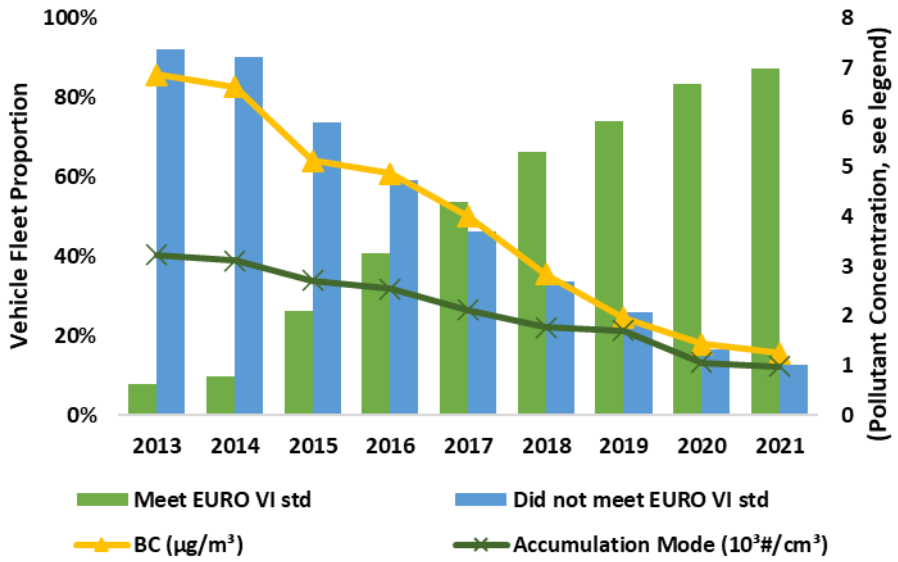

Fig. 3. Temporal trends in Black Carbon and Accumulation mode particle concentrations in relation to heavy duty truck traffic which did not meet the Euro VI emissions standard, 2013-2021. The continuous lines join annual averages for the particle metrics, and the bars show those heavy duty trucks which either did or did not meet the Euro VI emissions standard. A strong relationship is seen in the trends for Black Carbon and Euro VI non-compliant vehicles.

The Nucleation mode particles comprise mainly semi-volatile compounds and partition between the vapour and particulate phases. At the high temperature of the exhaust

gases, the vapour phase will predominate. The DPF is highly effective at removing particles of all sizes as indicated in the finding of present study that shows significant reduction of particle number but is not designed to remove vapour. This should be removed by the DOC, which has been a standard fitment on diesels since Euro 3. However, a laboratory study on a Euro 5 light duty diesel engine (Alam et al., 2019) found a reduction of organic carbon in the sum of both phases of only 56% by a diesel oxidation catalyst (DOC) and diesel particulate filter (DPF) relative to engine-out emissions, hence explaining the small effect of emission controls upon the Nucleation particle fraction. A further consideration is that the formation of Nucleation mode particles is competitive with vapour condensation onto larger particles (Harrison et al., 2018), and if the condensation sink provided by those larger particles declines, as reflected in the reduction of Aitken and accumulation mode particles, the formation of Nucleation mode particles is favoured. Calderón-Garcidueñas and Ayala (2022) report the formation of Nucleation mode particles in the exhaust of catalysed, but not uncatalyzed DPFs.

Two further factors need to be considered. The number of vehicles burning neither petrol or diesel, i.e. hydrogen fuelled, electric vehicles (EVs) or hybrid vehicles in electric mode, and hence unlikely to emit nanoparticles, except in small quantities from the tyres and brakes, has been increasing as shown in Fig. S4. However, by 2021 only 0.5% of passenger cars in inner London were electric vehicles. Taxis comprise 6.4% of the vehicles in central London, and by 2021, 50% were either battery-electric, hybrid or hydrogen fuel cell. Hence, even allowing for the greater distance travelled by taxis, it seems likely that only a few percent of vehicles on Marylebone Road were

neither petrol nor diesel, and hence would have little influence on the air quality trends observed. There has been a shift of petrol vehicles towards gasoline direct injection (GDI), which emit sub-23nm solid particles (Pfau et al., 2022). However, the particle number emission limit set by Euro 6 requires the fitting of particulate filters which are highly efficient at removing solid particles of all sizes, and hence no effect upon the sub-23 nm particles in the atmosphere is anticipated.

DISCUSSION

The long-term (2010-2021) trends of both particle number and size distribution and of some regulated pollutant concentrations have been analysed from an urban traffic site in the UK. The Aitken mode (Dp 30-100nm), Accumulation mode particles (Dp>100nm), and Black Carbon decreased faster than other pollutants, and reduced by 6.2%/year (CI: 6.5- 5.8%/year), 7.3%/year (CI: 7.64, 6.99%/year) and 8.3%/year (CI: 8.56, 7.98%/year), respectively. The most significant reduction occurred when the wind was blowing from the southerly sector, which at this site carries fresh emissions from traffic to the sampling station, confirming that the policy intervention in the road transport sector has effectively decreased those pollutant concentrations. The change in particle emissions is clearly seen in the changing size distribution. The Nucleation mode proportion of the entire particle population gradually rose from 23% in 2015 to 39% in 2021, and the Accumulation mode shows the opposite, decreasing from 22% in 2015 to 12% in 2021. Analysis of PNSD split by wind direction shows two different populations of data, in which the southerly winds (particularly 180°, 225°, and 270°) contribute higher concentrations than that from the northerly sector. Another study by Rönkkö et al (2017) that focused on nanocluster aerosol (Dp 1.3-3nm) has also found

a high concentration from wind sectors that were associated with emission from the road.

At LMR, a clear change was observed in the particle size distribution, most prominent in the 225° wind sector which is most influenced by the Marylebone Road traffic; a bimodal pattern is seen in the early years, in which a modal (~70nm) peak gradually disappeared by the end of the period, indicating a significant change in the sources of these particle size ranges.

DPFs were introduced as a measure to reduce air pollution by diesel exhaust particles. As the mass of particles became difficult to measure in laboratory regulatory tests, the Euro 5, 6 and VI emission standards were defined in terms of a particle number concentration. As the formation of the nucleation mode particles occurs in the diluting exhaust gases, it is inherently variable, depending upon the dilution ratio and environmental conditions, and consequently the emission standards were set in terms of the number concentrations of involatile (solid) particles >23nm in the exhaust gases. The introduction of DPFs has clearly had a major beneficial impact upon concentrations of Black Carbon and Accumulation mode particle emissions, but there remains an issue of poor control of the Nucleation mode particles. As a consequence, the total particle number count declined by only 26% between 2014 and 2021, which compares poorly with the 81% decline in Black Carbon. The relative toxicity of different particle components and sizes is not well understood, but there remains enhanced concern over ultrafine particles due to their high surface area to volume ratio and ability for translocation within the human body (WHO, 2021).

In the Good Practice Statement issued by WHO (2021) as part of its updated Air Quality Guidelines a concentration of ultrafine particles exceeding 10,000 cm^{-3} is defined as “high”. It is noted that compliance with the WHO guideline is not only exceeded at Marylebone Road but is also observed at a suburban background site in London at Honor Oak Park (Ciupek et al., 2022). Current concentrations at Marylebone Road exceed the threshold for “high” values by around a factor of two, and at the suburban Honor Oak Park site in south London also exceeded that level in one of the past three years. Compliance with the recommendation is likely to require a much-increased uptake of battery-electric vehicles with a much-reduced emission of ultrafine particles. High concentrations of ultrafine particles are a worldwide phenomenon (Kumar et al., 2014), and hence this is likely to be a widespread and persistent phenomenon.

Acknowledgments: SD would like to thank to Indonesia Endowment Fund for Education (LPDP), Ministry of Finance, Republic of Indonesia, for their financial support toward her PhD study. The authors are grateful to the UK Dept of Environment, Food and Rural Affairs (Defra) for funding the measurements of pollutants.

Funding: This work was supported by the National Centre for Atmospheric Science funded by the U.K. Natural Environment Research Council (R8/H12/83/011).

Author contributions: The study was conceived by RH and FP. DB provided initial scrutiny of the data and SD carried out the data analysis and wrote the first draft of the paper. RH refined the paper, with inputs from FP and DC.

Declaration of Competing Interests

The authors declare that they have no known competing financial interests or personal relationships that could have appeared to influence the work reported in this paper.

Data availability: Data supporting this publication are openly available from the UBIRA eData repository at https://doi.org/10.25500/edata.bham.00000862

REFERENCES

Alam, M.S., Zeraati-Rezaei, S., Xu, H., Harrison, R.M., 2019. Characterization of gas and particulate phase organic emissions (C_9-C_{37}) from a diesel engine and the effect of abatement devices. Environ. Sci. Technol. 53, 11,345-11,352.

AQEG, 2018. Air Quality Expert Group, Ultrafine Particles (UFP) in the UK. Air Quality Expert Group, Department for Environment, Food and Rural Affairs, https://uk-air.defra.gov.uk/assets/documents/reports/cat09/1807261113_180703_UFP_Report_FINAL_for_publication.pdf. [last accessed 30/07/2022].

Austin E., Xiang J., Gould T., Shirai J., Yun S., Yost M., Larson T., Seto E., 2019. Mobile ObserVations of ultrafine particles: The MOV-UP Study Report. University of Washington, Seattle, WA, USA.

Baldauf, R.W., Devlin, R.B., Gehr, P., Giannelli, R., Hassett-Sipple, B., Jung, H., Martini, G., McDonald, J., Sacks, J.D., Walker, K., 2016. Ultrafine particle metrics and research considerations: review of the 2015 UFP workshop. Int. J. Environ. Res. Public Health. 13, 1054.

Calderón-Garcidueñas, L., Ayala, A., 2022. Air pollution, ultrafine particles, and your brain: Are combustion nanoparticle emissions and engineered nanoparticles causing preventable fatal neurodegenerative diseases and common neuropsychiatric outcomes? Environ. Sci. Technol. 56, 6847-6856.

Carslaw D.C., Ropkins K., 2012. openair - an R package for air quality data analysis. Environ Modell Softw. 27-28, 52-61.

Cassee, F., Morawska, L., Peters, A., Wierzbicka, A., Buonanno, G., Cyrys, J., SchnelleKreis, J., Kowalski, M., Riediker, M., Birmili, W., Querol, X., 2019. White Paper: Ambient ultrafine particles: evidence for policy makers. European Federation of Clean Air and Environmental Protection Associations (EFCA), https://efca.net/files/WHITE%20PAPER-UFP%20evidence%20for%20policy%20makers%20(25%20OCT).pdf. [last accessed 30/07/2022].

Charron, A., Harrison, R.M., 2003. Primary particle formation from vehicle emissions during exhaust dilution in the roadside atmosphere. Atmos. Environ. 37, 4109-4119.

Ciupek, K., McGhee, E., Tompkins, J., Williams, K., Brown, A., Butterfield, D., Allerton, J., Bradshaw, C., Buckley, P., Lilley, A., Kantilal, V., Robins, C., Sweeney, B., Brown, R., Priestman, M., Font Font, A., Fuller, G., Green, D., Tremper, A., 2022. *Airborne particle concentrations, particle number and black carbon in the United Kingdom. Annual report 2022, National Physical Laboratory,* http://eprintspublications.npl.co.uk/id/eprint/9590. [last accessed 18/01/2023].

Ciupek, K., Butterfield, D., Quincey, P., Sweeney, B., Lilley, A., Bradshaw, C., Fuller, G., Green, D., Font Font, A., 2021. 2019 Annual Report for the UK Black Carbon Network. National Physic Laboratory Report, http://eprintspublications.npl.co.uk/id/eprint/9278. [last accessed 01/02/2023]

Cleveland, R. B., Cleveland, W. S., McRae, J.E., Terpenning, I., 1990. STL: A Seasonal-Trend Decomposition Procedure Based on Loess. J. Off. Stat, 6, 3-73.

Font, A., Fuller, G.W., 2016. Did policies to abate atmospheric emissions from traffic have a positive effect in London? Environ. Pollut. 218, 463-474.

Giemsa, E., Soentgen, J., Kusch, T., Beck, C., Münkel, C., Cyrys, J., Pitz, M., 2021. Influence of local sources and meteorological parameters on the spatial and temporal distribution of ultrafine particles in Augsburg, Germany. Front. Environ. Sci. 8, 609846.

Gualtieri, G., Crisci, A., Tartaglia, M., Toscano, P., Vagnoli, C., Andreini, B.P., Gioli, B., 2014. Analysis of 20-year air quality trends and relationship with emission data: The case of Florence (Italy). Urban Clim. 10, 530-549.

Harrison, R.M., Beddows, D., Alam, M.S., Singh, A., Brean, J., Xu, R., Kotthaus, S., Grimmond, S., 2019. Interpretation of particle number size distributions measured across an urban area during the FASTER campaign. Atmos. Chem. Phys. 19, 39-55.

Harrison, R.M., Beddows, D.C., 2017. Efficacy of recent emissions controls on road vehicles in Europe and implications for public health. Sci. Rep. 7, 1-5.

Harrison, R.M., MacKenzie, A.R., Xu, H., Alam, M.S., Nikolova, I., Zhong, J., Singh, A., Zeraati-Rezaei, S., Stark, C., Beddows, D.C., Liang, Z., 2018. Diesel exhaust nanoparticles and their behaviour in the atmosphere. Proc. R. Soc. A. 474, 20180492.

Harrison, R.M., Shi, J.P., Xi ,S., Khan, A., Mark, D., Kinnersley, R., Yin, J., 2000. Measurement of number, mass, and size distribution of particles in the atmosphere. Phil. Trans. R. Soc. Lond. 358, 2567-2580.

HEI, 2013. HEI Perspectives 3: Understanding the health effects of ambient ultrafine particles. Health Effects Institute, Boston, MA, https://www.healtheffects.org/system/files/Perspectives3.pdf. [last accessed 30/07/2022].

Helfter, C., Famulari, D., Phillips, G.J., Barlow, J.F., Wood, C.R., Grimmond, C.S.B., Nemitz, E., 2011. Controls of carbon dioxide concentrations and fluxes above central London. Atmos. Chem. Phys. 11, 1913-1928.

Hicks, W., Beevers, S., Tremper, A.H., Stewart, G., Priestman, M., Kelly, F.J., Lanoisellé, M., Lowry, D., Green, D.C., 2021. Quantification of non-exhaust particulate matter traffic emissions and the impact of COVID-19 lockdown at London Marylebone Road. Atmosphere 12, 190.

Holman, C., Harrison, R.,, Querol, X., 2015. Review of the efficacy of low emission zones to improve urban air quality in European cities. Atmos. Environ. 111, 161-169.

Jones, A.M., Harrison, R.M., Barratt, B., Fuller, G.A., 2012. Large reduction in airborne particle number concentrations at the time of the introduction of “sulphur free” diesel and the London Low Emission Zone. Atmos. Environ. 50, 129-138.

Kamara, A.A., Harrison, R.M., 2021. Analysis of the air pollution climate of a central urban roadside supersite: London, Marylebone Road. Atmos. Environ. 258, 118479.

Kittelson, D.B., Watts, W.F., Johnson, J.P., 2006. On-road and laboratory evaluation of combustion aerosols—Part1: Summary of diesel engine results. J Aerosol Sci. 37, 913-930.

Kumar, P., Morawska, L., Birmili, W., Paasonen, P., Hu, M., Kulmala, Harrison, R.M., Norford, L., Britter, R., 2014. Ultrafine particles in cities. Environ. Int. 66,1-10.

Ma, L., Graham, D.J., Stettler, M.E., 2021. Has the ultra low emission zone in London improved air quality? Environ. Res. Lett. 16, 124001

Manning, A.J., Nicholson, K.J., Middleton, D.R., Rafferty, S.C., 2000. Field study of wind and traffic to test a street canyon pollution model. Environ. Monit. Assess. 60, 283-313.

Mikkonen, S., Németh, Z., Varga, V., Weidinger, T., Leinonen, V., Yli-Juuti, T. and Salma, I., 2020. Decennial time trends and diurnal patterns of particle number concentrations in a central European city between 2008 and 2018. Atmos. Chem. Phys. 20, 12247-12263.

NAEI, (2022). Overview of Air Pollutants. National Atmospheric Emissions Inventory, https://naei.beis.gov.uk/overview/ap-overview. [last accessed 11/07/2022].

Oliveira C., Alves C., Pio C.A., 2009. Aerosol particle size distributions at a traffic exposed site and an urban background location in Oporto, Portugal. Química Nova 32, 928-933.

Pfau, S.A., La Rocca, A., Haffner-Staton, E., Fay, M.W., Cairns, A., 2022. Linking operating conditions of a GDI engine to the nature and nanostructure of ultrafine soot particles. Combust. Flame 245, 112315.

Sen P.K., 1968). Estimates of regression coefficient based on Kendall's Tau. J. Am. Stat. Assoc. 63, 1379-1389.

Rönkkö, T., Kuuluvainen, H., Karjalainen, P., Keskinen, J., Hillamo, R., Niemi, J.V., Pirjola, L., Timonen, H.J., Saarikoski, S., Saukko, E. and Järvinen, A., 2017. Traffic is a major source of atmospheric nanocluster aerosol. Proc. Natl. Acad. Sci. U.S.A. 114, 7549-7554.

Theil H.A., 1950. Rank Invariant Method of Linear and Polynomial Regression Analysis, I, II, III. Proc. Sect. Sci. K. Ned. Akad. Wet. Amst. 53, 386-392, 521–25, 1397–1412.

598 Tompkins J., McGhee E., Ciupek K., Williams K., Robins C., Allerton J., Quincey P.,
599 Brown R., Green D., Tremper A., Priestman M., Font Font A., 2021. Airborne
600 particulate concentrations and numbers in the United Kingdom. Annual report 2019,
601 National Physical Laboratory, https://eprintspublications.npl.co.uk/9292/. [last
602 accessed 11/07/2022].

603

604 Vu, T.V., Delgado-Saborit, J.M., Harrison, R.M., 2015. Particle number size
605 distributions from seven major sources and implications for source apportionment
606 studies. Atmos. Environ. 122, 114-132.

607

608 Wahlin, P., Palmgren, F., Van Dingenen, R., 2001. Experimental studies of ultrafine
609 particles in streets and the relationship to traffic. Atmos. Environ. 35, S63-S69.

610

611 WHO, 2021. WHO global air quality guidelines: particulate matter ($PM_{2.5}$ and PM_{10}),
612 ozone, nitrogen dioxide, sulfur dioxide and carbon monoxide. World Health
613 Organization, Copenhagen, Denmark.

614

615 WHO, 2012. World Health Organization, Health Effects of Black Carbon. World
616 Health Organization, Copenhagen, Denmark.

617

618

TABLE LEGENDS

Table 1. Overall trends for the period 2010-2021, and 2014-2021 at London Marylebone Road for de-seasonalised data. Trends are calculated for the various metrics using the Theil-Sen method. Negative values indicate a reduction with time. The brackets show 95% Confidence Intervals, while the statistical significance marked by "***", "**", "*", "+" represents $p<0.001$, $p<0.01$, $p<0.05$, and $p<0.1$, respectively.

FIGURE LEGENDS

Fig. 1. Annual mean concentration of each particle size mode split by year (2010-2021) and wind direction. Data are filtered according to hourly average wind direction and averaged over one-year intervals. The error bars correspond to one standard error. The Nucleation mode data show a sharp drop from 2013 to 2014, after which there is no clear upward or downward trend. The Aitken and Accumulation mode data show a steady decline. The 180º and 225º data show the greatest contribution of Marylebone Road traffic.

Fig. 2. Annual average particle number size distributions (PNSD) at London, Marylebone Road, 2010-2021. These show all data (left panel), and data only for the 225º wind direction (right panel) which is most affected by Marylebone Road traffic. A mode visible at around 70nm in the earlier years is no longer visible at the end of the time series.

Fig. 3. Temporal trends in Black Carbon and Accumulation mode particle concentrations in relation to heavy duty truck traffic which did not meet the Euro VI emissions standard, 2013-2021. The continuous lines join annual averages for the particle metrics, and the bars show those heavy duty trucks which either did or did not meet the Euro VI emissions standard. A strong relationship is seen in the trends for Black Carbon and Euro VI non-compliant vehicles.

Table 1. Overall trends for the period 2010-2021, and 2014-2021 at London Marylebone

Road for de-seasonalised data. Trends are calculated for the various metrics using the Thei-Sen method. Negative values indicate a reduction with time. The brackets show 95% Confidence Intervals, while the statistical significance marked by "***", "**", "*", "+" represents p<0.001, p<0.01, p<0.05, and p<0.1, respectively.

Parameter	Trends 2010-2021		Trends 2014-2021	
	# cm^{-3} $year^{-1}$	% $year^{-1}$	# cm^{-3} $year^{-1}$	% $year^{-1}$
Nucleation	-242 [-290, -191] ***	-4.86 [-5.52, -4.14] ***	28.6 [-44.5, 99.8]	0.98 [-1.41, 3.69]
Aitken	-643 [-700, -597] ***	-6.18 [-6.53, -5.84] ***	-541 [-581, -494] ***	-7.18 [-7.54, -6.9] ***
Accumulation	-328 [-352, -309] ***	-7.28 [-7.64, -6.99] ***	-305 [-323, -283] ***	-10.18 [-10.14, -9.75] ***
TNCS	-1211 [-1333, -1101] ***	-6.11 [-6.5, -5.72] ***	-853 [-951, -749] ***	-6.26 [-6.72, -5.63] ***
TNC	-1815 [-2351, -1364] ***	-5.2 [-6.39, -4.15] ***	-74.5 [-742, 804]	-0.38 [-3.32, 4.85]
	µg m^{-3} $year^{-1}$	% $year^{-1}$	µg m^{-3} $year^{-1}$	% $year^{-1}$
BC	-0.83 [-0.9, -0.77] ***	-8.26 [-8.56, -7.98] ***	-0.76 [-0.82, -0.7] ***	-12.1 [-12.5, -11.8] ***
CO	-0.04 [-0.04, -0.03] ***	-5.2 [-5.51, -4.69] ***	-0.04 [-0.04, -0.03] ***	-7.15 [-8.22, -5.54] ***
NOx	-18.3 [-22.4, -14.0] ***	-4.73 [-5.29, -3.90] ***	-36.5 [-39.8, -33.4] ***	-9.31 [-9.61, -8.88] ***

SUPPLEMENTARY MATERIALS

Limited Impact of Diesel Particle Filters on Road Traffic Emissions of Ultrafine Particles

Table S1. Data capture of TNC CPC, SMPS, and Regulated Pollutants.

Parameter	Data Capture (%)											
	2010	2011	2012	2013	2014	2015	2016	2017	2018	2019	2020	2021
Wind speed	100	95	100	100	100	100	100	100	100	100	100	99
Wind dir	100	96	100	100	100	100	100	100	100	100	100	98
CO	96	92	95	99	97	98	86	72	98	97	79	84
NO_x	97	93	94	99	99	99	99	99	98	95	97	94
NO_2	97	93	94	99	99	99	99	99	98	95	97	94
NO	97	93	94	99	99	99	99	99	99	95	97	94
O_3	94	54	96	98	95	98	97	98	96	98	92	93
SO_2	92	83	98	80	97	99	99	99	92	98	96	95
PM_{10}	93	90	85	94	93	97	95	96	97	96	75	76
$PM_{2.5}$	58	91	92	97	97	97	96	96	90	91	79	86
BC	97	92	97	99	99	99	98	95	89	95	86	97
TNC	84	79	74	57	51	47	8.4	39	73	80	63	38
TNCS	76	70	37	86	82	90	93	59	44	36	86	74

Table S2. Overall Change of Pollutant Concentration (in percentage) Over 2010-2021.

Year	CO	NO_x	NO_2	NO	O_3	SO_2	PM_{10}	$PM_{2.5}$	BC	TNC	TNCS	Nucleation	Aitken	Accumulation
2010														
2011	1%	9%	-1%	15%	1%	4%	21%	8%	17%	-7%	-12%	-21%	-9%	-7%
2012	-10%	2%	-3%	5%	-19%	19%	-20%	-12%	-14%	-9%	11%	20%	7%	8%
2013	-14%	-10%	-10%	-10%	18%	-27%	-5%	-6%	-23%	-13%	-20%	-13%	-21%	-26%
2014	3%	17%	10%	20%	-21%	50%	-10%	-9%	-3%	-4%	-15%	-35%	-8%	-4%
2015	-2%	-9%	-6%	-11%	8%	0%	-8%	-13%	-23%	-24%	-9%	-9%	-7%	-13%
2016	2%	-1%	1%	-1%	1%	-14%	8%	0%	-5%		-2%	13%	-6%	-6%
2017	-32%	-4%	-6%	-3%	5%	-13%	-8%	-3%	-18%		-5%	7%	-7%	-17%
2018	-9%	-16%	1%	-23%	28%	-21%	0%	2%	-29%		-13%	-7%	-15%	-16%
2019	-5%	-27%	-26%	-27%	7%	-24%	-7%	-9%	-31%	9%	-1%	3%	-3%	-4%

2020	-11%	-43%	-30%	-50%	43%	-48%	-27%	-37%	-27%	-39%	-17%	4%	-23%	-37%
2021	60%	0%	-2%	1%	-13%	2%	2%	17%	-12%	13%	-11%	-21%	-3%	-8%
Overall	**-34%**	**-64%**	**-56%**	**-68%**	**49%**	**-67%**	**-48%**	**-53%**	**-86%**	**-48%**	**-64%**	**-54%**	**-65%**	**-77%**

Some of data are excluded due to very low data capture (<10%)

Table S3. Annual change of vehicle non-compliance with DPF

Vehicle types	% year^{-1}
LDVs-Petrol Cars	-12%
LDVs-Diesel Cars	-17%
LGVs-Petrol Cars	-13%
LGVs-Diesel Cars	-11%
HDVs-Rigid and Artic	-21%
HDVs- Buses and Coaches	-15%
HDVs- TfL Buses	-26%

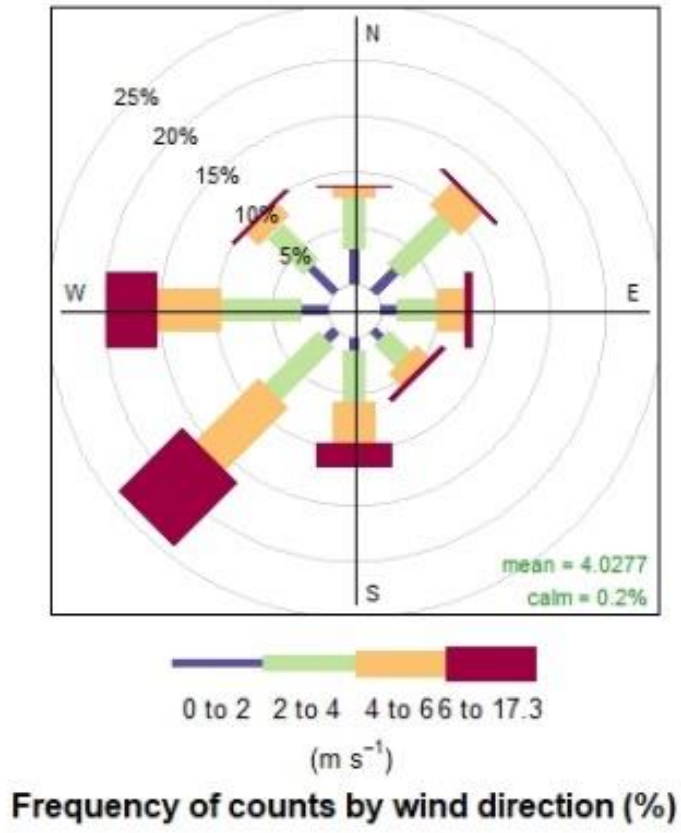

Fig. S1. Wind rose from LHR over 2010-2021.

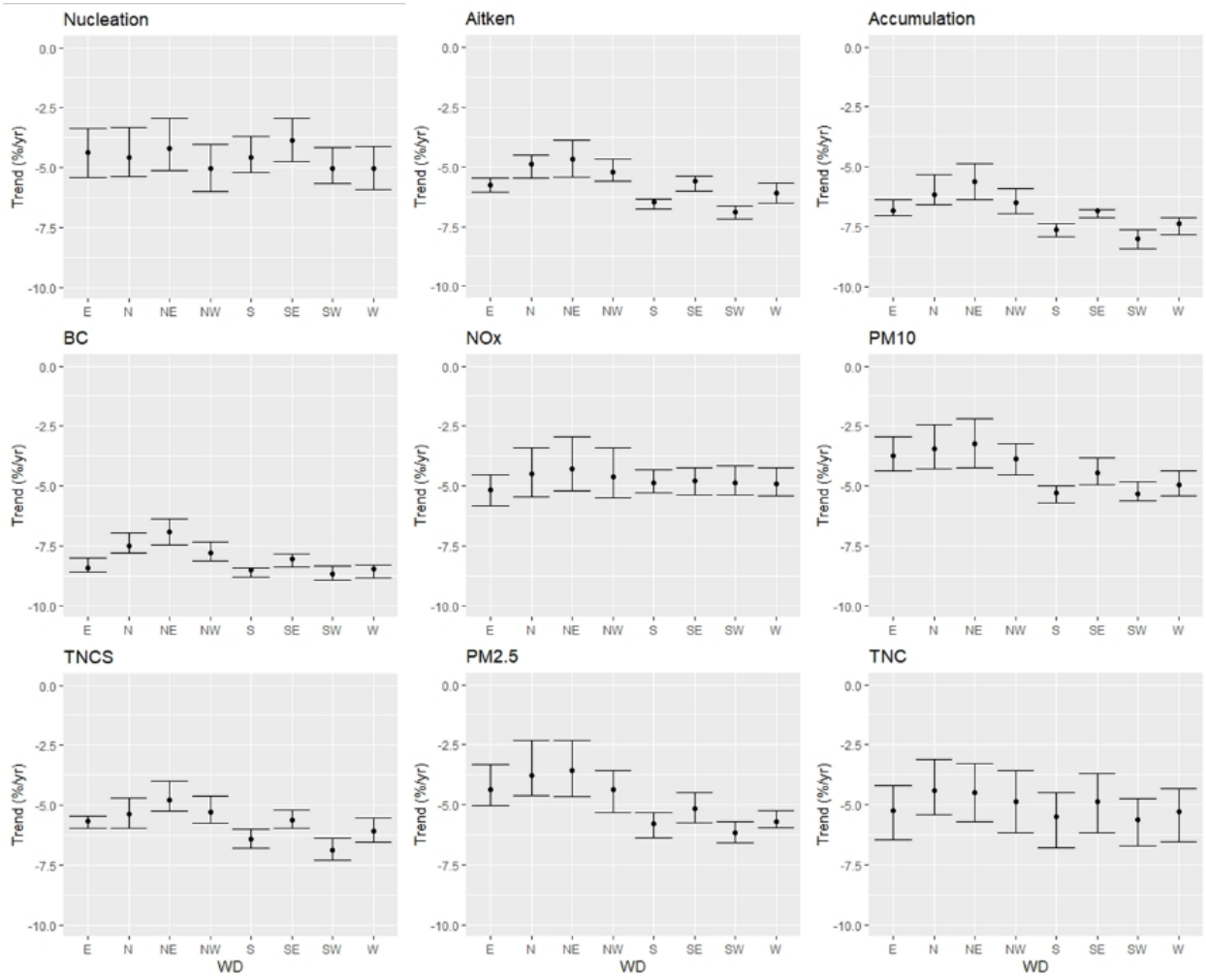

Fig. S2. Overall de-seasonalised trends split by wind direction for the period 2010-2021 at London, Marylebone Road. Error bars represent 95% CI. All of the trend estimation are statistically significant to the level of $p<0.001$.

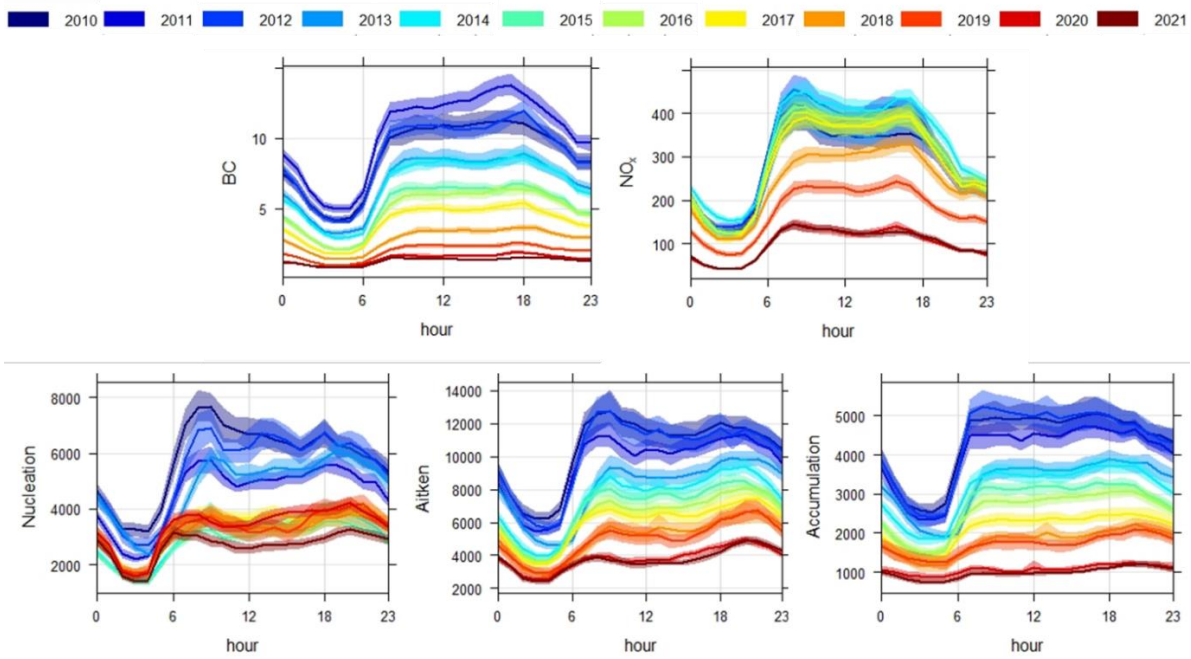

Fig. S3. Diurnal cycle of annual average pollutants concentration at LMR over 2010-2021 (Hour is local time).

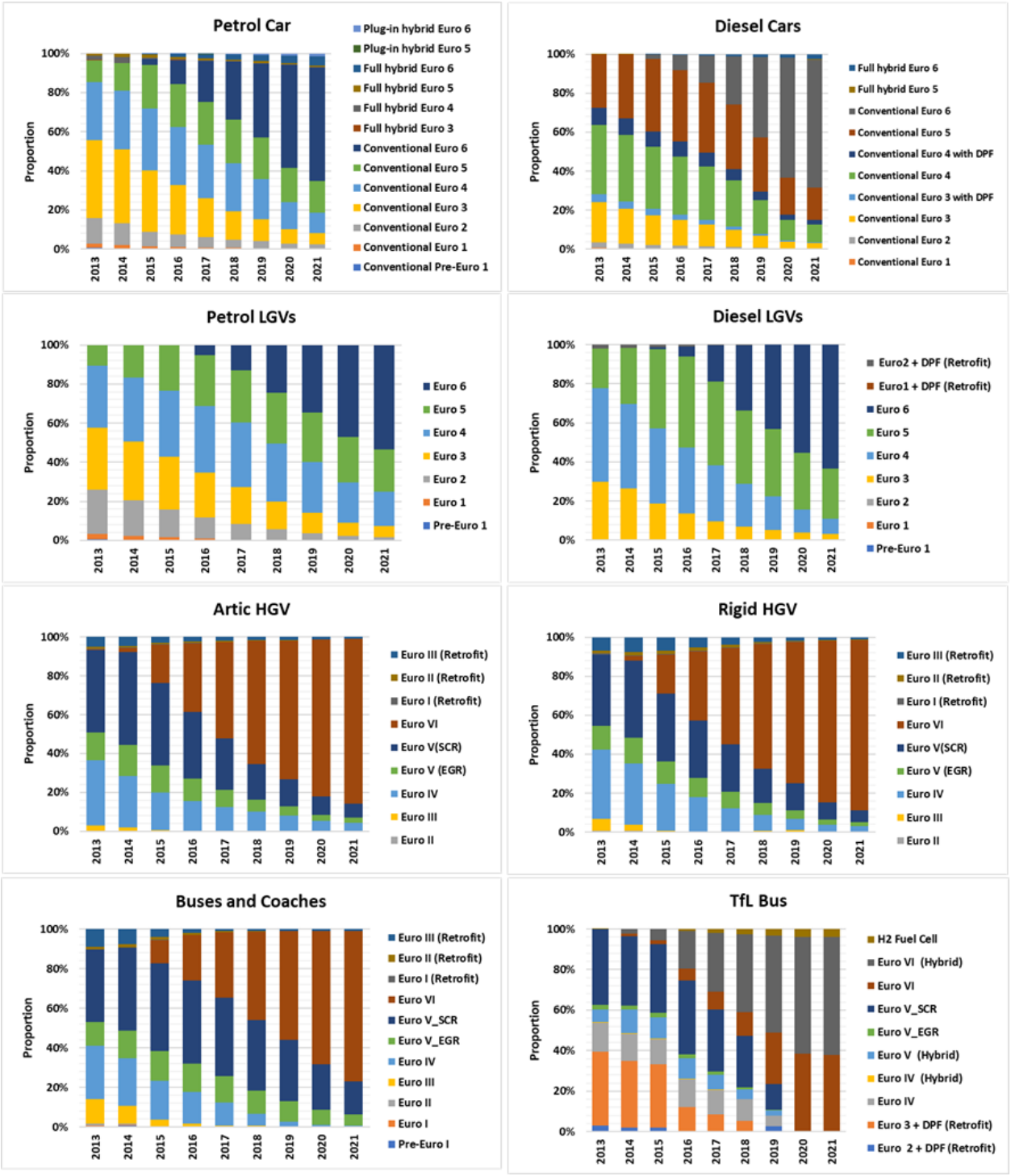

Source: NAEI, 2018 (https://naei.beis.gov.uk/data/ef-transport)

Fig. S4. Vehicle Fleet Composition within Inner London Area

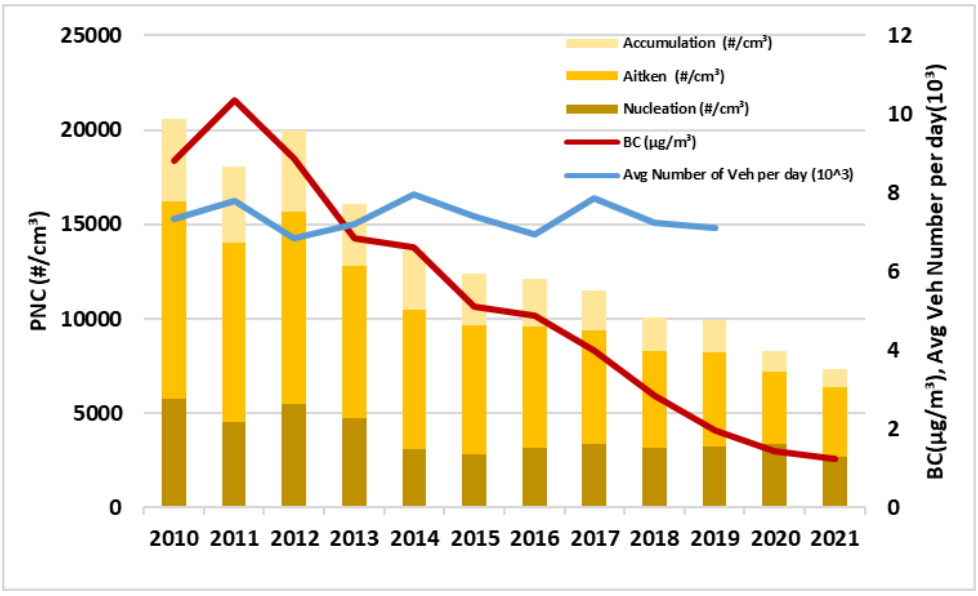

Fig. S5. PNC and BC concentration and Average Number of Vehicle per day at LMR.

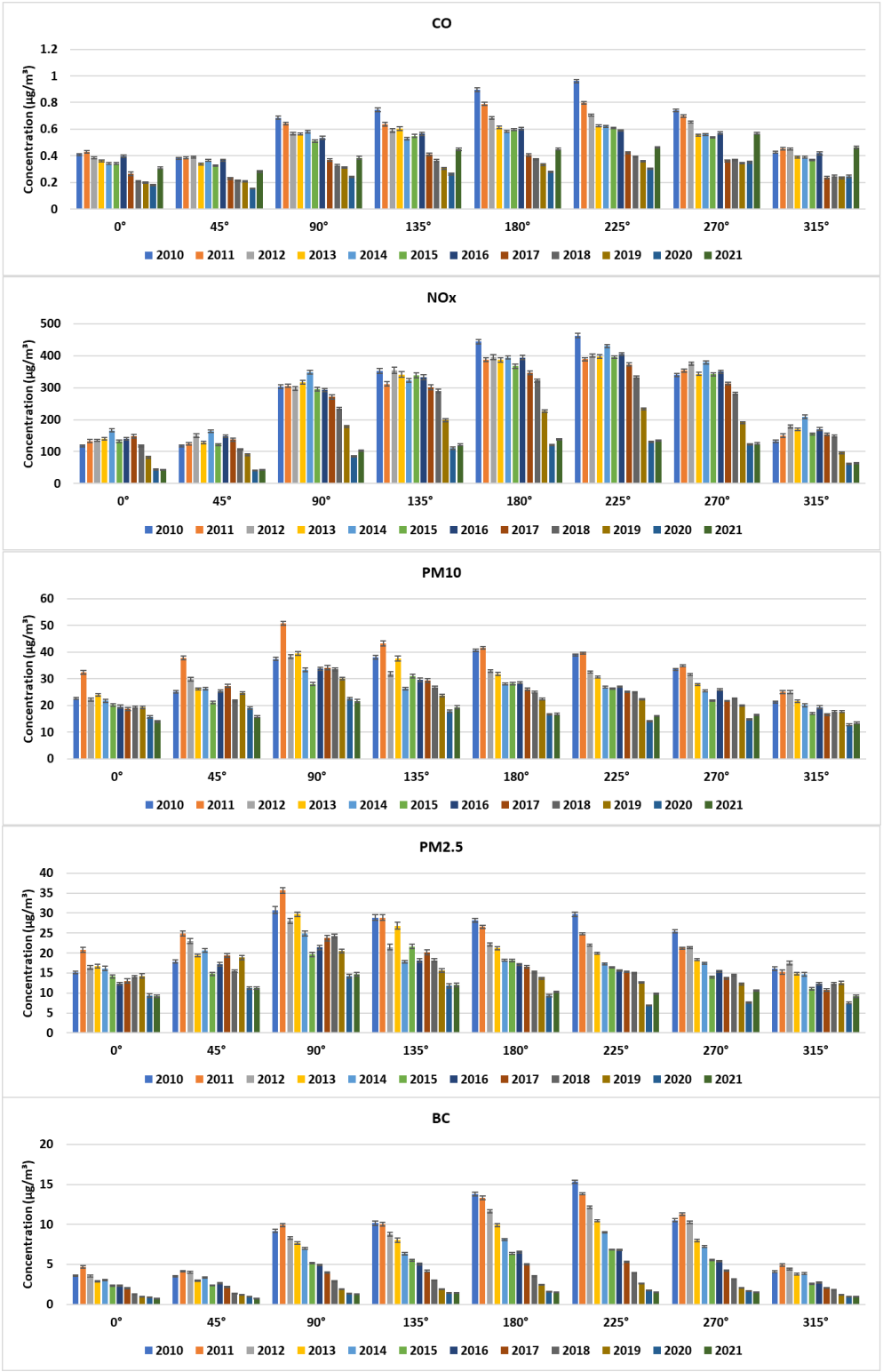

Fig. S6. Annual mean concentration of each regulated pollutant split by year (2010-2021) and wind direction. Data are filtered according to hourly average wind direction and averaged over one-year intervals. The error bars correspond to one standard error.

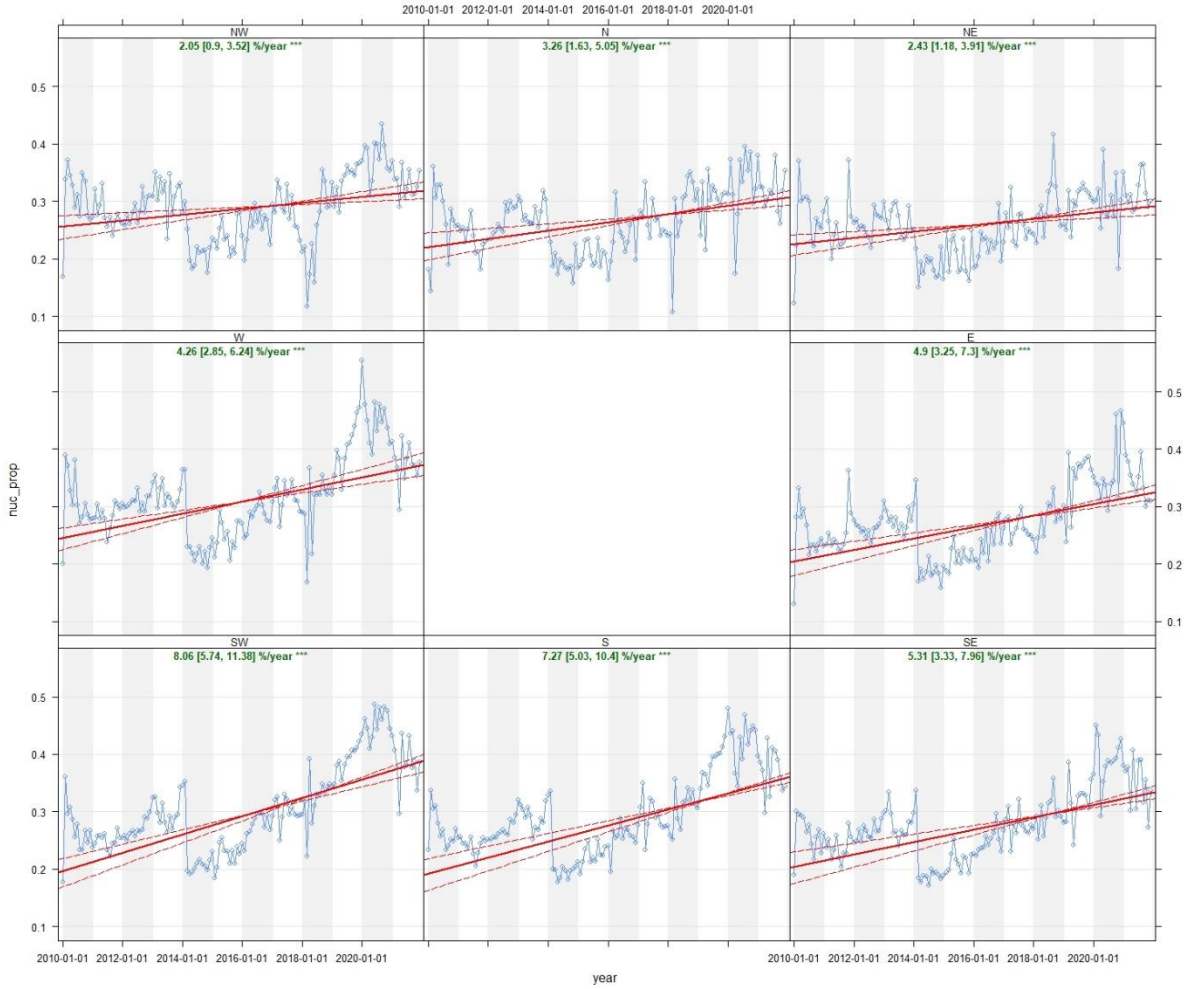

Fig. S7. Trend in the proportion Nucleation mode particles of total number of particles split by wind direction.

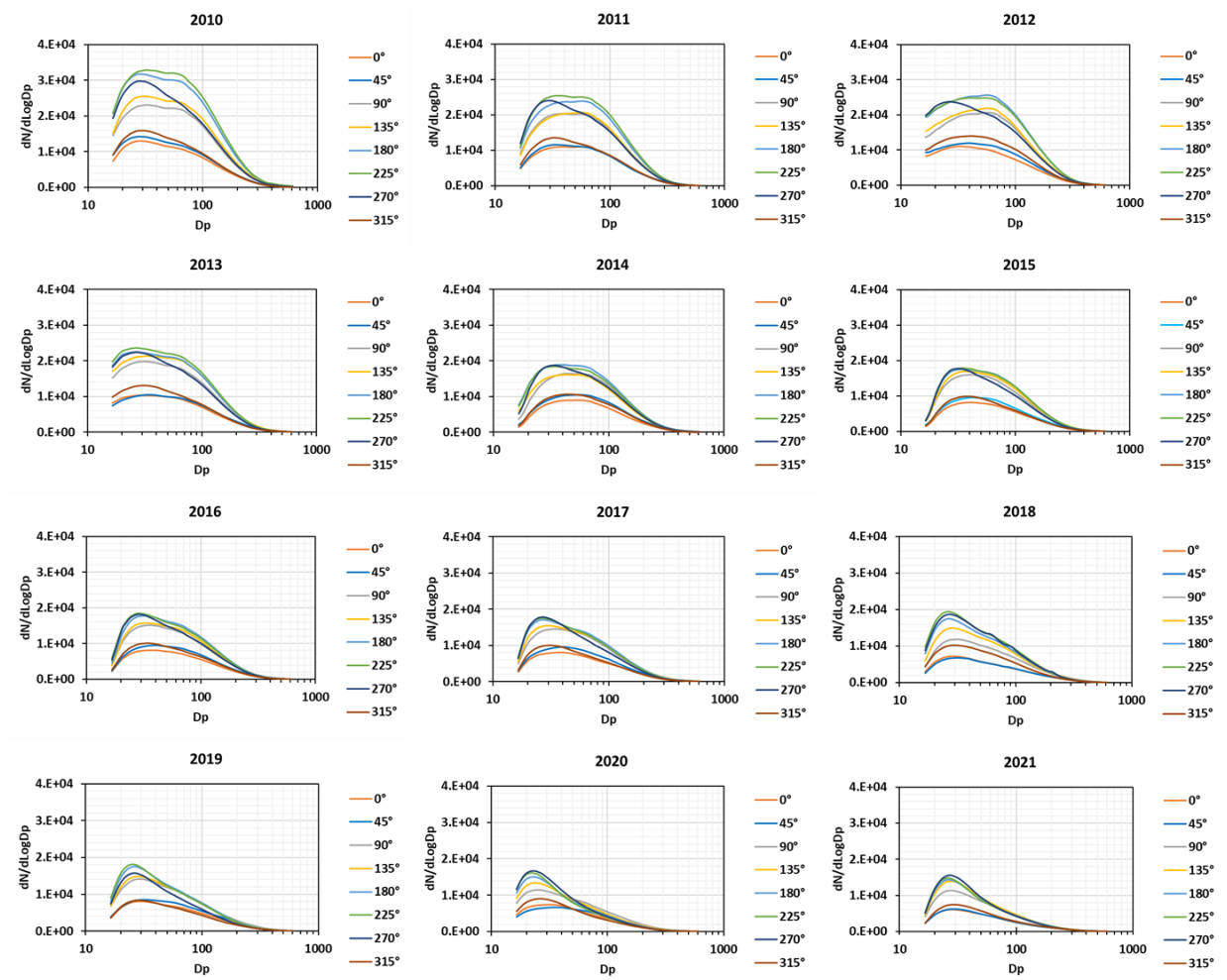

59

60

61 **Fig. S8.** Average PNSD split by wind direction at London Marylebone Road.

62

63

64

65

66

67 **Fig: S9.** Low Emission Zone Area (left), ULEZ area (right).

Chapter 4: Analysing Multiple Metrics of Ultrafine Particles from Personal Exposure Campaigns with Source Quantification

Authors: **Seny Damayanti**, Dimitrios Bousiotis, Arunik Baruah, Francis D. Pope, Roy M. Harrison

Submitted to: Environment International, 2025

Author Contributions: Seny Damayanti: Writing-original draft, Conceptualization, Resources, Visualization, Methodology. Dimitrios Bousiotis: Writing-review & editing, Resources. Arunik Baruah: Writing-review & editing, Resources. Francis D. Pope: Validation, Supervision, Conceptualization, Writing- review & editing. Roy M. Harrison: Validation, Supervision, Conceptualization, Writing- review & editing, Funding acquisition.

Analysing Multiple Metrics of Ultrafine Particles from Personal Exposure Campaigns with Source Quantification

Seny Damayanti[1], Dimitrios Bousiotis[1], Arunik Baruah[1,3,4] Francis D. Pope[1], Roy M. Harrison[1,2]

[1] Division of Environmental Health and Risk Management
School of Geography, Earth and Environmental Sciences
University of Birmingham
Edgbaston, Birmingham B15 2TT, United Kingdom

[2] Department of Environmental Sciences
Faculty of Meteorology Environment and Arid Land Agriculture
King Abdulaziz University, Jeddah 21589, Saudi Arabia

[3] University School for Advanced Studies IUSS Pavia
Palazzo Del Broletto, Pavia, 27100, Italy

[4] Dept of Engineering 'Enzo Ferrari'
University of Modena and Reggio Emilia, Modena, 41125, Italy

Corresponding author: Roy M. Harrison (r.m.harrison@bham.ac.uk)

ORCID ID – Roy M. Harrison: 0000-0002-2684-5226

ORCID ID – Francis Pope: 0000-0001-6583-8347

ABSTRACT

Assessment of personal air pollution exposure is crucial especially for pollutants that exhibit significant spatial and temporal variation. Multiple particle metrics, including particle number concentration (PNC), lung deposited surface area (LDSA), and average particle diameter (ranging from 10-700 nm) were evaluated to assess personal exposure to ultrafine particles (UFP) in a densely populated urban area in Birmingham, UK, using walking and bus journeys. A significant difference ($p < 0.01$) was found between the two transport modes in the average exposure levels to PNC and LDSA, with exposure on the bus higher compared to that of walking. A strong correlation between PNC and LDSA was observed across both commuting modes ($r > 0.85$). The highest average exposure to PNC was recorded on weekdays, particularly in the afternoon during bus trips (19820±18980 #cm^{-3}), and in the evening during walking trips (14510±19120 #cm^{-3}), which coincided with the smallest average particle diameter. Road vehicles and restaurant cooking activities, particularly those located on main roads, are likely responsible for these elevated levels. A close examination of the data shows many short-lived increases or "peaks" in PNC and LDSA accompanied by a reduction in average diameter, attributable to hyper-local emissions that may affect overall exposure. A new method has been developed to separate peak data (de-peaking) from walking datasets, enabling source quantification. Three sources are quantified in the data: general urban background (scale >1km), local increment on background (~1km) and short-lived peaks due to hyper-local emissions (metres).

Keywords: Personal exposure; Mapping; Ultrafine particles; Road traffic; Vehicle emissions

1. INTRODUCTION

Ambient particulate matter pollution is the leading environmental risk factor for the global burden of disease in 2021 (HEI, 2024). In Europe, it is estimated that approximately 253,000 deaths were attributable to fine particulate matter ($PM_{2.5}$, which is comprised of particles less than 2.5 μm in diameter) exposure in 2021 (EEA, 2023). In recent decades, $PM_{2.5}$ has been the main focus of air pollution exposure studies due to regulatory guidelines. However, due to growing concerns, there is an increase in studies investigating an emerging pollutant, specifically ultrafine particles (UFPs, particles with a diameter of 100 nm or less).

Although UFPs are included in $PM_{2.5,}$ their measurements are not indicative of one another. A study exploring ambient UFPs and $PM_{2.5}$ concentration across 10 cities worldwide revealed a poor correlation between UFP and $PM_{2.5}$ concentration, with the Pearson correlation coefficient, r, ranging from 0.09 - 0.69 (de Jesus et al., 2019). A weak correlation (r = 0.5) between these two pollutants was also observed in a personal exposure study conducted in a London Street canyon (Kaur et al., 2005). Furthermore, UFPs exhibit greater spatial variability than $PM_{2.5}$ (Jianyao et al., 2025; Saha et al., 2019; Wu et al., 2015) due to additional substantial emission sources, such as restaurant cooking, and industry processes (Saha et al., 2019; Shah et al., 2023; Ye et al., 2020b) and new particle formation (Gani et al., 2021; Schraufnagel, 2020a; Li Tao et al., 2023). This implies that controlling $PM_{2.5}$ does not necessarily reduce the UFP level, thus requiring a thorough evaluation of their exposure (Nair et al., 2023).

It has been postulated that UFP have a more adverse effect on human health than larger particles. Due to their small size, they can more easily enter the human lung, reach the alveolar region, and be retained longer than larger particles (Schraufnagel, 2020a). It has

been hypothesized that UFPs can penetrate biological membranes and then translocate to other organs, including the brain and nervous system, via systemic circulation (HEI, 2013a). Moreover, UFPs possess a large surface area to mass ratio, which enables them to adsorb more hazardous metals and organic compounds. This property may lead to the induction of oxidative stress, making UFPs more toxic per unit mass than larger particles (H.-S. Kwon et al., 2020; Lin et al., 2022; Schraufnagel, 2020a). A recent cohort study has shown that long-term exposures to ambient UFPs are linked to the occurrence of brain tumours in Canada's two major cities (Lloyd et al., 2024). In contrast, short-term exposure to UFPs has been linked to inflammatory and cardiovascular illness (Simone Ohlwein et al., 2019).

Although UFPs contribute very little to mass concentration, they are a major contributor to the total number of particles in the atmosphere. Therefore, UFPs are typically measured by particle count per volume of air rather than their mass (Harrison, 2020a; HEI, 2013a).

Emission from road vehicles serves as the major contributor to UFPs in most urban atmospheres (Brines et al., 2015; Chatain et al., 2021). A strong association was observed between the particle size range of 30-60 nm and light-duty vehicles (Charron & Harrison, 2003), whereas a range of 60-80 nm was associated with diesel vehicle exhaust (Hopke et al., 2022). As previously mentioned, cooking activities contribute greatly to UFP emissions, particularly those with a smaller diameter. A field measurement study using a mobile laboratory examined UFPs from nine restaurants in the urban US, found that the modal particle diameter across all sampling sites ranged from 8 nm to 29 nm (Kim et al., 2024).

Lung deposited surface area (LDSA) is an alternative metric for UFPs, linking the surface area of particles with different regions of deposition in the human respiratory tract (Lepistö et al., 2020). The deposition efficiency is dependent on the particle size. Larger particles (Dp > 10 μm are primarily retained in the upper respiratory tract due to impaction, while smaller particles ((Dp < 0.1 μm) will deposit in the tracheobronchial, and alveolar regions through diffusion (ICRP, 1994b). LDSA provides a more accurate predictor of UFP-induced inflammatory and oxidative stress responses, which can be utilised to examine the dose-response relationship (Baldauf et al., 2016; Lepistö et al., 2020). A prior study identified a stronger association between the LDSA and reduction in lung function compared to larger particles ($PM_{2.5}$ or PM_{10}) thereby suggesting the LDSA as a critical metric for evaluating the impact of particulate matter on lung function and population health (Patel et al., 2018; Rückerl et al., 2016). Additionally, toxicological research has suggested that surface area is the most relevant parameter influencing acute lung toxicity induced by UFPs (Schmid & Stoeger, 2016). A study demonstrated that around 50 % of ultrafine particles deposit in the alveolar region (X. Liu et al., 2023), where interaction between respiratory and pulmonary circulation occurs (Lepistö et al., 2022), and deposition in this region is dominated by particles with a diameter less than 100 nm (ICRP, 1994b). Lloyd et al. (2024) concluded that including average particle size as a variable in their epidemiological model was important, which demonstrated significant associations of UFP exposures with total and respiratory mortality. Their results indicate a stronger association between larger average UFP size (up to ~35 nm) and brain tumours.

In 2021, the WHO released updated global air quality guidelines, tightening the limits for particulate matter ($PM_{2.5}$ and PM_{10}) and gaseous pollutants. While there was ample evidence of the toxicological effect of UFPs (Ferin et al., 1990; Gilmour et al., 2004;

Renwick et al., 2004; Vora et al., 2014) at the time the WHO set their new PM standards, epidemiological studies did not provide sufficient evidence to set an air quality guideline for UFPs. Hence, WHO (2021) formulated Good Practice Statements for three pollutants, including UFP, to limit the adverse effect on human health and the environment. One specific recommendation is to increase population exposure assessment for UFP (WHO, 2021a). This has been adopted by the European Commission which has included UFPs monitoring as a requirement in the latest Air Quality Directive (EU, 2024).

Evaluating individual exposure to air pollutants is crucial, particularly within urban areas where sources of pollution are manifold and ambient concentrations frequently reach elevated levels. It is also essential for informing policy-based evidence to improve air quality (Cichowicz & Dobrzański, 2022). There is an increasing body of knowledge evaluating personal exposure to UFP, particularly by mobile monitoring (He & Qiu, 2022; Knibbs et al., 2011; Luengo-Oroz & Reis, 2019; Patel et al., 2023; Rivas et al., 2017b; Samad et al., 2022; Tran et al., 2020; Weichenthal et al., 2008). However, most prior studies have primarily focused only on PNC, while the analysis of LDSA and average diameter, which are other crucial metrics of UFPs, remains limited (Amin et al., 2024; Liu et al., 2022; Tran et al., 2020).

This study presents a comprehensive analysis of important UFP-related metrics, including PNC, LDSA, and average diameter, derived from personal exposure measurements in an urban setting in Birmingham, UK, using walking and onboard bus measurements. It is noted that the LDSA measured in this study refers to that deposited in the alveolar region. This study aimed to investigate the dynamics of measured metrics along a pre-defined study route and within various microenvironments, analyse the temporal variation of exposure, and identify areas of high concentration in the study region. While the PNC

147 metric provides information on the abundance of UFPs in the atmosphere, the average
148 size gives insight into the characteristics of emission sources (e.g., certain average
149 diameters are linked to certain emission source). Additionally, the LDSA, as mentioned
150 earlier, is valuable for dose-response analysis studies. Assessing these metrics together,
151 enables a more comprehensive analysis of sources and relationships and thus enhances
152 understanding of UFP exposure in urban environments.

153 In addition, further analysis was performed to evaluate the effect of short-term PNC peaks
154 on overall UFP exposure by excluding short-term peaks from the total data set and
155 comparing the result with urban background concentrations from a local monitoring
156 station. This approach facilitated the estimation of contributions from urban background,
157 local increment, and hyperlocal sources.

158

159 ## 2. METHODS

160 ### 2.1 Sampling Location and Period

161 Mobile measurements were performed to estimate personal exposure, between 20th May
162 to 26th June 2023, by either walking or bus travel at three different times i.e., morning (8
163 AM – 11 AM), afternoon (12 PM- 4 PM), and evening (5 PM – 8 PM) on both weekdays
164 and weekends. The walking route explores urban microenvironments in Selly Oak, a high-
165 density urban area, which is inhabited by more than 10,000 people, primarily consisting
166 of university students. The bus routes include two routes (a) a residential route and a (b)
167 a main road towards the walking route. Personal exposure measurement was conducted
168 along an approximately 3.5 km bus route, and 7 km walking route, as shown in Figure 1.
169 A total of 234,556 (walking) and 26,859 (bus) data points recorded at a 1-s resolution,

equivalent to 287 km (walking) and 95 km (bus) from 41 trips (walking) and 27 trips (bus) were collected over 24 sampling days (Table S1).

In addition to the walking and bus routes, assessment was conducted in various microenvironments to understand local sources of UFPs. This included bus stops (BS) located on two main roads (BS 1 and BS 2), as well as one on a secondary road (BS 3). Furthermore, measurements were carried out at two supermarkets, one that exclusively sells groceries (Supermarket 1) while the other includes a food-selling kitchen (Supermarket 2), as well as at a fast-food restaurant. Although the sample size collected at these microenvironments was smaller than the walking and bus measurement, which may affect statistical robustness, they provide valuable insight into probable local sources of UFPs.

Additional data derived from a nearby urban background station, namely Birmingham Air Quality Supersite (BAQS) was used for further analysis. The BAQS is located within the University of Birmingham campus, on the north-side of Selly Oak. There is a railway line and local through road to the west and east, respectively, as well as a few houses nearby.

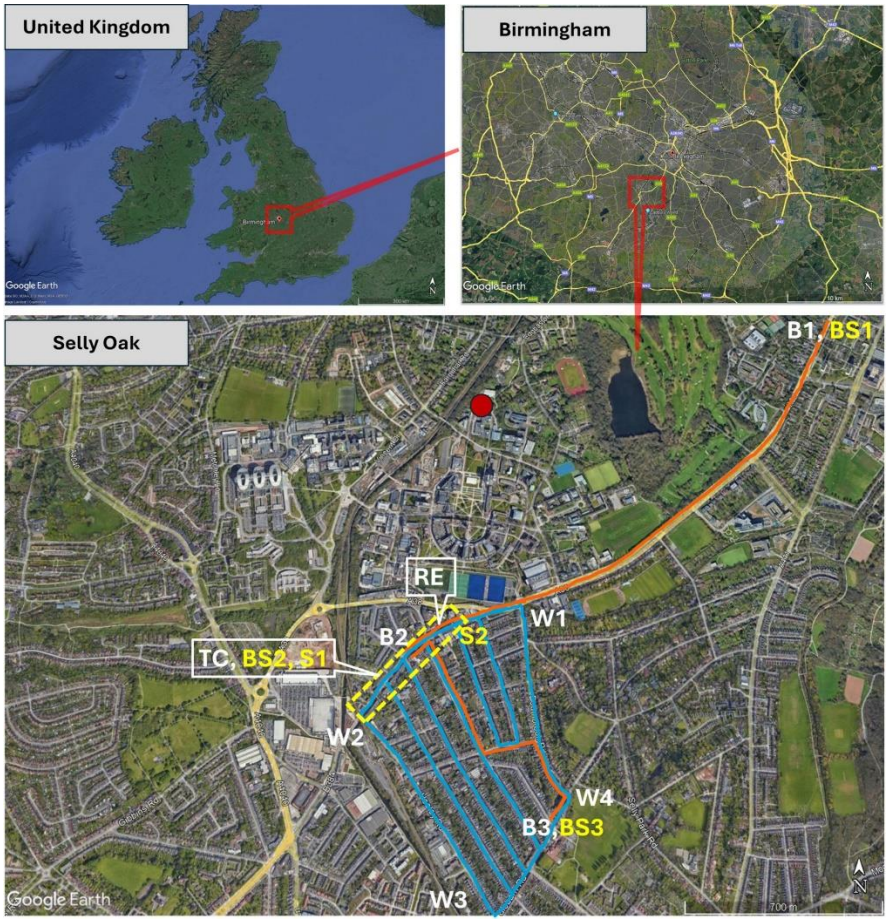

Figure 1. Map of study area. Fixed routes for walking and bus measurements are shown by the blue and orange lines, respectively. Segments B1-BS2, and W1-W2 represent routes along main roads for bus and walking, respectively. Segments B2-B3, and the roads within W1-W2-W3-W4 represent routes along the residential roads for bus and walking, respectively. The dashed-yellow line shows the restaurant area. TC shows the traffic count station. The yellow text labels the locations of microenvironment as BS (bus stop), S (supermarket), and RE (restaurant). The red dot shows the location of the urban background, Birmingham Air Quality Supersite (BAQS).

2.2 Sampling Instruments

A handheld particle counter (DiSCmini, Testo Inc.), was used to measure PNC, D, and LDSA at a time resolution of 1 s. The DiSCmini detects particle concentration between 10^3 and 10^6 #/cm^3, while the size range of particle diameter detected ranges from 10 – 700 nm. The average diameter recorded by the DiSCmini reflects the electrical mobility diameter of particles, which is defined as the diameter of a spherical particle exhibiting same electrical mobility in an electric field as the particle under study. Particles up to 10

μm can deposit in the alveolar region, however, the DiSCmini is reliable only for particles less than 300 nm (Todea et al., 2015). A study has shown that particles larger than 400 nm can substantially contribute to the LDSA in another region i.e., head airways (ICRP, 1994a). Therefore, this study focusses only on the suitable size range for the DiSCmini.

The DiSCmini operates by applying electrical charges to particles and measuring their subsequent diffusion. In a unipolar charger, particles are given positive charges so that the current they generate may later be detected. In a "diffusion stage," particles are deposited via diffusion and subsequently detected as an electrical current, which is selectively based on size (Martin Fierz et al., 2008; Fierz et al., 2011). The remaining particles create an electrical current in addition to ending up in a filter stage. The ratio of current at the filter stage and diffusion stage determines the average particle diameter. Once the diameter is determined, the particle number can be calculated based on the total charge and flow rate. Meanwhile, LDSA is estimated using the International Commission for Radiological Protection or ICRP model (ICRP, 1994b), which relies on the correlation with the total current signal. The calculation has been thoroughly explained in Fierz et al., (2008).

In this study, the DiSCmini was co-located with regulatory grade particle instruments (TSI CPC 3775 and TSI SMPS 3082) for 7 days at BAQS (Figure S1). The PNC from the DiSCmini was compared with the total number concentration from the SMPS within the selected diameter range of 10-300 nm, which is similar to the modal diameter range of the DiSCmini. The R^2 value of 0.97 between DiSCmini and SMPS indicates a satisfactory agreement. This is consistent with prior studies, both in controlled laboratory settings and in field measurements (Meier et al., 2013; Viana et al., 2015)), that demonstrated a strong correlation between DiSCmini and reference instruments, with $R^2 > 0.80$ (Viana et al.,

2015). Before and after the trip, a HEPA filter was attached to the inlet tube to perform a zero check for quality assurance. A GPS sensor was used to track the coordinate point during the trips. The instruments were carried in a backpack during measurements (Baruah et al., 2024; Bousiotis et al., 2024), and an inlet tube was positioned within the breathing zone, i.e., approximately 30 cm away from the mouth (Int Panis et al., 2010). More information regarding sampling methods was provided by Bousiotis et al. (2024).

The DiSCmini is recognised as a robust sensor for personal exposure assessment (Meier et al., 2013; Mills et al., 2013); however, it possesses several limitations. PNC is definitively measured by a condensation particle counter (CPC), and hence the result from the DiSCmini measurement is indicative PNC. The performance of the DiSCmini as well as other portable sensors has been comprehensively studied in another study, which suggested that those sensors, including the DiSCmini, are categorised as indicative instruments or tier 2 for airborne exposure studies (Viana et al., 2015). The accuracy of this instrument is typically around 15-20% relative to a CPC according to the manufacturer's report. Viana et al., (2015) reveal that the mean difference between DiSCmini and each stationary instrument was 10-18%, 12-18%, 7-13% for average PNC, average diameter, and alveolar LDSA, respectively. This uncertainty may arise from the mismatch between the aerosol size distribution used during laboratory calibration and that measured in actual field measurements. Specifically, the DiSCmini is calibrated using a monodisperse aerosol, after which its response is modelled for a polydisperse aerosol that assumes a lognormal size distribution with a geometric standard deviation (σ) of 1.9. In fact, the characteristics of real-world aerosol may differ, resulting in inaccuracies both in particle number and average diameter measurement. The DiSCmini has to make an approximation related to particle size and shape (i.e., spherical shape) and assumes

particles to be hydrophobic. The assumption of spherical particles may simplify the interpretation of particle movement under electric charge. Furthermore, the estimation of LDSA relies on the total current from charged particles, which is accurate for particles up to the size range of 300 to 600 nm. However, when the measured aerosol consists of particles larger than the upper limit, the absence of any size-dependency during the measurement may result in an underestimate of the LDSA concentration (Lepistö et al., 2020)

2.3 Data Analysis

Data analyses were performed using the Openair package in R (David C. Carslaw & Karl Ropkins, 2012), and Microsoft Excel.

All the measured data with 1 s resolution were used for analysis, with the exception when comparing with the SMPS data (5-minutes averaged, in Figure 7 and Figure 10), and in de-peaked analysis (10-minutes averaged), which will be elaborated below.

Figure 2 gives an example of a time series of the collected data. It may be seen to contain many short-term increases, or “spikes”. In section 3.6, short-term peaks in the PNC from walking exposure data were further investigated, including the following steps:

1. *Baseline calculation*

   The baseline was calculated for each trip individually. To do this, a centred moving median was applied using various time windows, specifically 1-minute averages, 5-minute averages, and 10-minute averages, before and after data points. The moving median is considered more robust to outliers compared to the moving average (Yaro et al., 2023). As the baseline is calculated by involving data before and after data points during the specific time window, there were some data points

where the baseline was unavailable. For instance, when using 10-minute averages, the initial and the final 10-minute segments of each trip were unavailable. Thus, only the original PNC data with available baseline data will be subjected to further investigation.

2. *Short-term peak (spike) identification*

The study conducted by De Kluizenaar et al. (2017) detected peak exposure to UFPs by both static and mobile measurements (walking, cycling, and motorized), with peak exposure defined as UFP levels above the 95th or 99th percentile that occurred for a duration of at least 10 minutes for each researcher. Nevertheless, employing the 95th and 99th percentile cutoffs is unsuitable for our dataset since rapid changes in PNC are frequently found, resulting in many spikes remaining in the dataset. Other approaches were tried, and a threshold of 10% of the baseline was selected for optimal spike detection based on visual observation.

3. *Exclusion of short-term peak (spike) data from dataset*

Peaks above the threshold were classified as spikes and separated from the data set.

4. *Data Interpolation*

A linear interpolation was used to replace the removed short-term peak data points. A 10-minute average time window was chosen as an optimum time window that yields the closest de-peaked interpolated PNC to the background level as seen in Fig. S2. In addition, this time window is also considered appropriate for walking measurement since the researcher passed through diverse microenvironments during the trip, resulting in a highly dynamic data concentration.

5. *Comparison of De-peaked mobile PNC data with Background PNC data*

De-peaked interpolated PNC data were corrected to the SMPS using the calibration obtained through the co-location study. A more detailed explanation of the co-location process is provided by Baruah et al. (2024) and Bousiotis et al., (2024). The baseline PNC was then compared to the total number concentration derived from the SMPS, and to the sum of the removed “spikes”.

2.4 Spatial Map Distribution

To generate a spatial map of the particle characteristics, the average PNC was calculated for individual street segments, specifically of 20 m for the walking route, and 50 m for the bus route. Route segmentation was carried out in R by grouping the GPS coordinate points according to distance. This discrepancy in scales is due to the difference in speed between walking and bus measurements.

3. RESULTS AND DISCUSSION

3.1 General Results

Table 1 displays the descriptive statistics for PNC, average diameter and LDSA for the entire measurement period. In general, we found a statistically significant difference ($p < 0.01$) between riding the bus and walking in the average exposure levels to both PNC and LDSA, with riding the bus giving higher values (17244 #/cm^3, and 29 μm²/cm³) compared to walking (10066 #/cm^3, and 22 μm²/cm³). Using a typical instrument (DiSCmini), the average PNC and LDSA exposure on the bus in our study is lower than that observed in Cambodia, specifically 22,600 and 37,200 #/cm³ for PNC, and 50.8 and 83.9 μm²/cm³ for LDSA from two distinct roads (Amin et al., 2024). Our walking exposure is also much lower

than that observed in a commercial area (62,400 #/cm³ for PNC, and 125 μm²/cm³ for LDSA) and at a background site (18,700 #/cm³ for PNC, and 42.4 μm²/cm³ for LDSA) in Singapore (Tran et al., 2020). The data indicates vehicle volume in their study area is approximately double compared to that passing on the main road in this study. In addition, other substantial UFP emission sources (i.e., incense from a temple) were presented, which may lead to their higher average PNC compared to that observed in the current study. Figure S3 displays the PNC measured from mobile measurements and the PNC derived from the SMPS at the local air quality station simultaneously with the bus and walking measurement. In addition, Figure 2 shows an example from a weekday morning trip. Notably, the SMPS reading indicated that there was no substantial change in PNC levels between walking and bus measurements times. This suggests that the higher PNC exposure during bus rides was likely attributed to other factors other than changes in the ambient air quality. Some possible factors are the infiltration of surrounding vehicle emissions into the cabin (Rivas et al., 2017a) and emission from the bus engines. Elevated exposure to pollutants inside the bus aligns with other prior personal exposure studies (Rivas et al., 2017a; Wang et al., 2024).

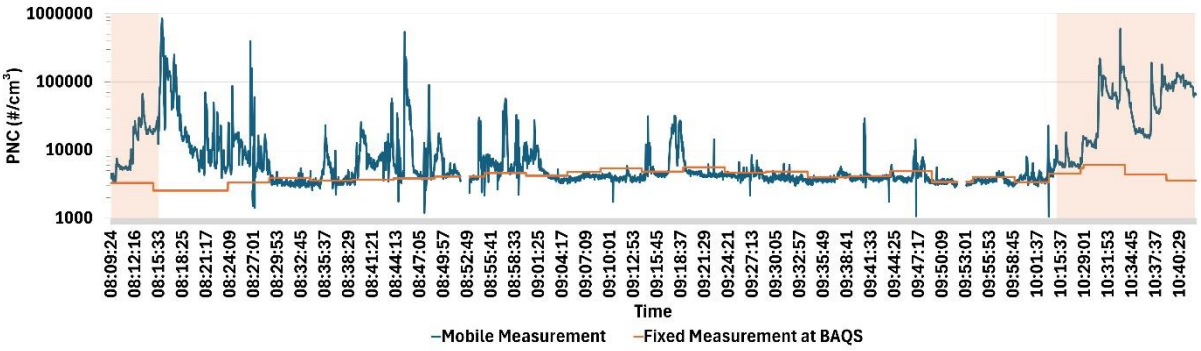

Figure 2. Example of PNC from a morning trip during mobile measurement by DiSCmini (blue line), and that derived from SMPS at the local urban background air monitoring site (orange line). A light orange shade shows the measurement on the bus journey, while the unshaded PNC was measured during walking.

The higher exposure during bus travel coincides with a smaller average particle diameter, i.e., 41±17 nm in contrast to walking trips (46 ±19 nm). Prior studies have indicated that taking the bus provides higher levels of pollutants compared to walking trips (Chaney et al., 2017; Weichenthal et al., 2008); Bus idling behaviour, ventilation, and elevated outdoor particle concentrations along the bus route may also affect exposure to particles while on the bus (Hammond et al., 2007; Singh et al., 2021; Zhang et al., 2013). The proximity to the vehicle exhaust, particularly at junctions where vehicles accelerate, thus increasing UFP emissions (Kim et al., 2024) may also contribute to the higher exposure level within the bus cabin. In addition, a study found that buses can experience self-pollution (Sabin et al., 2005), when the bus's own exhaust emission enter the cabin through doors during the passenger exchange, windows, and cracks (Zhang et al., 2013).

In addition to outdoor sources, in-cabin UFP sources can also contribute to the exposure levels during the bus journey. Prior studies have indicated that combustion equipment, particularly fuel-operated auxiliary heaters, could be an important UFP source within the bus cabin (Hallquist & Salberg, 2025; Oikarinen et al., 2025; Oikarinen et al., 2022). These heaters are used to heat the engine as well as the cabin, particularly in cold areas, and are commonly employed both in internal combustion engine and electric vehicles. The operation of such heaters has been shown to emit very high concentrations of smaller particles (Dp<23 nm) (Hallquist & Salberg, 2025), particularly during the start-up and shut-down phases. The quantity of UFP emissions from this source can be comparable to or even exceed those generated by idling engines, making it a significant yet neglected contributor to in-cabin UFP concentrations. Sources of UFP emissions within the cabin itself seem unlikely.

In this study, the smaller average particle size measured on the bus suggests that self-pollution and passenger exchange, especially along the main road where emissions from road transport are important and, are likely responsible for the higher PNC exposure and LDSA due to the introduction of small freshly vehicle-emitted particles. Even though all buses in the study area meet EURO VI emission standards and have been fitted with diesel particle filters, it should be noted that this technology is less effective in removing ultrafine particles, especially those in the liquid mode (Dp < 30 nm) when compared to the regulatory monitored $PM_{2.5}$ size fraction (Damayanti et al., 2023). Consequently, the concentration of particles within this size range (Dp < 30 nm or typically classified as nucleation mode) is expected to remain high during bus journeys. These circumstances may exacerbate the adverse impact of UFPs on bus passengers.

Table 1. Descriptive Statistics of PNC, Average Diameter, and LDSA from walking and bus measurements during the campaign period. The asterisks "*" and"**" represent walking data that include all trips (41 trips) and only include the same days as bus trips (27 trips), respectively. "N" is the number of data points, the "[a]" in the minimum and maximum average diameter columns, indicates the lowest and highest values of modal diameter obtainable from the DiSCmini.

Parameter		N	Mean	SD	Median	Min	Max
PNC (#/cm³)	Walking *	234556	11010	17236	7003	288	971987
	Walking **	152494	10066	18479	6409	288	971987
	Bus	26859	17244	19549	11357	656	406968
Average Diameter (nm	Walking *	234556	46.2	19.0	44.5	10[a]	300[a]
	Walking **	152494	48.4	20.1	46.4	10[a]	300[a]
	Bus	26859	41.4	16.8	37.9	10[a]	300[a]
LDSA (µm²/cm³)	Walking *	234556	22.6	22.0	19.3	2.3	1533.4
	Walking **	152494	22.0	23.5	18.9	2.3	1533.4
	Bus	26859	29.1	16.6	25.9	5.6	184.2

A study by Liu et al. (2023) analysed LDSA measurements from urban areas across Europe, reporting an annual average Alveolar LDSA in Birmingham of 15±11 µm²/cm³. A

higher average LDSA recorded in our study may be attributed to the use of a different instrument as Liu et al. (2023) used data from a fixed SMPS, most probably not in close proximity to emission sources, as during our mobile monitoring. Comparing the bus routes (Table S2), the average PNC and LDSA were found to be higher near a major road (18590 #/cm^3) compared with the route that passes through residential area, (11197 #/cm^3). Likewise, the LDSA, as with PNC exposure, exhibited lower levels along the residential route (24.5 μm²/cm³). However, this route also showed a larger average diameter (47.3 nm), indicating less influence from traffic and cooking emissions.

A stronger positive correlation between traffic volume and UFPs exposure was identified compared to other traffic-related pollutants (Nazneen et al., 2023). Prior research have shown road type as an important determinant influencing personal exposure to air pollutants (Fruin et al., 2008; MacNaughton et al., 2014; Rafiepourgatabi et al., 2021). For instance, a study in Canada found that UFP concentrations on motorways were much higher than those on residential roads by an order of magnitude (Fruin et al., 2008). In this study, the major road has a substantially higher traffic volume, with a higher proportion of heavy-duty vehicles compared to the residential road. Considering all identified potential factors, higher exposure during bus trips, particularly on major roads, is attributable to overall road emissions as well as in-cabin contributions. Figure 3 shows the temporal variation of average PNC exposure, average diameter, and LDSA, whereas Table S3 presents the statistical summary. Weekday PNC exposure was observed to be higher (12609 ± 21242 #/cm^3) than weekend exposure (9512 ± 14342 #/cm^3), in both walking, and bus measurements. This pattern aligns with the results of Amin et al., (2024), particularly for the bus measurement. Traffic count data from a main road on our study route showed that approximately 14000 vehicles pass along this road daily. Figure S4

408 shows time variation from that road, with less traffic on weekends, which may explain the
409 lower PNC exposure during that period. The hourly average of vehicle numbers over the
410 weekend shows a slight decrease relative to weekdays (Table S4). However, we observed
411 a substantial reduction in bus numbers with approximately 50% of the weekday count
412 during the weekend, which may lead to a decrease in PNC during that time. In addition,
413 weekday trips exhibited a smaller average particle size (43 ± 17 nm) than on the weekend
414 (50 ± 20 nm), suggesting a greater relative local background presence during the
415 weekend.

416 Statistical significance tests utilising non-parametric Kruskal-Wallis and *post hoc* pairwise
417 Wilcoxon tests revealed significant differences in all measured parameters ($p<0.001$)
418 across various times of day for each travel mode, indicating that commuting time
419 significantly influences pollutant exposure levels. The highest average exposure to PNC
420 was recorded during weekday afternoons (AWD), coinciding with the smallest average
421 diameter, from bus trips (19819 ± 18976 #cm^3, and 36 ± 13 nm), and on weekday evenings
422 (EWD) during walking trips (14514 ± 19118 #cm^3, and 40 ± 16 nm). The diurnal cycle of
423 vehicle count (Figure S3) indicates that the maximum traffic intensity occurs in the
424 afternoon, with buses peaking at around 1 PM. In addition, cooking activities from cafes
425 and restaurants located along the study routes are likely contributing to the elevated
426 exposure during that time. Our measurement results from a restaurant shows an
427 extremely high PNC in this microenvironment, which will be elaborated in section 3.3.
428 Morning weekend trips exhibited the lowest mean of PNC exposure, with the largest
429 average diameter from both walking (7307 ± 18196 #/cm^3, and 57 ± 18 nm) and bus
430 measurement (6762 ± 9949 #/cm^3, and 53 ± 13 nm), which is likely due to reduced
431 emissions from traffic. Furthermore, a reduction in restaurant cooking activities during

mornings at weekend may contribute to a decrease in the concentration of smaller particles, resulting in an increase in relative presence of coarser particles in the atmosphere during that period. Afternoon trips had a higher exposure to LDSA, both for walking and bus measurements.

To investigate the high exposure measured during the afternoon, a detailed analysis of individual trips was conducted. Two distinct days were identified during which the average exposure to PNC exceeded 20000 #/cm^3. Particle number size distribution data derived from the SMPS instrument at BAQS during the specified time period were also examined (Figure S5). The PNSD shows extremely high concentrations of smaller particles, probably indicating that a new particle formation event occurred on those specific days i.e., 24th May and 9th June 2023, as seen in Figure S5.

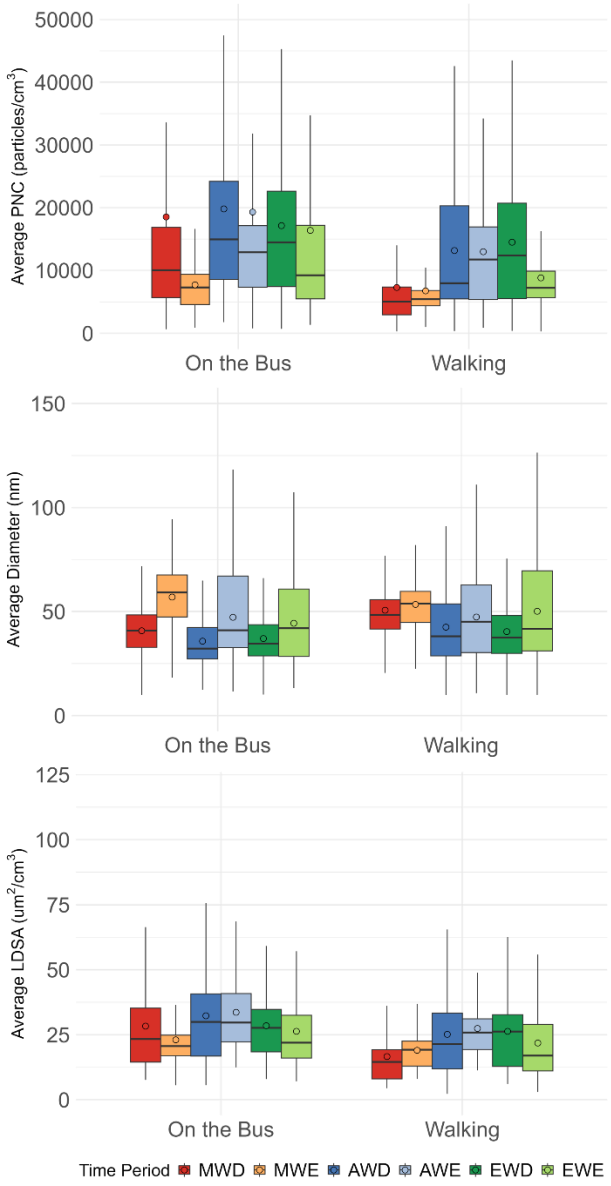

Figure 3. Box plots of mean PNC exposure, LDSA, and average diameter by travel mode and time. Black dots represent the mean concentration, horizontal lines represent the median, outliers are not displayed. Abbreviations: The first letter refers to: A= Afternoon, E=Evening, M=Morning; the last two letters refer to: WD= Weekday, WE= Weekend.

3.2 Correlation between PNC, LDSA, and Average Diameter

We examined the correlation between the three measured UFP metrics. The result indicates that both walking and bus trips exhibit very strong positive correlations between LDSA and PNC, with Spearman's correlation coefficients (r) of 0.86 and 0.84,

454 respectively. Conversely, a strong negative correlation (r) was observed between PNC
455 and average diameter, i.e., -0.63 and -0.73 for walking and bus data, respectively. Among
456 the bus routes, route 1, which passed along a main road, shows a stronger correlation
457 coefficient between PNC and LDSA (0.82, and 0.86) compared to route 2 (a residential
458 road, i.e., 0.78). This suggests that route 1 is more appreciably affected by traffic
459 emissions. These findings agree with a previous study (X. Liu et al., 2023) that identified
460 a strong correlation (r = 0.91) between PNC (range of 10–500 nm) and LDSA using data
461 from a Birmingham urban background site. Nonetheless, high LDSA is indeed not always
462 correlated with the high PNC, as demonstrated in the prior studies (Fung et al., 2022;
463 Kuula et al., 2020) that show that the LDSA/PNC ratio can be significantly higher in urban
464 background sites, attributed to the greater proportion of larger particles at those sites
465 compared to street canyons. This suggest that different sources, such as residential wood
466 combustion, potentially contribute to the LDSA in urban background measurements.

467 The correlation between PNC and LDSA by average particle size was explored (Figure
468 4). Particle size is categorised into three different groups: nucleation mode (10-25 nm),
469 Aitken mode (25-100 nm), and accumulation mode (>100 nm). Overall, there is a strong
470 correlation between PNC and LDSA across all modes (Pearson correlation, r= 0.80-0.98).
471 Nevertheless, there is a very strong correlation observed between higher PNC levels
472 (reaching up to 300,000#/cm^3 and 1,000,000#/cm^3 for bus and walking, respectively) and
473 higher LDSA in smaller particle sizes (nucleation mode). Additionally, we observed a good
474 association between LDSA and moderate PNC in the Aitken mode, as well as lower PNC
475 when the average diameter is in the accumulation mode. During the walking
476 measurement, we identified numerous short-term peaks in PNC, particularly in the

nucleation mode, indicating the presence of local sources that released smaller particles along the walking path.

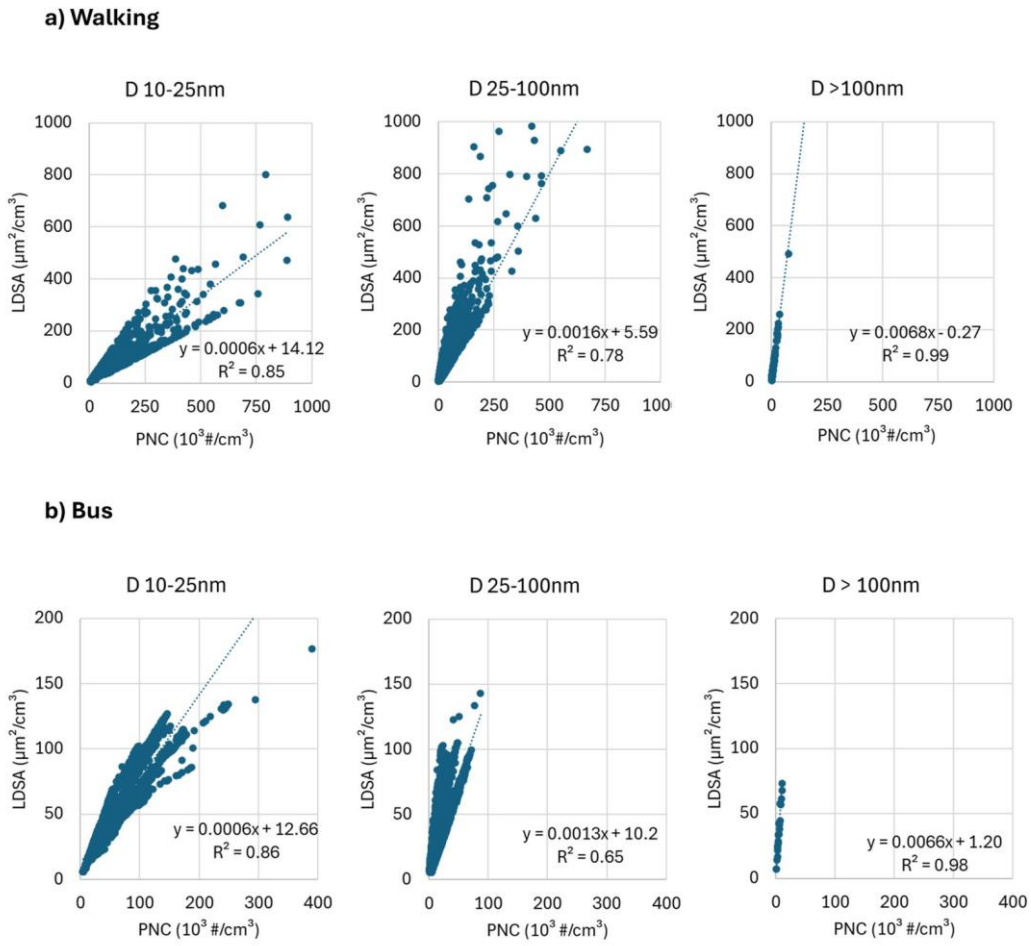

Figure 4. Scatterplot of PNC vs. LDSA by level of average diameter from walking (top) and bus (bottom) measurements

When examining the bus route type, it was found that there was a stronger association between PNC and LDSA with average diameter in the nucleation mode (Figure S6) along main roads (R^2 = 0.86) compared to residential roads (R^2 = 0.78), implying that vehicle emissions have a significant impact on the level of exposure. This agrees with a recent source apportionment study by Bousiotis et al (2024) in the same location, which also found a great association between LDSA and traffic source, suggesting that this metric was mainly driven by vehicle emissions.

Multiple trends were seen in the scatter plot (Fig.4 and Fig. S6), particularly from the bus ride in the nucleation mode range. We attempted to visually identify some prominent trends by separating the data set with higher PNC and LDSA, plotting it on a different graph and thereafter examining the location based on the coordinate points. Higher PNC and LDSA levels were recorded along the major road (Fig. S7). The various trends arose from the peak in PNC and LDSA that occurred around several bus stops, occurring immediately following passenger exchange (Fig S7.a-b). The bus accelerates upon departure, resulting in the increase in engine load and promoting the formation of volatile nucleation particles. The variation in slope is likely attributable to the variability of the bus engine load, passenger load, nearby traffic conditions, and local dispersion, which affect the level of multiple measured metrics during measurement.

3.3 Measurements in Other Microenvironments

Table S5 presents summary statistics of measured metrics in various microenvironments. In general, the fast-food restaurant had the highest level of PNC exposure and LDSA, reaching around 65000 ± 43000 #/cm^3, and 121 ± 82 μm²/cm^3 for PNC and LDSA, respectively. The restaurant's cooking activities, which primarily use the deep-fry method, are expected to be a significant source of PNC with high LDSA. There are previous studies that have examined the high concentrations of UFP related to cooking activities (Abdullahi et al., 2013; Geiss et al., 2016; See & Balasubramanian, 2006; Wallace, 2006). Geiss et al. (2016) examined the levels of UFP and LDSA concentrations in various occupational and non-occupational environments, including a canteen kitchen. During the 8-hour monitoring period, the recorded values for average LDSA and PNC were 400 μm²/cm³ and 500000 #/cm³, respectively. When the fryer was turned on, short-term peaks (spikes) in LDSA and PNC levels reached roughly 4000 μm²/cm³ and 500000 #/cm^3, respectively.

According to See and Balasubramanian (2006), deep-frying caused the most significant rise in PNC (up to 60000 #/cm^3) compared to background concentrations by a factor of 24.

Bus stop, BS 3, situated in a residential area and across a large park, exhibits a lower average PNC exposure level (10062 #/cm^3) compared to the other bus stops located on a major road. Comparable patterns were found in the LDSA, with BS 1 having the highest exposure, i.e., 41 μm²/cm³. An elevated level of PNC exposure and LDSA at bus stops located on major roads was expected due to the presence of road vehicles and a higher frequency of buses passing along these routes. Moreover, bus stop BS 1 was located near the supermarket's car park, and there were several restaurants across the road from the bus stop, potentially contributing to this high concentration.

A supermarket selling cooked food (Supermarket 2) exhibited higher PNC exposure (22570 #/cm^3) with the smallest average diameter of 25 nm, indicating that cooking activities significantly contribute appreciably to UFPs levels in that microenvironment. This average diameter falls within the particle mode range (8 to 29 nm) observed in various restaurants studied by Kim et al., (2024). The lowest levels of PNC and LDSA exposure (5485 #/cm^3 and 14 μm²/cm³, respectively), were measured inside a grocery-only supermarket (Supermarket 1) where no combustion activities took place inside the building, which coincided with a larger average diameter of 56 nm.

3.4 Spatial Variation of PNC and Average Diameter

Figure 5 and Figure S6 illustrate the spatial variation of PNC exposure and the average diameter along walking and bus routes at different times of day on weekdays. During walking trips, PNC were observed at lower levels in the morning period, with the average

diameter mostly ranging from 40-60nm. Hotspots, which are locations with higher concentrations of pollutant, were observed on major roads, specifically around junction areas where traffic lights, petrol stations, and pedestrian crossings were located. This high exposure coincided with a smaller average diameter and is marked with a red circle on the map (Figure 5). Pollutant levels remained high during afternoon and evening trips. In addition to this area, there are other hotspots (shown by a blue circle) that encompass a supermarket's car park, several restaurants, bus stops, and traffic lights, all of which can potentially be major sources of UFP emissions.

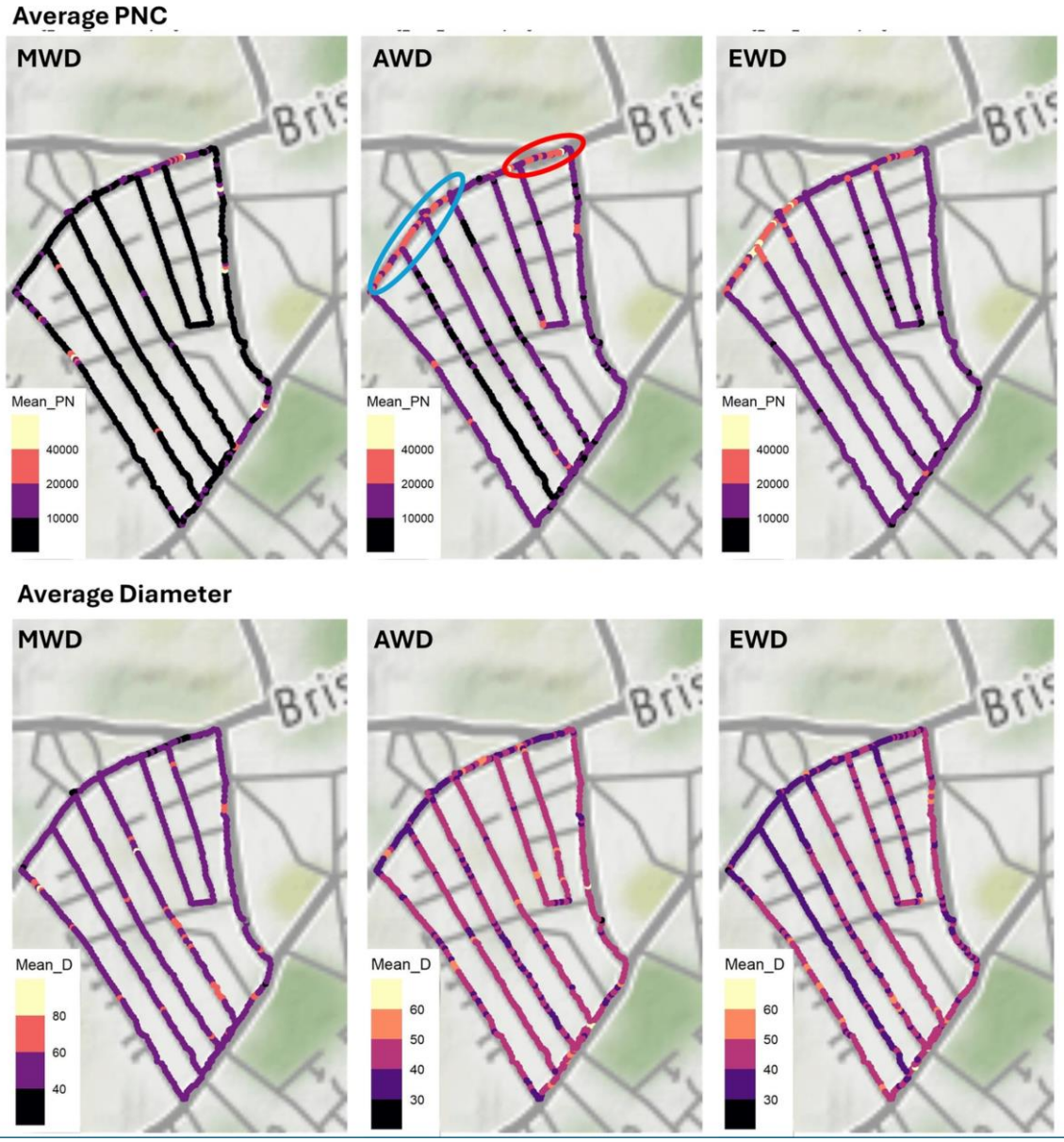

Figure 5. Spatial distribution of average PNC exposure (top panel) and average diameter (bottom panel) from walking measurement by time of day. The blue circle shows the region encompassing a supermarket's car park, several restaurants, bus stops, and traffic lights, while the red circle shows the junction area where traffic lights, a petrol station, and pedestrian crossings were located. The scale is adjusted for average diameter in the MWD, taking into account the larger average diameter during that period.

The bus measurements revealed that hotspots were predominantly seen at intersections along major roads (Figure S8), indicating a rapid exchange of external air with the interior of the bus. In addition, a spatial map of morning trips shows high exposure levels in an

area where a school gate and U-turn and a road that links two major roads were located, which is highlighted with a dark blue circle on the map. This situation may have resulted in busier traffic than other location, and hence higher UFP levels.

While doing bus measurements, hotspots along the walking route were also detected, i.e., around petrol stations and restaurant areas. This indicates that outdoor concentrations affected air quality inside the bus. Fewer hotspots with coarser average particle sizes were observed on the residential road, consistent with this conclusion.

3.5 Peak Pollution During Measurement

While conducting walking and bus measurements, abrupt changes sometimes occurred in the measured PNC, LDSA, and average diameter. It was evident that UFP varies greatly spatially and temporally, even over small distances, implying the need for more intense mobile measurement of this pollutant to better understand of its emission sources. Figure 6 shows short-term peaks recorded during an afternoon walk and a morning bus trip, including measurements taken on both a main and a residential road. During an afternoon walk, more short-term peaks were observed along the major road, particularly when passing through the junction and walking past restaurants. The sudden change in PNC and LDSA occurred simultaneously with the decrease in the average diameter. Upon entering the residential road, the levels of PNC and LDSA gradually decreased, and the average diameter became coarser.

During the bus measurement on the residential road, a lower PNC exposure and LDSA were observed. The average particle size ranged from 40 to 60 nm, with the exception of a sharp decrease to approximately 20 nm when the bus turned onto another road. The

particle's average diameter was relatively small during the measurement along the major road. The sudden change, an increase in PNC and LDSA, and a decrease in average particle diameter were predominantly observed at junctions and traffic lights. In contrast, the average diameter tended to increase while passing through greener areas with higher vegetation i.e., school field and park.

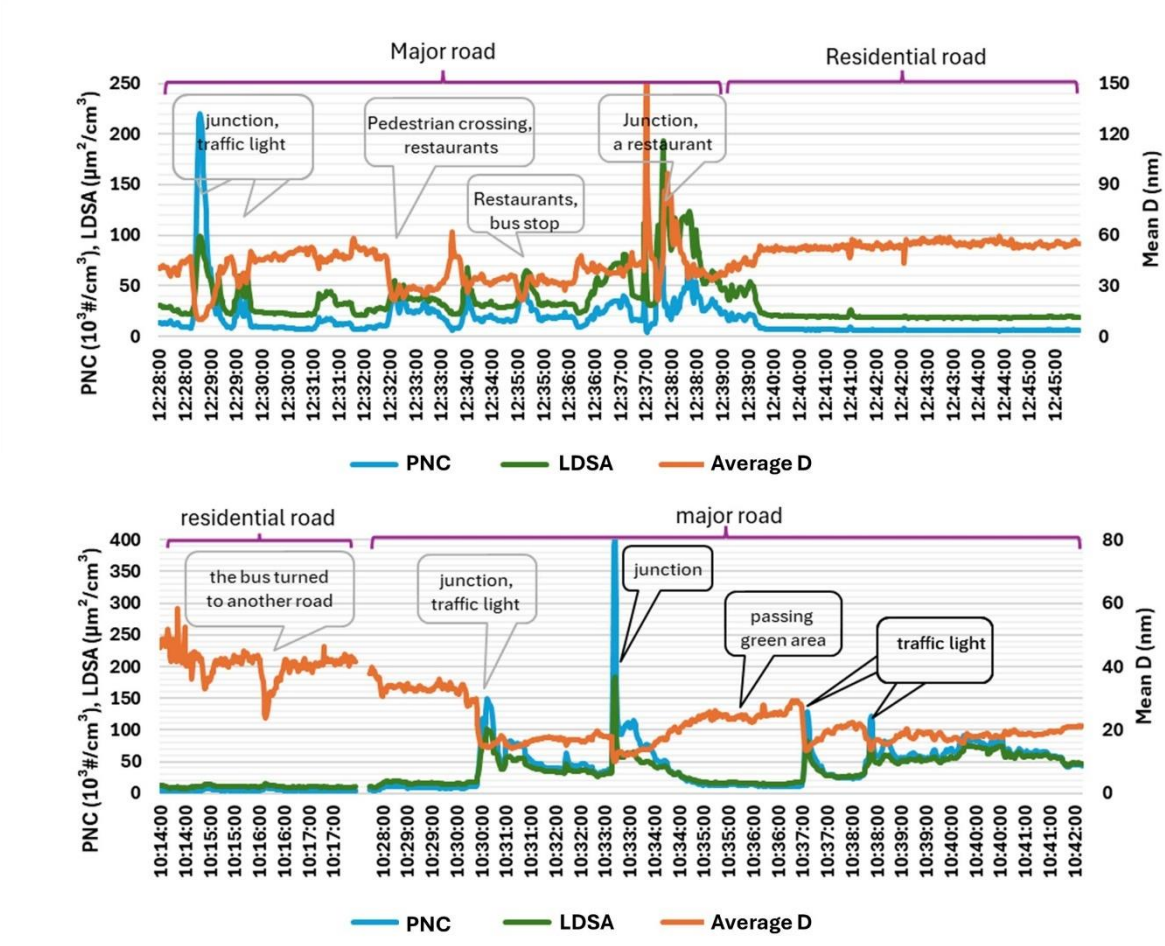

Figure 6. Examples of short-term peak (spike) events during an afternoon walking (top) and morning bus journey on 19th June 2025 (bottom) measurements.

3.6 UFPs Source Quantification from Walking measurements

Hotspots, which are typically defined as extremely high or short-term peaks concentrations, are frequently observed in personal exposure monitoring, especially when

conducted in urban areas. In this study, short-term peaks were recorded mostly during walking measurement as seen in Figure 7. It also shows that there are some periods when PNC levels during walking were comparable to the background concentration, while other periods were higher, suggesting the presence of local sources.

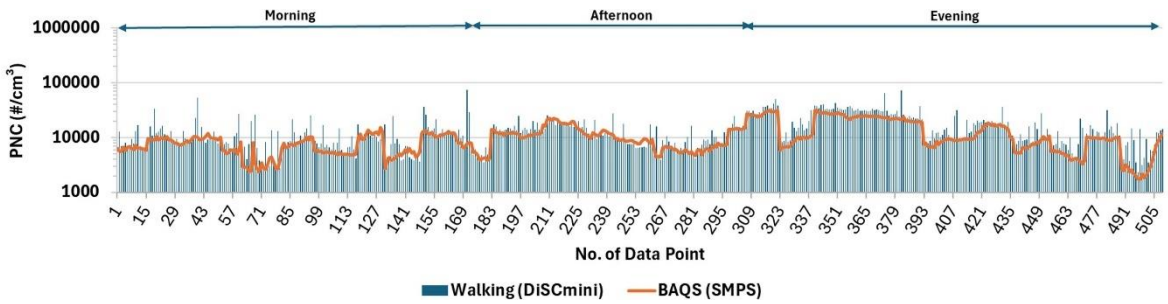

Figure 7. A compilation of PNC from all walking trips (blue bar chart) and that measured by SMPS at BAQS (orange line). PNC from DiSCmini was corrected to SMPS using the earlier collocation. PNC derived from walking in Selly Oak were average into 5-minute intervals to compare with that measured at BAQS.

Nevertheless, there is a scarcity of research which has examined the impact of this such hyperlocal concentrations on overall exposure. In this analysis, further examination was carried out by separating the short-term peaks that were observed predominantly when passing hotspot areas, particularly during walking measurement. Furthermore, this approach allows for the quantification of potential sources contributing to exposure levels during assessment.

Figure 8 presents an example of PNC during an afternoon weekday walk, displaying the raw PNC data and the concentration after removing the short-term peaks and interpolation (de-peaking). Meanwhile, Figure S9 presents the data for the entire campaign. Approximately 25% of the walking data (by time) was identified to consist of short-term peaks. Although it represents only a quarter of the measurement duration, in the

epidemiological context, its presence may impact the inhalation dose and hence health outcomes. A study investigated the exposure to UFPs peak concentration derived from a land use regression model based on mobile monitoring in the US, revealing a stronger association between peak UFPs exposure with inflammatory biomarkers compared to when using an annual average concentration metric (Lin et al., 2021). This underscores the importance of peak exposure evaluation in personal exposure monitoring, particularly in the active travel assessment.

Removal of the peaks, and subsequent interpolation, led to a decrease in the overall average PNC by approximately 19%, as shown in Figure 9.

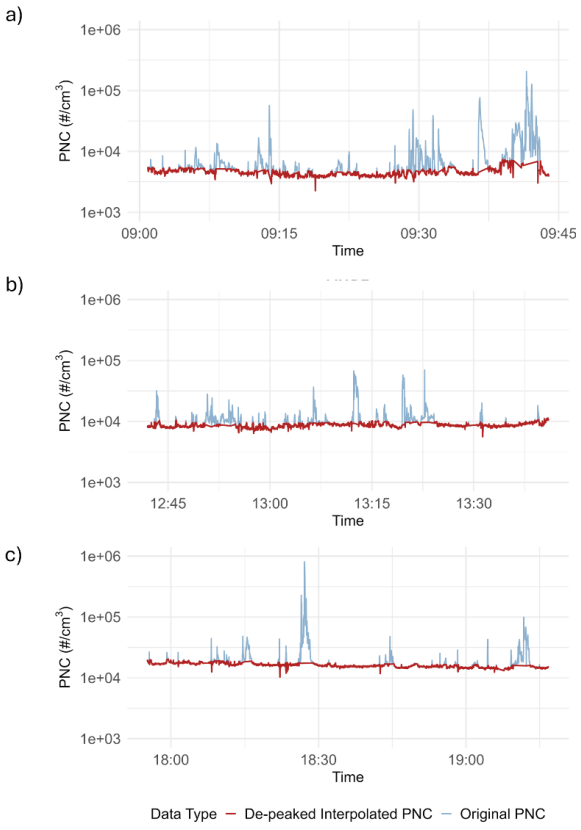

Figure 8. Examples of PNC from walking trips, which excluded the short-term peaks data (red line), are overlaid with the original PNC from a) a morning trip on 24th May 2023, (b) an afternoon trip on 23rd May 2023, and c) an evening trip on 9th June 2023.

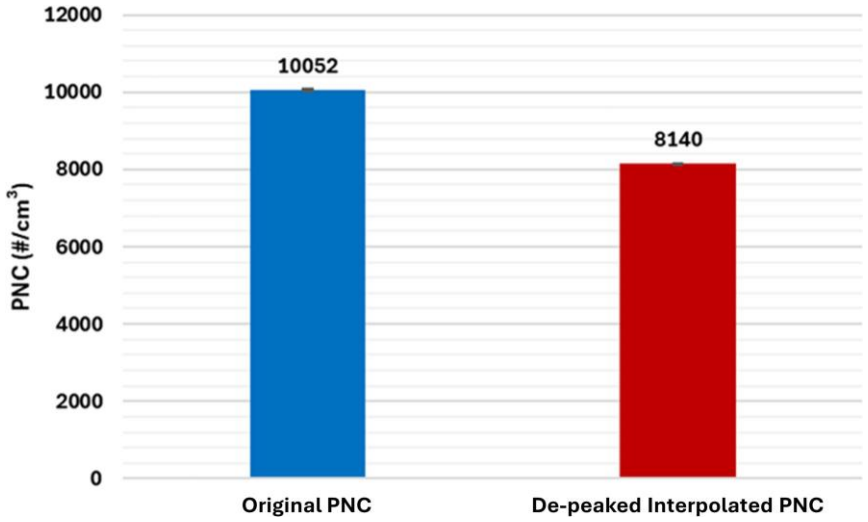

Figure 9. The average of PNC obtained from walking measurements from the whole campaign. The standard error indicates that the average PNC was significantly different between raw data and after removing the short-term peaks data.

Figure 10 clearly demonstrates a significant difference in the average PNC obtained from walking trips, before and after the removal of short-term peak data points. The decrease in average PNC ranges between 12-34%, of which the largest decrease occurred during the morning on weekdays (MWD), with a reduction of 34%. A large portion of spike data (31% of data,) was observed during morning trips (Table S6), leading to a more pronounced decline during that time in comparison to other periods.

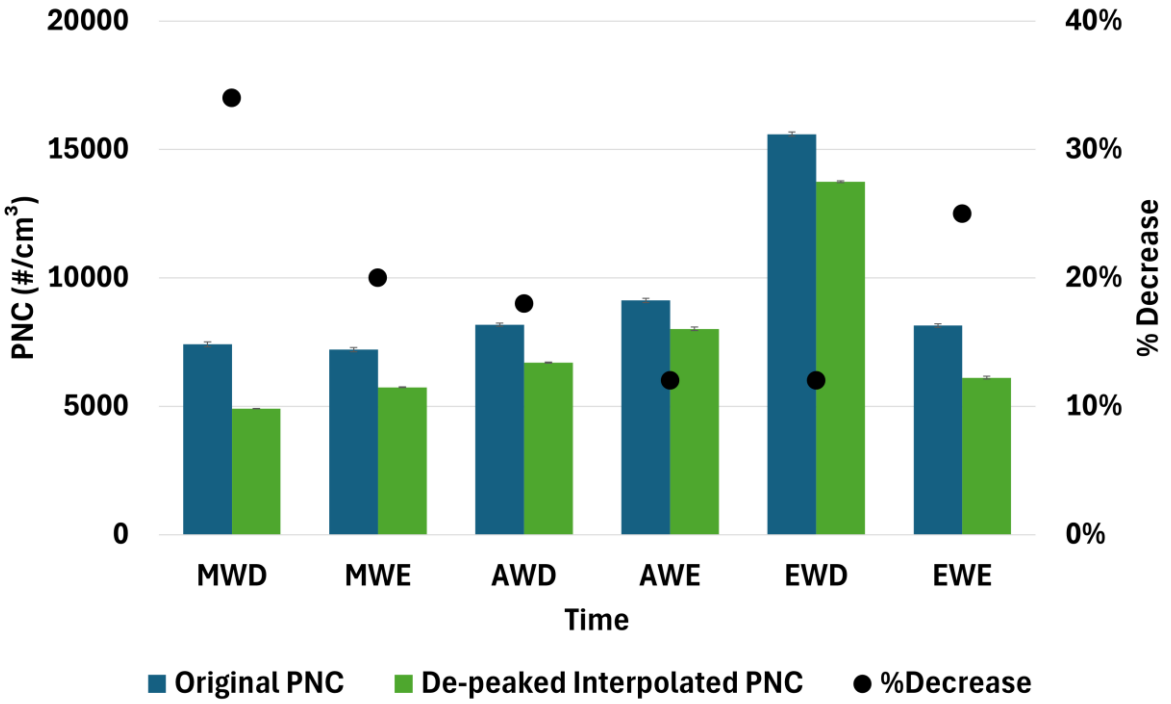

Figure 10. Comparison of the PNC average between the original data (the blue bar) and after removing short-term peaks (the green bar) from walking trips, categorised by measurement period. The black dots show the percentage of decline in the average PNC. The standard error indicates that the average PNC was significantly different between the two data groups.

To enhance understanding of whether the de-peaked interpolated PNC returns to the local background level, PNC derived from the SMPS deployed at a local urban background monitoring station was used as a comparator. Interpolated de-peaked PNCs were corrected to SMPS observations during the collocation period (Figure S1) and were subsequently compared to SMPS data at the time the measurements took place. Although a statistical test result indicates no significant difference between walking and background PNC (p-value of 0.2), the average corrected PNC from walking measurement was notably higher (11801±8357 #/cm^3) (Figure 11a) than that measured at the urban background (10816±6711 #/cm^3), likely attributable to the closer proximity to general traffic and cooking sources. However, PNC from walking (de-peaked) correlated very well with the measurements at BAQS as seen in Figure 11b.

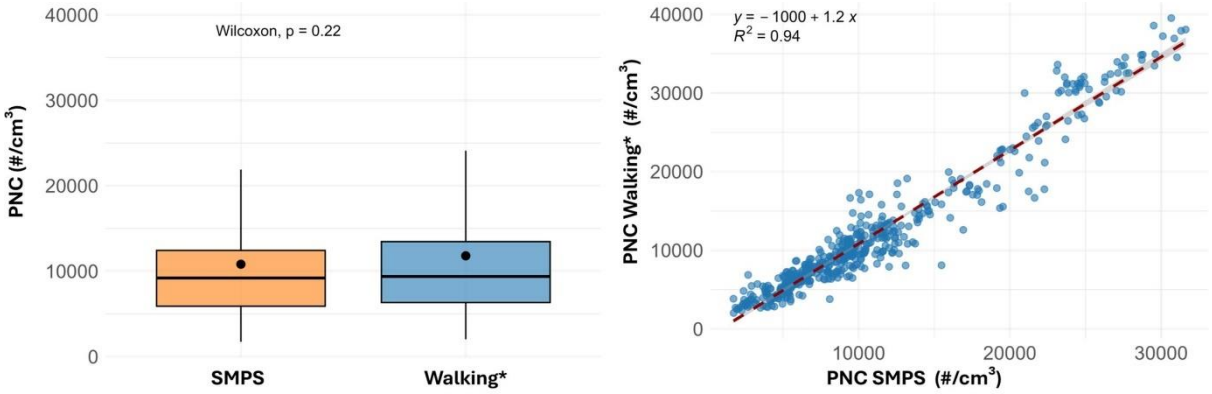

Figure 11. (a) Average PNC from walking derived from the DiSCmini and that measured by SMPS at the BAQS urban background. The black dot represents the average concentration, while the asterisk (*) indicates de-peaked interpolated PNC after being corrected to SMPS. **(b)** scatter plot between PNC walking (de-peaked and corrected) versus SMPS, using 5-minutes data averages.

Short-term peaks that were detected in personal exposure measurements revealed the presence of hyperlocal effects upon the exposure level. Nonetheless, the separation of such data from the personal exposure monitoring record suggests that some reduction in exposure to pollutants, particularly those with very high spatial and temporal variability as UFP, could potentially be achieved by reducing pollutant hotspots especially in densely populated areas.

4. CONCLUSION

In this study, walking and in-bus measurements were performed to evaluate personal exposure to UFPs. Multiple critical metrics of UFPs were assessed, including particle number concentration (PNC), lung deposited surface area (LDSA), and average diameter (D, ranging from 10 to 300 nm). Generally, higher exposure to PNC and LDSA coincide with smaller average diameter, and a higher exposure was typically recorded during public bus rides than walking measurement. A stronger association between PNC and LDSA

682 with average diameter in the nucleation mode (Dp < 30 nm) along a main road as opposed
683 to a residential route during bus measurement, suggests a substantial impact of traffic and
684 restaurant emission on the level of exposure. During the walking measurements,
685 numerous short-term peaks of PNC and LDSA were observed, indicating the presence of
686 multiple local UFPs sources within the study area. Additionally, measurements made in
687 other microenvironments to assess exposure levels and investigate potential local
688 sources found that the lowest exposure was recorded inside a grocery supermarket, while
689 a fast-food restaurant, which primarily uses the deep-fry method, exhibited the highest
690 exposure level to PNC and LDSA. Hotspots were detected, specifically where the major
691 sources of UFP emissions were concentrated, specifically at road junction areas, traffic
692 lights, supermarkets car parks, a petrol station, and restaurants. The dynamical behaviour
693 of the measured metrics was explored. An abrupt change and substantial increase in PNC
694 and LDSA, which occurred simultaneously with a drop in average diameter, were
695 observed while passing through the hotspots. On the other hand, upon entering the
696 residential road, a gradual decrease in PNC and LDSA with an increase in average
697 diameter was observed. A method has been developed to separate short-term peaks from
698 UFP exposure data obtained by walking measurement. We found by removing the short-
699 term peaks (de-peaking), which occurred during ~25% of the data time series, resulted in
700 a 19% drop in the average PNC. Hence, this approach effectively enables the
701 differentiation of hyper-local sources from the local background contribution. Furthermore,
702 de-peaked average PNC was on average 9% higher than urban background
703 measurements, indicating a general local increment, likely due to the proximity to the
704 emission sources (i.e., road traffics, and restaurant cooking). This novel approach

improves the distinction between episodic peaks and the “true” background exposure, and thus, enhances the comprehension of personal exposure assessments.

Acknowledgements: SD would like to thank to Indonesia Endowment Fund for Education (LPDP), Ministry of Finance, Republic of Indonesia, for their financial support toward her PhD study. We also thank to Jian Zhong for providing traffic count data.

Funding: This work was supported by the European Union RI-URBANS project under Grant Agreement No. 101036245.

Author Contributions: **Seny Damayanti**: Writing-original draft, Conceptualization, Resources, Visualization, Methodology. **Dimitrios Bousiotis**: Writing-review & editing, Resources. **Arunik Baruah**: Writing-review & editing, Resources. **Francis D. Pope**: Validation, Supervision, Conceptualization, Writing- review & editing. **Roy M. Harrison**: Validation, Supervision, Conceptualization, Writing- review & editing, Funding acquisition.

Declaration of Competing Interests

The authors declare that they have no known competing financial interests or personal relationships that could have appeared to influence the work reported in this paper.

Data Availability: Data supporting this publication are openly available from the UBIRA eData repository at https://doi.org/10.25500/edata.bham.00001260

REFERENCES

Abdullahi, K. L., Delgado-Saborit, J. M., & Harrison, R. M. (2013). Emissions and indoor concentrations of particulate matter and its specific chemical components from cooking: A review. *Atmospheric Environment*, *71*, 260-294. https://doi.org/https://doi.org/10.1016/j.atmosenv.2013.01.061

Amin, M., Aun, S., Hang, L., Hata, M., Phairuang, W., & Masami, F. (2024). Investigation into personal exposure to ultrafine particle (UFP) in Phnom Penh, Cambodia: A pilot study. *Atmospheric Pollution Research*, *15*(12), 102307. https://doi.org/https://doi.org/10.1016/j.apr.2024.102307

Baldauf, R., Devlin RB, Gehr P, Giannelli R, Hassett-Sipple B, Jung H, Martini G, McDonald J, Sacks JD, & K., W. (2016). Ultrafine Particle Metrics and Research Considerations: Review of the 2015 UFP Workshop. *Internatinal Journal of Environmental Research and Public Health.*, *11*. https://doi.org/10.3390/ijerph13111054

Baruah, A., Bousiotis, D., Damayanti, S., Bigi, A., Ghermandi, G., Ghaffarpasand, O., Harrison, R. M., & Pope, F. D. (2024). A novel spatiotemporal prediction approach to fill air pollution data gaps using mobile sensors, machine learning and citizen science techniques. *npj Climate and Atmospheric Science*, *7*(1), 310. https://doi.org/10.1038/s41612-024-00859-z

Bousiotis, D., Damayanti, S., Baruah, A., Bigi, A., Beddows, D. C. S., Harrison, R. M., & Pope, F. D. (2024). Pinpointing sources of pollution using citizen science and hyperlocal low-cost mobile source apportionment. *Environment International*, *193*, 109069. https://doi.org/https://doi.org/10.1016/j.envint.2024.109069

Brines, M., Dall'Osto, M., Beddows, D. C. S., Harrison, R. M., Gómez-Moreno, F., Núñez, L., Artíñano, B., Costabile, F., Gobbi, G. P., Salimi, F., Morawska, L., Sioutas, C., & Querol, X. (2015). Traffic and nucleation events as main sources of ultrafine particles in high-insolation developed world cities. *Atmospheric Chemistry and Physics*, *15*(10), 5929-5945. https://doi.org/10.5194/acp-15-5929-2015

Carslaw, D. C., & Ropkins, K. (2012). openair — An R package for air quality data analysis. *Environmental Modelling & Software*, *27-28*, 52-61. https://doi.org/https://doi.org/10.1016/j.envsoft.2011.09.008

Chaney, R. A., Sloan, C. D., Cooper, V. C., Robinson, D. R., Hendrickson, N. R., McCord, T. A., & Johnston, J. D. (2017). Personal exposure to fine particulate air pollution while commuting: An examination of six transport modes on an urban arterial roadway. *PLOS ONE*, *12*(11), e0188053. https://doi.org/10.1371/journal.pone.0188053

Charron, A., & Harrison, R. M. (2003). Primary particle formation from vehicle emissions during exhaust dilution in the roadside atmosphere. *Atmospheric Environment*, *37*(29), 4109-4119. https://doi.org/10.1016/s1352-2310(03)00510-7

Chatain, M., Alvarez, R., Ustache, A., Rivière, E., Favez, O., & Pallares, C. (2021). Simultaneous Roadside and Urban Background Measurements of Submicron Aerosol Number Concentration and Size Distribution (in the Range 20–800 nm), along with Chemical Composition in Strasbourg, France. *Atmosphere*, *12*. https://doi.org/https://doi.org/10.3390/atmos12010071

Cichowicz, R., & Dobrzański, M. (2022). 3D spatial dispersion of particulate matter and gaseous pollutants on a university campus in the center of an urban agglomeration. *Energy*, *259*, 125009. https://doi.org/https://doi.org/10.1016/j.energy.2022.125009

Damayanti, S., Harrison, R. M., Pope, F., & Beddows, D. C. S. (2023). Limited impact of diesel particle filters on road traffic emissions of ultrafine particles. *Environment International*, *174*, 107888. https://doi.org/https://doi.org/10.1016/j.envint.2023.107888

de Jesus, A. L., Rahman, M. M., Mazaheri, M., Thompson, H., Knibbs, L. D., Jeong, C., Evans, G., Nei, W., Ding, A., Qiao, L., Li, L., Portin, H., Niemi, J. V., Timonen, H., Luoma, K., Petäjä, T., Kulmala, M., Kowalski, M., Peters, A., . . . Morawska, L. (2019). Ultrafine particles and PM2.5 in the air of cities around the world: Are they representative of each other? *Environment International*, *129*, 118-135. https://doi.org/https://doi.org/10.1016/j.envint.2019.05.021

EEA. (2023). *Air pollution levels still too high across Europe – remains top environmental health risk.* Retrieved 2 August from

EU. (2024). *Directive (EU) 2024/2881 of the European Parliament and of the Council of 23 October 2024 on ambient air quality and cleaner air for Europe (recast), Brussels.*

Ferin, J., Oberdörster, G., Penney, D. P., Soderholm, S. C., Gelein, R., & Piper, H. C. (1990). Increased pulmonary toxicity of ultrafine particles? I. Particle clearance, translocation, morphology. *Journal of Aerosol Science*, *21*(3), 381-384. https://doi.org/https://doi.org/10.1016/0021-8502(90)90064-5

Fierz, M., Burtscher, H., Steigmeier, P., & Kasper, M. (2008). Field Measurement of Particle Size and Number Concentration with the Diffusion Size Classifier (Disc). *SAE Technical Papers*. https://doi.org/10.4271/2008-01-1179

Fierz, M., C., H., P., S., & and Burtscher, H. (2011). Design, Calibration, and Field Performance of a Miniature Diffusion Size Classifier. *Aerosol Science and Technology*, *45*(1), 1-10. https://doi.org/10.1080/02786826.2010.516283

Fung, P. L., Zaidan, M. A., Niemi, J. V., Saukko, E., Timonen, H., Kousa, A., Kuula, J., Rönkkö, T., Karppinen, A., Tarkoma, S., Kulmala, M., Petäjä, T., & Hussein, T. (2022). Input-adaptive linear mixed-effects model for estimating alveolar lung-deposited surface area (LDSA) using multipollutant datasets. *Atmos. Chem. Phys.*, *22*(3), 1861-1882. https://doi.org/10.5194/acp-22-1861-2022

Gani, S., Chambliss, S. E., Messier, K. P., Lunden, M. M., & Apte, J. S. (2021). Spatiotemporal profiles of ultrafine particles differ from other traffic-related air pollutants: lessons from long-term measurements at fixed sites and mobile monitoring [10.1039/D1EA00058F]. *Environmental Science: Atmospheres*, *1*(7), 558-568. https://doi.org/10.1039/D1EA00058F

Geiss, O., Bianchi, I., & Barrero-Moreno, J. (2016). Lung-deposited surface area concentration measurements in selected occupational and non-occupational environments. *Journal of Aerosol Science*, *96*, 24-37. https://doi.org/https://doi.org/10.1016/j.jaerosci.2016.02.007

Gilmour, P. S., Ziesenis, A., Morrison, E. R., Vickers, M. A., Drost, E. M., Ford, I., Karg, E., Mossa, C., Schroeppel, A., Ferron, G. A., Heyder, J., Greaves, M., MacNee, W., & Donaldson, K. (2004). Pulmonary and systemic effects of short-term inhalation exposure to ultrafine carbon black particles. *Toxicology*

and Applied Pharmacology, *195*(1), 35-44. https://doi.org/https://doi.org/10.1016/j.taap.2003.10.003

Hammond, D., Lalor, M., & Jones, S. (2007). In-Vehicle Measurement of Particle Number Concentrations on School Buses Equipped with Diesel Retrofits. *Water, Air, and Soil Pollution*, *179*, 217-225. https://doi.org/10.1007/s11270-006-9226-7

Harrison, R. M. (2020). Airborne particulate matter. *Philosophical Transactions of the Royal Society A: Mathematical, Physical and Engineering Sciences*, *378*(2183), 20190319. https://doi.org/10.1098/rsta.2019.0319

He, R., & Qiu, Z. (2022). Exposure characteristics of ultrafine particles on urban streets and its impact on pedestrians. *Environmental Monitoring and Assessment*, *194*(10), 735. https://doi.org/10.1007/s10661-022-10453-6

HEI. (2013). *Understanding the Health Effects of Ambient Ultrafine Particles* (HEI Perspectives 3, Issue.

HEI. (2024). *State of Global Air 2024*. HEI.

Hopke, P. K., Feng, Y., & Dai, Q. (2022). Source apportionment of particle number concentrations: A global review. *Science of the Total Environment*, *819*, 153104. https://doi.org/https://doi.org/10.1016/j.scitotenv.2022.153104

ICRP. (1994a). *Human Respiratory Tract Model for Radiological Protection* (Publication 66, Issue. E. S. Ltd.

ICRP. (1994b). Human Respiratory Tract Model for Radiological Protection, . *Publication 66: Human Respiratory Tract Model for Radiological Protection. Anns. ICRP, 24(4)*.

Int Panis, L., de Geus, B., Vandenbulcke, G., Willems, H., Degraeuwe, B., Bleux, N., Mishra, V., Thomas, I., & Meeusen, R. (2010). Exposure to particulate matter in traffic: A comparison of cyclists and car passengers. *Atmospheric Environment*, *44*(19), 2263-2270. https://doi.org/https://doi.org/10.1016/j.atmosenv.2010.04.028

Jianyao, Y., Yuan, H., Su, G., Wang, J., Weng, W., & Zhang, X. (2025). Machine learning-enhanced high-resolution exposure assessment of ultrafine particles. *Nature Communications*, *16*(1), 1209. https://doi.org/10.1038/s41467-025-56581-8

Kaur, S., Nieuwenhuijsen, M., & Colvile, R. (2005). Personal exposure of street canyon intersection users to PM2.5, ultrafine particle counts and carbon monoxide in Central London, UK. *Atmospheric Environment*, *39*(20), 3629-3641. https://doi.org/https://doi.org/10.1016/j.atmosenv.2005.02.046

Kim, S., Machesky, J., Gentner, D. R., & Presto, A. A. (2024). Real-world observations of reduced nitrogen and ultrafine particles in commercial cooking organic aerosol emissions. *Atmos. Chem. Phys.*, *24*(2), 1281-1298. https://doi.org/10.5194/acp-24-1281-2024

Knibbs, L. D., Cole-Hunter, T., & Morawska, L. (2011). A review of commuter exposure to ultrafine particles and its health effects. *Atmospheric Environment*, *45*(16), 2611-2622. https://doi.org/https://doi.org/10.1016/j.atmosenv.2011.02.065

Kuula, J., Heino, K., V., N. J., Erkka, S., Harri, P., Anu, K., Minna, A., Topi, R., & and Timonen, H. (2020). Long-term sensor measurements of lung deposited surface area of particulate matter emitted from local vehicular and residential

wood combustion sources. *Aerosol Science and Technology*, *54*(2), 190-202. https://doi.org/10.1080/02786826.2019.1668909

Kwon, H.-S., Ryu, M. H., & Carlsten, C. (2020). Ultrafine particles: unique physicochemical properties relevant to health and disease. *Experimental & Molecular Medicine*, *52*(3), 318-328. https://doi.org/10.1038/s12276-020-0405-1

Lepistö, T., Heino, K., Paxton, J., Anssi, J., Anssi, A., & and Rönkkö, T. (2020). Measurement of the human respiratory tract deposited surface area of particles with an electrical low pressure impactor. *Aerosol Science and Technology*, *54*(8), 958-971. https://doi.org/10.1080/02786826.2020.1745141

Lepistö, T., Kuuluvainen, H., Lintusaari, H., Kuittinen, N., Salo, L., Helin, A., Niemi, J. V., Manninen, H. E., Timonen, H., Jalava, P., Saarikoski, S., & Rönkkö, T. (2022). Connection between lung deposited surface area (LDSA) and black carbon (BC) concentrations in road traffic and harbour environments. *Atmospheric Environment*, *272*, 118931. https://doi.org/https://doi.org/10.1016/j.atmosenv.2021.118931

Lin, S., Ryan, I., Paul, S., Deng, X., Zhang, W., Luo, G., Dong, G.-H., Nair, A., & Yu, F. (2022). Particle surface area, ultrafine particle number concentration, and cardiovascular hospitalizations. *Environmental Pollution*, *310*, 119795. https://doi.org/https://doi.org/10.1016/j.envpol.2022.119795

Liu, X., Hadiatullah, H., Khedr, M., Zhang, X., Schnelle-Kreis, J., Zimmermann, R., & Adam, T. (2022). Personal exposure to various size fractions of ambient particulate matter during the heating and non-heating periods using mobile monitoring approach: A case study in Augsburg, Germany. *Atmospheric Pollution Research*, *13*(7), 101483. https://doi.org/https://doi.org/10.1016/j.apr.2022.101483

Liu, X., Hadiatullah, H., Zhang, X., Trechera, P., Savadkoohi, M., Garcia-Marlès, M., Reche, C., Pérez, N., Beddows, D. C. S., Salma, I., Thén, W., Kalkavouras, P., Mihalopoulos, N., Hueglin, C., Green, D. C., Tremper, A. H., Chazeau, B., Gille, G., Marchand, N., . . . Querol, X. (2023). Ambient air particulate total lung deposited surface area (LDSA) levels in urban Europe. *Science of the Total Environment*, *898*, 165466. https://doi.org/https://doi.org/10.1016/j.scitotenv.2023.165466

Lloyd, M., Olaniyan, T., Ganji, A., Xu, J., Simon, L., Zhang, M., Saeedi, M., Yamanouchi, S., Wang, A., Burnett, R. T., Tjepkema, M., Hatzopoulou, M., & Weichenthal, S. (2024). Airborne ultrafine particle concentrations and brain cancer incidence in Canada's two largest cities. *Environment International*, *193*, 109088. https://doi.org/https://doi.org/10.1016/j.envint.2024.109088

Luengo-Oroz, J., & Reis, S. (2019). Assessment of cyclists' exposure to ultrafine particles along alternative commuting routes in Edinburgh. *Atmospheric Pollution Research*, *10*(4), 1148-1158. https://doi.org/https://doi.org/10.1016/j.apr.2019.01.020

Meier, R., Katherine, C., & and Riediker, M. (2013). Comparative Testing of a Miniature Diffusion Size Classifier to Assess Airborne Ultrafine Particles Under Field Conditions. *Aerosol Science and Technology*, *47*(1), 22-28. https://doi.org/10.1080/02786826.2012.720397

Mills, J. B., Hong, P. J., & and Peters, T. M. (2013). Comparison of the DiSCmini Aerosol Monitor to a Handheld Condensation Particle Counter and a Scanning

Mobility Particle Sizer for Submicrometer Sodium Chloride and Metal Aerosols. *Journal of Occupational and Environmental Hygiene*, *10*(5), 250-258. https://doi.org/10.1080/15459624.2013.769077

Nair, A. A., Lin, S., Luo, G., Ryan, I., Qi, Q., Deng, X., & Yu, F. (2023). Environmental exposure disparities in ultrafine particles and PM2.5 by urbanicity and socio-demographics in New York state, 2013–2020. *Environmental Research*, *239*, 117246. https://doi.org/https://doi.org/10.1016/j.envres.2023.117246

Ohlwein, S., Kappeler, R., Kutlar Joss, M., Künzli, N., & Hoffmann, B. (2019). Health effects of ultrafine particles: a systematic literature review update of epidemiological evidence. *International Journal of Public Health*, *64*(4), 547-559. https://doi.org/10.1007/s00038-019-01202-7

Patel, H., Talbot, N., Dirks, K., & Salmond, J. (2023). The impact of low emission zones on personal exposure to ultrafine particles in the commuter environment. *Science of the Total Environment*, *874*, 162540. https://doi.org/https://doi.org/10.1016/j.scitotenv.2023.162540

Patel, S., Leavey, A., Sheshadri, A., Kumar, P., Kandikuppa, S., Tarsi, J., Mukhopadhyay, K., Johnson, P., Balakrishnan, K., Schechtman, K. B., Castro, M., Yadama, G., & Biswas, P. (2018). Associations between household air pollution and reduced lung function in women and children in rural southern India. *Journal of Applied Toxicology*, *38*(11), 1405-1415. https://doi.org/https://doi.org/10.1002/jat.3659

Renwick, L. C., Brown, D., Clouter, A., & Donaldson, K. (2004). Increased inflammation and altered macrophage chemotactic responses caused by two ultrafine particle types. *Occupational and Environmental Medicine*, *61*(5), 442. https://doi.org/10.1136/oem.2003.008227

Rivas, I., Kumar, P., & Hagen-Zanker, A. (2017). Exposure to air pollutants during commuting in London: Are there inequalities among different socio-economic groups? *Environment International*, *101*, 143-157. https://doi.org/https://doi.org/10.1016/j.envint.2017.01.019

Rivas, I., Kumar, P., Hagen-Zanker, A., Andrade, M. d. F., Slovic, A. D., Pritchard, J. P., & Geurs, K. T. (2017). Determinants of black carbon, particle mass and number concentrations in London transport microenvironments. *Atmospheric Environment*, *161*, 247-262. https://doi.org/https://doi.org/10.1016/j.atmosenv.2017.05.004

Rückerl, R., Schneider, A., Hampel, R., Breitner, S., Cyrys, J., Kraus, U., Gu, J., Soentgen, J., Koenig, W., & Peters, A. (2016). Association of novel metrics of particulate matter with vascular markers of inflammation and coagulation in susceptible populations –results from a panel study. *Environmental Research*, *150*, 337-347. https://doi.org/https://doi.org/10.1016/j.envres.2016.05.037

Sabin, L. D., Behrentz, E., Winer, A. M., Jeong, S., Fitz, D. R., Pankratz, D. V., Colome, S. D., & Fruin, S. A. (2005). Characterizing the range of children's air pollutant exposure during school bus commutes. *Journal of Exposure Science & Environmental Epidemiology*, *15*(5), 377-387. https://doi.org/10.1038/sj.jea.7500414

Saha, P. K., Zimmerman, N., Malings, C., Hauryliuk, A., Li, Z., Snell, L., Subramanian, R., Lipsky, E., Apte, J. S., Robinson, A. L., & Presto, A. A. (2019). Quantifying high-resolution spatial variations and local source impacts

of urban ultrafine particle concentrations. *Science of the Total Environment*, *655*, 473-481. https://doi.org/https://doi.org/10.1016/j.scitotenv.2018.11.197

Samad, A., Arango, K., Alvarez Florez, D., Chourdakis, I., & Vogt, U. (2022). Assessment of Coarse, Fine, and Ultrafine Particles in S-Bahn Trains and Underground Stations in Stuttgart. *Atmosphere*, *13*(11).

Schmid, O., & Stoeger, T. (2016). Surface area is the biologically most effective dose metric for acute nanoparticle toxicity in the lung. *Journal of Aerosol Science*, *99*, 133-143. https://doi.org/https://doi.org/10.1016/j.jaerosci.2015.12.006

Schraufnagel, D. E. (2020). The health effects of ultrafine particles. *Experimental & Molecular Medicine*, *52*(3), 311-317. https://doi.org/10.1038/s12276-020-0403-3

See, S. W., & Balasubramanian, R. (2006). Physical Characteristics of Ultrafine Particles Emitted from Different Gas Cooking Methods. *Aerosol and Air Quality Research*, *6*(1), 82-92. https://doi.org/10.4209/aaqr.2006.03.0007

Shah, R. U., Padilla, L. E., Peters, D. R., Dupuy-Todd, M., Fonseca, E. R., Ma, G. Q., Popoola, O. A. M., Jones, R. L., Mills, J., Martin, N. A., & Alvarez, R. A. (2023). Identifying Patterns and Sources of Fine and Ultrafine Particulate Matter in London Using Mobile Measurements of Lung-Deposited Surface Area. *Environmental Science & Technology*, *57*(1), 96-108. https://doi.org/10.1021/acs.est.2c08096

Singh, A., Ng'ang'a, D., Gatari, M. J., Kidane, A. W., Alemu, Z. A., Derrick, N., Webster, M. J., Bartington, S. E., Thomas, G. N., Avis, W., & Pope, F. D. (2021). Air quality assessment in three East African cities using calibrated low-cost sensors with a focus on road-based hotspots. *Environmental Research Communications*, *3*(7), 075007. https://doi.org/10.1088/2515-7620/ac0e0a

Tao, L., Zhou, Z., Tao, J., Zhang, L., Wu, C., Li, J., Yue, D., Wu, Z., Zhang, Z., Yuan, Z., Huang, J., & Wang, B. (2023). High contribution of new particle formation to ultrafine particles in four seasons in an urban atmosphere in south China. *Science of The Total Environment*, *889*, 164202. https://doi.org/https://doi.org/10.1016/j.scitotenv.2023.164202

Todea, A. M., Beckmann, S., Kaminski, H., & Asbach, C. (2015). Accuracy of electrical aerosol sensors measuring lung deposited surface area concentrations. *Journal of Aerosol Science*, *89*, 96-109. https://doi.org/https://doi.org/10.1016/j.jaerosci.2015.07.003

Tran, P. T. M., Ngoh, J. R., & Balasubramanian, R. (2020). Assessment of the Integrated Personal Exposure to Particulate Emissions in Urban Micro-environments: A Pilot Study. *Aerosol and Air Quality Research*, *20*(2), 341-357. https://doi.org/10.4209/aaqr.2019.04.0201

Viana, M., Rivas, I., Reche, C., Fonseca, A. S., Pérez, N., Querol, X., Alastuey, A., Álvarez-Pedrerol, M., & Sunyer, J. (2015). Field comparison of portable and stationary instruments for outdoor urban air exposure assessments. *Atmospheric Environment*, *123*, 220-228. https://doi.org/https://doi.org/10.1016/j.atmosenv.2015.10.076

Vora, R., Zareba, W., Utell, M. J., Pietropaoli, A. P., Chalupa, D., Little, E. L., Oakes, D., Bausch, J., Wiltshire, J., & Frampton, M. W. (2014). Inhalation of ultrafine carbon particles alters heart rate and heart rate variability in people with type 2 diabetes. *Particle and Fibre Toxicology*, *11*(1), 31. https://doi.org/10.1186/s12989-014-0031-y

Wallace, L. (2006). Indoor Sources of Ultrafine and Accumulation Mode Particles: Size Distributions, Size-Resolved Concentrations, and Source Strengths. *Aerosol Science and Technology*, *40*(5), 348-360. https://doi.org/10.1080/02786820600612250

Wang, W., Liu, X., Xiao, Y., Han, S., Liu, S., Wang, B., & Wang, H. (2024). Real-time evolution characteristics and potential reactions of contaminants in commuter bus cabin air. *Science of The Total Environment*, *946*, 174440. https://doi.org/https://doi.org/10.1016/j.scitotenv.2024.174440

Weichenthal, S., Dufresne, A., Infante-Rivard, C., & Joseph, L. (2008). Determinants of ultrafine particle exposures in transportation environments: findings of an 8-month survey conducted in Montréal, Canada. *Journal of Exposure Science & Environmental Epidemiology*, *18*(6), 551-563. https://doi.org/10.1038/sj.jes.7500644

WHO. (2021). *WHO Global Air Quality Guidelines: Particulate Matter (PM2.5 and PM10), Ozone, Nitrogen Dioxide, Sulfur Dioxide and Carbon Monoxide*.

Wu, H., Reis, S., Lin, C., Beverland, I. J., & Heal, M. R. (2015). Identifying drivers for the intra-urban spatial variability of airborne particulate matter components and their interrelationships. *Atmospheric Environment*, *112*, 306-316. https://doi.org/https://doi.org/10.1016/j.atmosenv.2015.04.059

Yaro, A., Maly, F., & Pražák, P. (2023). Outlier Detection in Time-Series Receive Signal Strength Observation Using Z-Score Method with Sn Scale Estimator for Indoor Localization. *Applied Sciences*, *13*, 3900. https://doi.org/10.3390/app13063900

Ye, Q., Li, H. Z., Gu, P., Robinson, E. S., Apte, J. S., Sullivan, R. C., Robinson, A. L., Donahue, N. M., & Presto, A. A. (2020). Moving beyond Fine Particle Mass: High-Spatial Resolution Exposure to Source-Resolved Atmospheric Particle Number and Chemical Mixing State. *Environmental Health Perspectives*, *128*(1), 017009. https://doi.org/doi:10.1289/EHP5311

Zhang, Q., Fischer, H. J., Weiss, R. E., & Zhu, Y. (2013). Ultrafine particle concentrations in and around idling school buses. *Atmospheric Environment*, *69*, 65-75. https://doi.org/https://doi.org/10.1016/j.atmosenv.2012.12.015

SUPPLEMENTARY INFORMATION

Analysing Multiple Metrics of Ultrafine Particles from Personal Exposure Campaigns with Source Quantification

Table S1. Number of sampling trips during the campaign period.

Period	Time	No. of Trip	
		Walking	Bus
Morning Weekday (MWD)	8 AM- 11.59 AM	10	6
Morning Weekend (MWE)		3	3
Afternoon Weekday (AWD)	12 PM- 4 PM	9	6
Afternoon Weekend (AWE)		5	3
Evening Weekday (EWD)	5 PM- 8 PM	10	6
Evening Weekend (EWE)		4	3
Total		**41**	**27**

Table S2. Descriptive Statistic of PNC, average diameter, LDSA and meteorological parameter by type of route during bus measurement (derived from 1-second average data).

	N	Mean	SD	Min	Pctl. 25	Pctl. 50	Pctl. 75	Max
Bus Route : Major Rd								
PNC (#/cm^3)	21966	18590	20978	656	7351	12131	22178.75	406968
Average Diameter (nm)	21966	40.1	16.0	10.0	29.1	36.9	49.1	300.0
LDSA (μm²/cm³)	21966	30.1	17.1	5.6	17.8	27.1	36.8	184.2
RH (%)	22097	53.7	11.4	29.7	45.1	54.2	60.6	88.1
Wind speed (m/s)	22097	3.7	1.7	0.3	2.4	3.6	4.8	9.4
Temperature (°C)	22097	24.9	4.4	12.4	22.2	24.5	27.7	33.6
Bus Route : Residential Rd								
PNC (#/cm^3)	4893	11197	8800	711	5068	8467	14288	96039
Average Diameter (nm)	4893	47.3	18.8	12.4	33.2	43.4	60.5	300.0
LDSA (μm²/cm³)	4893	24.5	13.1	7.1	14.8	22.3	29.8	142.9
RH (%)	5024	52.9	9.4	33.9	48.7	53.6	58.9	73.1
Wind speed (m/s)	5024	3.6	1.9	0.2	2.1	3.3	4.9	9.4
Temperature (°C)	5024	25.3	4.6	17.6	21.9	25.4	27.8	33.6

Table S3. Descriptive Statistic of PNC, average diameter, and LDSA by time period (derived from 1-second average data).

	Mode	Time of day	N	Mean	SD	Min	Pctl. 25	Pctl. 50	Pctl. 75	Max
PNC (#/cm³)	Walking	Weekday								
		Morning	59880	7307	18196	292	2960	5040	7383	890896
		Afternoon	51106	13185	16793	371	5484	7997	20317	792119
		Evening	59357	14514	19119	393	5521	12401	20730	935157
		Weekend								
		Morning	20377	6762	9949	601	4387	5427	6823	464257
		Afternoon	20297	13001	13406	872	5388	11762	16955	549162
		Evening	23539	8835	15605	288	5663.5	7247	9903.5	971987
	Bus	Weekday								
		Morning	5685	18541	24106	656	5689	10065	16880	406968
		Afternoon	5526	19819	18976	1789	8578	14973	24212	146238
		Evening	7305	17150	13794	711	7448	14493	22643	187267
		Weekend								
		Morning	2647	7723	4175	886	4590	7318	9407	68351
		Afternoon	3113	19318	26144	798	7348	12917	17152	249120
		Evening	2583	16398	20706	1353	5489	9250	17211	173854
LDSA (μm²/cm³)	Walking	Weekday								
		Morning	59880	16.6	18.8	4.5	8.1	14.6	19.3	956.0
		Afternoon	51106	25.2	26.5	2.3	11.9	21.4	33.3	1533.4
		Evening	59357	26.3	22.9	6.1	12.9	26.3	32.8	903.7
		Weekend								
		Morning	20377	19.0	15.6	8.0	13.0	19.2	22.6	929.9
		Afternoon	20297	27.4	18.9	11.3	19.3	25.9	31.1	889.0
		Evening	23539	21.8	19.9	3.0	11.1	17.0	29.0	980.7
	Bus	Weekday								
		Morning	5685	28.3	18.8	7.6	14.5	23.4	35.3	184.2
		Afternoon	5526	32.3	19.6	5.6	16.8	29.9	40.7	126.8
		Evening	7305	28.5	12.8	8.0	18.4	27.7	34.8	96.5
		Weekend								
		Morning	2647	23.0	11.4	5.6	17.0	20.6	24.8	102.7
		Afternoon	3113	33.6	17.2	12.5	22.2	29.7	40.9	134.4
		Evening	2583	26.3	15.1	7.1	16.1	22.0	32.5	142.9
Average Diameter (nm)	Walking	Weekday								
		Morning	59880	50.6	17.9	10.0	41.6	48.4	55.7	300.0
		Afternoon	51106	42.5	19.8	10.0	28.7	38.1	53.7	300.0
		Evening	59357	40.4	15.9	10.0	29.9	37.5	48.1	300.0
		Weekend								
		Morning	20377	53.4	13.1	10.0	44.8	53.8	59.7	300.0
		Afternoon	20297	47.4	18.6	10.8	30.3	45.1	62.8	300.0
		Evening	23539	50.1	24.6	10.0	31.1	41.7	69.6	300.0
	Bus	Weekday								
		Morning	5685	40.8	15.1	10.0	32.8	40.8	48.4	300.0
		Afternoon	5526	35.8	13.3	12.4	27.2	32.2	42.3	95.8
		Evening	7305	37.0	11.1	10.1	28.7	34.6	43.7	226.3
		Weekend								
		Morning	2647	56.9	17.7	14.3	47.4	59.2	67.6	300.0
		Afternoon	3113	47.2	21.0	11.6	32.7	41.0	67.1	300.0
		Evening	2583	44.4	20.5	13.2	28.4	42.0	60.9	300.0

Table S4. The hourly average of vehicle numbers during campaign period

Vehicle Type	Weekday		Weekend	
	mean	SD	mean	SD
Cars	316	160	303	143
Rigids	5	3	3	1
HGVs	2	2	1	1
Buses	24	21	13	9
Total Vehicles	311	143	298	120

Table S5. Descriptive Statistic within Microenvironments (derived from 1-second average data).

Location	N	Mean	SD	Min	Pctl. 25	Pctl. 50	Pctl. 75	Max
Bus Stop 1								
PNC	5223	18413	27680	303	4778	8151	19652	613777
Average Diameter	5223	45	16	11	32	42	56	284
LDSA	5223	35	41	5	13	21	35	346
Bus Stop 2								
PNC	11643	14600	27516	649	5672	8512	15898	668922
Average Diameter	11643	44	21	10	32	39	58	300
LDSA	11643	26	22	5	16	23	30	638
Bus Stop 3								
PNC	15769	10062	13877	281	4412	6985	10926	329119
Average Diameter	15769	47	17	11	35	45	56	300
LDSA	15769	23	26	5	10	19	27	718
Supermarket 1								
PNC	3892	5495	5466	169	1825	3533	7466	74629
Average Diameter	3892	56	19	10	39	57	70	300
LDSA	3892	14	10	2	7	10	21	124
Supermarket 2								
PNC	559	22570	3809	16567	19188	21461	25920	35838
Average Diameter	559	25	1	23	24	25	25	26
LDSA	559	28	5	22	25	27	32	46
Restaurant								
PNC	2164	65176	43131	1070	40455	58293	83492	361922
Average Diameter	2164	39	16	19	30	34	42	163
LDSA	2164	121	82	11	82	105	136	987

Table S6. Number of spike data by time period

Period	No of spike data	%
MWD	11208	31%
AWD	5623	15%
EWD	8529	23%
MWE	2758	8%
AWE	1994	5%
EWE	6284	17%
Total	36396	100%

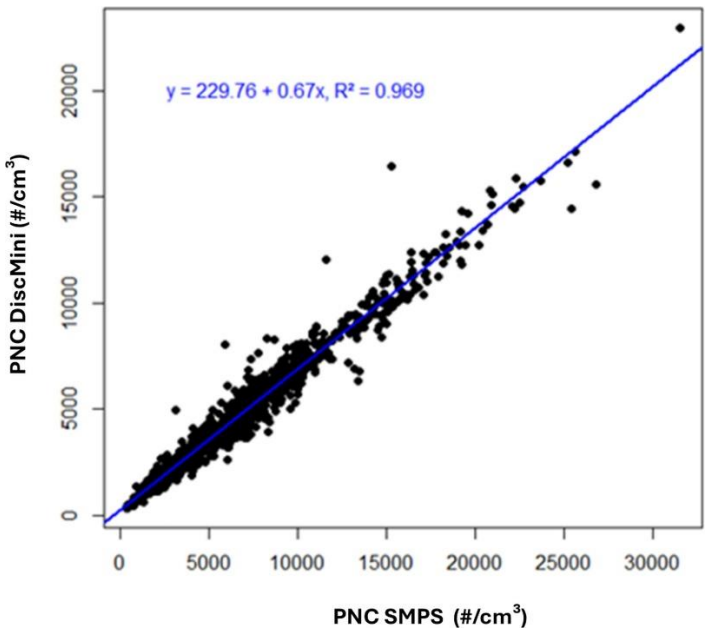

Figure S1. PNC (#/cm^3) derived from DiSCmini and SMPS during collocation period (5 minutes averaged data).

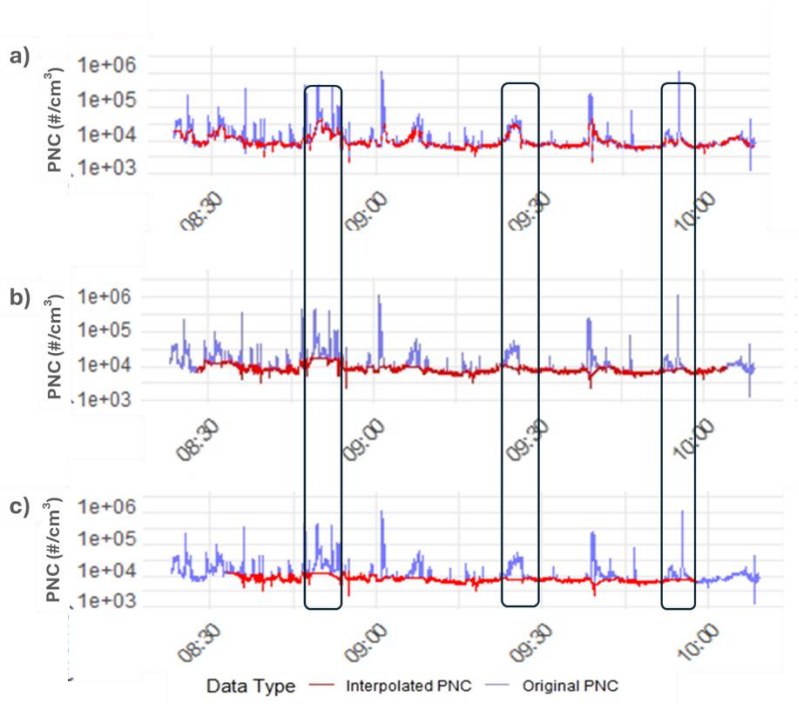

Figure S2. De-peaked interpolated PNC using (a) 1-minute average, (b) 5-minutes average, (c) 10-minutes average.

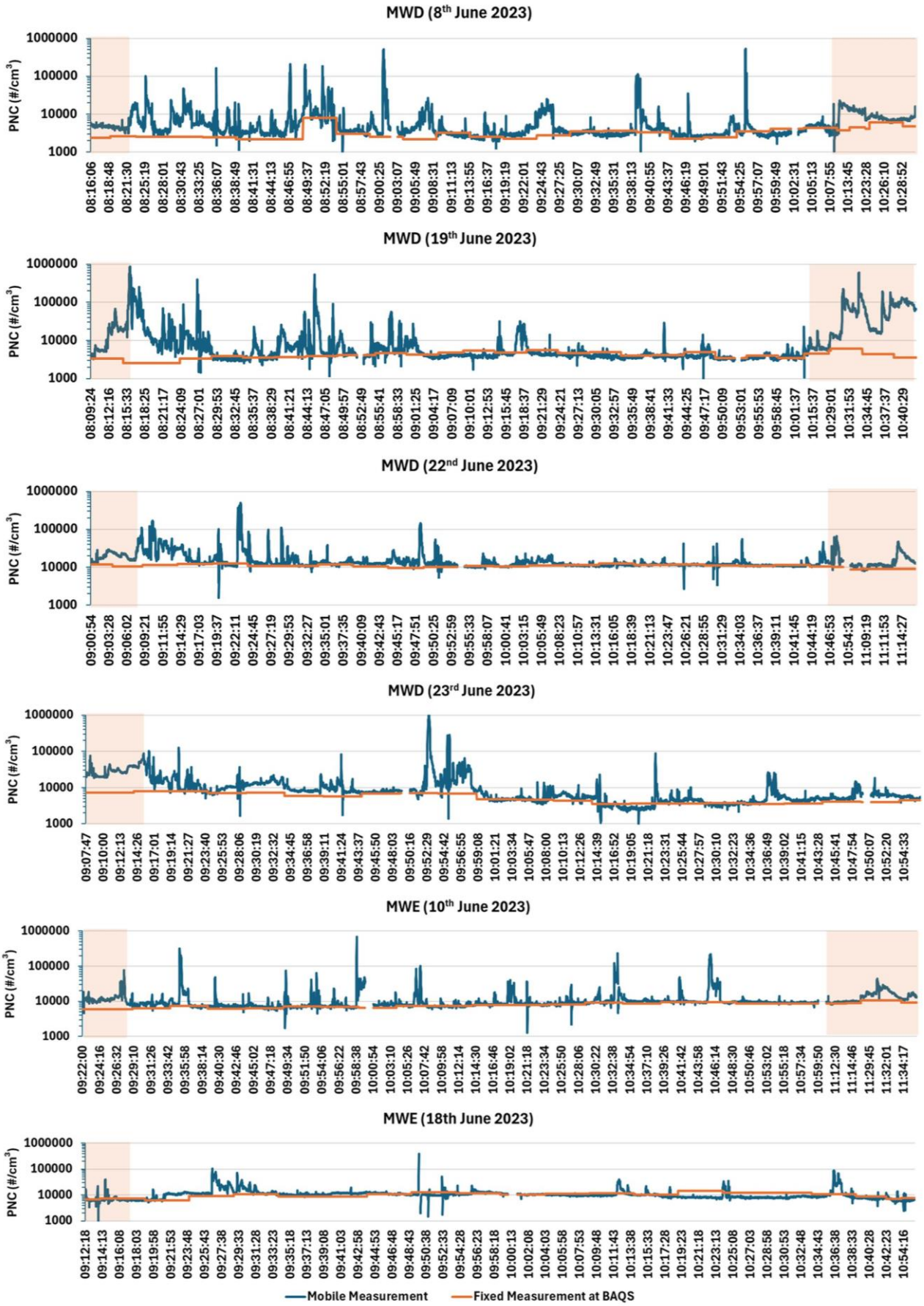
MWD (8th June 2023)
MWD (19th June 2023)
MWD (22nd June 2023)
MWD (23rd June 2023)
MWE (10th June 2023)
MWE (18th June 2023)
PNC (#/cm3)
1000000
100000
10000
1000
Mobile Measurement
Fixed Measurement at BAQS

38

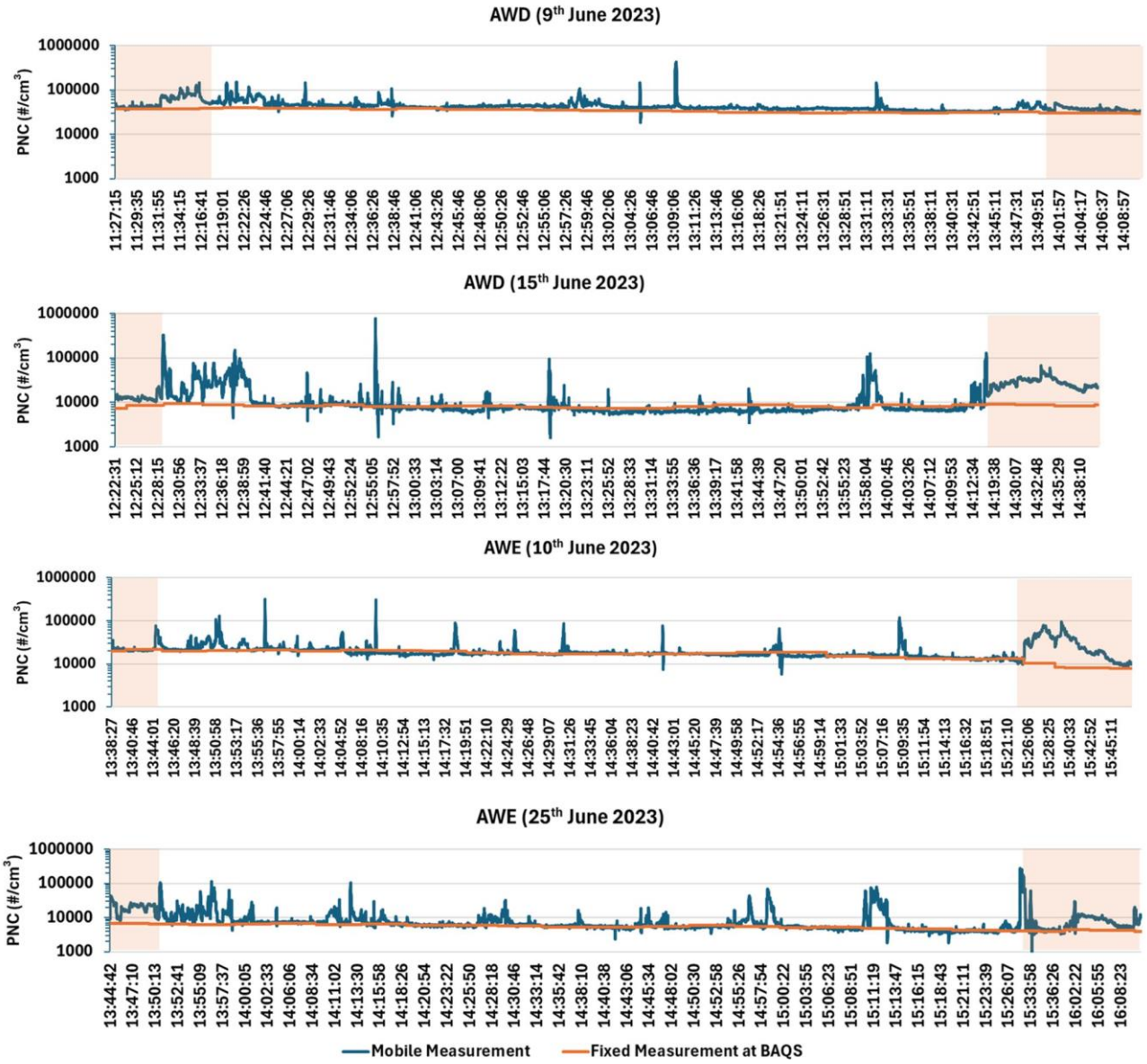
AWD (9th June 2023)
AWD (15th June 2023)
AWE (10th June 2023)
AWE (25th June 2023)
PNC (#/cm3)
1000000
100000
10000
1000
Mobile Measurement
Fixed Measurement at BAQS

39

40

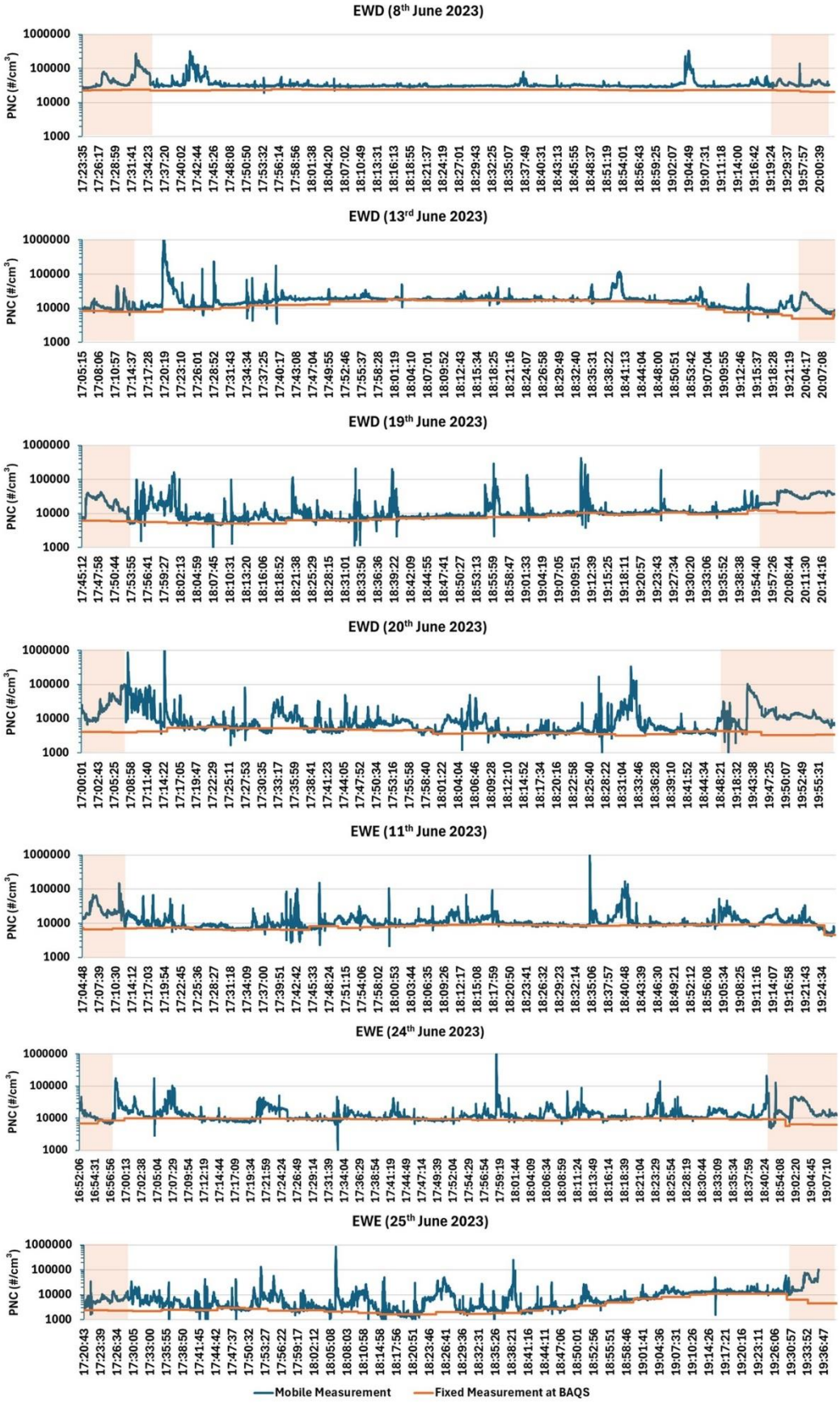
EWD (8th June 2023)
EWD (13rd June 2023)
EWD (19th June 2023)
EWD (20th June 2023)
EWE (11th June 2023)
EWE (24th June 2023)
EWE (25th June 2023)
PNC (#/cm3)
1000000
100000
10000
1000
Mobile Measurement
Fixed Measurement at BAQS

41

Figure S3. PNC from mobile measurement (blue line), and that derived from SMPS at BAQS during campaign period (orange line). The first letter refers to: A= Afternoon, E=Evening, M=Morning; the last two letters refer to: WD= Weekday, WE= Weekend, while the number indicates the sequence of trips. This figure presents only the trips for which SMPS data was available. A light orange shade shows the measurement on the bus journey, while the unshaded PNC measured during walking.

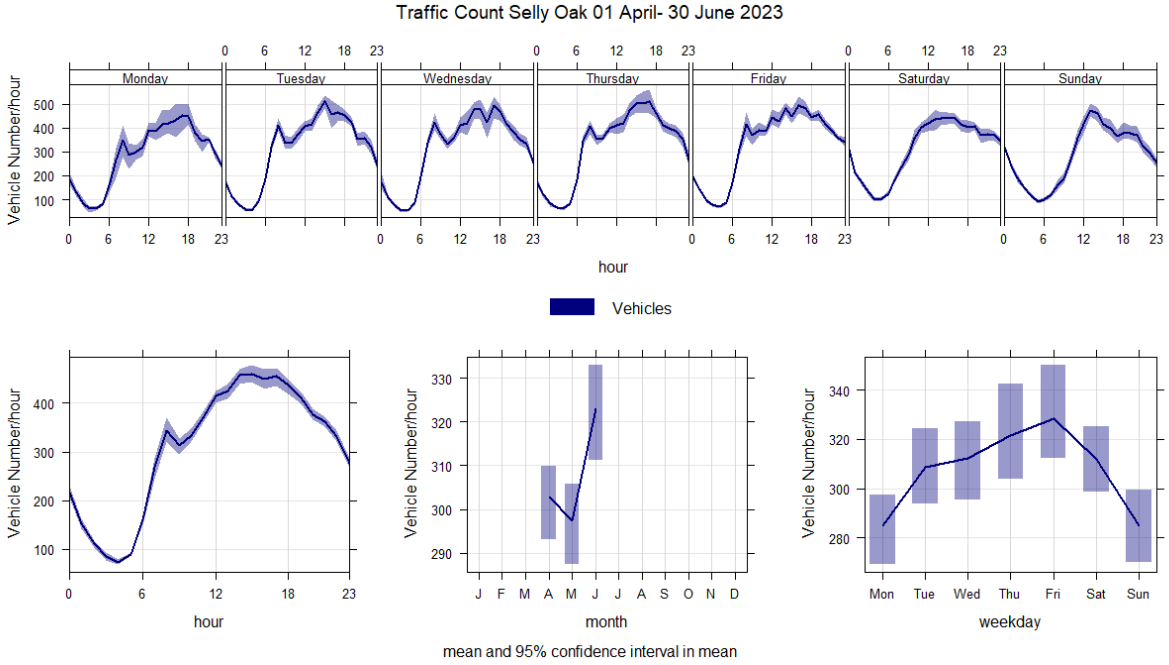

Figure S4. Time Variation of vehicle number per hour (from 1 lane) on a main road along study route during campaign period.

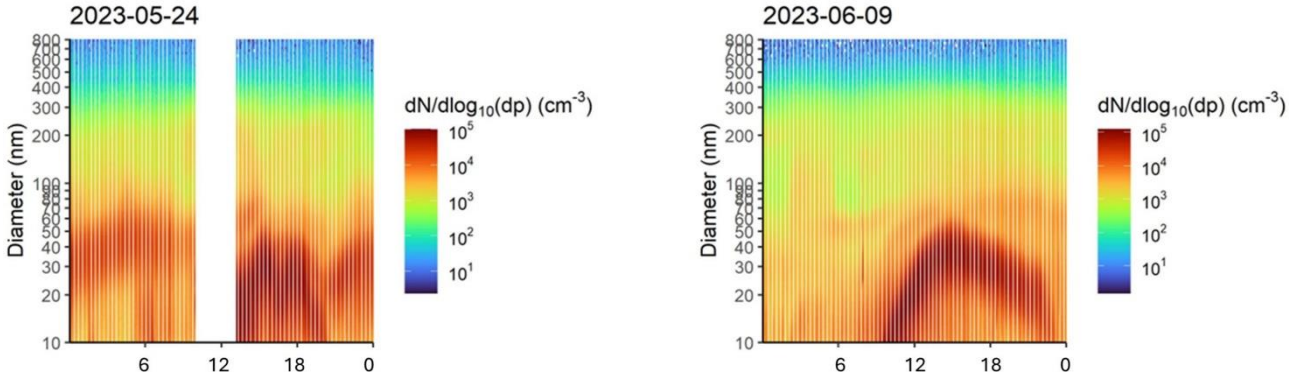

Figure S4. Particle Number Size Distribution derived from local air monitoring station on the specific days during high PNC exposure.

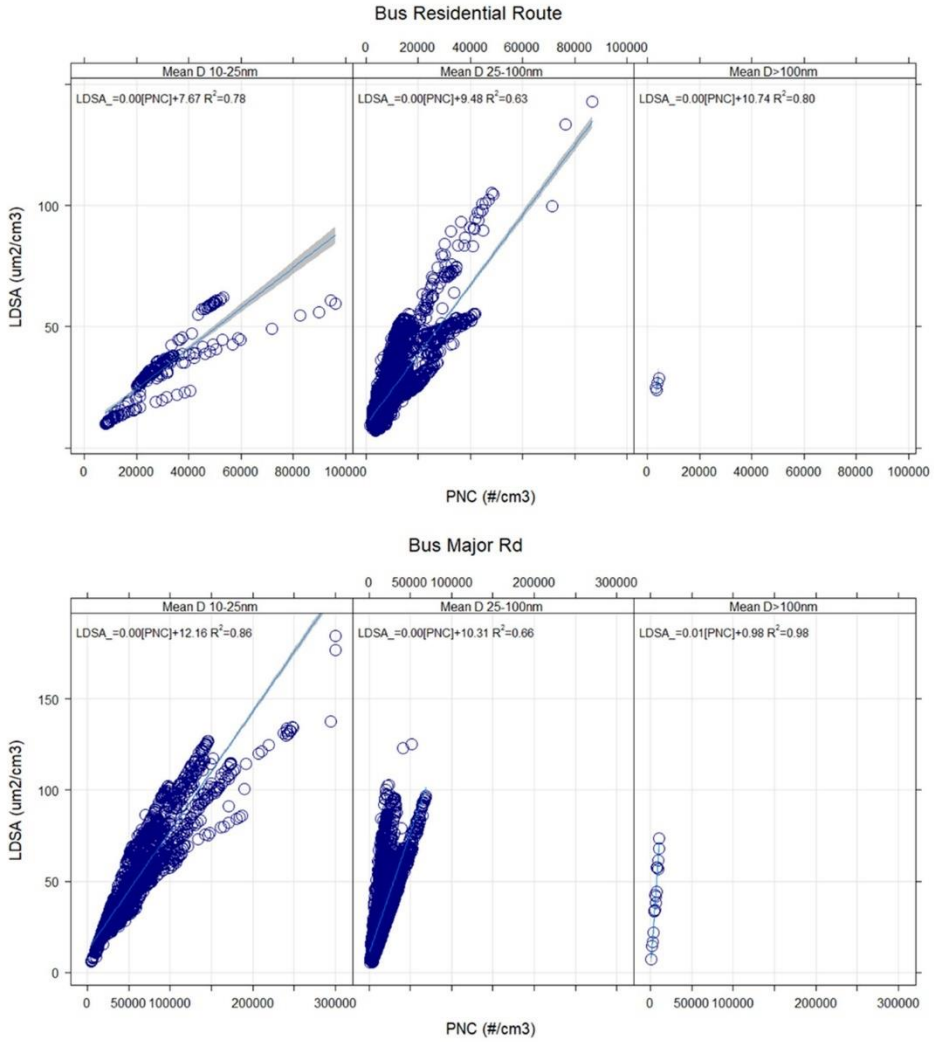

59

60 **Figure S6.** Scatter plot of PNC and LDSA by average particle diameter and route
61 types i.e., on residential route, and major road using 1-second data.)

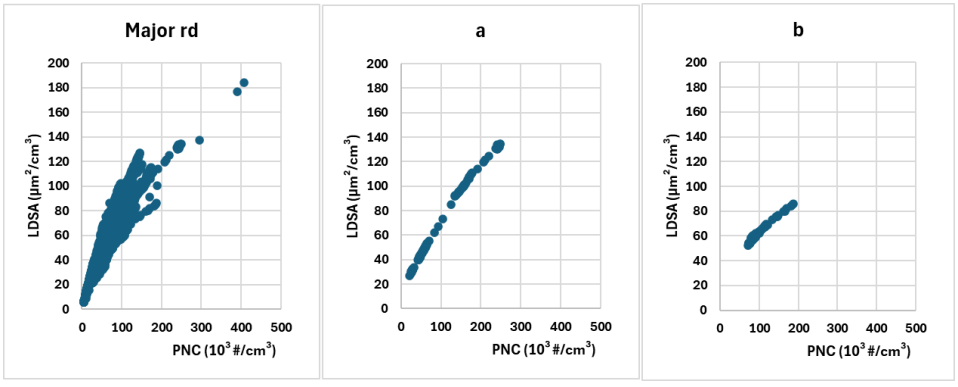

62

63 **Figure S7.** Scatter plot of PNC and LDSA from the bus journey within mean diameter
64 of 10-25 nm (nucleation mode) along major road. Multiple trends arose from several
65 short-term peaks in PNC and LDSA, occurring immediately after the passenger
66 exchange at two different bus stops (a) and (b) located near a petrol station.

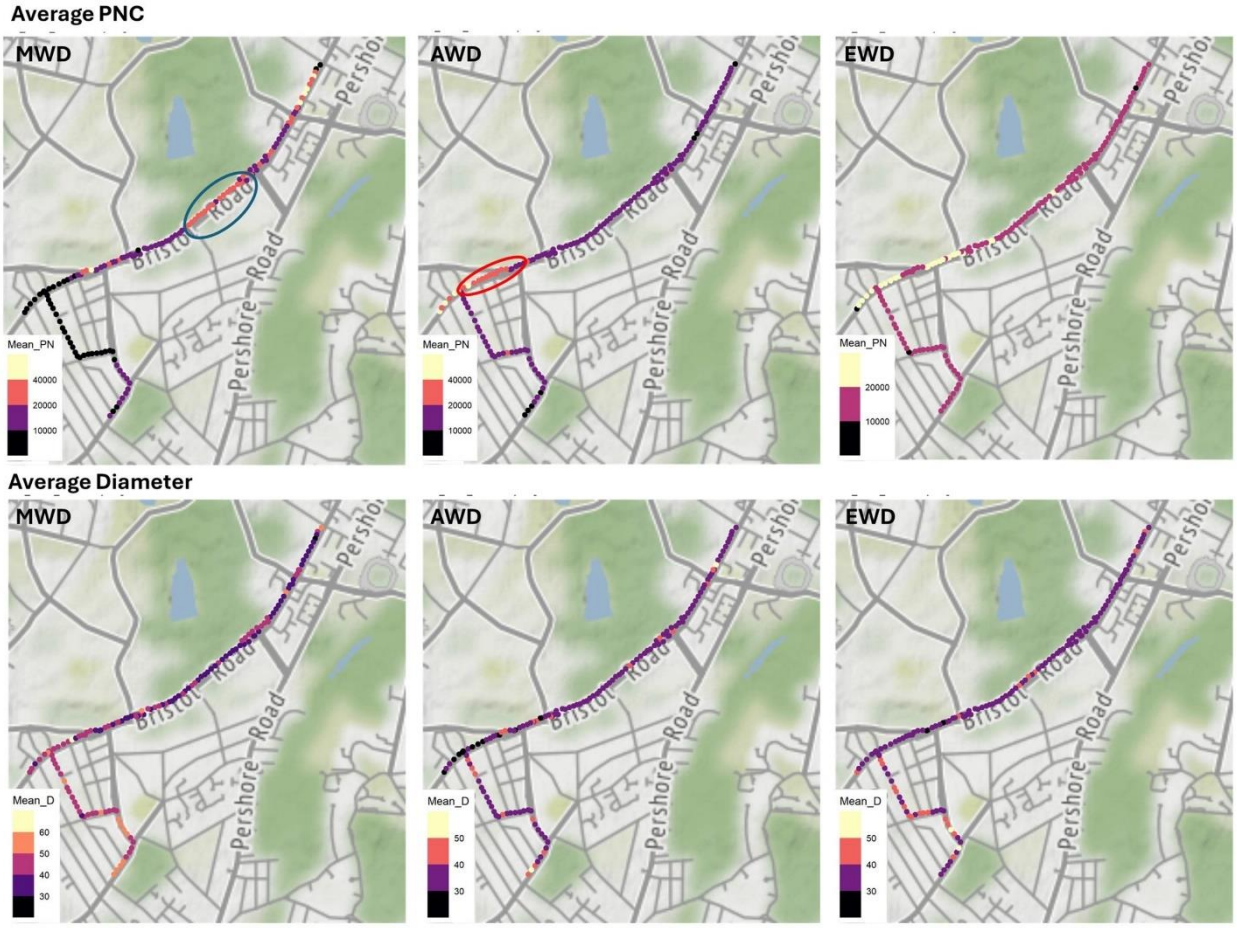

Figure S8. Spatial distribution of average PNC Exposure (top) and average diameter (bottom) from bus measurement by time of day. The red circle shows the junction area where traffic lights, a petrol station, and pedestrian crossings were located, while the dark blue circle encompasses a school gate and U-turn. The scale is adjusted for PNC in the EWD, and average diameter in the MWD because of the lower PNC, and larger average diameter, respectively.

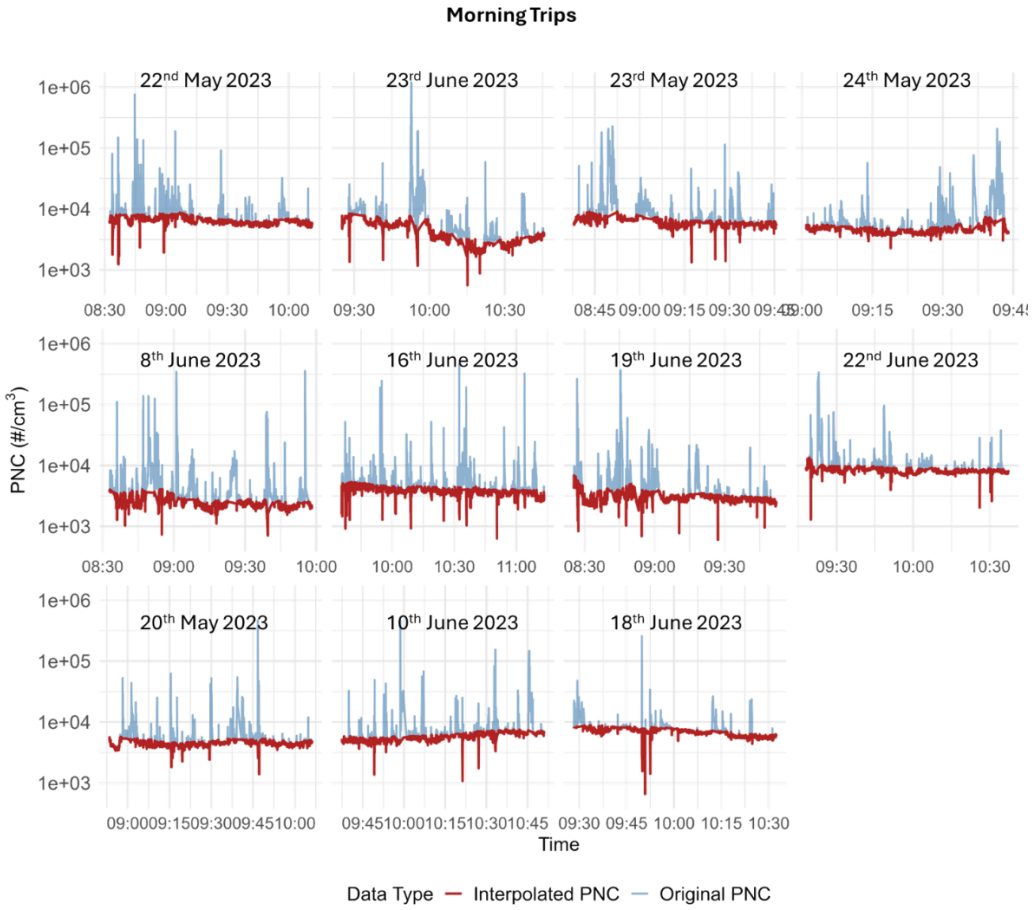
Morning Trips
22nd May 2023
23rd June 2023
23rd May 2023
24th May 2023
8th June 2023
16th June 2023
19th June 2023
22nd June 2023
20th May 2023
10th June 2023
18th June 2023
PNC (#/cm3)
Time
Data Type Interpolated PNC Original PNC

76

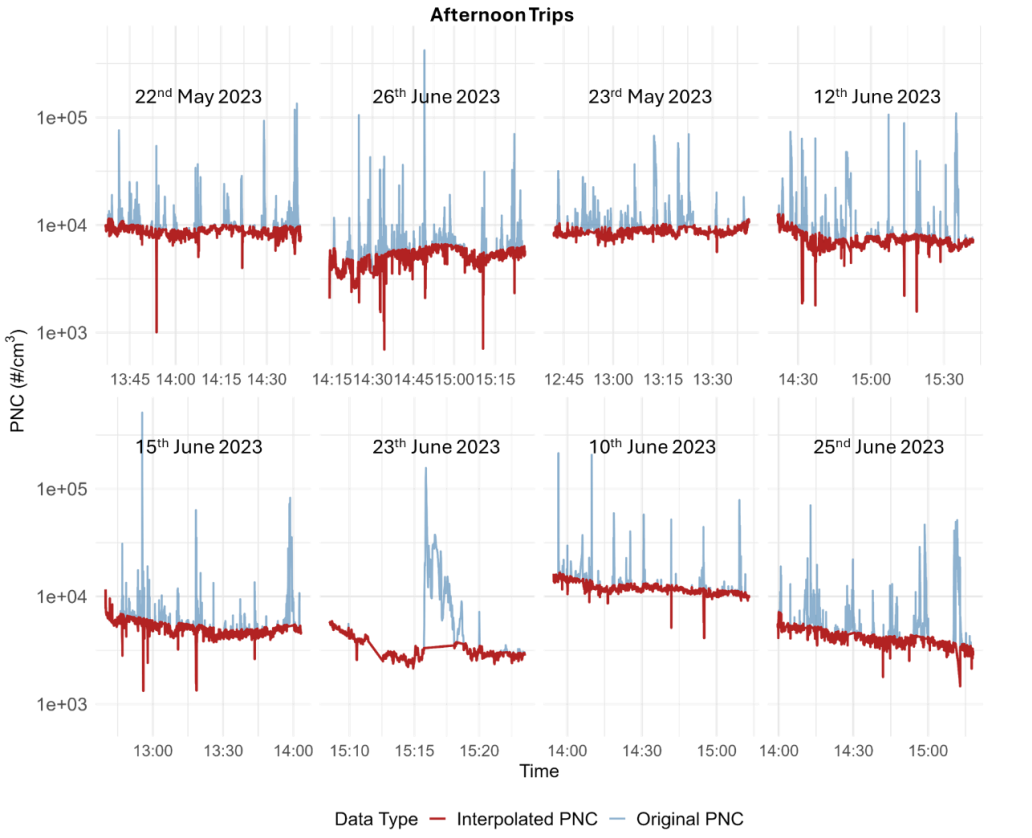
Afternoon Trips
22nd May 2023
26th June 2023
23rd May 2023
12th June 2023
15th June 2023
23th June 2023
10th June 2023
25nd June 2023
PNC (#/cm3)
Time
Data Type Interpolated PNC Original PNC

77

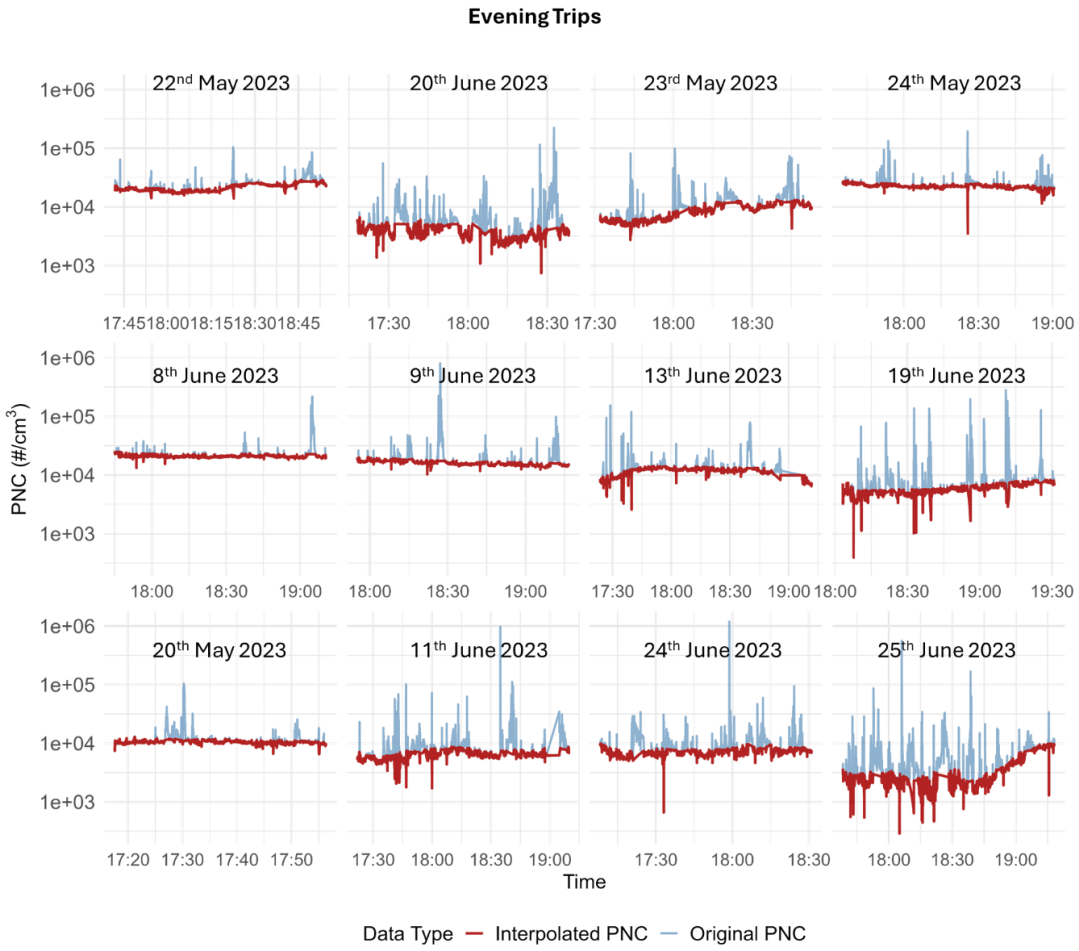

Figure S9. PNC obtained from walking measurements from the whole campaign (morning, afternoon, and evening trips). The blue line shows the raw concentration, whereas the red line represents the concentration after removing the short-term peaks.

Chapter 5: An Evaluation of Methods for Normalising Short Campaign Outdoor Personal Exposure Data to Reflect an Annual Mean

Authors: Seny Damayanti, Dimitrios Bousiotis, Arunik Baruah, Francis D. Pope, Roy M. Harrison

Submitted to: Atmospheric Environment, 2025

Author contributions: SD: Writing-original draft, Conceptualization, Resources, Visualization, Methodology. **DB**: Writing-review & editing, Resources. **AB**: Writing-review & editing, Resources**. FDP**: Validation, Supervision, Conceptualization, Writing-review & editing, Funding acquisition. **RMH**: Validation, Supervision, Conceptualization, Writing- review & editing, Funding acquisition.

An Evaluation of Methods for Normalising Short Campaign Outdoor Personal Exposure Data to Reflect an Annual Mean

Seny Damayanti[1], Dimitrios Bousiotis[1], Arunik Baruah[1,3,4], Francis D. Pope[1], Roy M. Harrison[1,2]

[1] Division of Environmental Health and Risk Management
School of Geography, Earth and Environmental Sciences
University of Birmingham
Edgbaston, Birmingham B15 2TT, United Kingdom

[2] Department of Environmental Sciences
Faculty of Meteorology Environment and Arid Land Agriculture
King Abdulaziz University, Jeddah 21589, Saudi Arabia

[3] University School for Advanced Studies IUSS Pavia
Palazzo Del Broletto, Pavia, 27100, Italy

[4] Dept of Engineering 'Enzo Ferrari'
University of Modena and Reggio Emilia, Modena, 41125, Italy

Corresponding author: Roy M. Harrison (r.m.harrison@bham.ac.uk)

ABSTRACT

Using a portable air sampler is a highly effective means to measure personal exposure to pollutants and also to map spatial distributions in high resolution. Nevertheless, the available data is descriptive only of the specific period of measurement, largely due to the influence of meteorological factors. Data normalisation has been conducted in air quality research to mitigate the impact of weather conditions on air pollutant concentration. However, this technique has been mostly used on long-term data obtained from stationary air monitoring stations using machine learning. In this paper, we evaluate several simple methods to minimise the influence of meteorological conditions on the personal exposure data collected in an urban neighbourhood in Birmingham based upon the use of data from a reference site. Data normalization to represent the annual mean was performed on the pollutant measurements of Particle Number Count (PNC), Particulate Matter mass (PM_1, $PM_{2.5}$, and PM_{10}), and Black Carbon (BC) obtained from walking measurements. Some methods appreciably altered the raw data, thereby making them comparable to the annual average. For certain pollutants (PNC and BC), the normalised concentration was still greater than the annual average at the reference site, which was expected due to the presence of additional local sources along the walking route. Data normalisation can be utilised to evaluate both personal exposure and the spatial distribution of pollutants so as to reflect conditions at a certain point in time or corresponding to a specified time interval differing from the conditions at the time of data collection.

Keywords: Data normalization; Personal exposure; spatial distribution**;** ultrafine particles

INTRODUCTION

Air pollution is a major environmental risk to human health. In 2019, it was estimated that around 4.2 million individuals died prematurely due to exposure to ambient (outdoor) air pollution (WHO, 2024). Of the various air pollutants, particulate matter (PM) is most closely linked to adverse effects upon human health. Long-term exposure to this pollutant is associated with respiratory and cardiovascular diseases (Guo et al., 2023; Liu et al., 2022; Liang et al., 2020). Ultrafine particles (UFP) with a diameter less than 100nm, have been considered to be potentially more harmful than larger particles due to their ability to translocate to other organs such as the liver, the brain, the kidney, and the heart (Schraufnagel, 2020; Peters et al., 2006; Oberdörster et al., 2004).

Ambient air quality monitoring stations play a key role in air quality management. Measurement data derived from such stations is widely used as a basis to estimate exposure to air pollutants (Xie et al., 2021; Evangelopoulos, 2021). Nevertheless, fixed air quality monitors are incapable of capturing the spatial variations in pollution at a hyperlocal level (Wang et al., 2023; Wang et al., 2021; Snyder et al., 2013). In recent years, portable air quality monitors have been widely used for personal exposure studies. The use of such monitors is an effective and more accurate approach to estimate the level of individual exposure to air pollutants (Vilcassim et al., 2023; Snyder et al., 2013) during the time of measurement. Implementing personal monitoring enables enhanced quantification of pollutant exposures potentially enabling associations of health effects with distinct sources (Koehler, and Peters., 2015), as well as reducing exposure misclassification in epidemiological studies. Personal exposure measurement can also be an effective method of high-resolution mapping of pollutant concentrations.

Despite its advantages, there are also limitations from the study of individual exposure to air pollutants. The data collected from such study is usually time-specific and only captures conditions at the time of measurement and will be influenced by local weather conditions occurring at that time.

Normalization of air quality data is increasingly used to remove the effects of weather conditions at the time of sampling so as to minimize bias or allow accurate assessment of policy interventions. However, most applications have used machine learning to analyze temporal trends in data derived from static monitoring stations. Grange and Carslaw (2019) used meteorological normalization to identify interventions in air quality time series from two UK sites, Dover, and London Marylebone Road, and Vu et al. (2019) removed weather effects from a time series of data from Beijing. Other study by Shi et al. (2021) utilized deweathering to evaluate the change in air quality in 11 cities due to the COVID-19 restrictions. Nevertheless, to the best of authors' knowledge, this is the first study that evaluates normalization upon air pollutant data from a short campaign of personal exposure monitoring.

The objective of this study was to develop simple normalization techniques to minimize the effects of external variables (e.g., weather) that might affect pollutant concentration during a sampling campaign and thus achieve a more representative assessment of air quality and its spatial distribution. In this work, personal exposure data for several air pollutants i.e. PNC, PM (PM_1, $PM_{2.5}$, and PM_{10}), and BC, has been normalised using measurement data derived from reference instruments at a local air quality monitoring station. As part of this work, local hotspots were identified by performing spatial distribution analysis.

METHODS

Data Collection and Calibration

Mobile measurements by walking were conducted between 20th May- 26th June 2023, to measure particle number concentration (PNC), Particulate Matter mass (PM_1, $PM_{2.5}$, and PM_{10}), and Black Carbon (BC) at three different times (morning, afternoon, and evening) on weekdays and weekends. The study area is situated in a densely populated area near the University of Birmingham, UK, as depicted in Figure 1.

A total of 43 trips were conducted to measure PNC and PM, and ten trips for BC measurements during the campaign. There were periods during which reference instrument data was unavailable, resulting in the selection of 33 trips for PNC and PM, and 10 trips for BC data in this analysis. The meteorological conditions during the campaign were predominantly sunny days, with average relative humidity between 50–65% and average wind speed of 2.9 to 4.4 m/s (Table S1). The temperature peaked at approximately 21° C in the afternoon (Figure S1).

Figure 1. The blue **line** shows the fixed **walking route** in Selly Oak, Birmingham. The yellow star depicts the location of local air quality monitoring at the Birmingham Air Quality Supersite (BAQS).

A miniature particle counter (DiSCmini), an optical particle counter (OPC-N3), and a micro Aethalometer were employed to measure particle number concentration (PNC), particulate matter mass (PM_1, $PM_{2.5}$, and PM_{10}), and BC concentration, respectively. A GPS was used to track the coordinate point during the measurements. All instruments were collocated for comparison with reference-grade instruments, specifically SMPS, FIDAS, and Aethalometer, which were deployed at BAQS. The instrument details, including reference grade, are presented in Table S2.

The OPC-N3 is known for its sensitivity to relative humidity (RH), leading to an overestimation of readings, particularly for $PM_{2.5}$ and PM_{10}, at elevated RH conditions (Crilley et al., 2020, 2018). Consequently, adjustment for RH was performed on the data obtained from this sensor for PM_1, $PM_{2.5}$, and $PM_{10,}$ leading to a significant improvement in PM concentrations. The correlation between mobile instruments after correction and the reference instruments is depicted in Figures S2-S4, demonstrating strong correlations with Pearson correlation (r) values of 0.98, 0.65, 0.85, and 0.78 for PNC, BC, PM_1, and $PM_{2.5}$, respectively, and a moderate correlation of 0.58 for PM_{10}. A comprehensive explanation of the instrument calibration process is available in Bousiotis et al. (2024) and Baruah et al. (2024). The regressions determined during the collocation were used to correct the personal sampler data.

Static data were taken from reference instruments located at the Birmingham Air Quality Supersite (BAQS), located on the University of Birmingham campus (see Figure 1). This is an urban background location with no immediate local source influences.

Normalization Methods

Normalization was done by scaling mobile personal exposure monitor data to fixed reference-grade instruments deployed at BAQS (urban background representation) in order to reflect longer periods, specifically annual mean concentrations. Four distinct methodologies were evaluated for calculating a correction factor or CF (Fig. 2), accounting for seasonal, diurnal, and weekly variability in pollutant levels. Data from continuous measurements derived from reference instruments, namely SMPS, FIDAS, and Aethalometer, which measured PNC, PM (PM_1, $PM_{2.5}$, and PM_{10}), and BC, respectively, during the year 2023 were utilized to determine the CF.

In terms of particle number, the PNC derived from SMPS refers to the total particle count within the size range of 10-300 nm, which is comparable to the modal diameter range recorded by the DiSCmini.

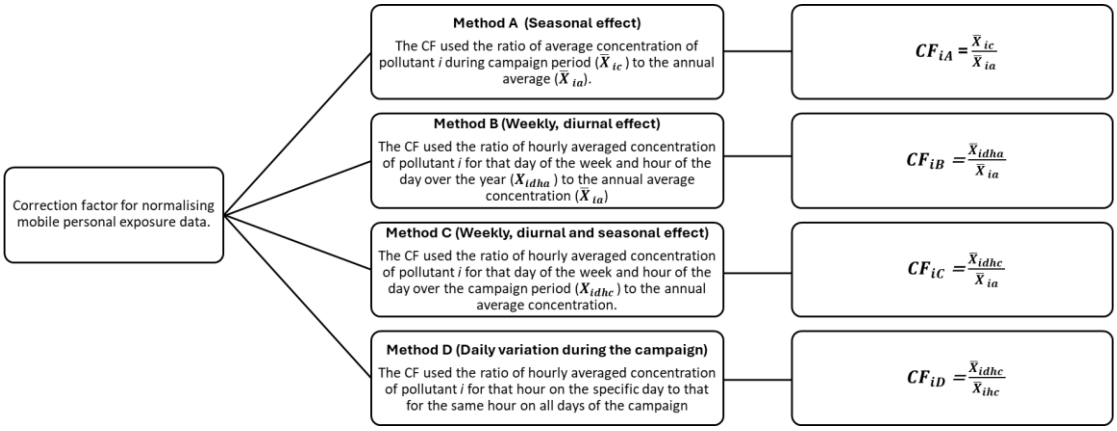

Figure 2. Four methods for determining correction factors, all utilising data derived from a reference instrument at BAQS.

- Method A

This method assumes that the campaign period may not accurately represent the full-year pollution level and utilises a seasonal correction factor based upon the ratio of the pollutant average concentration measured by the reference instrument during the campaign period to its annual mean. For example, higher UFPs in spring or summer can be attributed to new particle formation, and higher BC and $PM_{2.5}$ levels during winter are linked to intensified residential heating. This approach is straightforward to implement, however, it does not consider daily or hourly variations. Therefore, it is more suitable when detailed temporal data is unavailable.

- Method B

This approach improves upon the first method by incorporating both diurnal and weekly variations, specifically by using the average pollutant concentration measured during the same day of the week and hour of the day throughout the year. By averaging data across the entire year, it could mitigate bias from any single day or season and capture typical temporal patterns over the year. Nevertheless, it may not account for unusual events during the campaign, such as local pollution spikes or holiday traffic. This method is appropriate when the long-term hourly monitoring data is accessible.

- Method C

The third method incorporates campaign-specific condition. The numerator is calculated using the average concentration recorded at the reference station for the same hour and day, but only during the campaign period, while the denominator is the annual average concentration. This method takes into account diurnal, weekly, and seasonal effects, which may result in a more accurate representation of the

atmospheric conditions during the campaign. Nevertheless, this method requires a high-resolution reference station over the campaign period and presumes that the campaign duration is sufficient to account for typical variability.

- Method D

The fourth method uses the average concentration at a specific hour of the day as the numerator, while the average concentration for that same hour across all days during the campaign serves as the denominator. This approach considers daily variation within the campaign, highlighting how a specific walking exposure compares to typical values and is useful for identifying unusual events.

Each data point from mobile personal exposure data has a unique correction factor value that depends upon the employed method, with the exception of method A, which has the same value for all. Subsequently, the CF was used to normalize the mobile data utilizing Eq. 1 below:

$$x_{ij\,Norm} = \frac{x_i}{CF\,x_{ij}} \qquad \text{(Equation 1)}$$

Where:

$x_{ij\,Norm}$: normalized concentration of pollutant *i* from mobile measurement using method *j*.

x_i : non-normalized concentration of pollutant *i* from mobile measurement.

$CF x_{ij}$: correction factor of pollutant *i* using method *j.*

Spatial Distribution

Spatial distribution analysis was conducted using R software. Each data point on the walking route has its own coordinate derived from GPS measurement. The data were subsequently categorized based upon a distance of 20 meters for each segment. The average concentration of pollutants of each segment was calculated and plotted to identify local sources within the study area.

RESULTS AND DISCUSSION

Non-Normalized Concentration

A total of 33 trips for PNC, 41 trips for PM (PM_1, $PM_{2.5}$, and PM_{10}), and 10 trips for BC measurement were recorded during the campaign period. All reported data from walking measurements have been corrected against reference instruments. The average concentration of pollutants during walking was 15,870 #/cm³, 1.65 µg/m³, 3.9 µg/m³, 8.4 µg/m³, and 15.2 µg/m³ for PNC, BC, and PM (PM_1, $PM_{2.5}$, and PM_{10}), respectively. Figure 3 displays the measurements obtained when walking, alongside the readings from each reference-grade instrument deployed at BAQS during the walking trips. In general, certain periods exhibited concentrations during walking comparable to those recorded at the background site, although some short-term peaks were expected during mobile measurements due to proximity to local sources, particularly for PNC and BC. Nevertheless, the BAQS site primarily recorded elevated PM_1 concentrations compared to those recorded during walking. This discrepancy may arise from a difference in lower cut sizes between the two instruments, with FIDAS

measuring smaller particles (from 0.18 μm) compared to OPC-N3 (from 0.35 μm), resulting in a lower reading from the OPC.

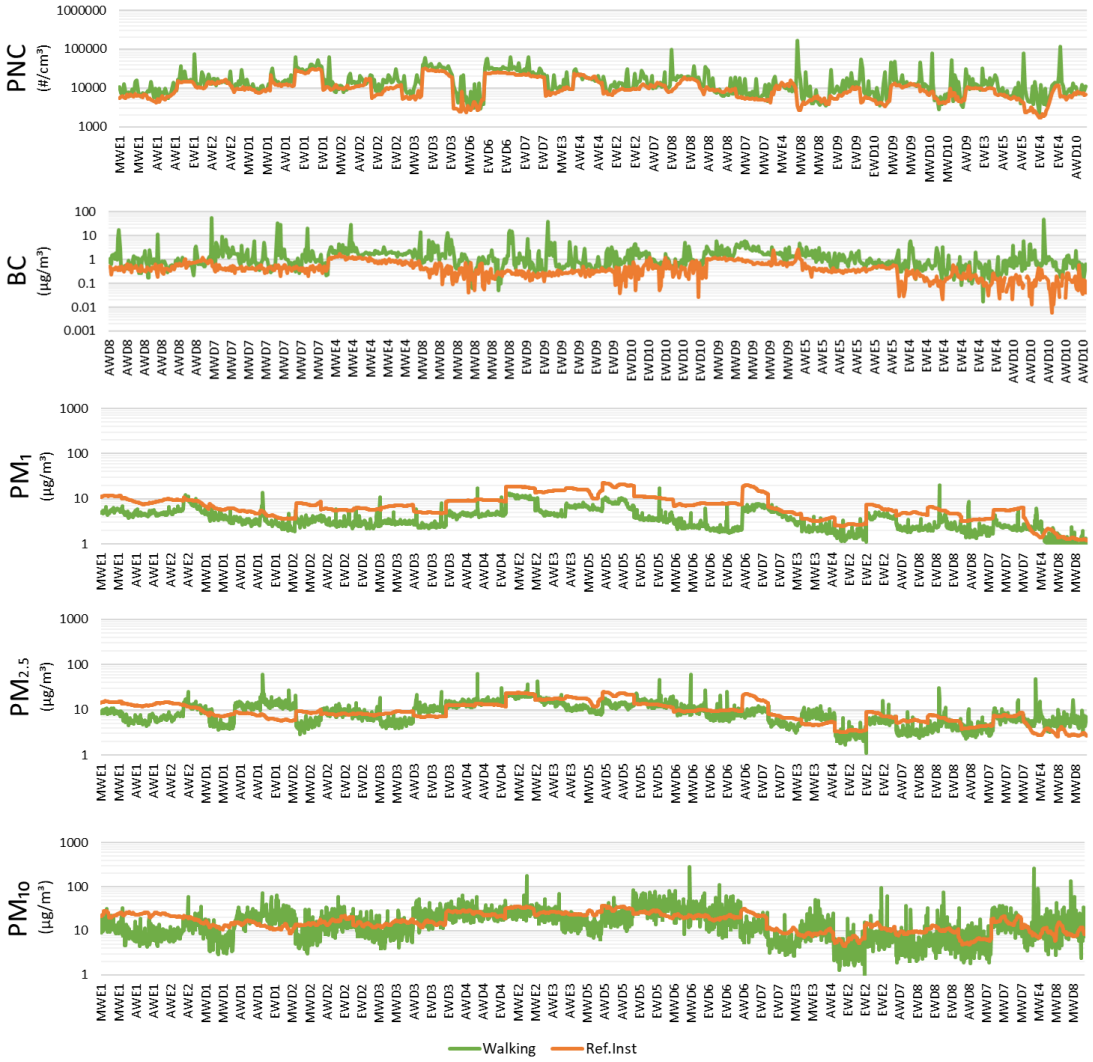

Figure 3. Concentration of pollutants from walking (green line), alongside from static measurement derived from reference-instrument at BAQS (orange line). In this plot, the concentration from walking was averaged based upon each reference-instrument, i.e., 5 minutes for PNC, and 1 minute for the remaining pollutants. The X-axis indicates the code of time of trips, with -WD and -WE stand for weekday and weekend, while M-A-E is for morning, afternoon, and evening, respectively.

Correction Factor (CF)

As described above, a correction factor (CF) was calculated to perform normalisation of personal exposure data from a short campaign in an urban neighbourhood in Birmingham. Four methods (Method A-D) were developed to calculate the CF, with the CF from method A presented in Table 1, while the results for the other methods are displayed in Figure 5.

Table 1. Average Concentration of each pollutant derived from reference instrument at BAQS and Correction Factor for Method A

Pollutant	Average Concentration*		Correction Factor A
	Campaign Period	2023	
PNC	9910	7330	1.35
BC	0.58	0.52	1.12
PM_1	7.48	5.55	1.35
$PM_{2.5}$	9.59	7.18	1.34
PM_{10}	16.91	10.54	1.60

*in #/cm³ for PNC, and µg/m³ for remaining pollutants.

The CF obtained from method A ranged from 1.1 to 1.6, with PNC, PM_1, and $PM_{2.5}$ around 1.3, while PM_{10} reached the highest value of 1.6, suggesting that the pollutant concentrations at BAQS during the campaign period were significantly higher compared to the annual average concentration. It was also indicated by the diurnal cycle of average concentration that is illustrated in Figure 4.

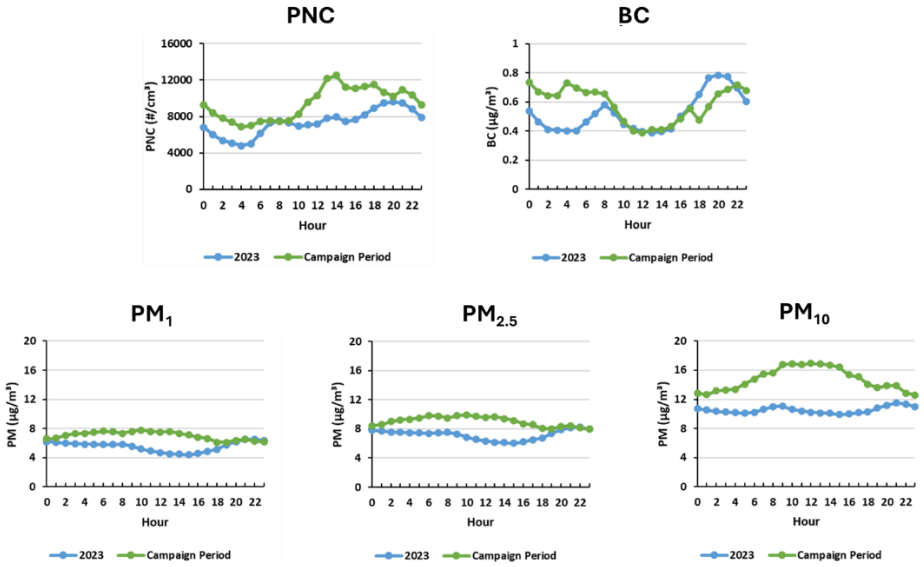

Figure 4. Diurnal Cycle of each pollutant in 2023 and campaign period

Variations in emission sources such as heating and traffic, including their regular temporal patterns may influence the fluctuation in pollutant concentration. The weather, however, greatly affects pollutant concentration in the atmosphere, especially during the campaign month (May-June), when wind speeds were lower than in other months in 2023, as seen in the monthly wind rose (Fig. S5). This condition may favour the accumulation in the atmosphere, leading to elevated concentration during that period (Gu et al., 2023). Moreover, elevated levels of pollutant ($PM_{2.5}$) throughout the spring season in the UK are typically associated with air masses transported from mainland Europe, affected particularly by agricultural activities (Harrison et al., 2022; UK Government, 2023).

Figure 4 shows that elevated levels of pollutant concentrations are more pronounced in the afternoon, with the exception of BC, which exhibits concentrations during the campaign comparable to their annual average level during the daylight hours. Further analysis of particle number size distribution data obtained from the SMPS revealed that new particle formation events occurred during the campaign period with a

frequency of 30%, as evidenced by a significantly higher concentration of small particles in the afternoon. The particle number size distribution on the sampling days is displayed in Figure S6.

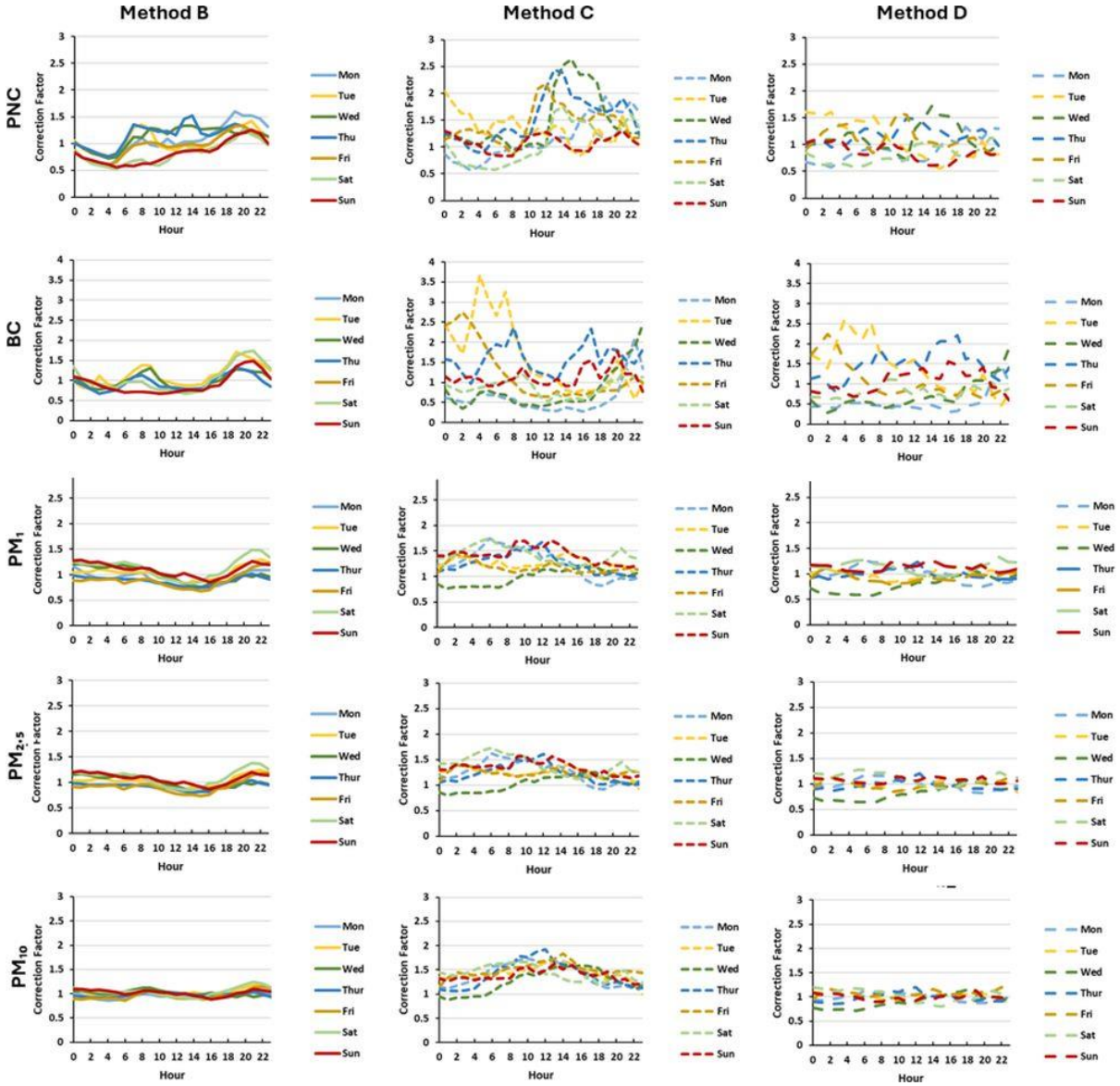

Figure 5. Correction Factor of each pollutant for method B, C, and D for the specific day of the week and hour of the day derived from the methods in Figure 2.

Since the campaign ran from 8 AM to 8 PM, we would only use the correction factor for this specific time period for data normalization. As shown in Figure 5, the CF for PNC derived from methods B and D exhibited a comparable range of approximately 0.5 to 1.5. Upon examining Figure 2, it is shown that these approaches have a typical ratio, with both the numerator and denominator employing data from either the annual period (method B) or the campaign period (method D). The correction factor (CF) for method C, which utilized a campaign-to-yearly data ratio, exhibits a higher value on specific days, peaking at 2.5, primarily during the afternoon period. This indicated that the pollutant concentration in those days of the campaign was more than twice the annual average. This suggests that the meteorological condition, characterised by predominantly calm weather with lower wind speed, contributed to elevated levels of pollutants in the atmosphere. These correction factor patterns were similarly detected in other pollutants, including PM_1, $PM_{2.5}$ and PM_{10}, only differing in magnitude. Nevertheless, the CF for these larger particles is more consistent compared to PNC and BC, indicating a higher contribution from regional sources to these pollutants.

Personal Exposure Normalized-Concentration

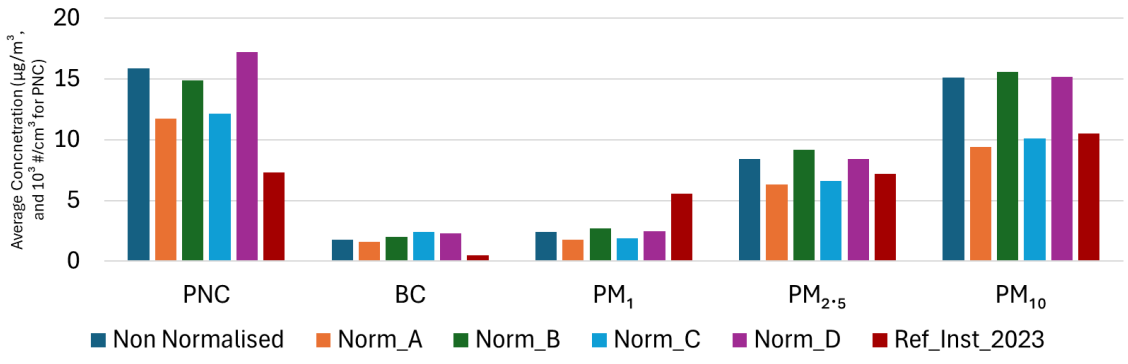

Figure 6. Average of non-normalized and normalized concentration of pollutant from each method. The normalised concentration was calculated using the respective

299 correction factor i.e., A (seasonal effect), B (weekly, diurnal effect), C (weekly, diurnal,
300 and seasonal effect), and D (daily variation during the campaign).

301

302 Figure 6 illustrates the average concentration of each pollutant, displaying both non-
303 normalized and normalized concentrations, alongside the annual average
304 concentration measured by a reference instrument at BAQS. A typical pattern of
305 normalized concentration for PNC, $PM_{2.5}$, and PM_{10} was observed, with Method A and
306 C significantly reducing their raw data, making them the most comparable to the annual
307 average. However, these methods yield a greater normalised concentration of PNC
308 than the annual average, perhaps due to the presence of additional local sources along
309 walking routes. Methods A and C have similarly reduced the PM_1 raw data, but it
310 remains lower than the annual mean across all methods, probably attributable to the
311 lower size cut issue as previously discussed in the beginning of this section.

312

313 Method A and C reduced the non-normalised concentration by 21-26% for PNC, PM_1,
314 and $PM_{2.5}$ and by up to 38% for PM_{10}. For BC, a minor change (11%) in normalised
315 concentration was observed when applying Method A, possibly due to slight
316 differences in concentration during the campaign period relative to its annual condition,
317 particularly during walking measurements, as indicated by its diurnal variation (see Fig
318 4). The remaining methods, namely B and D, yielded a slight change compared to non-
319 normalized concentrations, with method B generally yielding slightly higher results than
320 non-normalized concentrations, except for PNC.

321

Figure S7 illustrates the fluctuation in the day of the week and time of day for observed pollutants, both non-normalized and normalized concentration, including the annual mean from BAQS. Some of the non-normalised concentrations exhibited significantly higher levels, potentially attributable to meteorological factors or emission intensity. At certain points, several normalisation methods have effectively adjusted the non-normalised concentration to a level that reflects a yearly average, particularly for PNC and PM. For instance, PNC on Wednesday at 5 PM had an elevated raw concentration of nearly 30,000#/cm³, but when applying normalisation using method C (denoted as "Norm_C" on the graph), it was substantially reduced to approximately 20,000#/cm³. At that particular period, the normalized level remained above the yearly average at BAQS, which was expected due to the proximity of the walking route to local sources such as vehicle traffic and intensive cooking activities from restaurants, while BAQS does not have such local influences.

On the other hand, normalization by Method B led to an increase in the raw concentration, evident in the PM data (PM_1, $PM_{2.5}$, and PM_{10}), while Method D only slightly changed the diurnal pattern, apart from BC and PNC. Two populations of normalised data were identified, with Method A & C, as well as Method B & D exhibiting comparable levels, which is most clearly seen from $PM_{2.5}$ and PM_{10} at the weekend. The difference between the two groups may arise from distinct correction factors, with A and C taking into account two different time interval conditions i.e., during data collection and throughout an annual period. B & D, on the other hand, solely consider a single situation, which could be either annual or the campaign period.

With limited data on BC measurements, normalized concentrations exhibit elevated levels compared to their raw concentration. The higher annual average concentration of BC relative to its campaign period average is responsible for the increasing levels of this pollutant.

Method A averages pollutant data for both the entire campaign and the annual period at the background site. This allows for processes which affect both the sampling site and background site in a similar way, and includes simple effects of weather upon pollutant dispersion, as well as regional new particle formation processes. It will not readily accommodate effects upon street canyon concentrations where the effect of wind and mixing height may differ substantially from that at the more open background site, or for diurnal effects which differ between the sites. Method C adds an additional sophistication in conducting a similar exercise for each hour of the day and day of the week and relates it to the annual mean. Not surprisingly, the data normalised by methods A and C are very similar, as seen in Figure 6. The PNC data is reduced from the non-normalised concentration by Methods A and C, presumably because the campaign data are affected strongly by NPF events which do not occur with comparable frequency throughout the year. The corrected concentration is however greater than the annual mean at the background site, reflecting the emissions from local sources, which have been quantified in a companion paper during the campaign period (Damayanti et al., 2025). This is most notable for the PNC and BC data which are heavily influenced by road traffic in Selly Oak, but not at the background BAQS site. Method B differs from Method C by using mean data for each hour and day of the week over the entire year, rather than just over the campaign period. As such it allows explicitly for diurnal factors and reduces the variability in coefficients seen in Figure 5,

but not for differences in weather and NPF between the campaign period and the entire year. Method D again uses data for each hour of the day and day of the week in the normalisation process but normalises only to a campaign average rather than an annual average period. The outcome is concentrations which are broadly similar between Methods B and D, and to the non-normalised concentration (Figure 6). In the case of the typically spatially uniform $PM_{2.5}$, concentrations predicted by Methods A and C are alike, and similar to that at the background site. They are, however, notably smaller than the non-normalised mean which was presumably affected by seasonal weather-related factors. If the aim is to correct campaign data to an annual mean, both Methods A and C appear very suitable, and the results suggest that the added sophistication of Method C does not offer any great benefits, and for ease of use, Method A can be adopted. This may also be applicable in another manner, if the same analysis has been completed for all seasons and the correction factor for each season is available, it might potentially be utilized to estimate the personal exposure at a similar sampling site derived from the background site data.

Ratio of Walking Data to BAQS

The ratio of average concentrations from walking measurements to the annual concentration measured at BAQS, alongside the ratio during the measurement period was calculated (Figure 7). Both the raw and normalized PM_1 concentration ratios were below 1. As previously explained, the reason appears to be the difference in cut size between the two instruments. The ratio of $PM_{2.5}$ and PM_{10} was close to 1 across all methods, particularly in Methods A and C, which exhibit levels comparable to their annual average. This indicates a greater contribution from regional sources compared to local sources. The remaining pollutants exhibit a higher ratio, ranging from 1.7 to 2.4

for PNC and 3–4.6 for BC, indicating that local sources along the walking route contributed to the elevated concentration in this urban background area. Of all methods, ratios from A and C are consistent with the ratio during measurement, in particular of PNC, $PM_{2.5}$, PM_{10}, and thus more reliable to reflect annual conditions of personal exposure in the study area.

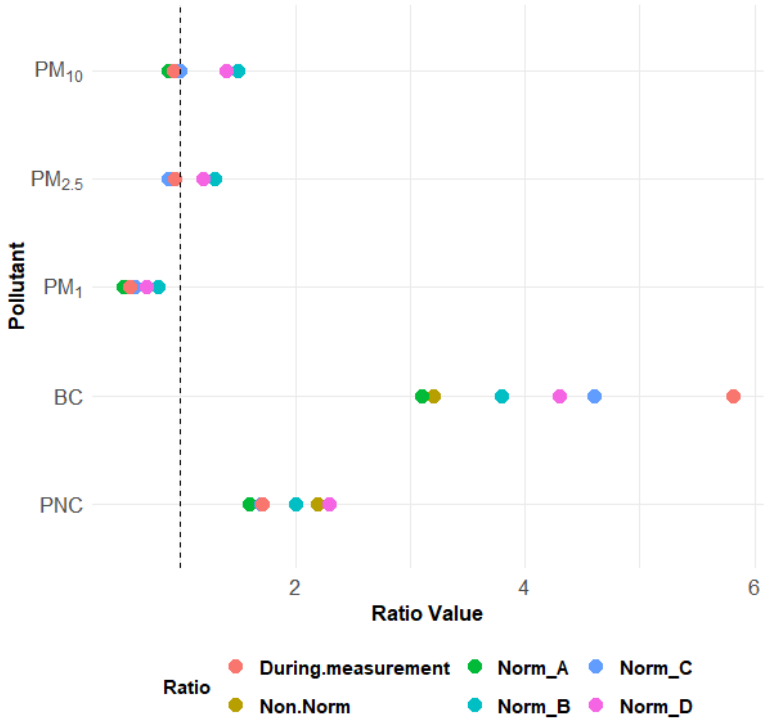

Figure 7. Ratio of pollutants from walking measurement (non-normalised and normalized concentration) to those measured at BAQS. The non-normalized values of PM_1, $PM_{2.5}$ and PM_{10} are nearly identical to Norm_D, resulting in their absence from the plot.

Spatial Map Distribution Analysis

Figure 8 illustrates an example of the spatial variation of PNC, presenting both non-normalized, and normalized average concentrations as determined by Method A, while the complete map is available in Figure S8. As expected, normalization of personal

408 exposure data, particularly with the application of Method A, resulted in a reduction of
409 the PNC level. Nonetheless, the normalization did not change its spatial distribution
410 pattern. Both maps still indicated hotspots (areas of higher concentration) in similar
411 locations.

412 Major roads generally exhibit normalized PNC pollution hotspots in proximity to
413 junctions and restaurant areas, reflecting emissions from vehicle exhaust and cooking
414 activities. We identified another PNC hotspot near the petrol station intersection.
415 However, hotspots of coarser PM ($PM_{2.5}$ and PM_{10}) were predominantly identified on
416 secondary roads, with one hotspot situated around a construction waste disposal site.
417 As with PM, hotspots of BC were also identified on secondary roads, one of which was
418 associated with a vehicle repair and service centre location.

419 Fig. S9 displays the spatial map of the difference in concentration between non-
420 normalized with normalized A (Δ Norm A), as well as normalized C (Δ Norm C). A
421 greater concentration difference indicates the influence of local sources along the
422 study route, as illustrated by this map, which highlights the major road for PNC and
423 $PM_{1,}$ and some points on secondary roads for coarser particles.

424

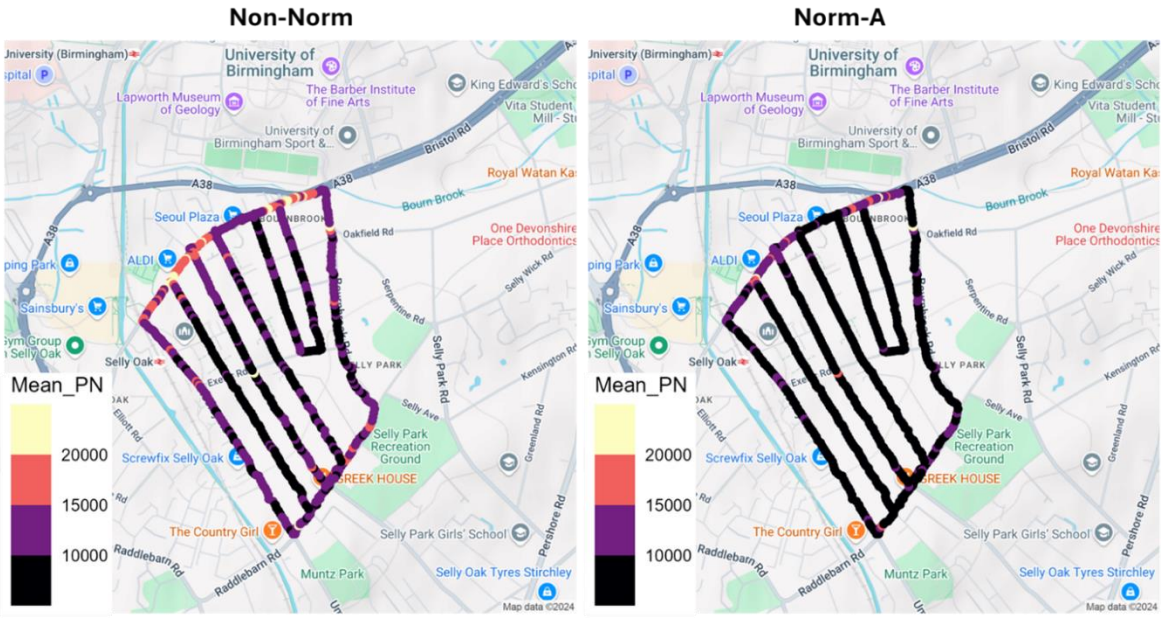

425

426 **Figure 8**. An example of the spatial distribution of PNC on the selected walking routes.
427 The average concentration was calculated for each small segment of street (20 m).
428
429
430 **Generalisability and Recommendations**

431 Generalisability is an important consideration in the development of a new
432 methodology. This study showed that Method A (seasonal correction) and Method C
433 (campaign-specific diurnal, weekly, and seasonal correction) generated normalised
434 concentrations that closely resembled the annual average at the reference station. The
435 evidence suggests that both methods are effective for the current context and broader
436 application. A simple methodology and minimal data requirements of Method A
437 enhance its generalisability, making it appropriate for study locations with limited
438 temporal resolution in monitoring data. Method C requires extensive data collection;
439 however, it enhances temporal sensitivity and is applicable to other regions where
440 hourly reference data are available during the campaign period. Method B, employing
441 long-term hourly reference data throughout the year, may exhibit less reliability in
442 campaigns conducted during unusual periods. Additionally, Method D is unsuitable for

predicting long-term exposure, as it solely captures intra-campaign variability. According to these findings, Method A provides a practical and sufficiently accurate option for general application in data-limited scenarios, whereas Method C is advisable when data availability allows.

CONCLUSIONS

Utilization of personal air monitors for outdoor measurements is an effective and potentially accurate means to assess exposure to pollutants at the individual level and allows mapping of pollutant concentration with high spatial resolution. However, such data are usually specific to the measurement time, mainly due to meteorological factors that affect pollutant concentrations in the ambient air. Data normalisation has been conducted in air quality research, mostly based on long-term data derived from fixed air quality monitoring stations. Here, we developed simple methods to normalize personal exposure data with the aim of minimising the effect of weather on the collected data and obtaining the adjusted personal exposure data that represents annual mean condition.

Personal exposure measurements of PNC, PM (PM_1, $PM_{2.5}$, and PM_{10}), and BC in an urban neighbourhood in Birmingham were conducted in the spring. The non-normalised concentrations of pollutants, particularly PNC, show very high concentrations during afternoon trips, apparently related to new particle formation which is more common during this season. The analysis of particle number size distribution data revealed that new particle formation occurred at a frequency of approximately 30% of days during the campaign, which significantly increased PNC

466 levels in the afternoon. This is a seasonally-related effect which can be captured by
467 using annual mean data for normalisation.

468 Among all the normalisation techniques develop in this study, the ratios from methods
469 A and C, which incorporate a correction factor for two distinct time intervals - during
470 data collection and over an annual period - align well with the ratios observed during
471 measurement, specifically for PNC, $PM_{2.5}$, and PM_{10}. Therefore, these methods have
472 the potential to accurately reflect the annual conditions of personal exposure in the
473 study area. The simpler Method A appears adequate for most purposes. It is far
474 simpler than the machine learning techniques now widely used in other applications,
475 and also likely to be less accurate as it is not based upon extensive model fitting with
476 explanatory variables. Nonetheless, the normalization method developed in this work
477 is easy to develop and execute, requires minimal computational resources to correct
478 the values, and is a simple yet effective approach that combines regulatory and low-
479 cost measurement data.

480 For smaller particles, the spatial map distribution identified several hotspots, primarily
481 around the intersection, supermarket, and restaurant areas on a major road. Higher
482 concentrations of coarser particles (PM_{10}) and BC were recorded in a residential area
483 adjacent to a construction waste disposal area and a vehicle repair centre,
484 respectively, which appear be substantial but localised sources of these pollutants in
485 this area

486 Despite data being normalized by the annual average, normalisation might be possible
487 with different time bases, e.g., seasonal averages or averages for a certain day of the

week; it depends on the study and research question. By doing so, it is possible to predict spatial distributions and personal exposures which reflect a certain time period.

ACKNOWLEDGEMENTS

SD would like to thank to Indonesia Endowment Fund for Education (LPDP), Ministry of Finance, Republic of Indonesia, for their financial support toward her PhD study.

FUNDING

This work was supported by European Union RI-URBANS project under grant agreement No. 101036245.

CRediT Authorship Contribution Statement

SD: Writing-original draft, Conceptualization, Resources, Visualization, Methodology. **DB**: Writing-review & editing, Resources. **AB**: Writing-review & editing, Resources**.** **FDP**: Validation, Supervision, Conceptualization, Writing- review & editing, Funding acquisition. **RMH**: Validation, Supervision, Conceptualization, Writing- review & editing, Funding acquisition.

Data Availability: Data supporting this publication are openly available from the UBIRA eData repository at https://doi.org/10.25500/edata.bham.00001260

REFERENCES

Baruah, A., Bousiotis, D., Damayanti, S., Bigi, A., Ghermandi, G., Ghaffarpasand, O., Harrison, R.M. Pope, F. D., 2024. A novel spatiotemporal prediction approach to fill air pollution data gaps using mobile sensors, machine learning and citizen science techniques. npj Climate and Atmospheric Science, 7, 310.

Bousiotis, D., Damayanti, S., Baruah, A., Bigi, A., Beddows, D. C., Harrison, R. M., Pope, F. D., 2024. Pinpointing sources of pollution using citizen science and hyperlocal low-cost mobile source apportionment. Environment International, 193, 109069.

Crilley, L. R., Singh, A., Kramer, L. J., Shaw, M. D., Alam, M.S., Apte, J. S., Bloss, W. J., Hildebrandt Ruiz, L., Fu, P., Fu, W., Gani, S., 2020. Effect of aerosol composition on the performance of low-cost optical particle counter correction factors. Atmospheric Measurement Techniques, 13, 1181-1193.

Crilley, L. R., Shaw, M., Pound, R., Kramer, L. J., Price, R., Young, S., Lewis, A.C., Pope, F. D., 2018. Evaluation of a low-cost optical particle counter (Alphasense OPC-N2) for ambient air monitoring. Atmospheric Measurement Techniques, 11, 709-720.

Damayanti, S., Bousiotis, D., Baruah, A., Pope, F. D., Harrison, R. M., 2025. Analysing multiple metrics of ultrafine particles from personal exposure campaigns with source quantification, Environment International in preparation .

Evangelopoulos, D., Chatzidiakou, L., Walton, H., Katsouyanni, K., Kelly, F.J., Quint, J.K., Jones, R.L., Barratt, B., 2021. Personal exposure to air pollution and respiratory health of COPD patients in London. European Respiratory Journal, 58, 2003432.

Grange, S. K., Carslaw, D. C., 2019. Using meteorological normalisation to detect interventions in air quality time series. Science of the Total Environment, 653, 578-588.

Gu, Y., Henze, D. K., Nawaz, M. O., Cao, H., Wagner, U. J., 2023. Sources of PM2.5-associated health risks in Europe and corresponding emission-induced changes during 2005–2015. GeoHealth, 7, e2022GH000767.

Guo, J., Chai, G., Song, X, Hui, X., Li, Z., Feng, X., Yang, K., 2023. Long-term exposure to particulate matter on cardiovascular and respiratory diseases in low- and

middle-income countries: A systematic review and meta-analysis. Frontiers in Public Health, 11, 1134341.

Harrison, R.M., Beddows, D.C.S., Tong, C., S. Damayanti, 2022. Non-Linearity of Secondary Pollutant Formation Estimated from Emissions Data and Measured Precursor-Secondary Pollutant Relationships, npj Climate and Atmospheric Science, 5, 71.

Koehler, K. A., Peters, T. M., 2015. New methods for personal exposure monitoring for airborne particles. Current Environmental Health Reports, 2, 399-411.

Liang, F., Liu, F., Huang, K., Yang, X., Li, J., Xiao, Q., Chen, J., Liu, X., Cao, J., Shen, C., Yu, L., Lu, F., Wu, X., Wu, X., Li, Y., Hu, D., Huang, J., Liu, Y, Lu, X., Gu, D., 2020. Long-term exposure to fine particulate matter and cardiovascular disease in China. Journal of the American College of Cardiology, 75, 707-717.

Liu C, Chan KH, Lv J, Lam H, Newell K, Meng X, Liu Y, Chen R, Kartsonaki C, Wright N, Du H, Yang L, Chen Y, Guo Y, Pei P, Yu C, Shen H, Wu T, Kan H, Chen Z, Li L, China Kadorrie Biobank Collaborative Group, 2022. Long-Term Exposure To Ambient Fine Particulate Matter And Incidence Of Major Cardiovascular Diseases: A prospective study of 0.5 million adults in China. Environmental Science and Technology, 56, 13200-13211.

Oberdörster, G, Sharp, Z, Atudorei, V, Elder, A, Gelein, R, Kreyling, W, Cox, C., 2004. Translocation of inhaled ultrafine particles to the brain. Inhalation Toxicology, 16, 437-445.

Peters, A., Veronesi, B., Calderón-Garcidueñas, L., Gehr, P., Chen, L. C., Geiser, M., Reed, W., Rothen-Rutishauser, B., Schürch, S., Schulz, H., 2006. Translocation and potential neurological effects of fine and ultrafine particles a critical update. Particle and Fibre Toxicology, 3, 13, https://doi.org/10.1186/1743-8977-3-13.

Schraufnagel, D. E., 2020. The health effects of ultrafine particles. Experimental and Molecular Medicine, 52, 311–317.

Shi, Z., Song, C., Liu, B., Lu, G., Xu, J., Van Vu, T., Elliott, R. J., Li, W., Bloss, W. J., Harrison, R. M., 2021. Abrupt but smaller than expected changes in surface air quality attributable to COVID-19 lockdowns. Science Advances, 7, eabd6696.

Snyder, E.G., Watkins, T.H., Solomon, P.A., Thoma, E.D., Williams, R.W., Hagler, G.S., Shelow, D., Hindin, D.A., Kilaru, V.J. Preuss, P.W., 2013. The changing paradigm of air pollution monitoring. Environmental Science and Technology, 47, 11369-11377.

UK Government, 2023). Air Quality Statistics in the UK, 1987 to 2022 - Particulate Matter (PM10/PM2.5) (last accessed on 3th April 2025 from https://www.gov.uk/government/statistics/air-quality-statistics/concentrations-of-particulate-matter-pm10-and-pm25).

Vilcassim, R., Thurston, G. D., 2023. Gaps and future directions in research on health effects of air pollution. EBioMedicine, 93, 104668.

Vu, T. V., Shi, Z., Cheng, J., Zhang, Q., He, K., Wang, S., Harrison, R. M., 2019). Assessing the impact of clean air action on air quality trends in Beijing using a machine learning technique. Atmospheric Chemistry and Physics, 19, 11303-11314.

Wang, A., Paul, S., deSouza, P., Machida, Y., Mora, S., Duarte, F., Ratti, C., 2023. Key themes, trends, and drivers of mobile ambient air quality monitoring: A systematic review and meta-analysis. Environmental Science and Technology, 57, 9427-9444.

Wang, S., Ma, Y., Wang, Z., Wang, L., Chi, X., Ding, A., Yao, M., Li, Y., Li, Q., Wu, M., Zhang, L., 2021. Mobile monitoring of urban air quality at high spatial resolution by low-cost sensors: impacts of COVID-19 pandemic lockdown. Atmospheric Chemistry and Physics, 21, 7199-7215.

WHO, 2024. Ambient (Outdoor) Air Pollution. https://www.who.int/news-room/fact-sheets/detail/ambient-%28outdoor%29-air-quality-and-health (last accessed on 6th March 2025).

Xie, S., Meeker, J. R., Perez, L., Eriksen, W., Localio, A., Park, H., A. Jen, Goldstein, M., Temeng, A. F., Morales, S. M., Christie, C., Greenblatt, R. E., Barg, F. K., Apter, A. J., Himes, B. E., 2021. Feasibility and acceptability of monitoring personal air pollution exposure with sensors for asthma self-management. Asthma Research and Practice, 7, 13.

SUPPLEMENTARY INFORMATION

An Evaluation of Methods for Normalising Short Campaign Outdoor Personal Exposure Data to Reflect an Annual Mean

Table S1. Meteorological Parameter measured at local weather station (Elms Cottage) during campaign period (Average ± Std.dev).

Met	AWD	AWE	EWD	EWE	MWD	MWE
RH (%)	56(14.9)	49.4(16.6)	58.9(16.9)	55.9(4.1)	65.3(11.4)	63.1(5.4)
ws (m/s)	3.9(1.8)	4.4(1.9)	3.8(1.5)	3.6(1.8)	2.9(1.5)	3.2(1.2)

Table S2. Instruments detail.

Type of measurement	Instrument	Parameter	Manufacturer	Time Interval
Walking measurement	DiSCmini	PNC	Testo	1 s
	OPC-N3	PM_1, $PM_{2.5}$, PM_{10}	Alphasense	10 s
	MicroAeth AE51	BC	Aethlabs	10 s
	GPS	Longitude, Latitude	Garmin	1 s
Static measurement at BAQS (a local air quality monitoring station)	SMPS	PNC	TSI	5 mins
	FIDAS 200E	PM_1, $PM_{2.5}$, PM_{10},	PALAS	1 min
	Aethalometer AE33	BC	MAGEE Scientific	1 min

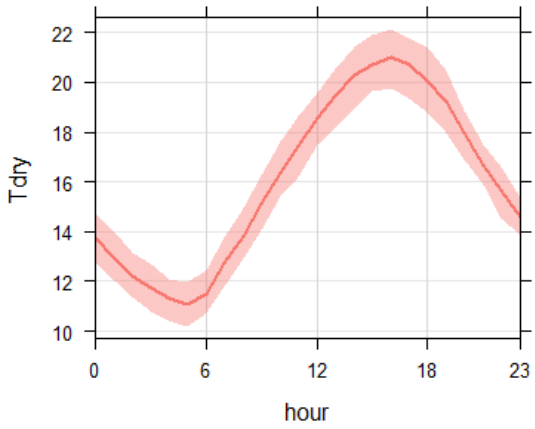

Figure S1. Diurnal cycle of temperature during the campaign period.

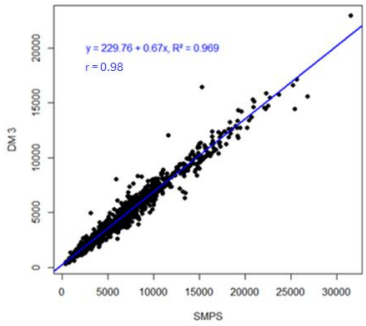

Figure S2. Collocation of instruments for mobile measurement (DM) with a reference instrument (SMPS) at BAQS.

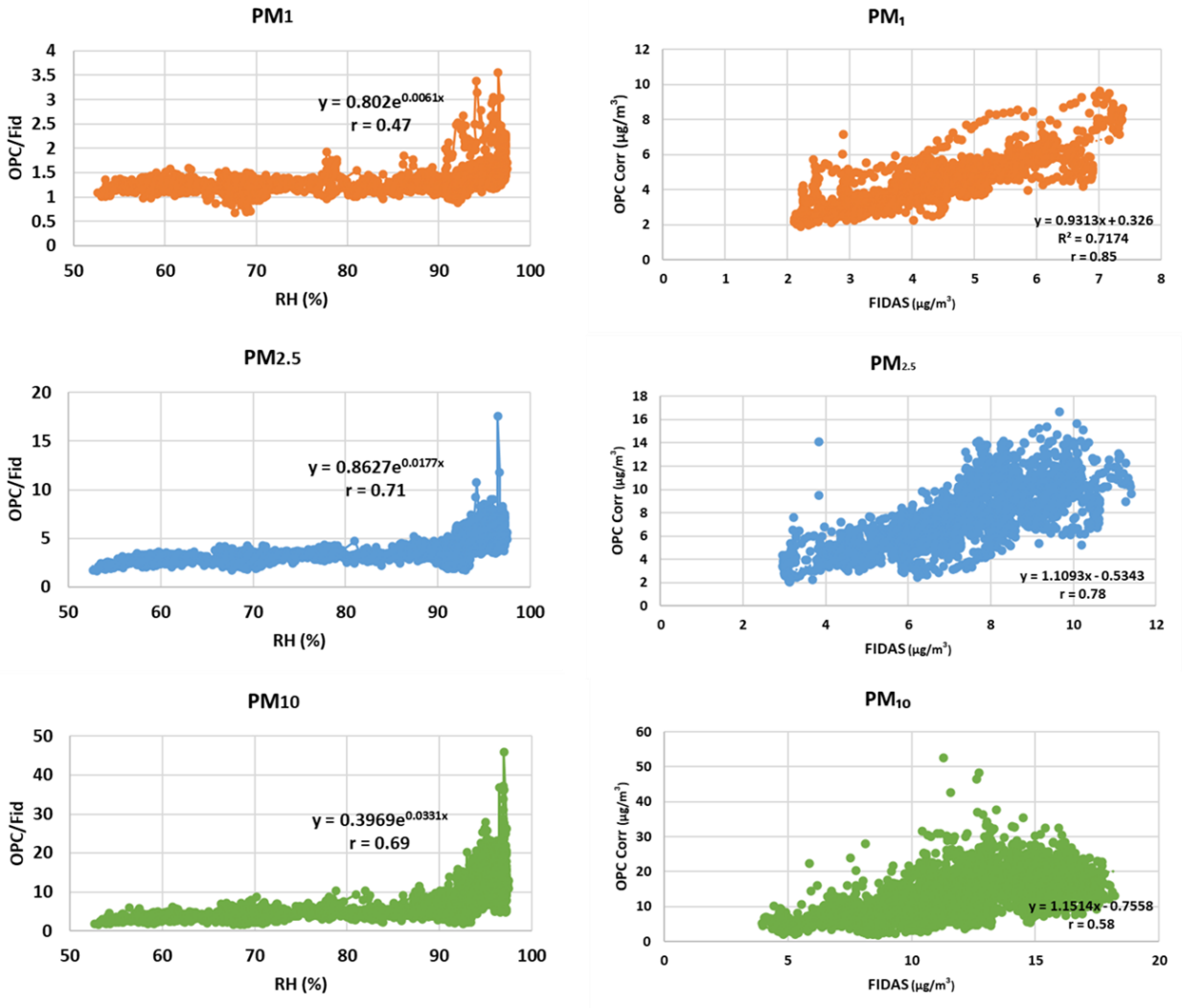

Figure S3. The left-hand panels show the relation between ratio OPC/Fidas vs RH, while the right-hand side panels represent OPC corrected for RH vs FIDAS.

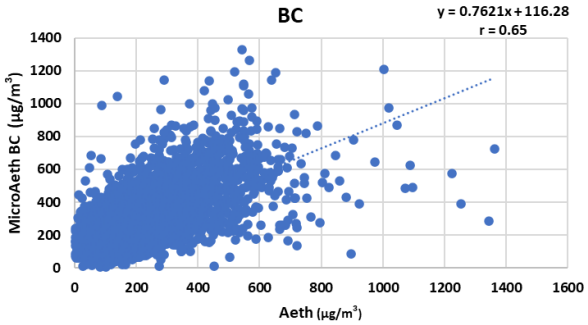

Figure S4. Micro Aeth vs Aethalometer.

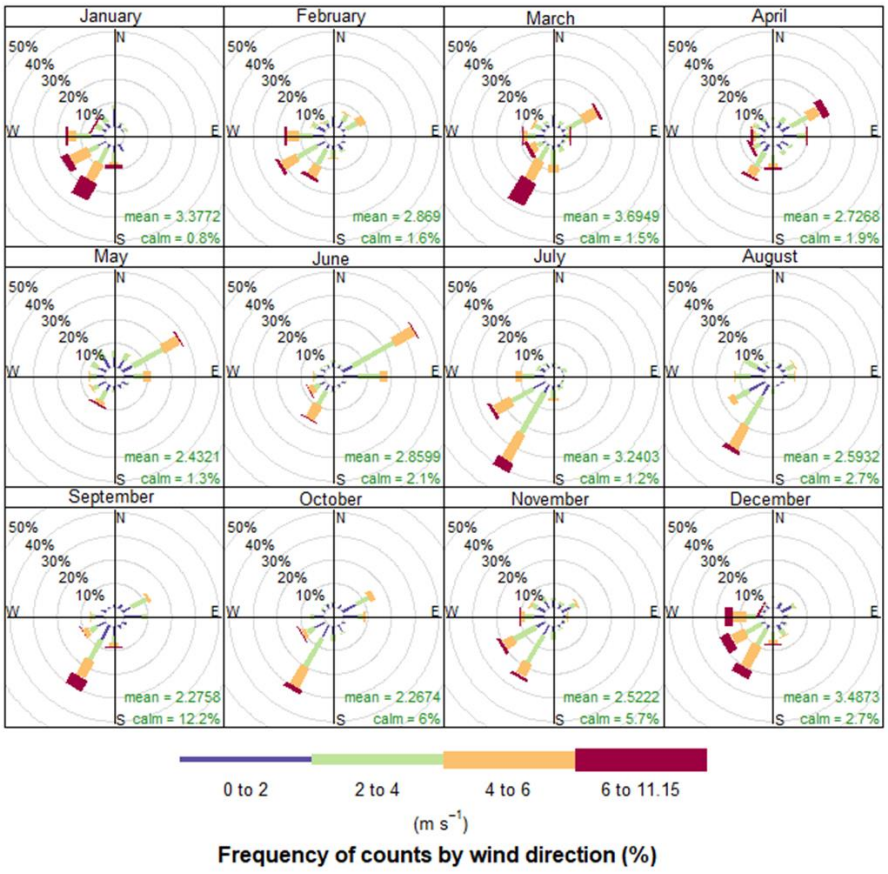

Figure S5. Monthly wind rose in 2023.

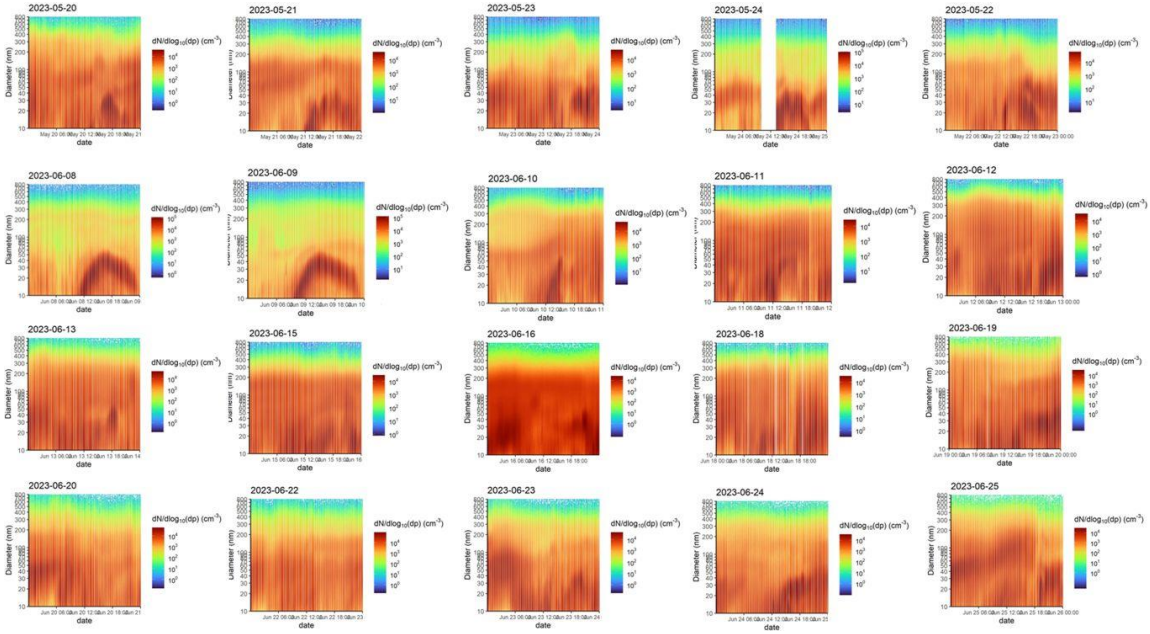

Figure S6. Particle number size distribution on the day of data collection. Data derived from SMPS at BAQS.

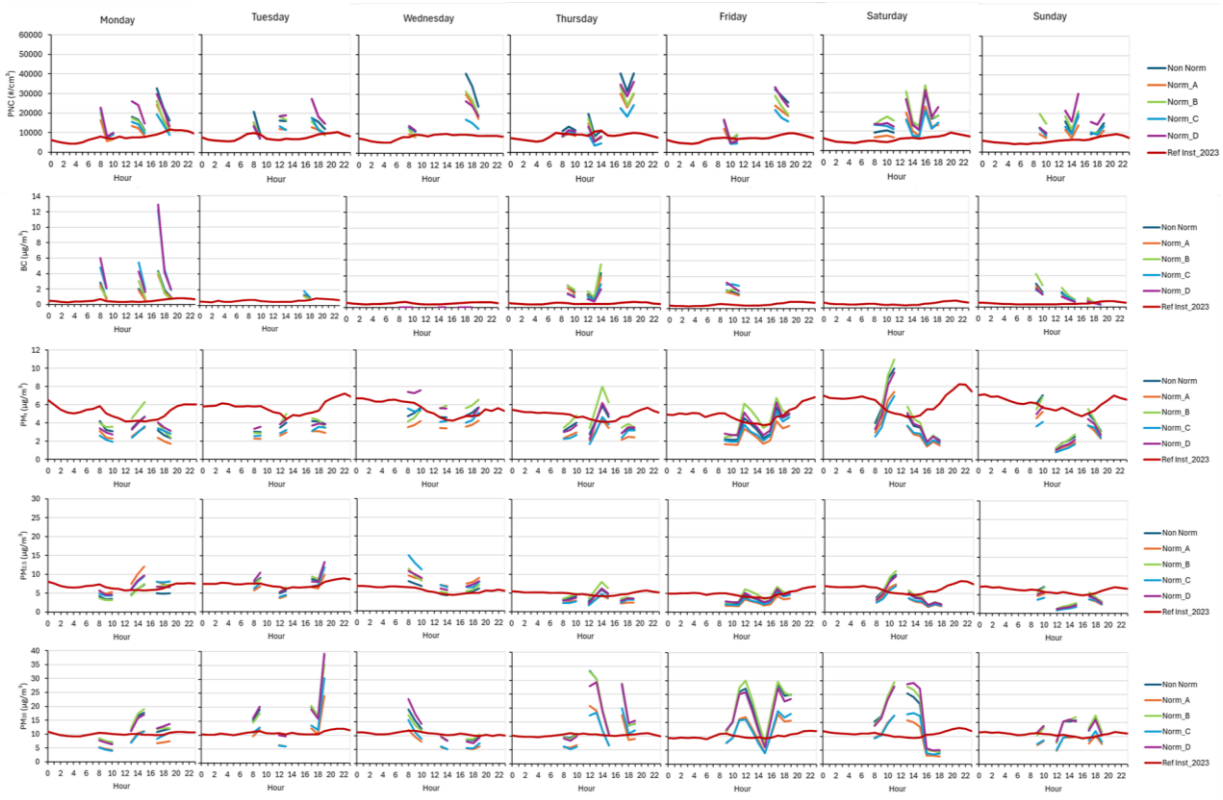

Figure S7. The day of the week and time of day variation of average non-normalized and normalized concentration of pollutant from each method and annual mean concentration derived from reference instruments.

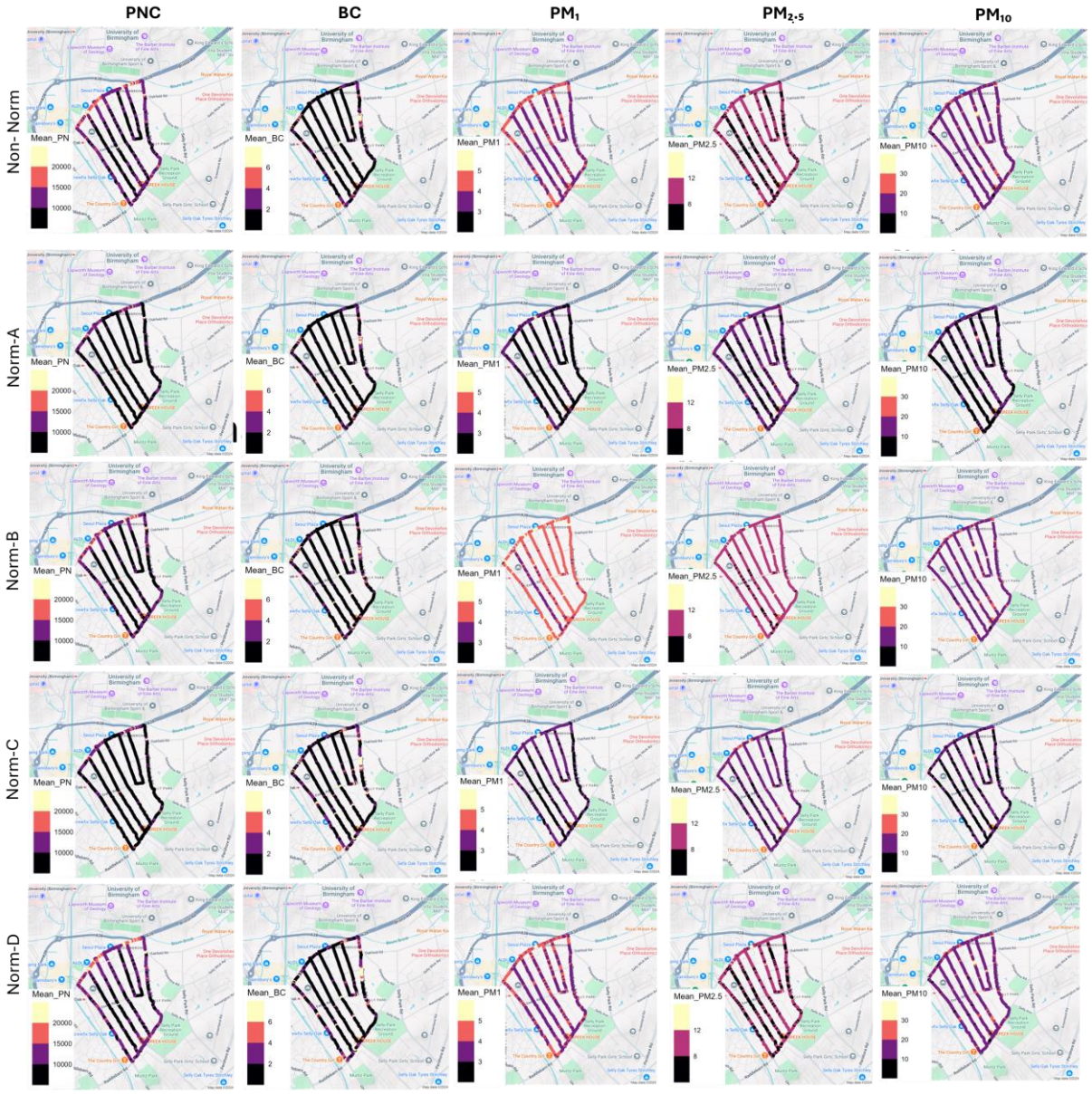

Figure S8. Spatial Map of each pollutant, showing non-normalised and normalised concentrations.

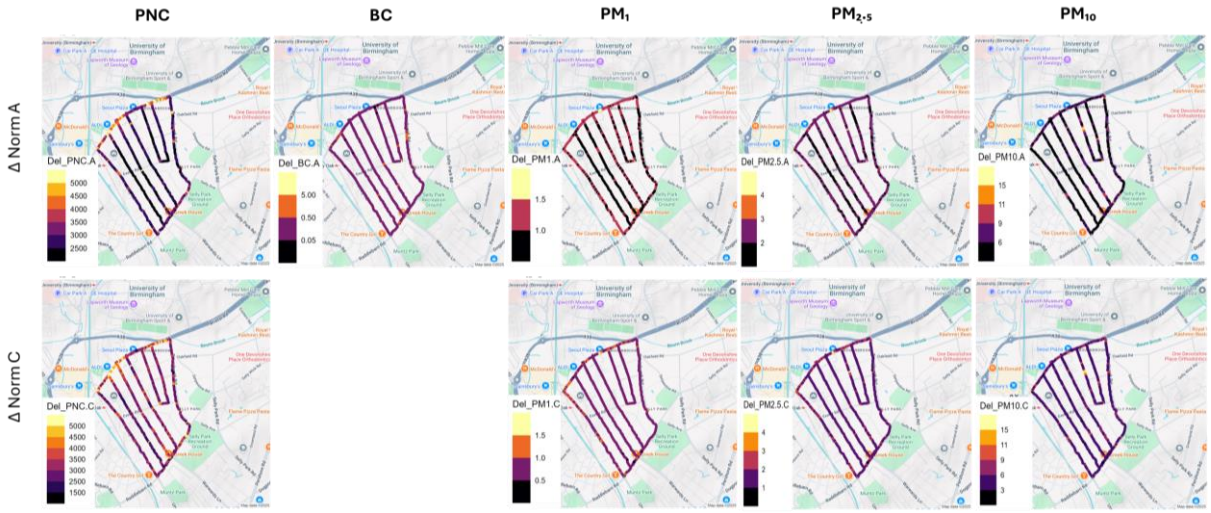

Figure S9. Spatial Map of each pollutant, showing delta (Δ) concentration of non-normalised and normalised concentrations utilizing method A (top) and method C (bottom). The Δ Norm C for BC and the other methods, i.e., B and D, are omitted due to the normalised concentration was higher than the non-normalised concentration and resulting in a negative value

Chapter 6: The Role of Highly Oxygenated Organic Molecules (HOMs) in Nucleation Particle Formation in an Urban Background in Northwestern UK.

Authors: Seny Damayanti[1], James Brean[1], David CS Beddows[1], Alex Rowell[1], James Allan[3,4], Michael Flynn[3], Nathan Watson[3], Francis D. Pope[1], Roy M. Harrison[1,2]

1 Division of Environmental Health and Risk Management, School of Geography, Earth and Environmental Sciences, University of Birmingham, Edgbaston, Birmingham B15 2TT, UK

2Department of Environmental Sciences, Faculty of Meteorology, Environment and Arid Land Agriculture, King Abdulaziz University, Jeddah 21589, Saudi Arabia

3 Department of Earth and Environmental Sciences, School of Natural Sciences, University of Manchester, Manchester M13 9PL, U.K.

4 National Centre for Atmospheric Science, University of Manchester, Manchester M13 9PL, U.K

Abstract:

New particle formation (NPF) serves as a major source of secondary ultrafine particles (UFPs, Dp < 100nm) in urban atmospheres. The interplay of atmospheric factors such as solar radiation and the condensation sink (CS) affects both the occurrence and characteristics of NPF, which may differ between urban areas. While urban NPF has been extensively studied in China and mainland Europe, there is no study examining NPF on a molecular level in the United Kingdom. This study investigated NPF by employing an observational dataset, comprising key gaseous precursors such as sulfuric acid, iodic acid, and highly oxygenated organic molecules (HOMs, i.e., ULVOC, ELVOC, and LVOC) derived from a 1-month summertime campaign in an urban background site in Manchester, UK. The results show that the NPF frequency was 20% of the measurement period, mostly occurred during daylight hours characterized by higher solar radiation, wind speed, and sulfuric acid level, and reduced CS. The particle formation rate correlated well with sulfuric acid concentrations. The origin of incoming air masses was also identified as another crucial factor influencing the NPF occurrence. The concentration of LVOC, important molecules for particle growth, was markedly lower on burst days (i.e., when nucleation occurs without subsequent particle growth). The correlation between particle formation rate (*J*) value, sulfuric acid, and ULVOC suggest that sulfuric acid is the primary driver of NPF, while ULVOC seem to contribute more to particle growth than to initial particle formation.

Keywords: NPF, summer, urban, HOMs, UK.

1. Introduction

Aerosol particles are acknowledged to adversely affect human health (Qin et al., 2024; Trees et al., 2024). The health effects of aerosol particles, specifically those with diameters less than 100 nm, defined as ultrafine particles (UFPs), differ from those of more commonly studied pollutants, such as $PM_{2.5}$. UFPs, which greatly contribute to number concentration in the atmosphere, can readily enter the human lung and subsequently translocating to other organs (Schraufnagel, 2020b).

New particle formation (NPF) is a major contributor to aerosol particle number in the atmosphere (Spracklen et al., 2006; Sun et al., 2024), contributing greatly (54%) to cloud condensation nuclei (CCN) numbers (Gordon et al., 2017), affecting cloud properties and hence Earth's radiative balance (Rosenfeld et al., 2014; Williamson et al., 2019).

Two main stages are involved in the NPF process, including the formation of molecular clusters through the clustering of vapours to form nanocluster aerosol, and their subsequent growth to a larger size (~100nm) over a few days (Kulmala et al., 2001; Lee et al., 2019), primarily via the condensation of oxygenated organic molecules (Kirkby et al., 2023; Kulmala et al., 2017; Lehtipalo et al., 2025; Schervish & Donahue, 2020).

Laboratory (Kirkby et al., 2011; Metzger et al., 2010; Xiao et al., 2021) and field studies (Alam et al., 2003; Ali et al., 2025; Brean et al., 2020a; Cai et al., 2022; Yao et al., 2018) indicate that sulfuric acid is a crucial factor in the initiation of NPF in the atmosphere.

Highly oxygenated organic molecules (HOMs) have been considered as the key species for particle growth in the early stage (Bianchi et al., 2019; Shrivastava et al., 2024; Tröstl et al., 2016). Research has shown that such molecules could also lead to a biogenic nucleation, however, this phenomenon is particularly observed in specific environment, such as boreal forest (Rose et al., 2018), peatland (Huang et al., 2024), and high altitude site (Bianchi et al., 2016). HOMs, organic compounds with a minimum of six oxygen atoms (Bianchi et al., 2019), are formed from autoxidation of volatile organic compounds involving peroxy radicals, or multi-generational oxidation (Garmash et al., 2020). HOMs are capable of driving rapid particle growth in the atmosphere, and the largest of them, typically large dimers, can even form new particles by themselves (Bianchi et al., 2019; Donahue et al., 2012; Schervish & Donahue, 2020; Simon et al., 2020). Other compounds such as ammonia, amines, large organic vapor molecules, and iodine oxoacids play important roles as stabilizer agents before clusters containing sulfuric acid grow to a diameter above 3 nm (He et al., 2023; Kulmala et al., 2017; Kulmala et al., 2013). Iodine oxoacids are particularly crucial in marine and polar regions, where ammonia levels are typically low (He et al., 2023).

Some conditions may inhibit the formation of new particles in the atmosphere. A more polluted atmosphere, characterized by higher concentration of pre-existing particles and thus a higher condensation sink (CS), can suppress NPF (Bousiotis et al., 2021a; Bousiotis et al., 2021b). Increased relative humidity (RH) may increase particle surface area (X. Li et al., 2019), hence enhancing CS. This diminishes sulfuric acid, and thereby decreasing particle formation rate (Hamed et al., 2011). At certain points, higher wind velocity may enhance pollutant dilution (Bousiotis et al., 2021a), whereas

low intensity of UVB during daylight (as a light intensity indicator) has been observed to inhibit NPF (Zhang et al., 2024).

While numerous NPF studies have been conducted in urban areas worldwide (Ali et al., 2025; Brean et al., 2020b; Jiang et al., 2021; H. Lee et al., 2024; Pushpawela et al., 2018; Sebastian et al., 2021; Siakavaras et al., 2016; L. Tao et al., 2023; Zhu et al., 2023), there are no studies showing the mechanism of NPF in the United Kingdom . In fact, NPF is sensitive to the atmospheric environment (Yao et al., 2018), leading to variability in the critical factors that govern this phenomenon.

Manchester is the third most populated city in the UK, with diverse emission sources, including traffic, industries, domestic combustion, and regional transport, all of which might contribute to NPF events. This study presents major NPF precursors, including sulfuric acid, iodic acid, and HOMs to elucidate their dynamics and NPF behaviour, thereby influencing UFP levels in this urban environment.

2. Method

2.1 Sampling Location and period

Sampling was conducted at an urban background site in Manchester, namely Manchester Air Quality Supersite (MAQS, at 53°26'39.2"N 2°12'51.9"W), situated approximately 5 km southeast of the city centre and 10 km northeast of Manchester Airport. The campaign took place for a period of 1.5 months in the summer in 2021, however, due to a technical issue, only data from 11th June to 5th July 2021 were evaluated in this study.

2.2 Instrumentation

A Nano Scanning Mobility Particle Sizer (SMPS, TSI Inc. USA) was deployed to measure particle number size distribution within the range of 4.5 – 65 nm. A nitrate-based Chemical Ionization Mass Spectrometry (CIMS, Aerodyne Inc. USA) was used to quantify a wide range of molecules, including sulfuric acid, iodic acid, and HOMs, with a time resolution of 1 s. The latter instruments ionize sample air using nitrate ions in the chemical ionization stage, then guide the ionised sample to a differentially pumped Atmospheric Pressure Interface (APi), and subsequently to a time-of-flight mass spectrometer for mass-to-charge ratio determination. Further information on the CIMS principles can be found elsewhere (Jokinen et al., 2012; Olin et al., 2022; Zhang et al., 2023). The flow rates of the Nano SMPS and CIMS are 1.5 L/min and 10 L/min, respectively. Both instruments were corrected for inlet line losses.

Several pollutants that have been routinely measured at this site were also analysed. These include PNSD (Dp 15.1 – 661.2 nm), the composition of non-refractory $PM_{2.5}$ (i.e., chloride, nitrate, sulfate, ammonium, and organic compounds), black carbon (BC) and NO_2. These were quantified using a Long SMPS (3082 SMPS and 3750, TSI Inc., USA), an Aerosol Chemical Species Monitor (ACSM, Aerodyne Inc., USA), an Aethalometer (AE33, Magee Scientific, Slovenia), and a Teledyne Model T500U (Teledyne, USA), respectively. The inlet height of the Nano SMPS and CIMS was around 1 metre, whereas other instruments were positioned between 6-7 metres above ground level. All this pollutant data as well as meteorological parameters (i.e., solar radiation, temperature and wind data) were downloaded from the Centre for Environmental Data Analysis (CEDA) archive. All data was averaged at a 10-minute period, with the exception of ACSM data which was measured at a 30-minute average.

2.3 NPF classification and parameters

The NPF classification was performed based on visual identification as described by Kulmala et al. (2012). Three primary features define a day as NPF event day, including (i) an increase in nucleation mode particle number (Dp < 25nm), particularly when a mode appeared at around 5 nm to differentiate it from traffic-source-related particles, (ii) the resultant formation of new, distinctive mode which persists for several hours, and (iii) subsequent growth of this mode.

Key parameters describing NPF events were calculated, including CS, particle formation rate (*J*), and particle growth rate (GR) (Kulmala et al., 2012) :

a) Condensation sink

Condensation sink is a metric that represents the rate at which gaseous molecules, here presumed sulfuric acid, condense onto pre-existing particles, calculated by:

$$\boldsymbol{CS = 4\pi D \sum_{d'_p} \beta_{m,d'_p} d'_p N_{d'_p}} \quad \textbf{Equation 11}$$

Where D is the diffusion coefficient of the condensing vapour as sulfuric acid, dp is particle diameter, Ndp is the particle number at diameter dp, and β_m is a transition-regime correction (Kulmala et al., 2012).

b) Formation Rate

The formation rate at size d_p is calculated by:

$$\boldsymbol{J_{dp} = \frac{dN_{dp}}{d_t} + CoagS_{dp}.N_{dp} + \frac{GR}{\Delta d_p}.N_{dp}} \quad \textbf{Equation 12}$$

Where $\frac{dN_{dp}}{d_t}$ represents the rate at which particles enter the size d_p, and the remaining terms represent the loss mechanism caused by coagulation sink and particle growth

rate. The NanoSMPS is able to measure particles with a diameter down to 5 nm, hence the formation rate of particles at 5 nm (J_5) was calculated. The formation rate at 1.7 nm was estimated from the J_5 values using a method proposed by Lehtinen et al., (2007) (Lehtinen et al., 2007).

c) Coagulation Sink (CoagS)

Coagulation sink is the rate at which a particle (dp) collides and coagulates into a larger particle (>dp) defined as Coagulation Sink ($CoagS_{dp}$). This is calculated by the equation below:

$$\boldsymbol{CoagS_{dp} = \sum_{d'_p=d_p}^{d'_p=max} K(d_p, d'_p) N_{d_p}} \quad \textbf{Equation 13}$$

Where $K(d_p, d'_p)$ refers to the coagulation coefficient between particles sizes dp and d'p.

d) Particle growth rate (GR)

Particle growth rate (GR) is defined as:

$$\boldsymbol{GR = \frac{dD_p}{dt}} \quad \textbf{Equation 14}$$

The calculation of GR is based on the equation proposed by Nieminen et al. (2010). The assumption of condensing vapour density, and concentration weighted mean mass is 1.5 g/cm^3, and ~276 g/mol, respectively, similar to the calculation by Brean et al (2020).

2.4 OOM classification

Organic aerosols exhibit substantial variability in the atmosphere. The volatility basis set (VBS) was introduced to classify this range of organic molecules according to their

volatility, which was subsequently adapted to describe highly oxygenated molecules (Bianchi et al., 2019; Donahue et al., 2011). Employing saturation mass concentrations (c_i^*), OOMs are commonly classified into six different groups, including ultra-low volatile organic compound (ULVOC) for c_i^* ≤ 10^{-9} µg/m^3, extremely low volatile organic compound (ELVOC) for $10^{-8} \leq c_i^* \leq 10^{-5}$ µg/m^3, low volatile organic compound (LVOC) for $10^{-4} \leq c_i^* \leq 10^{-1}$ µg/m^3, semi volatile organic compound (SVOC) for $10^0 \leq c_i^* \leq 10^2$ µg/m^3, intermediate volatile organic compound (IVOC) for $10^3 \leq c_i^* \leq 10^6$ µg/m^3, and volatile organic compound (VOC) for $c_i^* \geq 10^6$ µg/m^3 (Stolzenburg et al., 2022; Simon et al., 2020). HOMs, molecules that are primarily condense onto particles, mainly fall into the class of ULVOC, ELVOC, LVOC (Bianchi et al., 2019; Simon et al., 2020). Therefore, this study focused only on these molecules.

3 Results and discussion

3.1 General condition

Employing the criteria from the previous section, NPF events were recorded on 5 out of 25 measurement days (20%), as highlighted in yellow shade in Fig. S1, whereas 24% of the measurement days exhibited nucleation without subsequent growth, classified as Burst days. The event days had a banana shape, showing an increase to the nucleation mode to > 10^4 #/cm^3, followed by particle growth as seen by the increase in Aitken and Accumulation mode. The event days occurred during daylight hours when the solar radiation level was enhanced (Bousiotis et al., 2021b), with elevated hourly average concentrations of sulfuric acid peaking at 5.6 x 10^6 cm^3. This peak is approximately 50 % lower than that observed in urban Houston (Tiszenkel et al., 2025) and urban Barcelona (Brean et al., 2020a). Furthermore, a distinct air mass origin was

observed, showing that NPF event usually occurred when the wind direction ranged from 200°- 300°.

The NPF period varies from day-to-day, however, it typically takes place between 6 AM to 3 PM. Fig.11 displays the range of concentrations for each measured species, including data from the selected period (6 AM – 3 PM), whereas Fig. S2 shows the boxplot that include the entire day period. Comparing NPF days with non-NPF days, certain pollutants exhibit substantially higher concentrations, including nucleation and Aitken mode particles, sulfuric acid, and wind speed. On burst days, the average concentration was slightly higher than on non-NPF days, with the exception of the Aitken mode, which exhibits the lowest levels, and sulphuric acid, which shows a slight increase compared to NPF days. During those NPF days, accumulation mode, BC, NO_2, HOMs, $PM_{2.5}$ chemical species except for chloride, as well as CS were lower. This reduced concentration was also evident when comparing the NPF to the burst event; however, a higher CS was observed on the burst day.

A significance test was performed to check significant differences between event types for each measured species. A statistical test, specifically the Kruskal-Wallis test followed by a post-hoc pairwise test, was conducted using data from the selected period (6 AM to 3 PM) and revealed a significant difference in the concentrations of all species between NPF and Non-NPF days, except for iodic acid, solar radiation, ozone and chloride. Only ELVOC, solar radiation, and organic compounds exhibit no significant differences between NPF and Burst days. The lack of significant difference in solar radiation intensity between the three event types may indicate that other parameters are more decisive in determining the nucleation process at this study site.

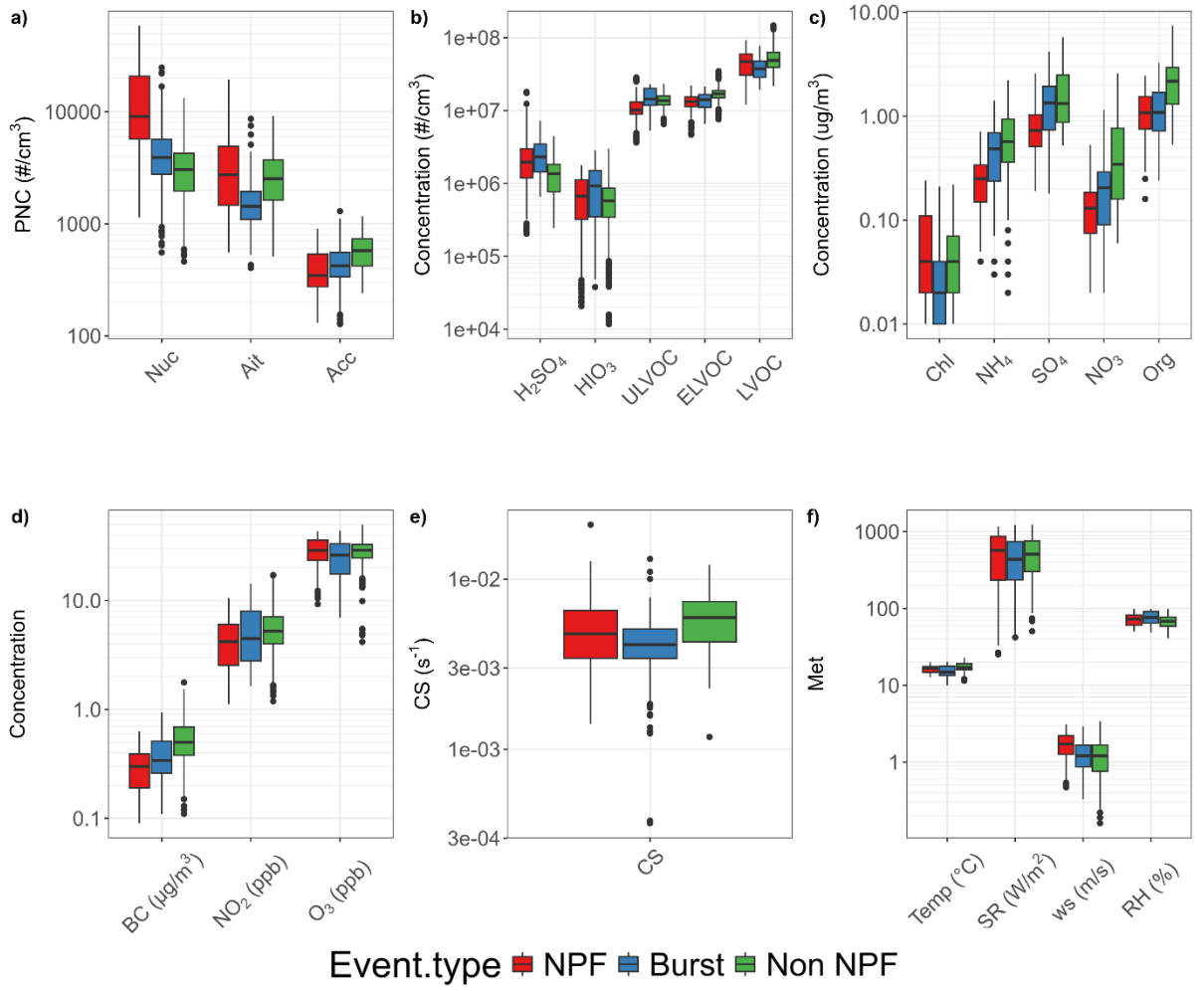

Figure 11. Boxplot of each investigated species using selected period (6 AM- 3 PM). Nuc, Ait, Acc represent nucleation, Aitken, and accumulation mode particles. Temp, SR, ws and RH shows meteorological parameters i.e, temperature, solar radiation intensity, wind speed, and relative humidity, respectively.

The average concentration of nucleation mode particles was significantly higher on NPF days (~1.4 x 10^4 #/cm^3) compared to that on Burst days (~4.7 x 10^3 #/cm^3) and non-NPF (~3.3 x 10^3 #/cm^3) days. Whereas the average concentration of sulfuric acid during this period (~2.5 x 10^6 /cm^3) was nearly double that observed on non-NPF days (1.3 x 10^6 /cm^3), although it was slightly lower than the concentration on Burst days

(2.6 x 10^6 /cm^3). The concentration of iodic acid was slightly higher on Burst days (~ 1 x 10^6 /cm^3) relative to other event types (~ 7 x 10^5 /cm^3 on both NPF and non-NPF days). Nevertheless, as previously mentioned, there was no significant difference in this pollutant concentration among all event types. HOMs were at their lowest during NPF days compared to other event types, with the exemption of LVOC which exhibited elevated level during this period.

Additional features of NPF days were lower concentrations of BC, NO_2, and $PM_{2.5}$ mass and thus lower CS in the atmosphere, suggesting that less polluted days promote nucleation processes in this study area. This finding is consistent with other European urbans studied by Bousiotis et al., (2021). NPF occurred on four weekdays and one weekend day, suggesting that the typical weekly cycle, characterised by elevated vehicle emissions on weekdays and reduced levels on weekends, may not be a substantial determinant at this study site.

A slightly elevated average air temperature was observed on non-NPF (17.4 °C) compared to Burst, and NPF days (15.5°C, and 16.4°C, respectively). On NPF days, a stronger wind speed of 1.7 m/s was recorded, whereas a slightly lower was found on burst and non-NPF (~1.2 m/s). Fig. S3 illustrates a clear variation in the origin of incoming air masses, with south-westerly to north-westerly wind predominating on NPF days. Meanwhile, the predominant easterly wind was consistently observed on burst and non-NPF days, likely carrying a higher pollutant concentration that elevates CS and hence inhibits the NPF.

3.2 Diurnal cycle by Event type

Fig. 12 illustrates the diurnal cycle of the average concentration of the investigated parameters categorized by event type, whilst the average diurnal ratios of NPF to Non-NPF and NPF to Burst is shown in Fig. S4. Nucleation on NPF days began in the early morning and intensified at around 9 AM, continuing until midday when solar radiation and temperature were elevated to a mean maximum of ~900 W/m^2 and 18 °C, respectively, as indicated by the increase in nucleation mode particles at around 1 PM to a mean maximum of 26 x 10^3 #/cm^3. The concentration at this peak was around sevenfold and fivefold more than that observed in non-NPF and burst days and was preceded by a sharp rise in sulfuric acid to a mean maximum of 5.7 x 10^6 #/cm^3. The peak in sulfuric acid has been linked to a photochemical reaction (Lu et al., 2019; Yang et al., 2021), this peak occurred when the generation of these molecules increases rapidly while its removal rate, as indicated by a low condensation sink, decreases during that period.

The increase in nucleation mode concentrations followed by an elevation of Aitken mode, indicating the growth of particles to a larger size. A clear diurnal cycle of iodic acid was observed, peaking at midday across all event types. This pattern aligns with a finding from a long-term observation in two polluted urban environments, i.e., Nanjing and Beijing, which shows elevated levels during the daytime across all seasons, attributing photochemical reactions as the primary source in those areas. Although there is no statistically significant difference in iodic acid concentration between the event types, a higher concentration of this pollutant (evidenced by its elevated ratio of NPF to Non-NPF at midday, Fig. S4) may also facilitate nucleation, as indicated by a study in an urban region which found that iodic acid could increase the survival

probability of particles with a diameter of less than < 3 nm (Zhang et al., 2024). And an analogous product, iodous acid (HIO_2) can enhance the nucleation rate of sulfuric acid particles more efficiently than dimethylamine (He et al., 2023).

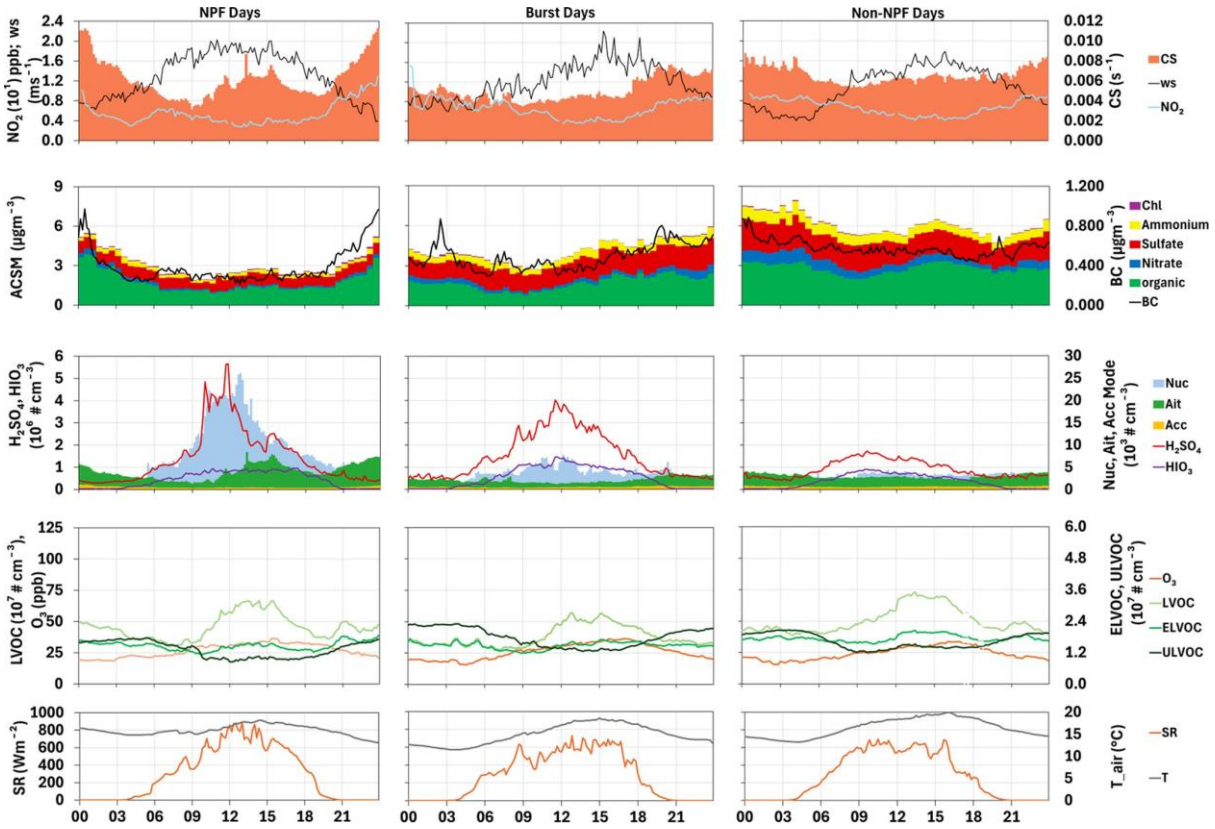

Figure 12. Diurnal cycle of average concentration of pollutant and meteorological factor differentiate by event type.

On NPF days, wind speed began to increase in the early morning and continue until the afternoon, whereas the CS and the concentration NO_2 and $PM_{2.5}$, particularly BC organics, nitrate, and ammonium, decreased during that period. This indicates that stronger wind in the early morning has facilitated the dispersion of existing particles, reducing pollution levels and suppressing CS, and thereby promotes NPF events at this study site. The initial nucleation phase, characterised by an increase in nucleation mode occurred at around 5 AM, following a period when BC and chemical composition

concentration (apart from chloride) were approximately 50% lower than those observed on non-NPF days (Fig. S4 b). A slight increase in BC and NO_2 concentrations during morning rush hours might be linked to the traffic emissions, however, this is concurrent with the increase to H_2SO_4 (Fig. S5), and therefore NPF and traffic emissions likely occur in parallel. On non-NPF days, a substantially higher concentration of BC and $PM_{2.5}$ chemical speciation was detected, occurring nearly throughout the day. This further supported that elevated pollution levels, which could serve as CS may inhibit the nucleation process.

The diurnal cycle of HOMs frequently exhibited peaks in the afternoon for ELVOC and LVOC, while a decline occurred in ULVOC. Elevated levels of ELVOC and LVOC alongside the ozone just after the increase of solar radiation during the daylight may result from photochemical reactions, which is also consistent with that observed in urban Beijing (Qiao et al., 2021) and in a forest environment (Lai et al., 2024). Whereas the nighttime peak in the ULVOC concentration is likely due to cross-reaction of peroxy radical (RO_2) (Zang et al., 2024) which is inhibited in the daytime by hydroperoxyl radical (HO_2) chemistry. This may explain the decrease of these large molecules as solar radiation increases.

3.3 Concentration and Mass Fraction of ACSM and HOMs

Utilising data from the selected timeframe (6 AM to 3 PM), the average $PM_{2.5}$ mass concentration on non-NPF days was approximately three times higher than that on NPF days (Fig, 13). The higher average concentration of VOC on Non-NPF (~ 46 x 10^6 /cm^3) compared to Burst (~ 38 x 10^6 /cm^3) and NPF days (~ 42 x 10^6 /cm^3) may have led to a higher concentration of HOMs. This is due to less condensation onto

newly-formed particles, as condensation is the primary removal mechanism for these molecules in the atmosphere (Bianchi et al., 2019) .

Nitrate-rich aerosol was identified on non-NPF days, with an average proportion of 11%, compared to 6% on NPF days. A higher fraction of aerosol nitrate on Non-NPF days was also observed in NPF studies in urban Beijing (Du et al., 2022), and urban Delhi (Ali et al., 2025). Such pollutant can be formed during daylight via a photochemical reaction between NO_2 and hydroxyl radicals (Yang et al., 2022). The substantially higher NO_2 concentration on non-NPF days, primarily originating from local sources as depicted in the polar plot (Fig. S6), may have led to an increased concentration of aerosol nitrate during that period.

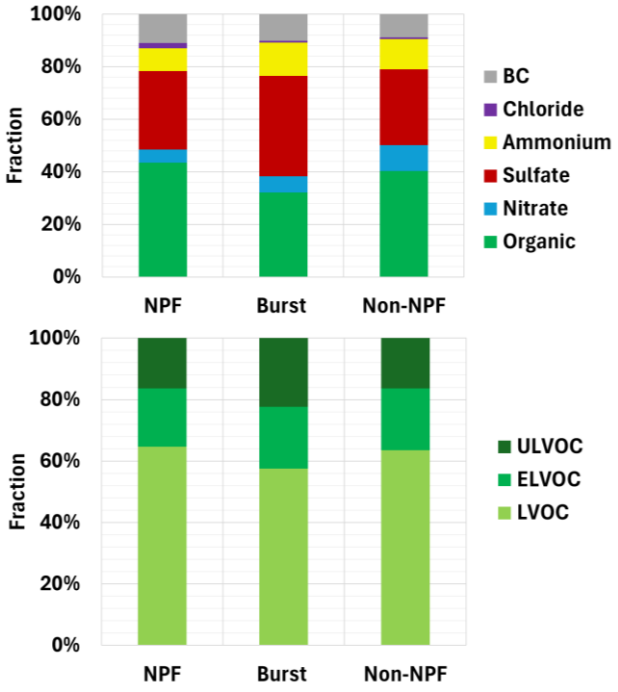

Figure 13. The average concentration and Mass Fraction of $PM_{2.5}$ (top) and HOMs (bottom) using selected period data (6 AM- 3 PM).

Globally, OOMs quantified by a nitrate- CIMS vary from 10^7 – 10^9 cm^{-3}, with the highest concentration in summer, and the lowest in winter (Y. Guo et al., 2022; Qiao et al., 2021). The total average concentration of HOMs from our measurement ranging from 7 x 10^7 to 8.6 x 10^8 cm^{-3}, utilising both selected data and all-day data period across all event types. The concentration of HOMs on non-NPF days was the highest among all event types, however, no notable difference was found between the fraction of ULVOC, ELVOC, and LVOC within the total HOMs on NPF and Non-NPF days. A substantial concentration of condensable vapors led to a high growth rate (Lee et al., 2024). The concentration of LVOC, a crucial component for particle growth, was markedly lower on burst days, which may explain the inability of newly formed particles to grow in the atmosphere during that period.

3.4 Mechanism of NPF

The particle growth rate on NPF days (Fig. S7) varied from 1.4 nm/h to 5.9 nm/h, with an average of 3.6 nm/h. This rate is comparable to that observed at other urban background sites in the UK and Europe (±3-4 nm/h) (Bousiotis et al., 2021, Bousiotis et al., 2019), and in urban Australia (4.6 nm/h, (Cheung et al., 2011), but is lower than that recorded in urban Korea, which is surrounded by agricultural, commercial, and residential areas (6.7 nm/h) (Haebum Lee et al., 2024). The most intense NPF event, characterised by the peak particle formation rate at 5 nm occurred on 11th June 2021, reaching a maximum of approximately 23 $cm^{-3}s^{-1}$ at noon (12 PM).

We further investigated the diurnal pattern of meteorological parameters and some gaseous precursors on that day, as presented in Fig.14. It is shown that J_5 increases as the solar radiation, temperature, and wind speed increase, with the peak of J_5

coincident with their peak when the origin of the air mass is coming from south-westerly wind. However, within an hour, it then abruptly drops from 23 $cm^{-3}s^{-1}$ to only 1 $cm^{-3}s^{-1}$, coinciding with a large decrease of solar radiation, and a change of wind direction to north-westerly that probably carried a cooler air mass, as indicated by lower air temperature. This indicates that all those meteorological parameters are crucial for NPF events in this area.

CS and chemical composition demonstrated a closely similar pattern, suggesting that the ions within $PM_{2.5}$ contribute substantially to the condensation sink. However, a sudden drop in chemical components and CS was observed as the wind direction substantially changed. However, it then continued to increase until the end of the day, which might explain the growth of newly formed particles, or the air mass coming from a new direction bringing more pollutants and hence increasing both CS and chemical component concentrations.

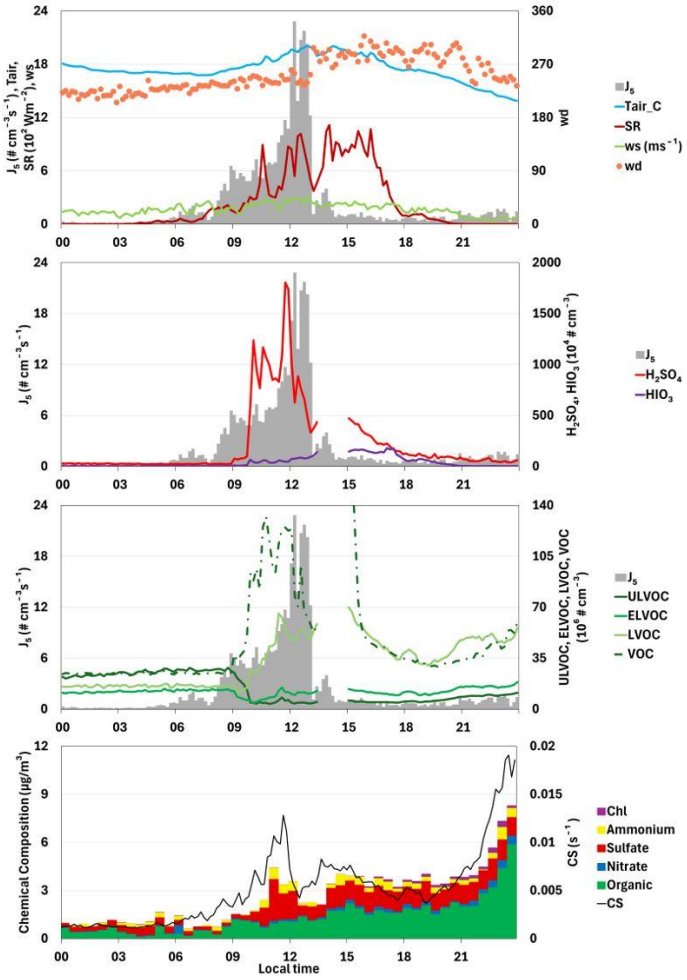

Figure 14. The diurnal cycle of J_5 and measured pollutants on 11th June 2021.

Iodic acid was observed to rise in the presence of sunlight, which occurred before the increase of sulfuric acid at around 9AM. This molecule, as well as iodous acid (HIO_2), are well known as an efficient nucleator particularly in marine environments (He et al., 2023), however, in urban environments, iodic and iodous acid are especially good at enhancing sulfuric acid nucleation, and can increase the survival probability of sub-3 nm particles through enhanced growth rates (Zhang et al., 2024). The coast is located approximately 50 km to the west side from our study area, and high concentrations of iodic acid precursors from this region are likely contributing to enhanced nucleation in the study site. Another study shows that iodic acid has also been detected at quite high

concentrations, with a maximum average concentration of $3x10^5$ molecules /cm^3, even at a remote location over 400 km from the nearest coast (Kürten et al., 2016). Other notable increases in J_5 occurred just before 12 PM, which was preceded by a substantial increase in sulfuric acid and iodic acid, in elevated solar radiation as well as temperature, further confirming their presence in governing NPF.

The concentrations of iodous acid (HIO_2) and iodic acid (HIO_3) were measured using the CIMS during the campaign. The detection limits are influenced by other compounds, leading to variability across different samples, and appear to be around 1x 10^3 /cm³.The table S1 presents a comparison of HIO_x concentrations from several NPF studies. Both Zhang et al. (2024), which used long-term urban measurements in Beijing and Nanjing, and the current study show that HIO_2 concentrations were an order of magnitude lower than those of HIO_3, consistent with prior studies (He et al., 2021; Zhang et al., 2024). The measured HIO_2 in this study were lower than those in coastal and boreal forest areas but comparable to or lower than those in Beijing and Nanjing. The relationship between HIO_2 and HIO_3 (Fig. S8) suggests that data below the detection limit or missing data (i.e., approximately 5% of the data for each compound) would lie in the lower left of the plot, while the gradient extending to the upper right is likely to reflect the actual iodous-to-iodic acid ratio in the air samples. There appear to be sufficient iodine acids in the samples to affect the nucleation process.

The sudden drop of HOMs, particularly ULVOC and ELVOC, concentration was observed at around 9AM, coinciding with a rise of sulfuric acid, and it was followed by the substantial increase in J_5. Given that important role of HOMs in the particle growth,

as highlighted by prior studies (Tröstl et al., 2016), the decrease in HOMs concentration may indicates that they were consumed during the growth of newly formed particles.

Fig 5. shows a positive correlation between sulfuric acid and *J*, both $J_{1.7}$ and J_5, implying its crucial role in initiating NPF at this study site, as frequently shown in previous studies (Brean et al., 2020a; Kirkby et al., 2016). The average value of J_5 (1.7 ± 2.6 cm^{-3} s^{-1}) was approximately sevenfold lower than that of $J_{1.7}$ (12.4 ± 52.8 cm^{-3} s^{-1}), indicating that a considerable number of particles at 1.7 nm are lost to coagulation rather than growing into larger particles of 5 nm. A markedly higher level of $J_{1.7}$ compared to J_5 was also seen in another study conducted in a forest environment (Yu et al., 2014). Both $J_{1.7}$ and J_5 occurred at a low sulfuric acid level (~1.7 x 10^5 molecules/cm^3), indicating that this minimal concentration was sufficient to initiate cluster formation, and further supports the concept that sulfuric acid is the primary driving factor for NPF at this study location, as is commonly observed in other urban NPF studies. Contrastingly, the increase in sulfuric acid concentration and thus formation rate is associated with a decrease in ULVOC levels. A chamber study that aimed to replicate NPF in a boreal forest by employing key components and NOx found a correlation between J and HOMs in the absence of NO_x. They concluded that sulfuric acid, ammonia, and HOMs interact mutually to promote particle formation, while NO_x inhibits NPF (Lehtipalo et al., 2018). This phenomenon was similarly observed in another chamber study that simulated polluted atmospheric conditions (Xiao et al., 2021). While such variables are difficult to control in field studies, our findings suggest that although ULVOC may not be the primary drivers of NPF in this study area, however, their high concentrations (>10^7 molecules/cm^3) likely contribute to the NPF. Quantifying the contribution of ULVOC to NPF is also notoriously challenging, and to

date, such studies have only been done through chamber experiments (Lehtipalo et al., 2018; Xiao et al., 2021) or in pristine environments (Bianchi et al., 2016; Huang et al., 2024; Rose et al., 2018).

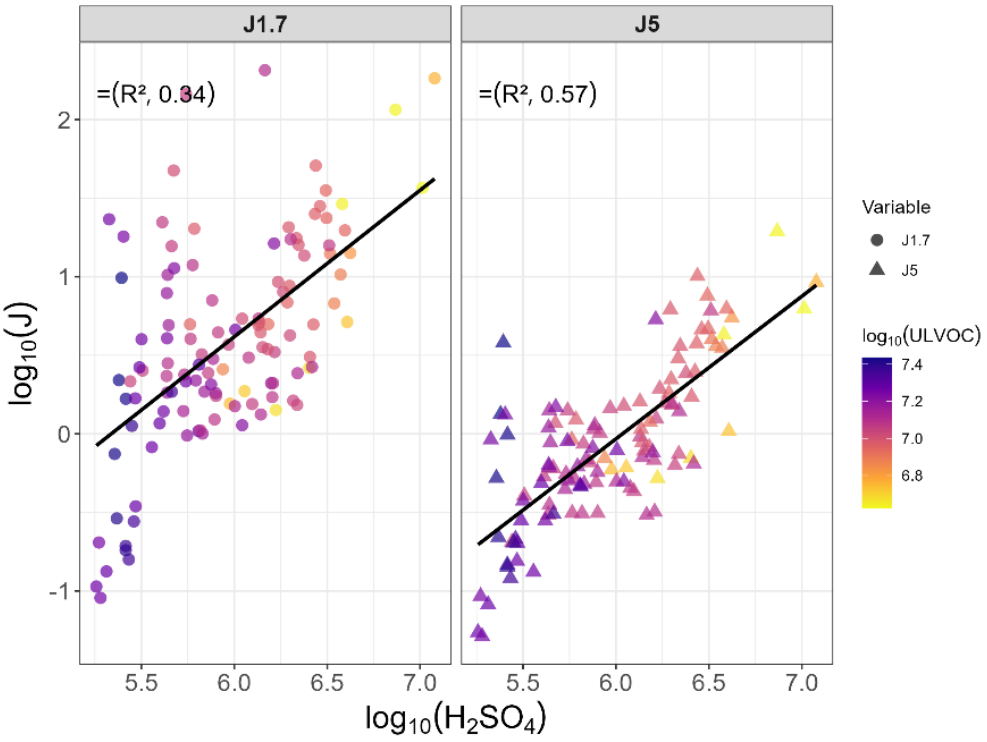

Figure 15. Formation rate at 1.7 nm ($J_{1.7}$) and 5 nm (J_5) Vs sulfuric acid concentration coloured by ULVOC concentration using selected period data.

Fig. S9 shows the diurnal cycle of the components of the *J* equation, showing that the coagulation sink is the dominant part compared to other components (Cai & Jiang, 2017). This evidence suggests that the majority of newly formed particles are eliminated from the atmosphere through the coagulation sink process.

3 Conclusions

This study examined the molecular characteristics of NPF at an urban background site in the UK, a country where no prior research has been conducted. NPF events occurred during daytime, marked by an increase in solar radiation intensity, wind speed, and a substantial rise in sulfuric acid levels, which were nearly double compared to non-NPF days. NPF mostly took place when wind direction varied between 200°- 300°, indicating either a source of clean air, or a source of NPF precursors. Aligned with most prior urban NPF studies, less polluted days promote nucleation, as indicated by the lower level of BC, NO_2, and $PM_{2.5}$ and thus CS during NPF days compared to burst and non-NPF days. The important role of ELVOC in particle growth is highlighted by the significantly lower levels of this molecule on burst days, which may explain the failure of newly formed particles to grow. On non-NPF days, the HOMs concentration was found to be the highest, however, the fraction of ULVOC, ELVOC, and LVOC within total HOMs was relatively similar to that observed on NPF days.

The average particle growth rate (GR) was comparable to that reported in other urban areas in the UK, Europe, and Australia, approximately 3.6 nm/h. An analysis of the diurnal pattern of particle formation rate at 5 nm (J_5) shows the substantial increase, which was preceded by a substantial increase in sulfuric acid and iodic acid under conditions of high solar radiation and temperature. A positive correlation was found between sulfuric acid and J (including both $J_{1.7}$ and J_5). The lowest level of J was detected at a low sulfuric acid level (~1.7×10^5 molecules/cm^3), thereby confirming the role of these molecules as a primary driver of NPF in this study site. The increase in J and sulfuric acid corresponds with the decrease in ULVOC levels. This suggest that

ULVOC may not be a major determinant of NPF, however, due to their elevated concentration, they may contribute more to particle growth than to the initial step of the nucleation process. These findings offer additional evidence that could improve the understanding of factors influencing NPF, particularly in the UK urban areas.

Acknowledgements

SD would like to thank to Indonesia Endowment Fund for Education (LPDP), Ministry of Finance, Republic of Indonesia, for their financial support toward her PhD study.

CRediT authorship contribution statement: **Seny Damayanti**: Writing-original draft, Conceptualization, Resources, Visualization, Methodology. **James Brean**: Conceptualization, Resources, Visualization, Methodology, Writing-review & editing. **Francis D. Pope**: Validation, Supervision, Conceptualization, Writing- review & editing. **Roy M. Harrison**: Validation, Supervision, Conceptualization, Writing- review & editing, Funding acquisition.

Funding

This work was supported by OSCA project under grant agreement NE/T001984/1

References

Alam, A., Shi, J. P., & Harrison, R. M. (2003). Observations of new particle formation in urban air. *Journal of Geophysical Research: Atmospheres*, *108*(D3). https://doi.org/https://doi.org/10.1029/2001JD001417

Ali, U., Singh, V., Faisal, M., Kumar, M., & Gani, S. (2025). Exploring the influence of physical and chemical factors on new particle formation in a polluted megacity [10.1039/D4EA00114A]. *Environmental Science: Atmospheres*, *5*(1), 25-47. https://doi.org/10.1039/D4EA00114A

Bianchi, F., Kurtén, T., Riva, M., Mohr, C., Rissanen, M. P., Roldin, P., Berndt, T., Crounse, J. D., Wennberg, P. O., Mentel, T. F., Wildt, J., Junninen, H., Jokinen, T., Kulmala, M., Worsnop, D. R., Thornton, J. A., Donahue, N.,

Kjaergaard, H. G., & Ehn, M. (2019). Highly Oxygenated Organic Molecules (HOM) from Gas-Phase Autoxidation Involving Peroxy Radicals: A Key Contributor to Atmospheric Aerosol. *Chemical Reviews*, *119*(6), 3472-3509. https://doi.org/10.1021/acs.chemrev.8b00395

Bianchi, F., Tröstl, J., Junninen, H., Frege, C., Henne, S., Hoyle, C. R., Molteni, U., Herrmann, E., Adamov, A., Bukowiecki, N., Chen, X., Duplissy, J., Gysel, M., Hutterli, M., Kangasluoma, J., Kontkanen, J., Kürten, A., Manninen, H. E., Münch, S., . . . Baltensperger, U. (2016). New particle formation in the free troposphere: A question of chemistry and timing. *Science*, *352*(6289), 1109-1112. https://doi.org/doi:10.1126/science.aad5456

Bousiotis, D., Brean, J., Pope, F. D., Dall'Osto, M., Querol, X., Alastuey, A., Perez, N., Petäjä, T., Massling, A., Nøjgaard, J. K., Nordstrøm, C., Kouvarakis, G., Vratolis, S., Eleftheriadis, K., Niemi, J. V., Portin, H., Wiedensohler, A., Weinhold, K., Merkel, M., . . . Harrison, R. M. (2021). The effect of meteorological conditions and atmospheric composition in the occurrence and development of new particle formation (NPF) events in Europe. *Atmos. Chem. Phys.*, *21*(5), 3345-3370. https://doi.org/10.5194/acp-21-3345-2021

Bousiotis, D., Pope, F. D., Beddows, D. C. S., Dall'Osto, M., Massling, A., Nøjgaard, J. K., Nordstrøm, C., Niemi, J. V., Portin, H., Petäjä, T., Perez, N., Alastuey, A., Querol, X., Kouvarakis, G., Mihalopoulos, N., Vratolis, S., Eleftheriadis, K., Wiedensohler, A., Weinhold, K., . . . Harrison, R. M. (2021). A phenomenology of new particle formation (NPF) at 13 European sites. *Atmos. Chem. Phys.*, *21*(15), 11905-11925. https://doi.org/10.5194/acp-21-11905-2021

Brean, J., Beddows, D. C. S., Shi, Z., Temime-Roussel, B., Marchand, N., Querol, X., Alastuey, A., Minguillón, M. C., & Harrison, R. M. (2020a). Molecular insights into new particle formation in Barcelona, Spain. *Atmos. Chem. Phys.*, *20*(16), 10029-10045. https://doi.org/10.5194/acp-20-10029-2020

Brean, J., Beddows, D. C. S., Shi, Z. B., Temime-Roussel, B., Marchand, N., Querol, X., Alastuey, A., Minguillón, M. C., & Harrison, R. M. (2020b). Molecular insights into new particle formation in Barcelona, Spain. *Atmospheric Chemistry and Physics*, *20*(16), 10029-10045. https://doi.org/10.5194/acp-20-10029-2020

Cai, R., & Jiang, J. (2017). A new balance formula to estimate new particle formation rate: reevaluating the effect of coagulation scavenging. *Atmos. Chem. Phys.*, *17*(20), 12659-12675. https://doi.org/10.5194/acp-17-12659-2017

Cai, R. L., Deng, C. J., Stolzenburg, D., Li, C. X., Guo, J. C., Kerminen, V. M., Jiang, J. K., Kulmala, M., & Kangasluoma, J. (2022). Survival probability of new atmospheric particles: closure between theory and measurements from 1.4 to 100 nm. *Atmospheric Chemistry and Physics*, *22*(22), 14571-14587. https://doi.org/10.5194/acp-22-14571-2022

Cheung, H. C., Morawska, L., & Ristovski, Z. D. (2011). Observation of new particle formation in subtropical urban environment. *Atmos. Chem. Phys.*, *11*(8), 3823-3833. https://doi.org/10.5194/acp-11-3823-2011

Donahue, N. M., Epstein, S. A., Pandis, S. N., & Robinson, A. L. (2011). A two-dimensional volatility basis set: 1. organic-aerosol mixing thermodynamics. *Atmos. Chem. Phys.*, *11*(7), 3303-3318. https://doi.org/10.5194/acp-11-3303-2011

Donahue, N. M., Kroll, J. H., Pandis, S. N., & Robinson, A. L. (2012). A two-dimensional volatility basis set – Part 2: Diagnostics of organic-aerosol evolution. *Atmos. Chem. Phys.*, *12*(2), 615-634. https://doi.org/10.5194/acp-12-615-2012

Du, W., Cai, J., Zheng, F., Yan, C., Zhou, Y., Guo, Y., Chu, B., Yao, L., Heikkinen, L. M., Fan, X., Wang, Y., Cai, R., Hakala, S., Chan, T., Kontkanen, J., Tuovinen, S., Petäjä, T., Kangasluoma, J., Bianchi, F., . . . Kulmala, M. (2022). Influence of Aerosol Chemical Composition on Condensation Sink Efficiency and New Particle Formation in Beijing. *Environmental Science & Technology Letters*, *9*(5), 375-382. https://doi.org/10.1021/acs.estlett.2c00159

Garmash, O., Rissanen, M. P., Pullinen, I., Schmitt, S., Kausiala, O., Tillmann, R., Zhao, D., Percival, C., Bannan, T. J., Priestley, M., Hallquist, Å. M., Kleist, E., Kiendler-Scharr, A., Hallquist, M., Berndt, T., McFiggans, G., Wildt, J., Mentel, T. F., & Ehn, M. (2020). Multi-generation OH oxidation as a source for highly oxygenated organic molecules from aromatics. *Atmos. Chem. Phys.*, *20*(1), 515-537. https://doi.org/10.5194/acp-20-515-2020

Gordon, H., Kirkby, J., Baltensperger, U., Bianchi, F., Breitenlechner, M., Curtius, J., Dias, A., Dommen, J., Donahue, N. M., Dunne, E. M., Duplissy, J., Ehrhart, S., Flagan, R. C., Frege, C., Fuchs, C., Hansel, A., Hoyle, C. R., Kulmala, M., Kürten, A., . . . Carslaw, K. S. (2017). Causes and importance of new particle formation in the present-day and preindustrial atmospheres. *Journal of Geophysical Research: Atmospheres*, *122*(16), 8739-8760. https://doi.org/https://doi.org/10.1002/2017JD026844

Guo, Y., Yan, C., Liu, Y., Qiao, X., Zheng, F., Zhang, Y., Zhou, Y., Li, C., Fan, X., Lin, Z., Feng, Z., Zhang, Y., Zheng, P., Tian, L., Nie, W., Wang, Z., Huang, D., Daellenbach, K. R., Yao, L., . . . Kulmala, M. (2022). Seasonal variation in oxygenated organic molecules in urban Beijing and their contribution to secondary organic aerosol. *Atmos. Chem. Phys.*, *22*(15), 10077-10097. https://doi.org/10.5194/acp-22-10077-2022

Hamed, A., Korhonen, H., Sihto, S.-L., Joutsensaari, J., Järvinen, H., Petäjä, T., Arnold, F., Nieminen, T., Kulmala, M., Smith, J. N., Lehtinen, K. E. J., & Laaksonen, A. (2011). The role of relative humidity in continental new particle formation. *Journal of Geophysical Research: Atmospheres*, *116*(D3). https://doi.org/https://doi.org/10.1029/2010JD014186

He, X.-C., Simon, M., Iyer, S., Xie, H.-B., Rörup, B., Shen, J., Finkenzeller, H., Stolzenburg, D., Zhang, R., Baccarini, A., Tham, Y. J., Wang, M., Amanatidis, S., Piedehierro, A. A., Amorim, A., Baalbaki, R., Brasseur, Z., Caudillo, L., Chu, B., . . . Kulmala, M. (2023). Iodine oxoacids enhance nucleation of sulfuric acid particles in the atmosphere. *Science*, *382*(6676), 1308-1314. https://doi.org/doi:10.1126/science.adh2526

Huang, W., Junninen, H., Garmash, O., Lehtipalo, K., Stolzenburg, D., Lampilahti, J. L. P., Ezhova, E., Schallhart, S., Rantala, P., Aliaga, D., Ahonen, L., Sulo, J., Quéléver, L. L. J., Cai, R., Alekseychik, P., Mazon, S. B., Yao, L., Blichner, S. M., Zha, Q., . . . Bianchi, F. (2024). Potential pre-industrial–like new particle formation induced by pure biogenic organic vapors in Finnish peatland. *Science Advances*, *10*(14), eadm9191. https://doi.org/doi:10.1126/sciadv.adm9191

Jiang, S. H., Zhang, F., Ren, J. Y., Chen, L., Yan, X., Liu, J. Y., Sun, Y. L., & Li, Z. Q. (2021). Evaluation of the contribution of new particle formation to cloud droplet number concentration in the urban atmosphere. *Atmospheric Chemistry and Physics*, *21*(18), 14293-14308. https://doi.org/10.5194/acp-21-14293-2021

Jokinen, T., Sipilä, M., Junninen, H., Ehn, M., Lönn, G., Hakala, J., Petäjä, T., Mauldin Iii, R. L., Kulmala, M., & Worsnop, D. R. (2012). Atmospheric sulphuric acid and neutral cluster measurements using CI-APi-TOF. *Atmos. Chem. Phys.*, *12*(9), 4117-4125. https://doi.org/10.5194/acp-12-4117-2012

Kirkby, J., Amorim, A., Baltensperger, U., Carslaw, K. S., Christoudias, T., Curtius, J., Donahue, N. M., Haddad, I. E., Flagan, R. C., Gordon, H., Hansel, A., Harder, H., Junninen, H., Kulmala, M., Kürten, A., Laaksonen, A., Lehtipalo, K., Lelieveld, J., Möhler, O., . . . Worsnop, D. R. (2023). Atmospheric new particle formation from the CERN CLOUD experiment. *Nature Geoscience*, *16*(11), 948-957. https://doi.org/10.1038/s41561-023-01305-0

Kirkby, J., Curtius, J., Almeida, J., Dunne, E., Duplissy, J., Ehrhart, S., Franchin, A., Gagné, S., Ickes, L., Kürten, A., Kupc, A., Metzger, A., Riccobono, F., Rondo, L., Schobesberger, S., Tsagkogeorgas, G., Wimmer, D., Amorim, A., Bianchi, F., . . . Kulmala, M. (2011). Role of sulphuric acid, ammonia and galactic cosmic rays in atmospheric aerosol nucleation. *Nature*, *476*(7361), 429-433. https://doi.org/10.1038/nature10343

Kirkby, J., Duplissy, J., Sengupta, K., Frege, C., Gordon, H., Williamson, C., Heinritzi, M., Simon, M., Yan, C., Almeida, J., Tröstl, J., Nieminen, T., Ortega, I. K., Wagner, R., Adamov, A., Amorim, A., Bernhammer, A.-K., Bianchi, F., Breitenlechner, M., . . . Curtius, J. (2016). Ion-induced nucleation of pure biogenic particles. *Nature*, *533*(7604), 521-526. https://doi.org/10.1038/nature17953

Kulmala, M., Dal, M. M., M., M. J., L., P., M., V., P., A., P., M., K., H., & and O'dowd, C. D. (2001). On the formation, growth and composition of nucleation mode particles. *Tellus B: Chemical and Physical Meteorology*, *53*(4), 479-490. https://doi.org/10.3402/tellusb.v53i4.16622

Kulmala, M., Kerminen, V. M., Petäjä, T., Ding, A. J., & Wang, L. (2017). Atmospheric gas-to-particle conversion: why NPF events are observed in megacities? [10.1039/C6FD00257A]. *Faraday Discussions*, *200*(0), 271-288. https://doi.org/10.1039/C6FD00257A

Kulmala, M., Kontkanen, J., Junninen, H., Lehtipalo, K., Manninen, H. E., Nieminen, T., Petäjä, T., Sipilä, M., Schobesberger, S., Rantala, P., Franchin, A., Jokinen, T., Järvinen, E., Äijälä, M., Kangasluoma, J., Hakala, J., Aalto, P. P., Paasonen, P., Mikkilä, J., . . . Worsnop, D. R. (2013). Direct Observations of Atmospheric Aerosol Nucleation. *Science*, *339*(6122), 943-946. https://doi.org/doi:10.1126/science.1227385

Kulmala, M., Petäjä, T., Nieminen, T., Sipilä, M., Manninen, H. E., Lehtipalo, K., Dal Maso, M., Aalto, P. P., Junninen, H., Paasonen, P., Riipinen, I., Lehtinen, K. E. J., Laaksonen, A., & Kerminen, V.-M. (2012). Measurement of the nucleation of atmospheric aerosol particles. *Nature Protocols*, *7*(9), 1651-1667. https://doi.org/10.1038/nprot.2012.091

Kürten, A., Bergen, A., Heinritzi, M., Leiminger, M., Lorenz, V., Piel, F., Simon, M., Sitals, R., Wagner, A. C., & Curtius, J. (2016). Observation of new particle formation and measurement of sulfuric acid, ammonia, amines and highly

oxidized organic molecules at a rural site in central Germany. *Atmos. Chem. Phys.*, *16*(19), 12793-12813. https://doi.org/10.5194/acp-16-12793-2016
Lai, S., Qi, X., Huang, X., Lou, S., Chi, X., Chen, L., Liu, C., Liu, Y., Yan, C., Li, M., Liu, T., Nie, W., Kerminen, V. M., Petäjä, T., Kulmala, M., & Ding, A. (2024). New particle formation induced by anthropogenic–biogenic interactions on the southeastern Tibetan Plateau. *Atmos. Chem. Phys.*, *24*(4), 2535-2553. https://doi.org/10.5194/acp-24-2535-2024
Lee, H., Cho, H., Yoon, Y. J., Kim, J., Lee, B. Y., & Park, K. (2024). Comparison of new particle formation events in urban, agricultural, and arctic environments. *Atmospheric Environment*, *333*, Article 120634. https://doi.org/10.1016/j.atmosenv.2024.120634
Lee, H., Cho, H., Yoon, Y. J., Kim, J., Lee, B. Y., & Park, K. (2024). Comparison of new particle formation events in urban, agricultural, and arctic environments. *Atmospheric Environment*, *333*, 120634. https://doi.org/https://doi.org/10.1016/j.atmosenv.2024.120634
Lee, S. H., Gordon, H., Yu, H., Lehtipalo, K., Haley, R., Li, Y. X., & Zhang, R. Y. (2019). New Particle Formation in the Atmosphere: From Molecular Clusters to Global Climate. *Journal of Geophysical Research-Atmospheres*, *124*(13), 7098-7146. https://doi.org/10.1029/2018jd029356
Lehtinen, K. E. J., Dal Maso, M., Kulmala, M., & Kerminen, V.-M. (2007). Estimating nucleation rates from apparent particle formation rates and vice versa: Revised formulation of the Kerminen–Kulmala equation. *Journal of Aerosol Science*, *38*(9), 988-994. https://doi.org/https://doi.org/10.1016/j.jaerosci.2007.06.009
Lehtipalo, K., Nieminen, T., Schobesberger, S., Ehn, M., Kulmala, M., & Kerminen, V.-M. (2025). How the understanding of atmospheric new particle formation has evolved along with the development of measurement and analysis methods. *Journal of Aerosol Science*, *184*, 106494. https://doi.org/https://doi.org/10.1016/j.jaerosci.2024.106494
Lehtipalo, K., Yan, C., Dada, L., Bianchi, F., Xiao, M., Wagner, R., Stolzenburg, D., Ahonen, L. R., Amorim, A., Baccarini, A., Bauer, P. S., Baumgartner, B., Bergen, A., Bernhammer, A.-K., Breitenlechner, M., Brilke, S., Buchholz, A., Mazon, S. B., Chen, D., . . . Worsnop, D. R. (2018). Multicomponent new particle formation from sulfuric acid, ammonia, and biogenic vapors. *Science Advances*, *4*(12), eaau5363. https://doi.org/doi:10.1126/sciadv.aau5363
Li, X., Chee, S., Hao, J., Abbatt, J. P. D., Jiang, J., & Smith, J. N. (2019). Relative humidity effect on the formation of highly oxidized molecules and new particles during monoterpene oxidation. *Atmos. Chem. Phys.*, *19*(3), 1555-1570. https://doi.org/10.5194/acp-19-1555-2019
Metzger, A., Verheggen, B., Dommen, J., Duplissy, J., Prevot, A. S. H., Weingartner, E., Riipinen, I., Kulmala, M., Spracklen, D. V., Carslaw, K. S., & Baltensperger, U. (2010). Evidence for the role of organics in aerosol particle formation under atmospheric conditions. *Proceedings of the National Academy of Sciences*, *107*(15), 6646-6651. https://doi.org/doi:10.1073/pnas.0911330107
Olin, M., Okuljar, M., Rissanen, M. P., Kalliokoski, J., Shen, J., Dada, L., Lampimäki, M., Wu, Y., Lohila, A., Duplissy, J., Sipilä, M., Petäjä, T., Kulmala, M., & Dal Maso, M. (2022). Measurement report: Atmospheric new particle formation in a coastal agricultural site explained with binPMF analysis of nitrate CI-APi-

TOF spectra. *Atmos. Chem. Phys.*, *22*(12), 8097-8115. https://doi.org/10.5194/acp-22-8097-2022

Pushpawela, B., Jayaratne, R., & Morawska, L. (2018). Differentiating between particle formation and growth events in an urban environment. *Atmospheric Chemistry and Physics*, *18*(15), 11171-11183. https://doi.org/10.5194/acp-18-11171-2018

Qiao, X., Yan, C., Li, X., Guo, Y., Yin, R., Deng, C., Li, C., Nie, W., Wang, M., Cai, R., Huang, D., Wang, Z., Yao, L., Worsnop, D. R., Bianchi, F., Liu, Y., Donahue, N. M., Kulmala, M., & Jiang, J. (2021). Contribution of Atmospheric Oxygenated Organic Compounds to Particle Growth in an Urban Environment. *Environmental Science & Technology*, *55*(20), 13646-13656. https://doi.org/10.1021/acs.est.1c02095

Qin, S. J., Zeng, Q. G., Zeng, H. X., Li, S. P., Andersson, J., Zhao, B., Oudin, A., Kanninen, K. M., Jalava, P., Jin, N. X., Yang, M., Lin, L. Z., Liu, R. Q., Dong, G. H., & Zeng, X. W. (2024). Neurotoxicity of fine and ultrafine particulate matter: A comprehensive review using a toxicity pathway-oriented adverse outcome pathway framework. *Science of the Total Environment*, *947*, Article 174450. https://doi.org/10.1016/j.scitotenv.2024.174450

Rose, C., Zha, Q., Dada, L., Yan, C., Lehtipalo, K., Junninen, H., Mazon, S. B., Jokinen, T., Sarnela, N., Sipilä, M., Petäjä, T., Kerminen, V.-M., Bianchi, F., & Kulmala, M. (2018). Observations of biogenic ion-induced cluster formation in the atmosphere. *Science Advances*, *4*(4), eaar5218. https://doi.org/doi:10.1126/sciadv.aar5218

Rosenfeld, D., Sherwood, S., Wood, R., & Donner, L. (2014). Climate Effects of Aerosol-Cloud Interactions. *Science*, *343*(6169), 379-380. https://doi.org/doi:10.1126/science.1247490

Schervish, M., & Donahue, N. M. (2020). Peroxy radical chemistry and the volatility basis set. *Atmos. Chem. Phys.*, *20*(2), 1183-1199. https://doi.org/10.5194/acp-20-1183-2020

Schraufnagel, D. E. (2020). The health effects of ultrafine particles. *Experimental & Molecular Medicine 52*.

Sebastian, M., Kanawade, V. P., & Pierce, J. R. (2021). Observation of sub-3nm particles and new particle formation at an urban location in India. *Atmospheric Environment*, *256*, Article 118460. https://doi.org/10.1016/j.atmosenv.2021.118460

Shrivastava, M., Zhang, J., Zaveri, R. A., Zhao, B., Pierce, J. R., O'Donnell, S. E., Fast, J. D., Gaudet, B., Shilling, J. E., Zelenyuk, A., Murphy, B. N., Pye, H. O. T., Zhang, Q., Trousdell, J., Zhang, R., Li, Y., & Chen, Q. (2024). Anthropogenic Extremely Low Volatility Organics (ELVOCs) Govern the Growth of Molecular Clusters Over the Southern Great Plains During the Springtime. *129*. https://doi.org/https://doi.org/10.1029/2024jd041212

Journal Name: Journal of Geophysical Research. Atmospheres; Journal Volume: 129; Journal Issue: 21

Siakavaras, D., Samara, C., Petrakakis, M., & Biskos, G. (2016). Nucleation events at a coastal city during the warm period: Kerbside versus urban background measurements. *Atmospheric Environment*, *140*, 60-68. https://doi.org/https://doi.org/10.1016/j.atmosenv.2016.05.054

Simon, M., Dada, L., Heinritzi, M., Scholz, W., Stolzenburg, D., Fischer, L., Wagner, A. C., Kürten, A., Rörup, B., He, X. C., Almeida, J., Baalbaki, R., Baccarini, A., Bauer, P. S., Beck, L., Bergen, A., Bianchi, F., Bräkling, S., Brilke, S., . . . Curtius, J. (2020). Molecular understanding of new-particle formation from α-pinene between −50 and +25 °C. *Atmos. Chem. Phys.*, *20*(15), 9183-9207. https://doi.org/10.5194/acp-20-9183-2020

Spracklen, D. V., Carslaw, K. S., Kulmala, M., Kerminen, V. M., Mann, G. W., & Sihto, S. L. (2006). The contribution of boundary layer nucleation events to total particle concentrations on regional and global scales. *Atmos. Chem. Phys.*, *6*(12), 5631-5648. https://doi.org/10.5194/acp-6-5631-2006

Sun, J., Hermann, M., Weinhold, K., Merkel, M., Birmili, W., Yang, Y., Tuch, T., Flentje, H., Briel, B., Ries, L., Couret, C., Elsasser, M., Sohmer, R., Wirtz, K., Meinhardt, F., Schütze, M., Bath, O., Hellack, B., Kerminen, V. M., . . . Wiedensohler, A. (2024). Measurement report: Contribution of atmospheric new particle formation to ultrafine particle concentration, cloud condensation nuclei, and radiative forcing – results from 5-year observations in central Europe. *Atmos. Chem. Phys.*, *24*(18), 10667-10687. https://doi.org/10.5194/acp-24-10667-2024

Tao, L., Zhou, Z., Tao, J., Zhang, L. M., Wu, C., Li, J. W., Yue, D. L., Wu, Z. J., Zhang, Z. S., Yuan, Z. Y., Huang, J. J., & Wang, B. G. (2023). High contribution of new particle formation to ultrafine particles in four seasons in an urban atmosphere in south China. *Science of the Total Environment*, *889*, Article 164202. https://doi.org/10.1016/j.scitotenv.2023.164202

Tiszenkel, L., Flynn, J. H., Dodero, A., & Lee, S.-H. (2025). Sulfuric acid, base, and low-volatility organics contribute to aerosol nucleation in urban Houston. *Communications Earth & Environment*, *6*(1), 364. https://doi.org/10.1038/s43247-025-02310-4

Trees, I., Yu, F. Q., Deng, X. L., Luo, G., Zhang, W. J., & Lin, S. (2024). Ultrafine Particles and Hospital Visits for Chronic Lower Respiratory Diseases in New York State. *Annals of the American Thoracic Society*, *21*(8), 1147-1155. https://doi.org/10.1513/AnnalsATS.202303-267OC

Tröstl, J., Chuang, W. K., Gordon, H., Heinritzi, M., Yan, C., Molteni, U., Ahlm, L., Frege, C., Bianchi, F., Wagner, R., Simon, M., Lehtipalo, K., Williamson, C., Craven, J. S., Duplissy, J., Adamov, A., Almeida, J., Bernhammer, A.-K., Breitenlechner, M., . . . Baltensperger, U. (2016). The role of low-volatility organic compounds in initial particle growth in the atmosphere. *Nature*, *533*(7604), 527-531. https://doi.org/10.1038/nature18271

Williamson, C. J., Kupc, A., Axisa, D., Bilsback, K. R., Bui, T., Campuzano-Jost, P., Dollner, M., Froyd, K. D., Hodshire, A. L., Jimenez, J. L., Kodros, J. K., Luo, G., Murphy, D. M., Nault, B. A., Ray, E. A., Weinzierl, B., Wilson, J. C., Yu, F., Yu, P., . . . Brock, C. A. (2019). A large source of cloud condensation nuclei from new particle formation in the tropics. *Nature*, *574*(7778), 399-403. https://doi.org/10.1038/s41586-019-1638-9

Xiao, M., Hoyle, C. R., Dada, L., Stolzenburg, D., Kürten, A., Wang, M., Lamkaddam, H., Garmash, O., Mentler, B., Molteni, U., Baccarini, A., Simon, M., He, X. C., Lehtipalo, K., Ahonen, L. R., Baalbaki, R., Bauer, P. S., Beck, L., Bell, D., . . . Dommen, J. (2021). The driving factors of new particle formation and growth in

the polluted boundary layer. *Atmos. Chem. Phys.*, *21*(18), 14275-14291. https://doi.org/10.5194/acp-21-14275-2021

Yang, S., Yuan, B., Peng, Y., Huang, S., Chen, W., Hu, W., Pei, C., Zhou, J., Parrish, D. D., Wang, W., He, X., Cheng, C., Li, X. B., Yang, X., Song, Y., Wang, H., Qi, J., Wang, B., Wang, C., . . . Shao, M. (2022). The formation and mitigation of nitrate pollution: comparison between urban and suburban environments. *Atmos. Chem. Phys.*, *22*(7), 4539-4556. https://doi.org/10.5194/acp-22-4539-2022

Yao, L., Garmash, O., Bianchi, F., Zheng, J., Yan, C., Kontkanen, J., Junninen, H., Mazon, S. B., Ehn, M., Paasonen, P., Sipilä, M., Wang, M., Wang, X., Xiao, S., Chen, H., Lu, Y., Zhang, B., Wang, D., Fu, Q., . . . Wang, L. (2018). Atmospheric new particle formation from sulfuric acid and amines in a Chinese megacity. *Science*, *361*(6399), 278-281. https://doi.org/doi:10.1126/science.aao4839

Yu, H., John, O., N., S. J., B., G. A., P., K. V., Yi, Y., Yiying, L., Kevin, H., Thomas, K., Roger, S., Chris, G., G., P. S., Lianhong, G., Jyri, M., & and Lee, S.-H. (2014). New Particle Formation and Growth in an Isoprene-Dominated Ozark Forest: From Sub-5 nm to CCN-Active Sizes. *Aerosol Science and Technology*, *48*(12), 1285-1298. https://doi.org/10.1080/02786826.2014.984801

Zang, H., Luo, Z., Li, C., Li, Z., Huang, D., & Zhao, Y. (2024). Nocturnal atmospheric synergistic oxidation reduces the formation of low-volatility organic compounds from biogenic emissions. *Atmos. Chem. Phys.*, *24*(20), 11701-11716. https://doi.org/10.5194/acp-24-11701-2024

Zhang, Y., Li, D. Z. T., He, X. C., Nie, W., Deng, C. J., Cai, R. L., Liu, Y. L., Guo, Y. S., Liu, C., Li, Y. R., Chen, L. D., Li, Y. Y., Hua, C. J., Liu, T. Y., Wang, Z. C., Xie, J. L., Wang, L., Petaejae, T., Bianchi, F., . . . Kulmala, M. (2024). Iodine oxoacids and their roles in sub-3 nm particle growth in polluted urban environments. *Atmospheric Chemistry and Physics*, *24*(3), 1873-1893. https://doi.org/10.5194/acp-24-1873-2024

Zhang, Y., Liu, R., Yang, D., Guo, Y., Li, M., & Hou, K. (2023). Chemical ionization mass spectrometry: Developments and applications for on-line characterization of atmospheric aerosols and trace gases. *TrAC Trends in Analytical Chemistry*, *168*, 117353. https://doi.org/https://doi.org/10.1016/j.trac.2023.117353

Zhu, W. B., Hu, B., Liu, Z. R., Pan, Y. P., Han, J. X., Li, C. H., Xu, M., Yang, S. H., Yin, Y. N., Zhou, J. X., Ji, D. S., & Wang, Y. S. (2023). Reduction of anthropogenic emissions enhanced atmospheric new particle formation: Observational evidence during the Beijing 2022 Winter Olympics. *Atmospheric Environment*, *314*, Article 120094. https://doi.org/10.1016/j.atmosenv.2023.120094

Supplementary Information

The Role of Highly Oxygenated Organic Molecules (HOMs) in Nucleation Particle Formation in an Urban Background in Northwestern UK.

Table S1. HIO_x typical range from various NPF studies

Study	Location	HIO_2 typical range ($molecules/cm^3$)	HIO_3 typical range ($molecules/cm^3$)
(Zhang et al., 2024)	Beijing (Urban)	$1x10^3 – 1x10^5$	$5x10^3 - 2x10^6$
	Nanjing (Urban)	$1x10^3 – 3x10^5$	$10^4 – 3x10^5$
Present study (Urban)	Manchester (Urban)	$< 1x10^3 - 1 \times 10^5$	$3 \times 10^3 - 3 \times 10^6$
(Jokinen et al., 2022)	Finland (Boreal Forest)		$10^6 - 10^7$
(Sipilä et al., 2016)	Mace head, Ireland (Pristine coastal site)		$10^7 - 10^8$

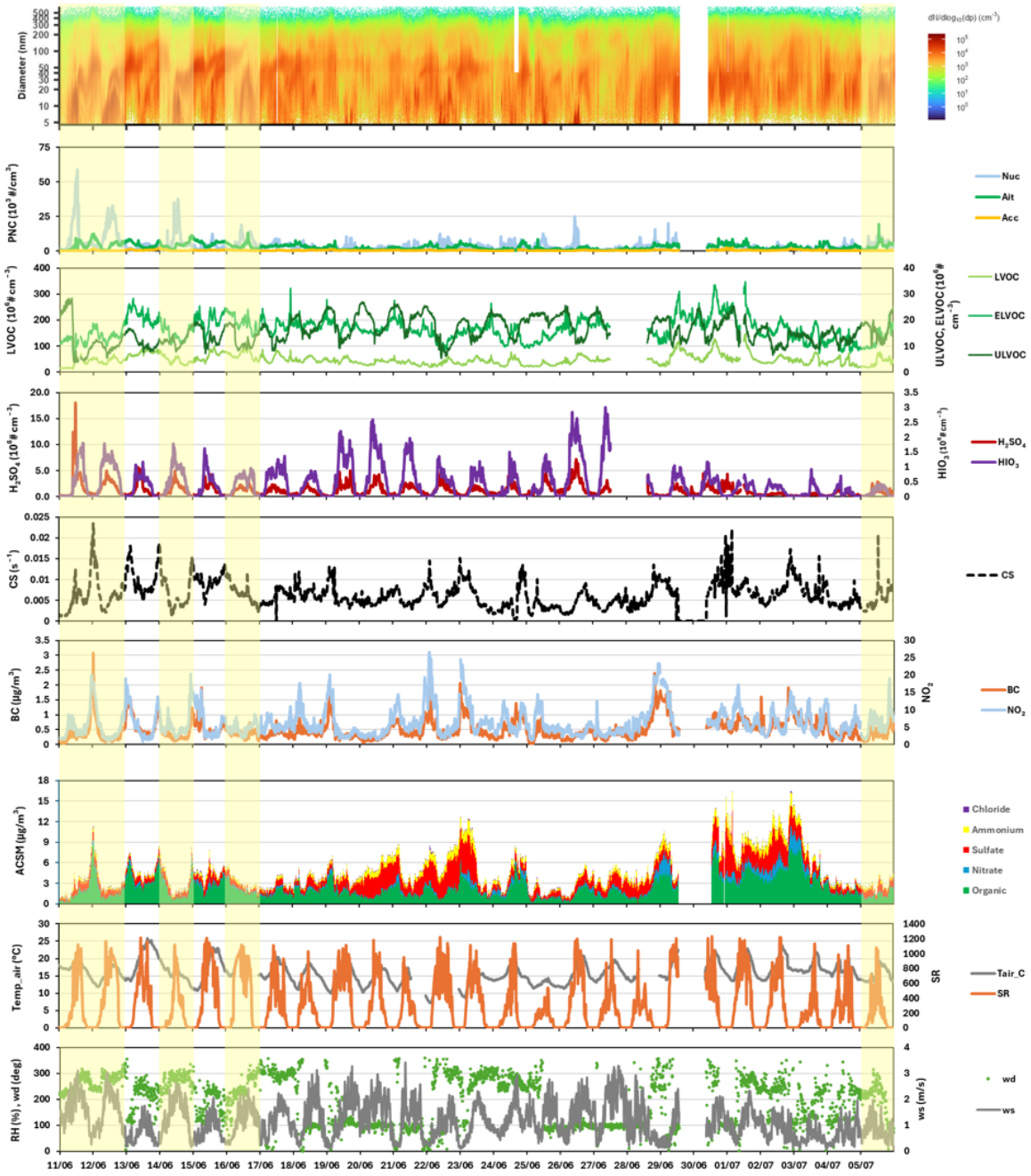

Fig S1. Time plot of investigated pollutant over campaign period. NPF event days are highlighted in yellow shade.

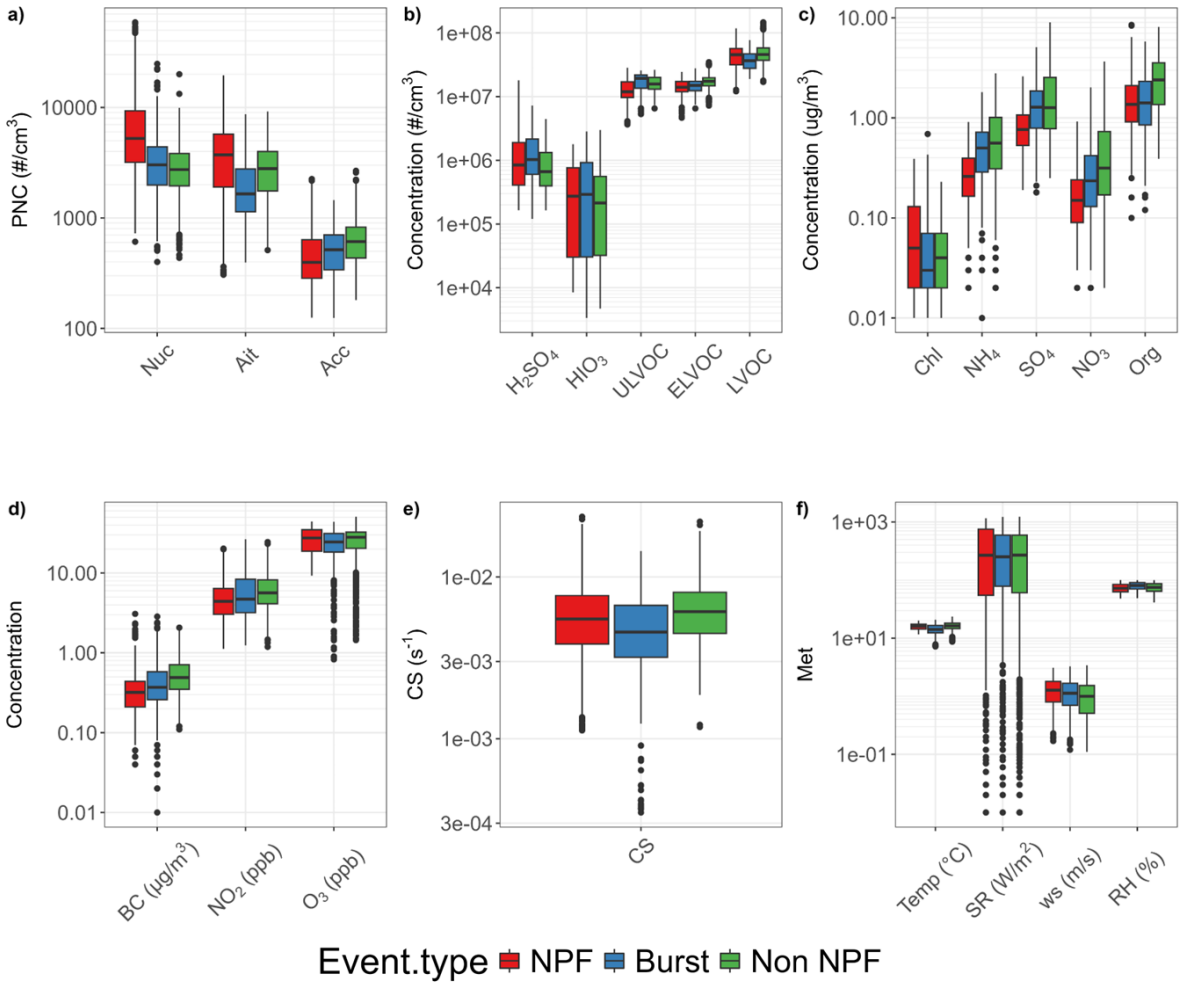

Figure S2. Boxplot of each investigated species using All day period.

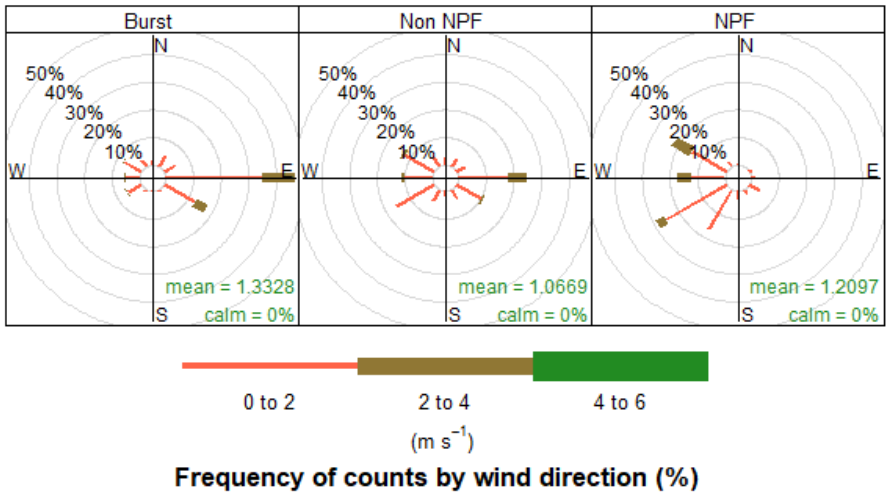

Figure S3. Windrose by event types.

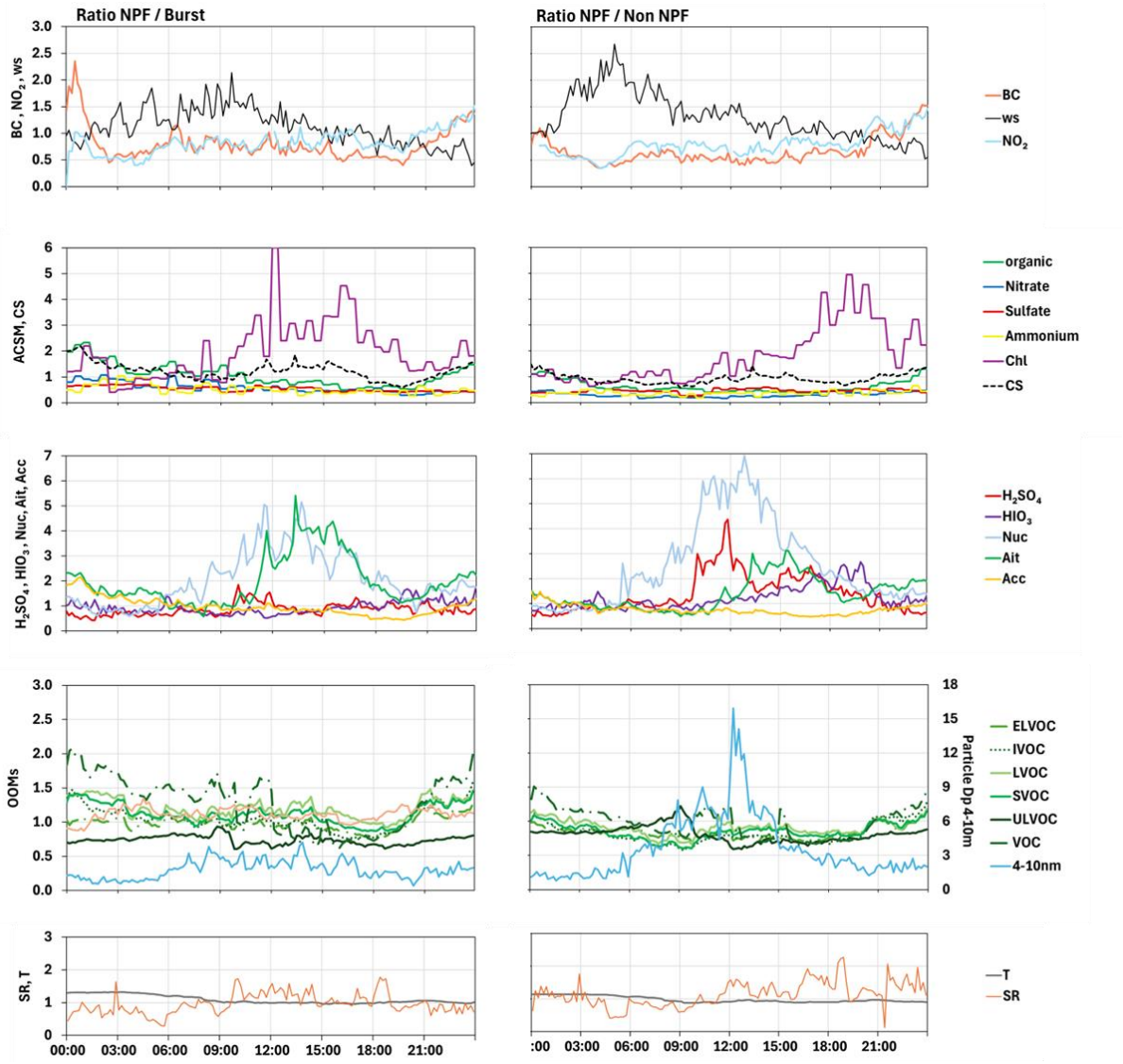

Figure S4. Diurnal cycle of Pollutant Ratio of NPF to Non-NPF (left panel) and NPF to Burst (right panel).

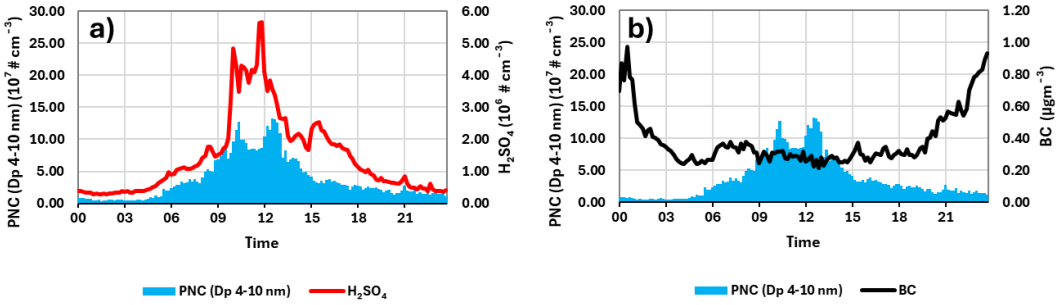

Figure S5. Diurnal cycle of average concentration (a) PNC (Dp 4 – 10 nm) and sulfuric acid, and (b) PNC (Dp 4 – 10 nm) and BC

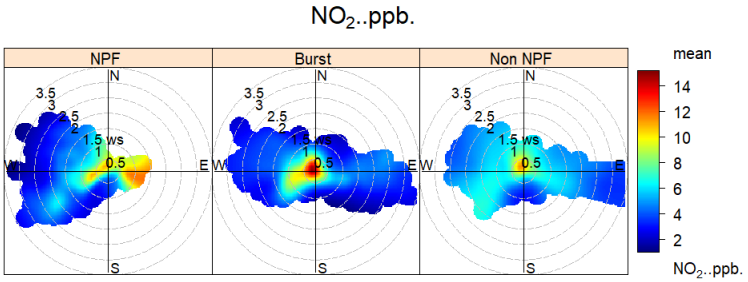

Figure S6. Polar plot of NO_2 concentration by event types.

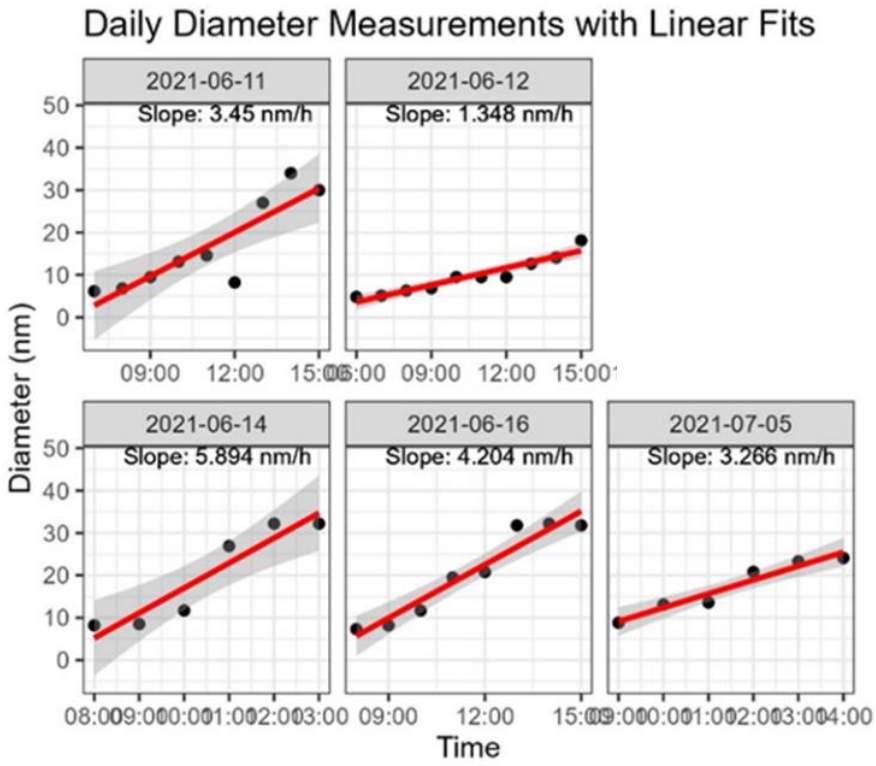

Figure S7. The linear fits between the mode of the growing diameter and time on NPF days.

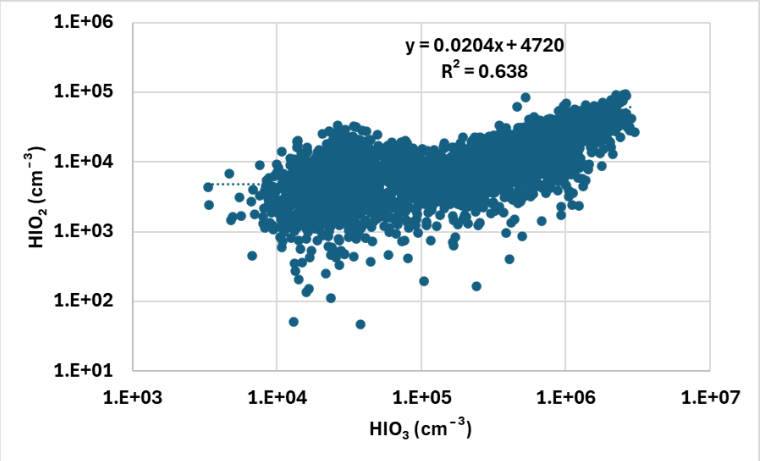

Figure S8. Scatter plot of iodic acid Vs iodous acid during the campaign

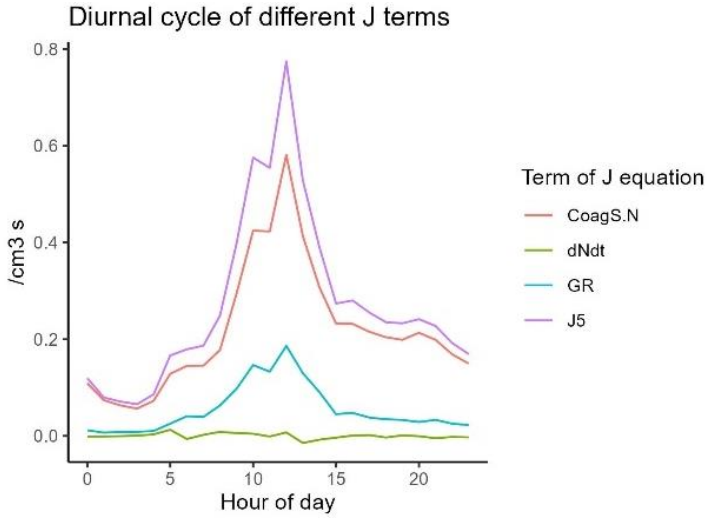

Figure S9. The diurnal cycle of each component of the J equation.

7. Conclusions and future directions

7.1 Conclusions

This thesis employed stationary and mobile monitoring air pollutant data collected from three urban environments in the UK. The former was obtained from three air quality supersites, including London, Birmingham, and Manchester, whereas the latter was collected from a measurement campaign in an urban neighbourhood area in Birmingham. The overarching aims are to investigate various aspects of UFPs, including control strategies, personal exposure assessments, and a major source of secondary UFP (i.e., NPF) in the urban atmosphere.

The first study examined the trend of pollutants by utilising long-term monitoring data (2010-2021) for both particle (PNC, and PNSD), and other traffic-related air pollutants measured at the London Marylebone Road supersite. A downward trend in all examined air pollutants was observed, ranging from 4.7 %/yr to 8.3%/yr. The most rapid decline was observed in BC and accumulation mode concentrations, whereas the decrease in nucleation mode occurs at a considerably slower rate compared to larger particles. A more substantial decline in BC and accumulation mode was noted from 2014 to 2021, coinciding with the progressive uptake of EURO 6/VI, however no comparable decline was observed in the nucleation mode. Trend analysis differentiated by the wind direction revealed a consistent pattern, with BC and accumulation mode decreasing rapidly during the study period, particularly from the direction associated with the vehicle exhaust emissions. In addition, a transition in PNSD from bimodal (i.e., the mode at ~30 nm, and ~70 nm) in 2010 to unimodal with the mode at ~70 no longer obvious was observed. These results further confirm the

substantial reduction of pollutants, particularly BC and accumulation mode, likely due to effective interventions in the road transport sector, especially diesel-powered vehicles. In the UK, it is mandatory for new light-duty diesel vehicle (EURO 5 and 6), and heavy-duty vehicles (EURO VI) to install a DPF within their exhaust systems. This is carried out to achieve the newly established particle number limit in those EURO standards. Prior studies, both in laboratory settings and on-road experiments, have demonstrated that this after-treatment technology is capable of removing particles with an extremely high efficiency, i.e., nearly 100%, particularly for involatile particles (Bergmann et al., 2009; Fiebig et al., 2014; Lee et al., 2015).

Our findings are supported by a recent experimental study that investigated the performance of DPF, focusing on particle number emission (PN) and size distribution during regeneration, utilising various soot loadings (Zhang et al., 2024).The results show that the reduction efficiency of PN increases with higher soot loading, particularly observed in the accumulation mode (50 nm – 560 nm), which can be attributed to the formation of filter cake. Additionally, a change in PNSD was noted, where a bimodal distribution was observed (at ~7 nm and ~25 nm) prior to DPF installation. This distribution then shifted to a trimodal (modes at ~ 12 nm -16 nm, ~ 50 nm -60 nm, and ~200 nm) when soot loading was moderate (0-2 g/L, the unit g/L represents the mass of soot collected per unit volume of the filter), with the mode in the range 50-60 nm being further removed at higher soot loading levels (4-6 g/L). They found a greater removal efficiency of the nucleation mode from the clean DPF (i.e., without soot loading). However, as soot loading increased (between 2 g/L and 4 g/L), the removal efficiency of the nucleation mode was not as high as that of the accumulation mode.

Consequently, the particles in the downstream of the DPF were dominantly within the nucleation mode range, accounting for up to 90%.

The particles accumulated in the DPF are periodically burnt off during the regeneration process, which aims to prevent additional fuel consumption caused by higher exhaust backpressure, diminished performance, and possible filter clogging ((Luo et al., 2023; Shi et al., 2022). However, the regeneration process may result in a short-term peak in particle number concentration. A previous study performed an on-road assessment of various light-duty diesel trucks revealed that the particle number emission factor during the regeneration phase was 5 times higher than that during the normal DPF stage (Li et al., 2024). This increase was likely attributed to the formation of volatile substances from lubricants under high-temperature conditions (Shi et al., 2022). Another study has observed a substantial increase in volatile particles within the size range of 5 and 10 nm emitted during the regeneration process (Dwyer et al., 2010). Nonetheless, the net advantage of DPF remains substantial at reducing UFPs emissions from diesel vehicle exhaust, as evidenced by our findings that reflect the real-world driving conditions at the London Marylebone Roadside site.

In addition, our results shows a consistent result with the experimental investigation, which demonstrates a large reduction in the accumulation mode, whereas the concentration in the nucleation mode remains high in the atmosphere. As a result, the concentration of UFPs may remain high, especially in the regions that are heavily influenced by diesel traffic or could even exceed levels found in areas where emission regulation standards are less stringent than EURO 5 (for light-duty vehicles) and EURO VI (for heavy-duty vehicles) or equivalent. Considering the negative impact of UFPs on human health, our findings from the first study underscore the necessity for

a more effective control technology to reduce UFP emissions, particularly for diesel vehicles in urban areas.

In addition to tailpipe emissions, non-exhaust emissions also significantly contribute to particulate matter emissions from the road transport sector. Non-exhaust emissions (NEE) are primarily generated from the abrasion of brakes, tyres, and road surfaces (Harrison, 2020b). An experimental study indicated that elevating the temperature of brake pads, ranging from 100°C to 300°C, is associated with elevated UFP emissions (Perricone et al., 2018). A laboratory-scaled study observed a substantial increase in particle number concentration due to tyre wear during slip events, likely attributed to the nucleation of evaporated compounds released from the tyre surface (Kim & Lee, 2018).

NEE contributes considerably less to UFP emissions in comparison to the exhaust emissions. Prior research carried out source apportionment analysis at a similar site to this study, i.e., London Marylebone Road that identified a minor contribution to particle number concentration from NEE, specifically from brake dust (1.7%) and resuspension dust (4.8 %) (Harrison et al., 2011b). NEE UFPs remains unregulated and not controlled by the DPF or any aftertreatment technologies. Despite the potential of electric vehicles to eliminate tailpipe emissions, they are considered as having a significant contribution to NEE due to their heavier weight. Nevertheless, research on NEE UFPs remains limited, pointing to a need for further investigation to comprehensively understand UFPs emission from the road transport sector.

It is noted that in Chapter 3 we introduce the terminology of “liquid mode” and “solid mode” to describe particles emitted from vehicle exhaust. In this thesis, the term “liquid

mode" refers to volatile/ semi-volatile particles, while "solid mode" denotes non-volatile particles, as smaller particles are not exclusively liquid.

The second and third studies analysed data derived from a personal exposure assessment to air pollutants using portable sensors. The former focused on UFP metrics, while the latter employed all measured pollutants, including UFP (only PNC), PM_1, $PM_{2.5}$, PM_{10}, and BC. In addition, both studies utilised data from BAQS, a local air quality monitoring station.

The second study evaluated personal exposure to not only PNC, which is frequently reported, but also to average diameter (Dp 10 – 700 nm) and LDSA. There are small numbers of existing personal exposure studies that have examined such additional metrics (average diameter and LDSA), which are considered as crucial proxies for epidemiological studies. The measurement took place in an area of high population density in urban Birmingham. In this study, we highlighted a higher exposure to PNC and LDSA with smaller average diameter during bus journeys compared to walking, particularly on major roads compared to residential roads. Many factors may affect this higher exposure, including traffic conditions, emissions from nearby vehicles, and emissions from the bus's own exhaust that enter the cabin through infiltration (Rivas et al., 2017; Sabin et al., 2005). Additionally, factors such as fuel type, bus fleet technology, and driving behaviour e.g., peak PNC while idling (Sabin et al., 2005), collectively contribute to the elevated exposure to air pollutants experienced by bus commuters. According to the information provided by the bus providers, the entire bus fleet in West Midland meets EURO VI standards, which means a DPF has been installed within the bus exhaust systems. Nevertheless, based on our findings from the first study, this technology demonstrated limited impact on reducing the smaller

particles, particularly in the nucleation mode. Consequently, an elevated level of UFP inside the bus cabin, which also increases the exposure level is expected. The Result from spatial distribution identified common hotspots, such as intersection areas, traffic lights, supermarket car parks, a petrol station, and restaurant areas, attributed to a higher intensity of combustion activity compared to other locations along the study route. Therefore, minimising commute time in hotspot locations, particularly those located on busy roads, is anticipated to reduce exposure to UFP. In addition, we leveraged PNC during walking measurements as well as PNC from a regulatory-grade instrument at BAQS to develop a novel approach. This method enables the estimation of source contributions, including general background, local increments due to the close proximity to the emission sources, and hyperlocal sources that are frequently observed in hotspot areas. The findings from this study provide evidence and a new method to support UFP control strategies.

Nonetheless, due to some limitations (e.g., time, cost and instrumentation), personal exposure studies in both the second study and most prior research represent only the exposure during the sampling period, typically within a brief campaign period and a specific season. This is mainly influenced by meteorological factors affecting pollutant concentrations in the atmosphere. As indicated by the PNSD analysis that shows NPF events occurred with a frequency of 30% of measurement days, potentially affecting personal exposure levels.

In the third study, we aimed to develop simple methods to obtain personal exposure concentrations that reflect longer periods, specifically annual personal exposure. This was achieved by minimising meteorological conditions that influence exposure levels measured during the campaign, a process known as the data normalisation technique.

While many studies normalize air pollutant data from long-term stationary monitoring data, no prior research has utilised short-period mobile or personal exposure data. As previously mentioned, we focused on data from walking measurements, employing 5 pollutants (PNC, PM_1, $PM_{2.5}$, and PM_{10}). Measurement data of these pollutants obtained from regulatory instruments at BAQS were used to determine correction factors, which were subsequently used to adjust personal exposure data collected over a ± 1-month campaign during the spring season of 2023.

Four distinct methods were developed, differing according to the time interval used for calculating the correction factor. Results show that two of the four methods (specifically, methods A and C), which incorporate a correction factor for two different time intervals (during the campaign and over a yearly period), have effectively reduced the non-normalised concentration for the majority of examined pollutants, making them more comparable to the annual average concentration measured at BAQS. The difference was still higher for PNC, likely attributable to the local increment resulting from the proximity to local sources, as identified in the second study.

Unlike existing data normalisation techniques that mainly use machine learning (ML) and thus require more explanatory variables and extensive model fitting, the normalisation ratio in our study relies solely on the BAQS data, potentially resulting in lower accuracy compared to the ML methods. However, our findings indicate that certain methods show the potential to accurately represent annual personal exposure concentrations in the study area. This indicates that, despite limited data and minimal computational resources, these methods are capable of effectively predicting longer-term exposure at individual levels. This technique may facilitate the estimation of exposure with different time bases and could be applicable in other typical studies.

In the fourth study, we aimed to gain a molecular understanding of how the UFP are generated from their main secondary source, i.e., NPF. No prior studies have been done in the UK. Here, we analysed data collected during a 1-month summer campaign at Manchester Air Quality Supersite, located in an urban background area in northwestern UK. The data includes gaseous precursors, such as sulfuric acid, iodic acid, and HOMs, in addition to other regularly monitored pollutants. This study site exhibits a common feature of NPF days, characterized by higher solar radiation and sulfuric acid levels. Less polluted atmospheric conditions, and higher wind speed seem to be favourable factors for NPF. The origin of air masses appears to influence NPF, with events mostly observed when the wind is from 200 to 300 degrees, suggesting the transport of either cleaner air or substantial gaseous precursors. The average concentration of sulfuric acid on NPF days was nearly double that on non-NPF, leading to an increase in the average PNC in nucleation mode by a factor of ~3 (based on data from 6 AM to 3 PM). Sulfuric acid is a critical component for initiating nucleation, as evidenced by observations in many locations worldwide, (Brean et al., 2020; Cai et al., 2024; Tiszenkel et al., 2025; Yao et al., 2018). On the other hand, ULVOC are hypothesised as efficient nucleators at specific atmospheric conditions such as boreal forests, peatlands, and high-altitude areas. We conducted a further analysis of the correlation between the *J* values ($J_{1.7}$ and J_5), sulfuric acid, and ULVOC. The results indicate a positive correlation between *J* values and sulfuric acid concentration, however, the increase in these parameters is associated with a decrease in ULVOC. This suggests that sulfuric acid is the primary driver of nucleation, while ULVOC may play a more important role in particle growth. However, the complexity of real atmospheric conditions makes the quantification of HOMs' contribution more

challenging. The findings of this study underscore the importance of reducing key gaseous pollutants, including SO_2 and VOC, to minimise UFPs produced by NPF mechanisms.

7.2 Future directions

- This thesis has explored several aspects of UFPs in urban environments. Nevertheless, there are limitations and opportunities for future research that require investigation to improve the understanding of UFPs, as follows:
- The first study underscores the importance of long-term monitoring data in evaluating the effectiveness of enacted policies. The study site is situated in a street canyon, allowing for effective sampling of air from specific directions linked to traffic emissions. Further analysis by wind direction facilitates the examination under actual driving conditions. Nonetheless, this study did not examine all pollutants measured at this site, it focused only on BC, PNC, and some regularly measured air pollutants (e.g., CO, NO_x, SO_2, O_3). Given that the nucleation mode emitted from diesel vehicles primarily consists of the liquid phase, mainly generated from vaporised condensed engine oil (hydrocarbon). Hence, future studies might include other pollutants, specifically hydrocarbons. In addition, other pollutants that play a crucial role in new particle formation (i.e., another UFPs source), such as sulfuric acid, iodic acid, and HOMs are important to be measured. To date, there has been no continuous monitoring of these pollutants in the UK. Evaluating both additional and existing measured pollutants, particularly with the availability of long-term data, may greatly improve our knowledge about sources and processes of UFPs. This could provide valuable information for determining

future policy or evaluating existing policy, particularly for the transport sector in urban areas.

- While we have examined assessment of the individual exposure to multimeric of UFPs from walking and bus journeys, there remain opportunities to explore and compare other common commuting modes in this study area, including in-car travel, cycling, and train use. Furthermore, it is essential to evaluate individual exposure in other microenvironments apart from those investigated in this study, such as office settings and laboratories. Prior studies demonstrate that laser printers emit significant quantities of UFPs (Azimi et al., 2016; Stephens et al., 2013), potentially increasing exposure levels in office environments. Examining multiple metrics of UFPs across various types of travel and different microenvironments will give important information to better understand how UFPs change over time and space, filling a key gap in research.
- To our knowledge, this is the first study to perform data normalisation utilising a short campaign of personal exposure data. Consequently, limitations may have emerged not only from the instrument's limitations (elaborated in Chapter 4), but also from the quantity of data available. This study presents methods that may accurately reflect annual exposure. However, repetition of the typical study with extended duration and across different seasons may assist in validating the methods we have developed.
- The findings from the NPF study presented in Chapter 6 further support the concept that sulfuric acid is a primary driver factor of NPF in urban atmospheres. The analysis of HOMs provides additional understanding of the particle growth process. However, since this is the first study examining NPF in the UK at a

molecular level, comparing it with previous studies is challenging. NPF is sensitive to atmospheric conditions, therefore, more studies should be undertaken in other cities and seasons to improve our understanding of NPF, particularly in urban areas of the UK.

- Various sources of UFP may possess unique chemical compositions, leading to differing health outcomes. However, few prior studies have examined the chemical composition of UFPs, with only one recent study reporting the chemical composition of UFPs from continuous monitoring in Greece (Argyropoulou et al., 2025). The absence of such studies is likely due to the limitations of instrumentation capable of characterizing UFPs, which exist in very small mass concentrations. Therefore, future recommendations include conducting studies aimed at developing instruments for UFP characterisation, which will enhance the understanding of the chemical composition present in UFPs. The findings will provide important evidence to support the epidemiological studies related to the adverse effects of UFPs.

References

Abdullahi, K. L., Delgado-Saborit, J. M., & Harrison, R. M. (2013). Emissions and indoor concentrations of particulate matter and its specific chemical components from cooking: A review. *Atmospheric Environment*, *71*, 260-294. https://doi.org/https://doi.org/10.1016/j.atmosenv.2013.01.061

Alage, S., Michoud, V., Harb, S., Picquet-Varrault, B., Cirtog, M., Kumar, A., Rissanen, M., & Cantrell, C. (2024). A nitrate ion chemical-ionization atmospheric-pressure-interface time-of-flight mass spectrometer (NO3− ToFCIMS) sensitivity study. *Atmos. Meas. Tech.*, *17*(15), 4709-4724. https://doi.org/10.5194/amt-17-4709-2024

Alam, A., Shi, J. P., & Harrison, R. M. (2003). Observations of new particle formation in urban air. *Journal of Geophysical Research: Atmospheres*, *108*(D3). https://doi.org/https://doi.org/10.1029/2001JD001417

Alas, H. D. C., Müller, T., Weinhold, K., Pfeifer, S., Glojek, K., Gregorič, A., Močnik, G., Drinovec, L., Costabile, F., Ristorini, M., & Wiedensohler, A. (2020). Performance of microAethalometers: Real-world Field Intercomparisons from Multiple Mobile Measurement Campaigns in Different Atmospheric Environments. *Aerosol and Air Quality Research*, *20*(12), 2640-2653. https://doi.org/10.4209/aaqr.2020.03.0113

Ali, U., Singh, V., Faisal, M., Kumar, M., & Gani, S. (2025). Exploring the influence of physical and chemical factors on new particle formation in a polluted megacity [10.1039/D4EA00114A]. *Environmental Science: Atmospheres*, *5*(1), 25-47. https://doi.org/10.1039/D4EA00114A

Amin, M., Aun, S., Hang, L., Hata, M., Phairuang, W., & Masami, F. (2024). Investigation into personal exposure to ultrafine particle (UFP) in Phnom Penh, Cambodia: A pilot study. *Atmospheric Pollution Research*, *15*(12), 102307. https://doi.org/https://doi.org/10.1016/j.apr.2024.102307

Anderson, J. O., Thundiyil, J. G., & Stolbach, A. (2012). Clearing the Air: A Review of the Effects of Particulate Matter Air Pollution on Human Health. *Journal of Medical Toxicology*, *8*(2), 166-175. https://doi.org/10.1007/s13181-011-0203-1

Apte, J. S., Kirchstetter, T. W., Reich, A. H., Deshpande, S. J., Kaushik, G., Chel, A., Marshall, J. D., & Nazaroff, W. W. (2011). Concentrations of fine, ultrafine, and black carbon particles in auto-rickshaws in New Delhi, India. *Atmospheric Environment*, *45*(26), 4470-4480. https://doi.org/https://doi.org/10.1016/j.atmosenv.2011.05.028

Apte, J. S., Messier, K. P., Gani, S., Brauer, M., Kirchstetter, T. W., Lunden, M. M., Marshall, J. D., Portier, C. J., Vermeulen, R. C. H., & Hamburg, S. P. (2017). High-Resolution Air Pollution Mapping with Google Street View Cars: Exploiting Big Data [Article]. *Environmental Science & Technology*, *51*(12), 6999-7008. https://doi.org/10.1021/acs.est.7b00891

AQEG. (2004). *Nitrogen Dioxide in the United Kingdom*.

AQEG. (2008). *Ozone in the United Kingdom*.

Atkinson, R. W., Barratt, B., Armstrong, B., Anderson, H. R., Beevers, S. D., Mudway, I. S., Green, D., Derwent, R. G., Wilkinson, P., & Tonne, C. (2009). The impact of the congestion charging scheme on ambient air pollution concentrations in London. *Atmospheric Environment*, *43*(34), 5493-5500.

Baldauf, R., Devlin RB, Gehr P, Giannelli R, Hassett-Sipple B, Jung H, Martini G, McDonald J, Sacks JD, & K., W. (2016). Ultrafine Particle Metrics and Research Considerations: Review of the 2015 UFP Workshop. *Internatinal Journal of Environmental Research and Public Health.*, *11*. https://doi.org/10.3390/ijerph13111054

Baruah, A., Bousiotis, D., Damayanti, S., Bigi, A., Ghermandi, G., Ghaffarpasand, O., Harrison, R. M., & Pope, F. D. (2024). A novel spatiotemporal prediction approach to fill air pollution data gaps using mobile sensors, machine learning and citizen science techniques. *npj Climate and Atmospheric Science*, *7*(1), 310. https://doi.org/10.1038/s41612-024-00859-z

Beevers, S. D., & Carslaw, D. C. (2005). The impact of congestion charging on vehicle emissions in London. *Atmospheric Environment*, *39*(1), 1-5.

Belkacem, I., Khardi, S., Helali, A., Slimi, K., & Serindat, S. (2020). The influence of urban road traffic on nanoparticles:

Roadside measurements *Atmospheric Environment 242*.

Bergmann, M., Kirchner, U., Vogt, R., & Benter, T. (2009). On-road and laboratory investigation of low-level PM emissions of a modern diesel particulate filter equipped diesel passenger car. *Atmospheric Environment*, *43*(11).

Bergmann, M. L., Andersen, Z. J., Amini, H., Ellermann, T., Hertel, O., Lim, Y. H., Loft, S., Mehta, A., Westendorp, R. G., & Cole-Hunter, T. (2021). Exposure to ultrafine particles while walking or bicycling during COVID-19closures:ArepeatedmeasuresstudyinCopenhagen,Denmark. *Science of the Total Environment*, *791*. https://doi.org/10.1016/j.scitotenv.2021.148301

Bianchi, F., Kurtén, T., Riva, M., Mohr, C., Rissanen, M. P., Roldin, P., Berndt, T., Crounse, J. D., Wennberg, P. O., Mentel, T. F., Wildt, J., Junninen, H., Jokinen, T., Kulmala, M., Worsnop, D. R., Thornton, J. A., Donahue, N., Kjaergaard, H. G., & Ehn, M. (2019). Highly Oxygenated Organic Molecules (HOM) from Gas-Phase Autoxidation Involving Peroxy Radicals: A Key Contributor to Atmospheric Aerosol. *Chemical Reviews*, *119*(6), 3472-3509. https://doi.org/10.1021/acs.chemrev.8b00395

Bianchi, F., Tröstl, J., Junninen, H., Frege, C., Henne, S., Hoyle, C. R., Molteni, U., Herrmann, E., Adamov, A., Bukowiecki, N., Chen, X., Duplissy, J., Gysel, M., Hutterli, M., Kangasluoma, J., Kontkanen, J., Kürten, A., Manninen, H. E., Münch, S., . . . Baltensperger, U. (2016). New particle formation in the free troposphere: A question of chemistry and timing. *Science*, *352*(6289), 1109-1112. https://doi.org/doi:10.1126/science.aad5456

Bista, S., Dureau, C., & Chaix, B. (2022). Personal exposure to concentrations and inhalation of black carbon according to transport mode use: The MobiliSense sensor-based study. *Environment International*, *158*, 106990. https://doi.org/https://doi.org/10.1016/j.envint.2021.106990

Borck, R., & Schrauth, P. (2021). Population density and urban air quality. *Regional Science and Urban Economics*, *86*, Article 103596. https://doi.org/10.1016/j.regsciurbeco.2020.103596

Borck, R., & Schrauth, P. (2024). Urban pollution: A global perspective. *Journal of Environmental Economics and Management*, *126*, Article 103013. https://doi.org/10.1016/j.jeem.2024.103013

Bousiotis, D., Brean, J., Pope, F. D., Dall'Osto, M., Querol, X., Alastuey, A., Perez, N., Petäjä, T., Massling, A., Nøjgaard, J. K., Nordstrøm, C., Kouvarakis, G., Vratolis, S., Eleftheriadis, K., Niemi, J. V., Portin, H., Wiedensohler, A., Weinhold, K., Merkel, M., . . . Harrison, R. M. (2021a). The effect of meteorological conditions and atmospheric composition in the occurrence and development of new particle formation (NPF) events in Europe. *Atmos. Chem. Phys.*, *21*(5), 3345-3370. https://doi.org/10.5194/acp-21-3345-2021

Bousiotis, D., Damayanti, S., Baruah, A., Bigi, A., Beddows, D. C. S., Harrison, R. M., & Pope, F. D. (2024). Pinpointing sources of pollution using citizen science and hyperlocal low-cost mobile source apportionment. *Environment International*, *193*, 109069. https://doi.org/https://doi.org/10.1016/j.envint.2024.109069

Bousiotis, D., Pope, F. D., Beddows, D. C. S., Dall'Osto, M., Massling, A., Nøjgaard, J. K., Nordstrøm, C., Niemi, J. V., Portin, H., Petäjä, T., Perez, N., Alastuey, A., Querol, X., Kouvarakis, G., Mihalopoulos, N., Vratolis, S., Eleftheriadis, K., Wiedensohler, A., Weinhold, K., . . . Harrison, R. M. (2021b). A phenomenology of new particle formation (NPF) at 13 European sites. *Atmos. Chem. Phys.*, *21*(15), 11905-11925. https://doi.org/10.5194/acp-21-11905-2021

Brean, J., Beddows, D. C. S., Shi, Z., Temime-Roussel, B., Marchand, N., Querol, X., Alastuey, A., Minguillón, M. C., & Harrison, R. M. (2020a). Molecular insights into new particle formation in Barcelona, Spain. *Atmos. Chem. Phys.*, *20*(16), 10029-10045. https://doi.org/10.5194/acp-20-10029-2020

Brean, J., Beddows, D. C. S., Shi, Z. B., Temime-Roussel, B., Marchand, N., Querol, X., Alastuey, A., Minguillón, M. C., & Harrison, R. M. (2020b). Molecular insights into new particle formation in Barcelona, Spain. *Atmospheric Chemistry and Physics*, *20*(16), 10029-10045. https://doi.org/10.5194/acp-20-10029-2020

Brean, J., Harrison, R. M., Shi, Z., Beddows, D. C. S., Acton, W. J. F., Hewitt, C. N., Squires, F. A., & Lee, J. (2019). Observations of highly oxidized molecules and particle nucleation in the atmosphere of Beijing. *Atmos. Chem. Phys.*, *19*(23), 14933-14947. https://doi.org/10.5194/acp-19-14933-2019

Brean, J., Rowell, A., Beddows, D. C. S., Weinhold, K., Mettke, P., Merkel, M., Tuch, T., Rissanen, M., Maso, M. D., Kumar, A., Barua, S., Iyer, S., Karppinen, A., Wiedensohler, A., Shi, Z., & Harrison, R. M. (2024). Road Traffic Emissions Lead to Much Enhanced New Particle Formation through Increased Growth Rates. *Environmental Science & Technology*, *58*(24), 10664-10674. https://doi.org/10.1021/acs.est.3c10526

Brines, M., Dall'Osto, M., Beddows, D. C. S., Harrison, R. M., Gómez-Moreno, F., Núñez, L., Artíñano, B., Costabile, F., Gobbi, G. P., Salimi, F., Morawska, L., Sioutas, C., & Querol, X. (2015). Traffic and nucleation events as main sources of ultrafine particles in high-insolation developed world cities. *Atmospheric Chemistry and Physics*, *15*(10), 5929-5945. https://doi.org/10.5194/acp-15-5929-2015

Buzea, C., Pacheco, II, & Robbie, K. (2007). Nanomaterials and nanoparticles: Sources and toxicity. *Biointerphases*, *2*(4), MR17-MR71. https://doi.org/10.1116/1.2815690

Cai, R., & Jiang, J. (2017). A new balance formula to estimate new particle formation rate: reevaluating the effect of coagulation scavenging. *Atmos. Chem. Phys.*, *17*(20), 12659-12675. https://doi.org/10.5194/acp-17-12659-2017

Cai, R., Yan, C., Yang, D., Yin, R., Lu, Y., Deng, C., Fu, Y., Ruan, J., Li, X., Kontkanen, J., Zhang, Q., Kangasluoma, J., Ma, Y., Hao, J., Worsnop, D. R., Bianchi, F., Paasonen, P., Kerminen, V. M., Liu, Y., . . . Jiang, J. (2021). Sulfuric acid–amine nucleation in urban Beijing. *Atmos. Chem. Phys.*, *21*(4), 2457-2468. https://doi.org/10.5194/acp-21-2457-2021

Cai, R. L., Deng, C. J., Stolzenburg, D., Li, C. X., Guo, J. C., Kerminen, V. M., Jiang, J. K., Kulmala, M., & Kangasluoma, J. (2022). Survival probability of new atmospheric particles: closure between theory and measurements from 1.4 to 100 nm. *Atmospheric Chemistry and Physics*, *22*(22), 14571-14587. https://doi.org/10.5194/acp-22-14571-2022

Campbell, S. J., Barth, A., Chen, G. I., Tremper, A. H., Priestman, M., Ek, D., Gu, S., Kelly, F. J., Kalberer, M., & Green, D. C. (2024). High time resolution quantification of PM2.5 oxidative potential at a Central London roadside supersite. *Environment International*, *193*, 109102. https://doi.org/https://doi.org/10.1016/j.envint.2024.109102

Carslaw, D. C., & Ropkins, K. (2012). openair - An R package for air quality data analysis. *Environmental Modelling & Software*, *27-28*, 52-61. https://doi.org/10.1016/j.envsoft.2011.09.008

Carslaw, D. C., & Ropkins, K. (2012). openair — An R package for air quality data analysis. *Environmental Modelling & Software*, *27-28*, 52-61. https://doi.org/https://doi.org/10.1016/j.envsoft.2011.09.008

CAS. (2025). *Manchester Air Quality Super Site at the Firs Environmental Research Station, Fallowfield Campus*. Centre for Atmospheric Science. Retrieved 06 May from

Chalupa, D. C., Morrow, P. E., Oberdörster, G., Utell, M. J., & Frampton, M. W. (2004). Ultrafine particle deposition in subjects with asthma. *Environmental Health Perspectives*, *112*(8), 879-882. https://doi.org/10.1289/ehp.6851

Chaney, R. A., Sloan, C. D., Cooper, V. C., Robinson, D. R., Hendrickson, N. R., McCord, T. A., & Johnston, J. D. (2017). Personal exposure to fine particulate air pollution while commuting: An examination of six transport modes on an urban arterial roadway. *PLOS ONE*, *12*(11), e0188053. https://doi.org/10.1371/journal.pone.0188053

Charron, A., & Harrison, R. M. (2003). Primary particle formation from vehicle emissions during exhaust dilution in the roadside atmosphere. *Atmospheric Environment*, *37*(29), 4109-4119. https://doi.org/10.1016/s1352-2310(03)00510-7

Chatain, M., Alvarez, R., Ustache, A., Rivière, E., Favez, O., & Pallares, C. (2021). Simultaneous Roadside and Urban Background Measurements of Submicron Aerosol Number Concentration and Size Distribution (in the Range 20–800 nm), along with Chemical Composition in Strasbourg, France. *Atmosphere*, *12*. https://doi.org/https://doi.org/10.3390/atmos12010071

Cheung, H. C., Morawska, L., & Ristovski, Z. D. (2011). Observation of new particle formation in subtropical urban environment. *Atmos. Chem. Phys.*, *11*(8), 3823-3833. https://doi.org/10.5194/acp-11-3823-2011

Cichowicz, R., & Dobrzański, M. (2022). 3D spatial dispersion of particulate matter and gaseous pollutants on a university campus in the center of an urban agglomeration. *Energy*, *259*, 125009. https://doi.org/https://doi.org/10.1016/j.energy.2022.125009

Crilley, L. R., Singh, A., Kramer, L. J., Shaw, M. D., Alam, M. S., Apte, J. S., Bloss, W. J., Hildebrandt Ruiz, L., Fu, P., Fu, W., Gani, S., Gatari, M., Ilyinskaya, E., Lewis, A. C., Ng'ang'a, D., Sun, Y., Whitty, R. C. W., Yue, S., Young, S., & Pope, F. D. (2020). Effect of aerosol composition on the performance of low-cost optical particle counter correction factors. *Atmos. Meas. Tech.*, *13*(3), 1181-1193. https://doi.org/10.5194/amt-13-1181-2020

Damayanti, S., Harrison, R. M., Pope, F., & Beddows, D. C. S. (2023). Limited impact of diesel particle filters on road traffic emissions of ultrafine particles. *Environment International*, *174*, 107888. https://doi.org/https://doi.org/10.1016/j.envint.2023.107888

de Jesus, A. L., Rahman, M. M., Mazaheri, M., Thompson, H., Knibbs, L. D., Jeong, C., Evans, G., Nei, W., Ding, A., Qiao, L., Li, L., Portin, H., Niemi, J. V., Timonen, H., Luoma, K., Petäjä, T., Kulmala, M., Kowalski, M., Peters, A., . . . Morawska, L. (2019). Ultrafine particles and PM2.5 in the air of cities around the world: Are they

representative of each other? *Environment International*, *129*, 118-135. https://doi.org/https://doi.org/10.1016/j.envint.2019.05.021
DEFRA, U. (2025a). *Site Information for London Marylebone Road(UKA00315)*. Department for Environment Food & Rural Affairs. Retrieved 3 May from
DEFRA, U. (2025b). *Standard Methods for monitoring and UK Approach*. UK DEFRA. Retrieved 8 May from https://uk-air.defra.gov.uk/networks/monitoring-methods?view=eu-standards
Diaz Resquin, M., Lichtig, P., Alessandrello, D., De Oto, M., Gómez, D., Rössler, C., Castesana, P., & Dawidowski, L. (2023). A machine learning approach to address air quality changes during the COVID-19 lockdown in Buenos Aires, Argentina. *Earth Syst. Sci. Data*, *15*(1), 189-209. https://doi.org/10.5194/essd-15-189-2023
Donahue, N. M., Epstein, S. A., Pandis, S. N., & Robinson, A. L. (2011). A two-dimensional volatility basis set: 1. organic-aerosol mixing thermodynamics. *Atmos. Chem. Phys.*, *11*(7), 3303-3318. https://doi.org/10.5194/acp-11-3303-2011
Donahue, N. M., Kroll, J. H., Pandis, S. N., & Robinson, A. L. (2012). A two-dimensional volatility basis set – Part 2: Diagnostics of organic-aerosol evolution. *Atmos. Chem. Phys.*, *12*(2), 615-634. https://doi.org/10.5194/acp-12-615-2012
Du, W., Cai, J., Zheng, F., Yan, C., Zhou, Y., Guo, Y., Chu, B., Yao, L., Heikkinen, L. M., Fan, X., Wang, Y., Cai, R., Hakala, S., Chan, T., Kontkanen, J., Tuovinen, S., Petäjä, T., Kangasluoma, J., Bianchi, F., . . . Kulmala, M. (2022). Influence of Aerosol Chemical Composition on Condensation Sink Efficiency and New Particle Formation in Beijing. *Environmental Science & Technology Letters*, *9*(5), 375-382. https://doi.org/10.1021/acs.estlett.2c00159
Dwyer, H., Ayala, A., Zhang, S., Collins, J., Huai, T., Herner, J., & Chau, W. (2010). Emissions from a diesel car during regeneration of an active diesel particulate filter. *Journal of Aerosol Science*, *41*(6), 541-552. https://doi.org/https://doi.org/10.1016/j.jaerosci.2010.04.001
EEA. (2023). *Air pollution levels still too high across Europe – remains top environmental health risk.* Retrieved 2 August from
Ellison, R. B., Greaves, S. P., & Hensher, D. A. (2013). Five years of London's low emission zone: Effects on vehicle fleet composition and air quality. *Transportation Research Part D: Transport and Environment*, *23*. https://doi.org/https://doi.org/10.1016/j.trd.2013.03.010
EU. (2024). *Directive (EU) 2024/2881 of the European Parliament and of the Council of 23 October 2024 on ambient air quality and cleaner air for Europe (recast), Brussels.*
Falocchi, M., Zardi, D., & Giovannini, L. (2021). Meteorological normalization of NO2 concentrations in the Province of Bolzano (Italian Alps). *Atmospheric Environment*, *246*, 118048. https://doi.org/https://doi.org/10.1016/j.atmosenv.2020.118048
Ferin, J., Oberdörster, G., Penney, D. P., Soderholm, S. C., Gelein, R., & Piper, H. C. (1990). Increased pulmonary toxicity of ultrafine particles? I. Particle clearance, translocation, morphology. *Journal of Aerosol Science*, *21*(3), 381-384. https://doi.org/https://doi.org/10.1016/0021-8502(90)90064-5
Fiebig, M., Wiartalla, A., Holderbaum, B., & Kiesow, S. (2014). Particulate emissions from diesel engines: correlation between engine technology and emissions. *Journal of Occupational Medicine and Toxicology*, *9*(1), 6. https://doi.org/10.1186/1745-6673-9-6
Fierz, M., Burtscher, H., & Steigmeier, P. (2008). Field measurement of particle size and number concentration with the Diffusion Size Classifier (DiSC) *SAE Technical Paper*.

Fierz, M., Burtscher, H., Steigmeier, P., & Kasper, M. (2008). Field Measurement of Particle Size and Number Concentration with the Diffusion Size Classifier (Disc). *SAE Technical Papers*. https://doi.org/10.4271/2008-01-1179

Fierz, M., C., H., P., S., & and Burtscher, H. (2011). Design, Calibration, and Field Performance of a Miniature Diffusion Size Classifier. *Aerosol Science and Technology*, *45*(1), 1-10. https://doi.org/10.1080/02786826.2010.516283

Franchini, M., & Manucci, P. M. (2007). Short-term effects of air pollution on cardiovascular diseases: outcomes and mechanisms. *Journal of Thrombosis and Haemostasis*, *5*(11).

Frederickson, L. B., Russell, H. S., Fessa, D., Khan, J., Schmidt, J. A., Johnson, M. S., & Hertel, O. (2023). Hyperlocal air pollution in an urban environment - measured with low-cost sensors. *Urban Climate*, *52*, 101684. https://doi.org/https://doi.org/10.1016/j.uclim.2023.101684

Frederickson, L. B., Sidaraviciute, R., Schmidt, J. A., Hertel, O., & Johnson, M. S. (2022). Are dense networks of low-cost nodes really useful for monitoring air pollution? A case study in Staffordshire. *Atmos. Chem. Phys.*, *22*(21), 13949-13965. https://doi.org/10.5194/acp-22-13949-2022

Fruin, S., Westerdahl, D., Sax, T., Sioutas, C., & Fine, P. M. (2008). Measurements and predictors of on-road ultrafine particle concentrations and associated pollutants in Los Angeles. *Atmospheric Environment*, *42*(2), 207-219. https://doi.org/https://doi.org/10.1016/j.atmosenv.2007.09.057

Fuller, G. W., & Green, D. (2006). Evidence for increasing concentrations of primary PM10 in London. *Atmospheric Environment*, *40*(32), 6134-6145. https://doi.org/10.1016/j.atmosenv.2006.05.031

Fuller, R., Landrigan, P. J., Balakrishnan, K., Bathan, G., Bose-O'Reilly, S., Brauer, M., Caravanos, J., Chiles, T., Cohen, A., Corra, L., Cropper, M., Ferraro, G., Hanna, J., Hanrahan, D., Hu, H., Hunter, D., Janata, G., Kupka, R., Lanphear, B., . . . Yan, C. H. (2022). Pollution and health: a progress update. *Lancet Planetary Health*, *6*(6), E535-E547. https://doi.org/10.1016/s2542-5196(22)00090-0

Fung, P. L., Zaidan, M. A., Niemi, J. V., Saukko, E., Timonen, H., Kousa, A., Kuula, J., Rönkkö, T., Karppinen, A., Tarkoma, S., Kulmala, M., Petäjä, T., & Hussein, T. (2022). Input-adaptive linear mixed-effects model for estimating alveolar lung-deposited surface area (LDSA) using multipollutant datasets. *Atmos. Chem. Phys.*, *22*(3), 1861-1882. https://doi.org/10.5194/acp-22-1861-2022

Gani, S., Chambliss, S. E., Messier, K. P., Lunden, M. M., & Apte, J. S. (2021). Spatiotemporal profiles of ultrafine particles differ from other traffic-related air pollutants: lessons from long-term measurements at fixed sites and mobile monitoring [10.1039/D1EA00058F]. *Environmental Science: Atmospheres*, *1*(7), 558-568. https://doi.org/10.1039/D1EA00058F

Garmash, O., Rissanen, M. P., Pullinen, I., Schmitt, S., Kausiala, O., Tillmann, R., Zhao, D., Percival, C., Bannan, T. J., Priestley, M., Hallquist, Å. M., Kleist, E., Kiendler-Scharr, A., Hallquist, M., Berndt, T., McFiggans, G., Wildt, J., Mentel, T. F., & Ehn, M. (2020). Multi-generation OH oxidation as a source for highly oxygenated organic molecules from aromatics. *Atmos. Chem. Phys.*, *20*(1), 515-537. https://doi.org/10.5194/acp-20-515-2020

Geiss, O., Bianchi, I., & Barrero-Moreno, J. (2016). Lung-deposited surface area concentration measurements in selected occupational and non-occupational environments. *Journal of Aerosol Science*, *96*, 24-37. https://doi.org/https://doi.org/10.1016/j.jaerosci.2016.02.007

Gilmour, P. S., Ziesenis, A., Morrison, E. R., Vickers, M. A., Drost, E. M., Ford, I., Karg, E., Mossa, C., Schroeppel, A., Ferron, G. A., Heyder, J., Greaves, M., MacNee, W., & Donaldson, K. (2004). Pulmonary and systemic effects of short-term inhalation exposure to ultrafine carbon black particles. *Toxicology and Applied Pharmacology*, *195*(1), 35-44. https://doi.org/https://doi.org/10.1016/j.taap.2003.10.003

Gordon, H., Kirkby, J., Baltensperger, U., Bianchi, F., Breitenlechner, M., Curtius, J., Dias, A., Dommen, J., Donahue, N. M., Dunne, E. M., Duplissy, J., Ehrhart, S., Flagan, R. C., Frege, C., Fuchs, C., Hansel, A., Hoyle, C. R., Kulmala, M., Kürten, A., . . . Carslaw, K. S. (2017). Causes and importance of new particle formation in the present-day and preindustrial atmospheres. *Journal of Geophysical Research: Atmospheres*, *122*(16), 8739-8760. https://doi.org/https://doi.org/10.1002/2017JD026844

Grange, S. K., & Carslaw, D. C. (2019). Using meteorological normalisation to detect interventions in air quality time series. *Science of the Total Environment*, *653*, 578-588. https://doi.org/https://doi.org/10.1016/j.scitotenv.2018.10.344

Grange, S. K., Carslaw, D. C., Lewis, A. C., Boleti, E., & Hueglin, C. (2018). Random forest meteorological normalisation models for Swiss PM10 trend analysis. *Atmos. Chem. Phys.*, *18*(9), 6223-6239. https://doi.org/10.5194/acp-18-6223-2018

Green, C. P., Heywood, J. S., & Navarro Paniagua, M. (2020). Did the London congestion charge reduce pollution? *Regional Science and Urban Economics*, *84*, 103573. https://doi.org/https://doi.org/10.1016/j.regsciurbeco.2020.103573

Guerreiro, C. B. B., Foltescu, V., & de Leeuw, F. (2014). Air quality status and trends in Europe [Article]. *Atmospheric Environment*, *98*, 376-384. https://doi.org/10.1016/j.atmosenv.2014.09.017

Guo, S., Hu, M., Peng, J., Wu, Z., Zamora, M. L., Shang, D., Du, Z., Zheng, J., Fang, X., Tang, R., Wu, Y., Zeng, L., Shuai, S., Zhang, W., Wang, Y., Ji, Y., Li, Y., Zhang, A. L., Wang, W., . . . Zhang, R. (2020). Remarkable nucleation and growth of ultrafine particles from vehicular exhaust. *Proceedings of the National Academy of Sciences*, *117*(7), 3427-3432. https://doi.org/doi:10.1073/pnas.1916366117

Guo, Y., Li, K., Zhao, B., Shen, J., Bloss, W. J., Azzi, M., & Zhang, Y. (2022). Evaluating the real changes of air quality due to clean air actions using a machine learning technique: Results from 12 Chinese mega-cities during 2013–2020. *Chemosphere*, *300*, 134608. https://doi.org/https://doi.org/10.1016/j.chemosphere.2022.134608

Guo, Y., Yan, C., Liu, Y., Qiao, X., Zheng, F., Zhang, Y., Zhou, Y., Li, C., Fan, X., Lin, Z., Feng, Z., Zhang, Y., Zheng, P., Tian, L., Nie, W., Wang, Z., Huang, D., Daellenbach, K. R., Yao, L., . . . Kulmala, M. (2022). Seasonal variation in oxygenated organic molecules in urban Beijing and their contribution to secondary organic aerosol. *Atmos. Chem. Phys.*, *22*(15), 10077-10097. https://doi.org/10.5194/acp-22-10077-2022

Gurjar, B. R., Ravindra, K., & Nagpure, A. S. (2016). Air pollution trends over Indian megacities and their local-to-global implications [Review]. *Atmospheric Environment*, *142*, 475-495. https://doi.org/10.1016/j.atmosenv.2016.06.030

Hagler, G. S. W., Baldauf, R. W., Thoma, E. D., Long, T. R., Snow, R. F., Kinsey, J. S., Oudejans, L., & Gullett, B. K. (2009). Ultrafine particles near a major roadway in Raleigh, North Carolina: Downwind attenuation and correlation with traffic-related pollutants. *Atmospheric Environment*, *43*(6), 1229-1234. https://doi.org/10.1016/j.atmosenv.2008.11.024

Hajmohammadi, H., & Heydecker, B. (2022). Evaluation of air quality effects of the London ultra-low emission zone by state-space modelling. *Atmospheric Pollution Research*, *13*(8), 101514. https://doi.org/https://doi.org/10.1016/j.apr.2022.101514
Hallquist, Å. M., & Salberg, H. (2025). Emissions from fuel-operated heaters in battery-electric buses. *Atmospheric Environment: X*, *26*, 100332. https://doi.org/https://doi.org/10.1016/j.aeaoa.2025.100332
Hamed, A., Korhonen, H., Sihto, S.-L., Joutsensaari, J., Järvinen, H., Petäjä, T., Arnold, F., Nieminen, T., Kulmala, M., Smith, J. N., Lehtinen, K. E. J., & Laaksonen, A. (2011). The role of relative humidity in continental new particle formation. *Journal of Geophysical Research: Atmospheres*, *116*(D3). https://doi.org/https://doi.org/10.1029/2010JD014186
Hammond, D., Lalor, M., & Jones, S. (2007). In-Vehicle Measurement of Particle Number Concentrations on School Buses Equipped with Diesel Retrofits. *Water, Air, and Soil Pollution*, *179*, 217-225. https://doi.org/10.1007/s11270-006-9226-7
Han, B., Hu, L.-W., & Bai, Z. (2017). Human Exposure Assessment for Air Pollution. In G.-H. Dong (Ed.), *Ambient Air Pollution and Health Impact in China* (pp. 27-57). Springer Singapore. https://doi.org/10.1007/978-981-10-5657-4_3
Han, L. J., Zhou, W. Q., Li, W. F., & Li, L. (2014). Impact of urbanization level on urban air quality: A case of fine particles (PM2.5) in Chinese cities [Article]. *Environmental Pollution*, *194*, 163-170. https://doi.org/10.1016/j.envpol.2014.07.022
Harrison, R. M. (2020a). Airborne particulate matter. *Philosophical Transactions of the Royal Society A: Mathematical, Physical and Engineering Sciences*, *378*(2183), 20190319. https://doi.org/10.1098/rsta.2019.0319
Harrison, R. M. (2020b). Airborne particulate matter. *Philosophical Transaction of the royal society A*, *378*(2183). https://doi.org/https://doi.org/10.1098/rsta.2019.0319
Harrison, R. M., Beddows, D. C. S., & Dall'Osto, M. (2011a). PMF Analysis of Wide-Range Particle Size Spectra Collected on a Major Highway. *Environmental Science & Technology*, *45*(13), 5522-5528. https://doi.org/10.1021/es2006622
Harrison, R. M., Beddows, D. C. S., & Dall'Osto, M. (2011b). PMF Analysis of Wide-Range Particle Size Spectra Collected on a Major Highway. *Environmental Science & Technology*, *45*(13), 5522-5528. https://doi.org/10.1021/es2006622
Harrison, R. M., Jones, A. M., Gietl, J., Yin, J. X., & Green, D. C. (2012). Estimation of the Contributions of Brake Dust, Tire Wear, and Resuspension to Nonexhaust Traffic Particles Derived from Atmospheric Measurements. *Environmental Science & Technology*, *46*(12), 6523-6529. https://doi.org/10.1021/es300894r
Harrison, R. M., Shi, J. P., Xi, S., Khan, A., Mark, D., Kinnersley, R., & Yin, J. (2000). Measurement of Number, Mass and Size Distribution of Particles in the Atmosphere. *Philosophical Transactions: Mathematical, Physical and Engineering Sciences*, *358*, 2567-2580
Harrison, R. M., & Yin, J. X. (2000). Particulate matter in the atmosphere: which particle properties are important for its effects on health? *Science of the Total Environment*, *249*(1-3), 85-101. <Go to ISI>://WOS:000086743100009
He, R., & Qiu, Z. (2022). Exposure characteristics of ultrafine particles on urban streets and its impact on pedestrians. *Environmental Monitoring and Assessment*, *194*(10), 735. https://doi.org/10.1007/s10661-022-10453-6
He, X.-C., Simon, M., Iyer, S., Xie, H.-B., Rörup, B., Shen, J., Finkenzeller, H., Stolzenburg, D., Zhang, R., Baccarini, A., Tham, Y. J., Wang, M., Amanatidis, S., Piedehierro, A. A., Amorim, A., Baalbaki, R., Brasseur, Z., Caudillo, L., Chu, B., . . . Kulmala, M.

(2023). Iodine oxoacids enhance nucleation of sulfuric acid particles in the atmosphere. *Science*, *382*(6676), 1308-1314. https://doi.org/doi:10.1126/science.adh2526

He, X.-C., Tham, Y. J., Dada, L., Wang, M., Finkenzeller, H., Stolzenburg, D., Iyer, S., Simon, M., Kürten, A., Shen, J., Rörup, B., Rissanen, M., Schobesberger, S., Baalbaki, R., Wang, D. S., Koenig, T. K., Jokinen, T., Sarnela, N., Beck, L. J., . . . Sipilä, M. (2021). Role of iodine oxoacids in atmospheric aerosol nucleation. *Science*, *371*(6529), 589-595. https://doi.org/doi:10.1126/science.abe0298

Heal, M. R., Kumar, P., & Harrison, R. M. (2012). Particles, air quality, policy and health. *Chemical Society Reviews*, *41*(19), 6606-6630. https://doi.org/10.1039/c2cs35076a

HEI. (2013a). *Understanding the Health Effects of Ambient Ultrafine Particles* (HEI Perspectives 3, Issue.

HEI. (2013b). *Understanding the Health Effects of Ambient Ultrafine Particles* (HEI Perspectives 3. , Issue. HEI.

HEI. (2024). *State of Global Air 2024*. HEI.

Hinds, W. C., & Zhu, Y. (2022). *Aerosol Technology:*

Properties, Behavior, and Measurement of Airborne Particles (Third edition). John Wiley & Sons, Inc.

Hoek, G., Kerckhoffs, J., Poppel, M. v., Hofman, J., Harrison, R., & Elshout, S. v. d. (2024). *Guidance Documents on Measurement & Modelling of Novel Air Quality Pollutant : Urban Mapping & Citizen Science* (WP6 Deliverable D46 (D6.1) urban mapping & citizen science Issue.

Holman, C., Harrison, R., & Querol, X. (2015). Review of the efficacy of low emission zones to improve urban air quality in European cities. *Atmospheric Environment*, *111*, 161-169. https://doi.org/https://doi.org/10.1016/j.atmosenv.2015.04.009

Holmes, N. S. (2007). A review of particle formation events and growth in the atmosphere in the various environments and discussion of mechanistic implications. *Atmospheric Environment*, *41*(10), 2183-2201. https://doi.org/https://doi.org/10.1016/j.atmosenv.2006.10.058

Hopke, P. K., Feng, Y., & Dai, Q. (2022). Source apportionment of particle number concentrations: A global review. *Science of the Total Environment*, *819*, 153104. https://doi.org/https://doi.org/10.1016/j.scitotenv.2022.153104

Huang, W., Junninen, H., Garmash, O., Lehtipalo, K., Stolzenburg, D., Lampilahti, J. L. P., Ezhova, E., Schallhart, S., Rantala, P., Aliaga, D., Ahonen, L., Sulo, J., Quéléver, L. L. J., Cai, R., Alekseychik, P., Mazon, S. B., Yao, L., Blichner, S. M., Zha, Q., . . . Bianchi, F. (2024). Potential pre-industrial–like new particle formation induced by pure biogenic organic vapors in Finnish peatland. *Science Advances*, *10*(14), eadm9191. https://doi.org/doi:10.1126/sciadv.adm9191

ICRP. (1994a). *Human Respiratory Tract Model for Radiological Protection* (Publication 66, Issue. E. S. Ltd.

ICRP. (1994b). Human Respiratory Tract Model for Radiological Protection, . *Publication 66: Human Respiratory Tract Model for Radiological Protection. Anns. ICRP, 24(4).*

Int Panis, L., de Geus, B., Vandenbulcke, G., Willems, H., Degraeuwe, B., Bleux, N., Mishra, V., Thomas, I., & Meeusen, R. (2010). Exposure to particulate matter in traffic: A comparison of cyclists and car passengers. *Atmospheric Environment*, *44*(19), 2263-2270. https://doi.org/https://doi.org/10.1016/j.atmosenv.2010.04.028

Jiang, S. H., Zhang, F., Ren, J. Y., Chen, L., Yan, X., Liu, J. Y., Sun, Y. L., & Li, Z. Q. (2021). Evaluation of the contribution of new particle formation to cloud droplet

number concentration in the urban atmosphere. *Atmospheric Chemistry and Physics*, *21*(18), 14293-14308. https://doi.org/10.5194/acp-21-14293-2021

Jianyao, Y., Yuan, H., Su, G., Wang, J., Weng, W., & Zhang, X. (2025). Machine learning-enhanced high-resolution exposure assessment of ultrafine particles. *Nature Communications*, *16*(1), 1209. https://doi.org/10.1038/s41467-025-56581-8

Jokinen, T., Lehtipalo, K., Thakur, R. C., Ylivinkka, I., Neitola, K., Sarnela, N., Laitinen, T., Kulmala, M., Petäjä, T., & Sipilä, M. (2022). Measurement report: Long-term measurements of aerosol precursor concentrations in the Finnish subarctic boreal forest. *Atmos. Chem. Phys.*, *22*(4), 2237-2254. https://doi.org/10.5194/acp-22-2237-2022

Jokinen, T., Sipilä, M., Junninen, H., Ehn, M., Lönn, G., Hakala, J., Petäjä, T., Mauldin Iii, R. L., Kulmala, M., & Worsnop, D. R. (2012). Atmospheric sulphuric acid and neutral cluster measurements using CI-APi-TOF. *Atmos. Chem. Phys.*, *12*(9), 4117-4125. https://doi.org/10.5194/acp-12-4117-2012

Kamara, A. A., & Harrison, R. M. (2021). Analysis of the air pollution climate of a central urban roadside supersite: London, Marylebone Road. *Atmospheric Environment*, *258*, Article 118479. https://doi.org/10.1016/j.atmosenv.2021.118479

Kaur, S., Nieuwenhuijsen, M., & Colvile, R. (2005). Personal exposure of street canyon intersection users to PM2.5, ultrafine particle counts and carbon monoxide in Central London, UK. *Atmospheric Environment*, *39*(20), 3629-3641. https://doi.org/https://doi.org/10.1016/j.atmosenv.2005.02.046

Kerminen, V.-M., Chen, X., Vakkari, V., Petäjä, T., Kulmala, M., & Bianchi, F. (2018). Atmospheric new particle formation and growth: review of field observations. *Environmental Research Letters*, *13*(10), 103003. https://doi.org/10.1088/1748-9326/aadf3c

Kerminen, V. M., Paramonov, M., Anttila, T., Riipinen, I., Fountoukis, C., Korhonen, H., Asmi, E., Laakso, L., Lihavainen, H., Swietlicki, E., Svenningsson, B., Asmi, A., Pandis, S. N., Kulmala, M., & Petäjä, T. (2012). Cloud condensation nuclei production associated with atmospheric nucleation: a synthesis based on existing literature and new results. *Atmos. Chem. Phys.*, *12*(24), 12037-12059. https://doi.org/10.5194/acp-12-12037-2012

Khreis, H., Sanchez, K. A., Foster, M., Burns, J., Nieuwenhuijsen, M. J., Jaikumar, R., Ramani, T., & Zietsman, J. (2023). Urban policy interventions to reduce traffic-related emissions and air pollution: A systematic evidence map *Environment International 172*. https://doi.org/https://doi.org/10.1016/j.envint.2023.107805

Kim, G., & Lee, S. (2018). Characteristics of Tire Wear Particles Generated by a Tire Simulator under Various Driving Conditions. *Environmental Science & Technology*, *52*(21), 12153-12161. https://doi.org/10.1021/acs.est.8b03459

Kim, S., Machesky, J., Gentner, D. R., & Presto, A. A. (2024). Real-world observations of reduced nitrogen and ultrafine particles in commercial cooking organic aerosol emissions. *Atmos. Chem. Phys.*, *24*(2), 1281-1298. https://doi.org/10.5194/acp-24-1281-2024

Kirkby, J., Amorim, A., Baltensperger, U., Carslaw, K. S., Christoudias, T., Curtius, J., Donahue, N. M., Haddad, I. E., Flagan, R. C., Gordon, H., Hansel, A., Harder, H., Junninen, H., Kulmala, M., Kürten, A., Laaksonen, A., Lehtipalo, K., Lelieveld, J., Möhler, O., . . . Worsnop, D. R. (2023). Atmospheric new particle formation from the CERN CLOUD experiment. *Nature Geoscience*, *16*(11), 948-957. https://doi.org/10.1038/s41561-023-01305-0

Kirkby, J., Curtius, J., Almeida, J., Dunne, E., Duplissy, J., Ehrhart, S., Franchin, A., Gagné, S., Ickes, L., Kürten, A., Kupc, A., Metzger, A., Riccobono, F., Rondo, L., Schobesberger, S., Tsagkogeorgas, G., Wimmer, D., Amorim, A., Bianchi, F., . . . Kulmala, M. (2011). Role of sulphuric acid, ammonia and galactic cosmic rays in atmospheric aerosol nucleation. *Nature*, *476*(7361), 429-433. https://doi.org/10.1038/nature10343

Kirkby, J., Duplissy, J., Sengupta, K., Frege, C., Gordon, H., Williamson, C., Heinritzi, M., Simon, M., Yan, C., Almeida, J., Tröstl, J., Nieminen, T., Ortega, I. K., Wagner, R., Adamov, A., Amorim, A., Bernhammer, A.-K., Bianchi, F., Breitenlechner, M., . . . Curtius, J. (2016). Ion-induced nucleation of pure biogenic particles. *Nature*, *533*(7604), 521-526. https://doi.org/10.1038/nature17953

Kittelson, D. B., Watts, W. F., & Johnson, J. P. (2004). Nanoparticle emissions on Minnesota highways. *Atmospheric Environment*, *38*(1), 9-19. https://doi.org/10.1016/j.atmosenv.2003.09.037

Klompmakera, J. O., Montagnea, D. R., Meliefstea, K., Hoeka, G., & Brunekreef, B. (2015). Spatial variation of ultrafine particles and black carbon in two cities: Results from a short-term measurement campaign. *Science of the Total Environment*, *508*, 266-275.

Knibbs, L. D., Cole-Hunter, T., & Morawska, L. (2011). A review of commuter exposure to ultrafine particles and its health effects. *Atmospheric Environment*, *45*(16), 2611-2622. https://doi.org/10.1016/j.atmosenv.2011.02.065

Kuang, C., McMurry, P. H., McCormick, A. V., & Eisele, F. L. (2008). Dependence of nucleation rates on sulfuric acid vapor concentration in diverse atmospheric locations. *Journal of Geophysical Research: Atmospheres*, *113*.

Kulmala, M., Dal, M. M., M., M. J., L., P., M., V., P., A., P., M., K., H., & and O'dowd, C. D. (2001). On the formation, growth and composition of nucleation mode particles. *Tellus B: Chemical and Physical Meteorology*, *53*(4), 479-490. https://doi.org/10.3402/tellusb.v53i4.16622

Kulmala, M., Kerminen, V. M., Petäjä, T., Ding, A. J., & Wang, L. (2017). Atmospheric gas-to-particle conversion: why NPF events are observed in megacities? [10.1039/C6FD00257A]. *Faraday Discussions*, *200*(0), 271-288. https://doi.org/10.1039/C6FD00257A

Kulmala, M., Kontkanen, J., Junninen, H., Lehtipalo, K., Manninen, H. E., Nieminen, T., Petäjä, T., Sipilä, M., Schobesberger, S., Rantala, P., Franchin, A., Jokinen, T., Järvinen, E., Äijälä, M., Kangasluoma, J., Hakala, J., Aalto, P. P., Paasonen, P., Mikkilä, J., . . . Worsnop, D. R. (2013). Direct Observations of Atmospheric Aerosol Nucleation. *Science*, *339*(6122), 943-946. https://doi.org/doi:10.1126/science.1227385

Kulmala, M., Petäjä, T., Nieminen, T., Sipilä, M., Manninen, H. E., Lehtipalo, K., Dal Maso, M., Aalto, P. P., Junninen, H., Paasonen, P., Riipinen, I., Lehtinen, K. E. J., Laaksonen, A., & Kerminen, V.-M. (2012). Measurement of the nucleation of atmospheric aerosol particles. *Nature Protocols*, *7*(9), 1651-1667. https://doi.org/10.1038/nprot.2012.091

Kulmala, M., Riipinen, I., Sipilä, M., Manninen, H. E., Petäjä, T., Junninen, H., Maso, M. D., Mordas, G., Mirme, A., Vana, M., Hirsikko, A., Laakso, L., Harrison, R. M., Hanson, I., Leung, C., Lehtinen, K. E. J., & Kerminen, V.-M. (2007). Toward Direct Measurement of Atmospheric Nucleation. *Science*, *318*(5847), 89-92. https://doi.org/doi:10.1126/science.1144124

Kumar, P., Ketzel, M., Vardoulakis, S., Pirjola, L., & Britter, R. (2011). Dynamics and dispersion modelling of nanoparticles from road traffic in the urban atmospheric

environment-A review. *Journal of Aerosol Science*, *42*(9), 580-603. https://doi.org/10.1016/j.jaerosci.2011.06.001
Kumar, P., Morawska, L., Birmili, W., Paasonen, P., Hu, M., Kulmala, M., Harrison, R. M., Norford, L., & Britter, R. (2014). Ultrafine particles in cities. *Environment International*, *66*.
Kumar, P., Morawska, L., Martani, C., Biskos, G., Neophytou, M., Di Sabatino, S., Bell, M., Norford, L., & Britter, R. (2015). The rise of low-cost sensing for managing air pollution in cities. *Environment International*, *75*, 199-205. https://doi.org/https://doi.org/10.1016/j.envint.2014.11.019
Kumar, P., Robins, A., Vardoulakis, S., & Britter, R. (2010). A review of the characteristics of nanoparticles in the urban atmosphere and the prospects for developing regulatory controls.
Kürten, A., Bergen, A., Heinritzi, M., Leiminger, M., Lorenz, V., Piel, F., Simon, M., Sitals, R., Wagner, A. C., & Curtius, J. (2016). Observation of new particle formation and measurement of sulfuric acid, ammonia, amines and highly oxidized organic molecules at a rural site in central Germany. *Atmos. Chem. Phys.*, *16*(19), 12793-12813. https://doi.org/10.5194/acp-16-12793-2016
Kuula, J., Heino, K., V., N. J., Erkka, S., Harri, P., Anu, K., Minna, A., Topi, R., & and Timonen, H. (2020). Long-term sensor measurements of lung deposited surface area of particulate matter emitted from local vehicular and residential wood combustion sources. *Aerosol Science and Technology*, *54*(2), 190-202. https://doi.org/10.1080/02786826.2019.1668909
Kwon, H.-S., Ryu, M. H., & Carlsten, C. (2020). Ultrafine particles: unique physicochemical properties relevant to health and disease. *Experimental & Molecular Medicine*, *52*(3), 318-328. https://doi.org/10.1038/s12276-020-0405-1
Kwon, H. S., Ryu, M. H., & Carlsten, C. (2020). Ultrafine particles: unique physicochemical properties relevant to health and disease. *Experimental and Molecular Medicine*, *52*(3), 318-328. https://doi.org/10.1038/s12276-020-0405-1
Lai, S., Qi, X., Huang, X., Lou, S., Chi, X., Chen, L., Liu, C., Liu, Y., Yan, C., Li, M., Liu, T., Nie, W., Kerminen, V. M., Petäjä, T., Kulmala, M., & Ding, A. (2024). New particle formation induced by anthropogenic–biogenic interactions on the southeastern Tibetan Plateau. *Atmos. Chem. Phys.*, *24*(4), 2535-2553. https://doi.org/10.5194/acp-24-2535-2024
Lee, B. J., Kim, B., & Lee, K. (2014). Air Pollution Exposure and Cardiovascular Disease. *Toxicological Research*, *30*(2), 71-75. https://doi.org/10.5487/tr.2014.30.2.071
Lee, H., Cho, H., Yoon, Y. J., Kim, J., Lee, B. Y., & Park, K. (2024). Comparison of new particle formation events in urban, agricultural, and arctic environments. *Atmospheric Environment*, *333*, Article 120634. https://doi.org/10.1016/j.atmosenv.2024.120634
Lee, H., Cho, H., Yoon, Y. J., Kim, J., Lee, B. Y., & Park, K. (2024). Comparison of new particle formation events in urban, agricultural, and arctic environments. *Atmospheric Environment*, *333*, 120634. https://doi.org/https://doi.org/10.1016/j.atmosenv.2024.120634
Lee, S. H., Gordon, H., Yu, H., Lehtipalo, K., Haley, R., Li, Y. X., & Zhang, R. Y. (2019). New Particle Formation in the Atmosphere: From Molecular Clusters to Global Climate. *Journal of Geophysical Research-Atmospheres*, *124*(13), 7098-7146. https://doi.org/10.1029/2018jd029356
Lee, S. H., Kwak, J. H., Lee, S. Y., & Lee, J. H. (2015). On-Road Chasing and Laboratory Measurements of Exhaust Particle Emissions of Diesel Vehicles Equipped with

Aftertreatment Technologies (DPF, Urea-SCR). *International Journal of Automotive Technology*, *16*, 551-559. https://doi.org/10.1007/s12239−015−0056−8
Lehtinen, K. E. J., Dal Maso, M., Kulmala, M., & Kerminen, V.-M. (2007). Estimating nucleation rates from apparent particle formation rates and vice versa: Revised formulation of the Kerminen–Kulmala equation. *Journal of Aerosol Science*, *38*(9), 988-994. https://doi.org/https://doi.org/10.1016/j.jaerosci.2007.06.009
Lehtipalo, K., Nieminen, T., Schobesberger, S., Ehn, M., Kulmala, M., & Kerminen, V.-M. (2025). How the understanding of atmospheric new particle formation has evolved along with the development of measurement and analysis methods. *Journal of Aerosol Science*, *184*, 106494. https://doi.org/https://doi.org/10.1016/j.jaerosci.2024.106494
Lehtipalo, K., Yan, C., Dada, L., Bianchi, F., Xiao, M., Wagner, R., Stolzenburg, D., Ahonen, L. R., Amorim, A., Baccarini, A., Bauer, P. S., Baumgartner, B., Bergen, A., Bernhammer, A.-K., Breitenlechner, M., Brilke, S., Buchholz, A., Mazon, S. B., Chen, D., . . . Worsnop, D. R. (2018). Multicomponent new particle formation from sulfuric acid, ammonia, and biogenic vapors. *Science Advances*, *4*(12), eaau5363. https://doi.org/doi:10.1126/sciadv.aau5363
Lepistö, T., Heino, K., Paxton, J., Anssi, J., Anssi, A., & and Rönkkö, T. (2020). Measurement of the human respiratory tract deposited surface area of particles with an electrical low pressure impactor. *Aerosol Science and Technology*, *54*(8), 958-971. https://doi.org/10.1080/02786826.2020.1745141
Lepistö, T., Kuuluvainen, H., Lintusaari, H., Kuittinen, N., Salo, L., Helin, A., Niemi, J. V., Manninen, H. E., Timonen, H., Jalava, P., Saarikoski, S., & Rönkkö, T. (2022). Connection between lung deposited surface area (LDSA) and black carbon (BC) concentrations in road traffic and harbour environments. *Atmospheric Environment*, *272*, 118931. https://doi.org/https://doi.org/10.1016/j.atmosenv.2021.118931
Lewis, A., Carslaw, D., & Moller, S. J. (2018). Ultrafine Particles (UFP) in the UK.
Li, C., Wang, Z., Li, B., Peng, Z.-R., & Fu, Q. (2019). Investigating the relationship between air pollution variation and urban form. *Building and Environment*, *147*, 559-568. https://doi.org/https://doi.org/10.1016/j.buildenv.2018.06.038
Li, D., Wu, D., Gui, X., Liao, S., Zhu, M., Yu, F., & Zheng, J. (2024). Exploring ultrafine particle emission characteristics from in-use light-duty diesel trucks in China using a portable measurement system. *Environmental Research*, *263*, 120234. https://doi.org/https://doi.org/10.1016/j.envres.2024.120234
Li, X., Chee, S., Hao, J., Abbatt, J. P. D., Jiang, J., & Smith, J. N. (2019). Relative humidity effect on the formation of highly oxidized molecules and new particles during monoterpene oxidation. *Atmos. Chem. Phys.*, *19*(3), 1555-1570. https://doi.org/10.5194/acp-19-1555-2019
Lin, C., Lane, K. J., Griffiths, J. K., & Brugge, D. D. (2021). Associations between Long-term UFP Exposure and Certain Inflammatory Biomarkers and Blood Lipid Indicators: An Analysis Featuring Peak Exposure Metrics. *ISEE Conference Abstracts*, *2021*(1). https://doi.org/doi:10.1289/isee.2021.O-LT-017
Lin, J. C., Fasoli, B., Mitchell, L., Bares, R., Hopkins, F., Thompson, T. M., & Alvarez, R. A. (2023). Towards hyperlocal source identification of pollutants in cities by combining mobile measurements with atmospheric modeling. *Atmospheric Environment*, *311*, 119995. https://doi.org/https://doi.org/10.1016/j.atmosenv.2023.119995
Lin, S., Ryan, I., Paul, S., Deng, X., Zhang, W., Luo, G., Dong, G.-H., Nair, A., & Yu, F. (2022). Particle surface area, ultrafine particle number concentration, and

cardiovascular hospitalizations. *Environmental Pollution*, *310*, 119795. https://doi.org/https://doi.org/10.1016/j.envpol.2022.119795

Liu, B., Bryson, J. R., Sevinc, D., Cole, M. A., Elliott, R. J. R., Bartington, S. E., Bloss, W. J., & Shi, Z. (2023). Assessing the Impacts of Birmingham's Clean Air Zone on Air Quality: Estimates from a Machine Learning and Synthetic Control Approach. *Environmental and Resource Economics*, *86*(1), 203-231. https://doi.org/10.1007/s10640-023-00794-2

Liu, H. J., Niu, S. N., Chen, Y. K., Dai, W. T., Liu, Y. L., Shen, M. X., Guo, X., Qi, W. N., Zhang, Y. F., Li, L., Jiang, Y. K., Wang, Q. Y., & Li, J. J. (2024). Comparison of aerosol number size distribution and new particle formation in summer at alpine and urban regions in the Guanzhong Plain, Northwest China. *Science of the Total Environment*, *954*, Article 176601. https://doi.org/10.1016/j.scitotenv.2024.176601

Liu, X., Hadiatullah, H., Khedr, M., Zhang, X., Schnelle-Kreis, J., Zimmermann, R., & Adam, T. (2022). Personal exposure to various size fractions of ambient particulate matter during the heating and non-heating periods using mobile monitoring approach: A case study in Augsburg, Germany. *Atmospheric Pollution Research*, *13*(7), 101483. https://doi.org/https://doi.org/10.1016/j.apr.2022.101483

Liu, X., Hadiatullah, H., Zhang, X., Trechera, P., Savadkoohi, M., Garcia-Marlès, M., Reche, C., Pérez, N., Beddows, D. C. S., Salma, I., Thén, W., Kalkavouras, P., Mihalopoulos, N., Hueglin, C., Green, D. C., Tremper, A. H., Chazeau, B., Gille, G., Marchand, N., . . . Querol, X. (2023). Ambient air particulate total lung deposited surface area (LDSA) levels in urban Europe. *Science of The Total Environment*, *898*, 165466. https://doi.org/https://doi.org/10.1016/j.scitotenv.2023.165466

Lloyd, M., Olaniyan, T., Ganji, A., Xu, J., Simon, L., Zhang, M., Saeedi, M., Yamanouchi, S., Wang, A., Burnett, R. T., Tjepkema, M., Hatzopoulou, M., & Weichenthal, S. (2024). Airborne ultrafine particle concentrations and brain cancer incidence in Canada's two largest cities. *Environment International*, *193*, 109088. https://doi.org/https://doi.org/10.1016/j.envint.2024.109088

Lu, Y., Yan, C., Fu, Y., Chen, Y., Liu, Y., Yang, G., Wang, Y., Bianchi, F., Chu, B., Zhou, Y., Yin, R., Baalbaki, R., Garmash, O., Deng, C., Wang, W., Liu, Y., Petäjä, T., Kerminen, V. M., Jiang, J., . . . Wang, L. (2019). A proxy for atmospheric daytime gaseous sulfuric acid concentration in urban Beijing. *Atmos. Chem. Phys.*, *19*(3), 1971-1983. https://doi.org/10.5194/acp-19-1971-2019

Luengo-Oroz, J., & Reis, S. (2019). Assessment of cyclists' exposure to ultrafine particles along alternative commuting routes in Edinburgh. *Atmospheric Pollution Research*, *10*(4), 1148-1158. https://doi.org/https://doi.org/10.1016/j.apr.2019.01.020

Luo, J., Zhang, H., Liu, Z., Zhang, Z., Pan, Y., Liang, X., Wu, S., Xu, H., Xu, S., & Jiang, C. (2023). A review of regeneration mechanism and methods for reducing soot emissions from diesel particulate filter in diesel engine. *Environmental Science and Pollution Research*, *30*(37), 86556-86597. https://doi.org/10.1007/s11356-023-28405-z

Lv, Y., Tian, H., Luo, L., Liu, S., Bai, X., Zhao, H., Lin, S., Zhao, S., Guo, Z., Xiao, Y., & Yang, J. (2022). Meteorology-normalized variations of air quality during the COVID-19 lockdown in three Chinese megacities. *Atmospheric Pollution Research*, *13*(6), 101452. https://doi.org/https://doi.org/10.1016/j.apr.2022.101452

Ma, L., Graham, D. J., & Stettler, M. E. J. (2021). Has the ultra low emission zone in London improved air quality? *Environmental Research Letters*, *16*(12), 124001. https://doi.org/10.1088/1748-9326/ac30c1

MacNaughton, P., Melly, S., Vallarino, J., Adamkiewicz, G., & Spengler, J. D. (2014). Impact of bicycle route type on exposure to traffic-related air pollution. *Science of the Total Environment*, *490*, 37-43. https://doi.org/https://doi.org/10.1016/j.scitotenv.2014.04.111

Mărmureanu, L., Antonia, M. C., Jeni, V., Jean-Eudes, P., Tanguy, A., Francois, T., Bogdan, A., Cruz, M. M., C., G. D., Bibi, Z., Jurgita, O., Thomas, E., Esther, C., James, A., L., C. P., John, J., R., C. M., Leah, W., Valerie, G., . . . and Freney, E. (2025). Evaluation of aerosol chemical speciation monitor response to different mixtures of organic and inorganic aerosols. *Aerosol Science and Technology*, *59*(1), 16-33. https://doi.org/10.1080/02786826.2024.2412999

Meier, R., Katherine, C., & and Riediker, M. (2013). Comparative Testing of a Miniature Diffusion Size Classifier to Assess Airborne Ultrafine Particles Under Field Conditions. *Aerosol Science and Technology*, *47*(1), 22-28. https://doi.org/10.1080/02786826.2012.720397

Metzger, A., Verheggen, B., Dommen, J., Duplissy, J., Prevot, A. S. H., Weingartner, E., Riipinen, I., Kulmala, M., Spracklen, D. V., Carslaw, K. S., & Baltensperger, U. (2010). Evidence for the role of organics in aerosol particle formation under atmospheric conditions. *Proceedings of the National Academy of Sciences*, *107*(15), 6646-6651. https://doi.org/doi:10.1073/pnas.0911330107

Mills, J. B., Hong, P. J., & and Peters, T. M. (2013). Comparison of the DiSCmini Aerosol Monitor to a Handheld Condensation Particle Counter and a Scanning Mobility Particle Sizer for Submicrometer Sodium Chloride and Metal Aerosols. *Journal of Occupational and Environmental Hygiene*, *10*(5), 250-258. https://doi.org/10.1080/15459624.2013.769077

Moreno-Ríos, A. L., Tejeda-Benítez, L. P., & Bustillo-Lecompte, C. F. (2022). Sources, characteristics, toxicity, and control of ultrafine particles: An overview. *Geoscience Frontiers*, *13*(1), 101147. https://doi.org/https://doi.org/10.1016/j.gsf.2021.101147

Motlagh, N. H., Lagerspetz, E., Nurmi, P., Li, X., Varjonen, S., Mineraud, J., Siekkinen, M., Rebeiro-Hargrave, A., Hussein, T., Petaja, T., Kulmala, M., & Tarkoma, S. (2020). Toward Massive Scale Air Quality Monitoring. *IEEE Communications Magazine*, *58*(2). https://doi.org/10.1109/MCOM.001.1900515

Murray, C. J. L., Aravkin, A. Y., Zheng, P., Abbafati, C., Abbas, K. M., Abbasi-Kangevari, M., Abd-Allah, F., Abdelalim, A., Abdollahi, M., Abdollahpour, I., Abegaz, K. H., Abolhassani, H., Aboyans, V., Abreu, L. G., Abrigo, M. R. M., Abualhasan, A., Abu-Raddad, L. J., Abushouk, A. I., Adabi, M., . . . Lim, S. S. (2020). Global burden of 87 risk factors in 204 countries and territories, 1990-2019: a systematic analysis for the Global Burden of Disease Study 2019. *Lancet*, *396*(10258), 1223-1249. https://doi.org/10.1016/s0140-6736(20)30752-2

Nair, A. A., Lin, S., Luo, G., Ryan, I., Qi, Q., Deng, X., & Yu, F. (2023). Environmental exposure disparities in ultrafine particles and PM2.5 by urbanicity and socio-demographics in New York state, 2013–2020. *Environmental Research*, *239*, 117246. https://doi.org/https://doi.org/10.1016/j.envres.2023.117246

Nazneen, Patra, A. K., Kolluru, S. S. R., Dubey, R., & Kumar, S. (2023). Determinants of traffic related atmospheric particulate matter concentrations and their associated health risk at a highway toll plaza in India. *Atmospheric Pollution Research*, *14*(6), 101778. https://doi.org/https://doi.org/10.1016/j.apr.2023.101778

Németh, Z., Rosati, B., Zíková, N., Salma, I., Bozó, L., Dameto de España, C., Schwarz, J., Ždímal, V., & Wonaschütz, A. (2018). Comparison of atmospheric new particle

formation events in three Central European cities. *Atmospheric Environment*, *178*, 191-197. https://doi.org/https://doi.org/10.1016/j.atmosenv.2018.01.035

Ng, N. L., C., H. S., A., T., R., C. M., L., C. P., B., O. T., D., S., R., W. D., Q., Z., L., S. Y., & and Jayne, J. T. (2011). An Aerosol Chemical Speciation Monitor (ACSM) for Routine Monitoring of the Composition and Mass Concentrations of Ambient Aerosol. *Aerosol Science and Technology*, *45*(7), 780-794. https://doi.org/10.1080/02786826.2011.560211

Oberdörster, G., Oberdörster, E., & Oberdörster, J. (2005). Nanotoxicology: An Emerging Discipline Evolving from Studies of Ultrafine Particles. *Environmental Health Perspectives 113*.

Oberdörster, G., Oberdörster, E., & Oberdörster, J. (2005). Nanotoxicology:: An emerging discipline evolving from studies of ultrafine particles. *Environmental Health Perspectives*, *113*(7), 823-839. https://doi.org/10.1289/ehp.7339

Ohlwein, S., Kappeler, R., Joss, M. K., Künzli, N., & Hoffmann, B. (2019). Health effects of ultrafine particles: a systematic literature review update of epidemiological evidence. *International Journal of Public Health*, *64*(4), 547-559. https://doi.org/10.1007/s00038-019-01202-7

Ohlwein, S., Kappeler, R., Kutlar Joss, M., Künzli, N., & Hoffmann, B. (2019). Health effects of ultrafine particles: a systematic literature review update of epidemiological evidence. *International Journal of Public Health*, *64*(4), 547-559. https://doi.org/10.1007/s00038-019-01202-7

Oikarinen, H., Hartikainen, A., Simonen, P., Olin, M., Mäkinen, U. V., Marjanen, P., Salo, L., Silvonen, V., Martikainen, S., Hoivala, J., Ihalainen, M., Miettinen, P., Yli-Pirilä, P., Sippula, O., Mikkonen, S., & Karjalainen, P. (2025). The role of fuel and environmental conditions on the amount and composition of primary, fresh, and aged aerosol emissions originating from diesel- and gasoline-operated auxiliary heaters of passenger cars. *Atmos. Meas. Tech.*, *18*(17), 4271-4292. https://doi.org/10.5194/amt-18-4271-2025

Oikarinen, H., Olin, M., Martikainen, S., Leinonen, V., Mikkonen, S., & Karjalainen, P. (2022). Particle number, mass, and black carbon emissions from fuel-operated auxiliary heaters in real vehicle use. *Atmospheric Environment: X*, *16*, 100189. https://doi.org/https://doi.org/10.1016/j.aeaoa.2022.100189

Olin, M., Okuljar, M., Rissanen, M. P., Kalliokoski, J., Shen, J., Dada, L., Lampimäki, M., Wu, Y., Lohila, A., Duplissy, J., Sipilä, M., Petäjä, T., Kulmala, M., & Dal Maso, M. (2022). Measurement report: Atmospheric new particle formation in a coastal agricultural site explained with binPMF analysis of nitrate CI-APi-TOF spectra. *Atmos. Chem. Phys.*, *22*(12), 8097-8115. https://doi.org/10.5194/acp-22-8097-2022

Padró-Martínez, L. T., Patton, A. P., Trull, J. B., Zamore, W., Brugge, D., & Durant, J. L. (2012). Mobile monitoring of particle number concentration and other traffic-related air pollutants in a near-highway neighborhood over the course of a year. *Atmospheric Environment*, *61*, 253-264. https://doi.org/10.1016/j.atmosenv.2012.06.088

Park, D., & Lim, B. I. (2025). The effect of the ultra-low emission zone on PM2.5 concentration in Seoul, South Korea. *Atmospheric Environment*, *340*, 120908. https://doi.org/https://doi.org/10.1016/j.atmosenv.2024.120908

Patel, H., Talbot, N., Dirks, K., & Salmond, J. (2023). The impact of low emission zones on personal exposure to ultrafine particles in the commuter environment. *Science of the Total Environment*, *874*, 162540. https://doi.org/https://doi.org/10.1016/j.scitotenv.2023.162540

Patel, S., Leavey, A., Sheshadri, A., Kumar, P., Kandikuppa, S., Tarsi, J., Mukhopadhyay, K., Johnson, P., Balakrishnan, K., Schechtman, K. B., Castro, M., Yadama, G., & Biswas, P. (2018). Associations between household air pollution and reduced lung function in women and children in rural southern India. *Journal of Applied Toxicology*, *38*(11), 1405-1415. https://doi.org/https://doi.org/10.1002/jat.3659

Perricone, G., Matějka, V., Alemani, M., Valota, G., Bonfanti, A., Ciotti, A., Olofsson, U., Söderberg, A., Wahlström, J., Nosko, O., Straffelini, G., Gialanella, S., & Ibrahim, M. (2018). A concept for reducing PM10 emissions for car brakes by 50%. *Wear*, *396-397*, 135-145. https://doi.org/https://doi.org/10.1016/j.wear.2017.06.018

Peters, A., Veronesi, B., Calderón-Garcidueñas, L., Gehr, P., Chen, L. C., Geiser, M., Reed, W., Rothen-Rutishauser, B., Schürch, S., & Schulz, H. (2006). Translocation and potential neurological effects of fine and ultrafine particles a critical update. *Particle and Fibre Toxicology*, *3*(1), Article 13. https://doi.org/10.1186/1743-8977-3-13

Peters, A., Wichmann, H. E., Tuch, T., Heinrich, J., & Heyder, J. (1997). Respiratory effects are associated with the number of ultrafine particles. *American Journal of Respiratory and Critical Care Medicine*, *155*(4), 1376-1383. <Go to ISI>://WOS:A1997WR65700031

Petetin, H., Bowdalo, D., Soret, A., Guevara, M., Jorba, O., Serradell, K., & Pérez García-Pando, C. (2020). Meteorology-normalized impact of the COVID-19 lockdown upon NO2 pollution in Spain. *Atmos. Chem. Phys.*, *20*(18), 11119-11141. https://doi.org/10.5194/acp-20-11119-2020

Pushpawela, B., Jayaratne, R., & Morawska, L. (2018). Differentiating between particle formation and growth events in an urban environment. *Atmospheric Chemistry and Physics*, *18*(15), 11171-11183. https://doi.org/10.5194/acp-18-11171-2018

Qian, S., Sakurai, H., & McMurry, P. H. (2007). Characteristics of regional nucleation events in urban East St. Louis. *Atmospheric Environment*, *41*(19), 4119-4127. https://doi.org/https://doi.org/10.1016/j.atmosenv.2007.01.011

Qiao, X., Yan, C., Li, X., Guo, Y., Yin, R., Deng, C., Li, C., Nie, W., Wang, M., Cai, R., Huang, D., Wang, Z., Yao, L., Worsnop, D. R., Bianchi, F., Liu, Y., Donahue, N. M., Kulmala, M., & Jiang, J. (2021). Contribution of Atmospheric Oxygenated Organic Compounds to Particle Growth in an Urban Environment. *Environmental Science & Technology*, *55*(20), 13646-13656. https://doi.org/10.1021/acs.est.1c02095

Qin, S. J., Zeng, Q. G., Zeng, H. X., Li, S. P., Andersson, J., Zhao, B., Oudin, A., Kanninen, K. M., Jalava, P., Jin, N. X., Yang, M., Lin, L. Z., Liu, R. Q., Dong, G. H., & Zeng, X. W. (2024). Neurotoxicity of fine and ultrafine particulate matter: A comprehensive review using a toxicity pathway-oriented adverse outcome pathway framework. *Science of the Total Environment*, *947*, Article 174450. https://doi.org/10.1016/j.scitotenv.2024.174450

Rafiepourgatabi, M., Woodward, A., Salmond, J. A., & Dirks, K. N. (2021). The Effect of Route Choice in Children's Exposure to Ultrafine Particles Whilst Walking to School. *International Journal of Environmental Research and Public Health,*, *18*. https://doi.org/https://doi.org/10.3390/ijerph18157808

Renwick, L. C., Brown, D., Clouter, A., & Donaldson, K. (2004). Increased inflammation and altered macrophage chemotactic responses caused by two ultrafine particle types. *Occupational and Environmental Medicine*, *61*(5), 442. https://doi.org/10.1136/oem.2003.008227

Rivas, I., Beddows, D. C. S., Amato, F., Green, D. C., Järvi, L., Hueglin, C., Reche, C., Timonen, H., Fuller, G. W., Niemi, J. V., Pérez, N., Aurela, M., Hopke, P. K.,

Alastuey, A., Kulmala, M., Harrison, R. M., Querol, X., & Kelly, F. J. (2020). Source apportionment of particle number size distribution in urban background and traffic stations in four European cities. *Environment International*, *135*, 105345. https://doi.org/https://doi.org/10.1016/j.envint.2019.105345

Rivas, I., Kumar, P., & Hagen-Zanker, A. (2017a). Exposure to air pollutants during commuting in London: Are there inequalities among different socio-economic groups? *Environment International*, *101*, 143-157. https://doi.org/https://doi.org/10.1016/j.envint.2017.01.019

Rivas, I., Kumar, P., Hagen-Zanker, A., Andrade, M. d. F., Slovic, A. D., Pritchard, J. P., & Geurs, K. T. (2017b). Determinants of black carbon, particle mass and number concentrations in London transport microenvironments. *Atmospheric Environment*, *161*, 247-262. https://doi.org/https://doi.org/10.1016/j.atmosenv.2017.05.004

Rodríguez, M. C., Dupont-Courtade, L., & Oueslati, W. (2016). Air pollution and urban structure linkages: Evidence from European cities [Review]. *Renewable & Sustainable Energy Reviews*, *53*, 1-9. https://doi.org/10.1016/j.rser.2015.07.190

Rönkkö, T., Kuuluvainen, H., Karjalainen, P., Keskinen, J., Hillamo, R., Niemi, J. V., Pirjola, L., Timonen, H. J., Saarikoski, S., Saukko, E., Järvinen, A., Silvennoinen, H., Rostedt, A., Olin, M., Yli-Ojanperä, J., Nousiainene, P., Kousa, A., & Dal Maso, M. (2017). Traffic is a major source of atmospheric nanocluster aerosol. *Proceedings of the National Academy of Sciences of the United States of America*, *114*(29), 7549-7554. https://doi.org/10.1073/pnas.1700830114

Rose, C., Zha, Q., Dada, L., Yan, C., Lehtipalo, K., Junninen, H., Mazon, S. B., Jokinen, T., Sarnela, N., Sipilä, M., Petäjä, T., Kerminen, V.-M., Bianchi, F., & Kulmala, M. (2018). Observations of biogenic ion-induced cluster formation in the atmosphere. *Science Advances*, *4*(4), eaar5218. https://doi.org/doi:10.1126/sciadv.aar5218

Rosenfeld, D., Sherwood, S., Wood, R., & Donner, L. (2014). Climate Effects of Aerosol-Cloud Interactions. *Science*, *343*(6169), 379-380. https://doi.org/doi:10.1126/science.1247490

Rückerl, R., Schneider, A., Hampel, R., Breitner, S., Cyrys, J., Kraus, U., Gu, J., Soentgen, J., Koenig, W., & Peters, A. (2016). Association of novel metrics of particulate matter with vascular markers of inflammation and coagulation in susceptible populations – results from a panel study. *Environmental Research*, *150*, 337-347. https://doi.org/https://doi.org/10.1016/j.envres.2016.05.037

Sabin, L. D., Behrentz, E., Winer, A. M., Jeong, S., Fitz, D. R., Pankratz, D. V., Colome, S. D., & Fruin, S. A. (2005). Characterizing the range of children's air pollutant exposure during school bus commutes. *Journal of Exposure Science & Environmental Epidemiology*, *15*(5), 377-387. https://doi.org/10.1038/sj.jea.7500414

Saha, P. K., Robinson, E. S., Shah, R. U., Zimmerman, N., Apte, J. S., Robinson, A. L., & Presto, A. A. (2018). Reduced Ultrafine Particle Concentration in Urban Air: Changes in

Nucleation and Anthropogenic Emissions. *Environmental Science & Technology*, *52*(12).

Saha, P. K., Zimmerman, N., Malings, C., Hauryliuk, A., Li, Z., Snell, L., Subramanian, R., Lipsky, E., Apte, J. S., Robinson, A. L., & Presto, A. A. (2019). Quantifying high-resolution spatial variations and local source impacts of urban ultrafine particle concentrations. *Science of The Total Environment*, *655*, 473-481. https://doi.org/https://doi.org/10.1016/j.scitotenv.2018.11.197

Samad, A., Arango, K., Alvarez Florez, D., Chourdakis, I., & Vogt, U. (2022). Assessment of Coarse, Fine, and Ultrafine Particles in S-Bahn Trains and Underground Stations in Stuttgart. *Atmosphere*, *13*(11).

Samet, J. M., Rappold, A., Graff, D., Cascio, W. E., Berntsen, J. H., Huang, Y. C. T., Herbst, M., Bassett, M., Montilla, T., Hazucha, M. J., Bromberg, P. A., & Devlin, R. B. (2009). Concentrated ambient ultrafine particle exposure induces cardiac changes in young healthy volunteers. *American Journal of Respiratory and Critical Care Medicine*, *179*(11).

Schervish, M., & Donahue, N. M. (2020). Peroxy radical chemistry and the volatility basis set. *Atmos. Chem. Phys.*, *20*(2), 1183-1199. https://doi.org/10.5194/acp-20-1183-2020

Schmid, O., & Stoeger, T. (2016). Surface area is the biologically most effective dose metric for acute nanoparticle toxicity in the lung. *Journal of Aerosol Science*, *99*, 133-143. https://doi.org/https://doi.org/10.1016/j.jaerosci.2015.12.006

Schraufnagel, D. E. (2020a). The health effects of ultrafine particles. *Experimental & Molecular Medicine*, *52*(3), 311-317. https://doi.org/10.1038/s12276-020-0403-3

Schraufnagel, D. E. (2020b). The health effects of ultrafine particles. *Experimental & Molecular Medicine 52*.

Sebastian, M., Kanawade, V. P., & Pierce, J. R. (2021). Observation of sub-3nm particles and new particle formation at an urban location in India. *Atmospheric Environment*, *256*, Article 118460. https://doi.org/10.1016/j.atmosenv.2021.118460

See, S. W., & Balasubramanian, R. (2006). Physical Characteristics of Ultrafine Particles Emitted from Different Gas Cooking Methods. *Aerosol and Air Quality Research*, *6*(1), 82-92. https://doi.org/10.4209/aaqr.2006.03.0007

Shah, R. U., Padilla, L. E., Peters, D. R., Dupuy-Todd, M., Fonseca, E. R., Ma, G. Q., Popoola, O. A. M., Jones, R. L., Mills, J., Martin, N. A., & Alvarez, R. A. (2023). Identifying Patterns and Sources of Fine and Ultrafine Particulate Matter in London Using Mobile Measurements of Lung-Deposited Surface Area. *Environmental Science & Technology*, *57*(1), 96-108. https://doi.org/10.1021/acs.est.2c08096

Shi, J. P., Khan, A. A., & Harrison, R. M. (1999). Measurements of ultrafine particle concentration and size distribution in the urban atmosphere. *Science of the Total Environment*, *235*(1-3), 51-64. <Go to ISI>://WOS:000082966700006

Shi, Y., Lu, Y., Cai, Y., He, Y., Zhou, Y., & Fang, J. (2022). Evolution of particulate matter deposited in the DPF channel during low-temperature regeneration by non-thermal plasma. *Fuel*, *318*, 123552. https://doi.org/https://doi.org/10.1016/j.fuel.2022.123552

Shi, Z., Song, C., Liu, B., Lu, G., Xu, J., Van Vu, T., Elliott, R. J. R., Li, W., Bloss, W. J., & Harrison, R. M. (2021). Abrupt but smaller than expected changes in surface air quality attributable to COVID-19 lockdowns. *Science Advances*, *7*(3), eabd6696. https://doi.org/doi:10.1126/sciadv.abd6696

Shrivastava, M., Zhang, J., Zaveri, R. A., Zhao, B., Pierce, J. R., O'Donnell, S. E., Fast, J. D., Gaudet, B., Shilling, J. E., Zelenyuk, A., Murphy, B. N., Pye, H. O. T., Zhang, Q., Trousdell, J., Zhang, R., Li, Y., & Chen, Q. (2024). Anthropogenic Extremely Low Volatility Organics (ELVOCs) Govern the Growth of Molecular Clusters Over the Southern Great Plains During the Springtime. *129*. https://doi.org/https://doi.org/10.1029/2024jd041212

Journal Name: Journal of Geophysical Research. Atmospheres; Journal Volume: 129; Journal Issue: 21

Siakavaras, D., Samara, C., Petrakakis, M., & Biskos, G. (2016). Nucleation events at a coastal city during the warm period: Kerbside versus urban background

measurements. *Atmospheric Environment*, *140*, 60-68. https://doi.org/https://doi.org/10.1016/j.atmosenv.2016.05.054

Sicard, P., Agathokleous, E., De Marco, A., Paoletti, E., & Calatayud, V. (2021). Urban population exposure to air pollution in Europe over the last decades [Article]. *Environmental Sciences Europe*, *33*(1), 12, Article 28. https://doi.org/10.1186/s12302-020-00450-2

Simon, M., Dada, L., Heinritzi, M., Scholz, W., Stolzenburg, D., Fischer, L., Wagner, A. C., Kürten, A., Rörup, B., He, X. C., Almeida, J., Baalbaki, R., Baccarini, A., Bauer, P. S., Beck, L., Bergen, A., Bianchi, F., Bräkling, S., Brilke, S., . . . Curtius, J. (2020). Molecular understanding of new-particle formation from α-pinene between −50 and +25 °C. *Atmos. Chem. Phys.*, *20*(15), 9183-9207. https://doi.org/10.5194/acp-20-9183-2020

Singh, A., Ng'ang'a, D., Gatari, M. J., Kidane, A. W., Alemu, Z. A., Derrick, N., Webster, M. J., Bartington, S. E., Thomas, G. N., Avis, W., & Pope, F. D. (2021). Air quality assessment in three East African cities using calibrated low-cost sensors with a focus on road-based hotspots. *Environmental Research Communications*, *3*(7), 075007. https://doi.org/10.1088/2515-7620/ac0e0a

Sipilä, M., Sarnela, N., Jokinen, T., Henschel, H., Junninen, H., Kontkanen, J., Richters, S., Kangasluoma, J., Franchin, A., Peräkylä, O., Rissanen, M. P., Ehn, M., Vehkamäki, H., Kurten, T., Berndt, T., Petäjä, T., Worsnop, D., Ceburnis, D., Kerminen, V.-M., . . . O'Dowd, C. (2016). Molecular-scale evidence of aerosol particle formation via sequential addition of HIO3. *Nature*, *537*(7621), 532-534. https://doi.org/10.1038/nature19314

Sowlat, M. H., Hasheminassab, S., & Sioutas, C. (2016). Source apportionment of ambient particle number concentrations in central Los Angeles using positive matrix factorization (PMF). *Atmospheric Chemistry and Physics*, *16*.

Spracklen, D. V., Carslaw, K. S., Kulmala, M., Kerminen, V. M., Mann, G. W., & Sihto, S. L. (2006). The contribution of boundary layer nucleation events to total particle concentrations on regional and global scales. *Atmos. Chem. Phys.*, *6*(12), 5631-5648. https://doi.org/10.5194/acp-6-5631-2006

Stolzenburg, D., Wang, M., Schervish, M., & Donahue, N. M. (2022). Tutorial: Dynamic organic growth modeling with a volatility basis set. *Journal of Aerosol Science*, *166*, 106063. https://doi.org/https://doi.org/10.1016/j.jaerosci.2022.106063

Sun, J., Hermann, M., Weinhold, K., Merkel, M., Birmili, W., Yang, Y., Tuch, T., Flentje, H., Briel, B., Ries, L., Couret, C., Elsasser, M., Sohmer, R., Wirtz, K., Meinhardt, F., Schütze, M., Bath, O., Hellack, B., Kerminen, V. M., . . . Wiedensohler, A. (2024). Measurement report: Contribution of atmospheric new particle formation to ultrafine particle concentration, cloud condensation nuclei, and radiative forcing – results from 5-year observations in central Europe. *Atmos. Chem. Phys.*, *24*(18), 10667-10687. https://doi.org/10.5194/acp-24-10667-2024

Tao, L., Zhou, Z., Tao, J., Zhang, L., Wu, C., Li, J., Yue, D., Wu, Z., Zhang, Z., Yuan, Z., Huang, J., & Wang, B. (2023). High contribution of new particle formation to ultrafine particles in four seasons in an urban atmosphere in south China. *Science of The Total Environment*, *889*, 164202. https://doi.org/https://doi.org/10.1016/j.scitotenv.2023.164202

Tao, L., Zhou, Z., Tao, J., Zhang, L. M., Wu, C., Li, J. W., Yue, D. L., Wu, Z. J., Zhang, Z. S., Yuan, Z. Y., Huang, J. J., & Wang, B. G. (2023). High contribution of new particle formation to ultrafine particles in four seasons in an urban atmosphere in south China.

Science of the Total Environment, *889*, Article 164202. https://doi.org/10.1016/j.scitotenv.2023.164202
Terzano, C., Di Stefano, F., Conti, V., Graziani, E., & Petroianni, A. (2010). Air pollution ultrafine particles: toxicity beyond the lung. *European Review for Medical and Pharmacological Sciences*, *14*(10), 809-821. <Go to ISI>://WOS:000283750900001
Testo. (2015). *Handheld difusion size classifier for nanoparticle measurement.* (testo-DiSCmini-Application-Notes, Issue.
TfL. (2023). *Congestion Charge marks 20 years of keeping London moving sustainably*. Transport for London Retrieved 29 april from
TfL. (2025). *Ultra Low Emission Zone*. Transport for London. Retrieved 23 April from
Tiszenkel, L., Flynn, J. H., Dodero, A., & Lee, S.-H. (2025). Sulfuric acid, base, and low-volatility organics contribute to aerosol nucleation in urban Houston. *Communications Earth & Environment*, *6*(1), 364. https://doi.org/10.1038/s43247-025-02310-4
Todea, A. M., Beckmann, S., Kaminski, H., & Asbach, C. (2015). Accuracy of electrical aerosol sensors measuring lung deposited surface area concentrations. *Journal of Aerosol Science*, *89*, 96-109. https://doi.org/https://doi.org/10.1016/j.jaerosci.2015.07.003
Tran, P. T. M., Kalairasan, M., Beshay, P. F. R., Biswal, B. K., Nguyen, T., & Balasubramanian, R. (2025). Evaluating pedestrian exposure to traffic-related airborne particles: Insights for sustainable and healthier urban environments. *Atmospheric Environment*, 121255. https://doi.org/https://doi.org/10.1016/j.atmosenv.2025.121255
Tran, P. T. M., Ngoh, J. R., & Balasubramanian, R. (2020). Assessment of the Integrated Personal Exposure to Particulate Emissions in Urban Micro-environments: A Pilot Study. *Aerosol and Air Quality Research*, *20*(2), 341-357. https://doi.org/10.4209/aaqr.2019.04.0201
Trees, I., Yu, F. Q., Deng, X. L., Luo, G., Zhang, W. J., & Lin, S. (2024). Ultrafine Particles and Hospital Visits for Chronic Lower Respiratory Diseases in New York State. *Annals of the American Thoracic Society*, *21*(8), 1147-1155. https://doi.org/10.1513/AnnalsATS.202303-267OC
Tröstl, J., Chuang, W. K., Gordon, H., Heinritzi, M., Yan, C., Molteni, U., Ahlm, L., Frege, C., Bianchi, F., Wagner, R., Simon, M., Lehtipalo, K., Williamson, C., Craven, J. S., Duplissy, J., Adamov, A., Almeida, J., Bernhammer, A.-K., Breitenlechner, M., . . . Baltensperger, U. (2016). The role of low-volatility organic compounds in initial particle growth in the atmosphere. *Nature*, *533*(7604), 527-531. https://doi.org/10.1038/nature18271
TSI. (2014). *Fundamentals of CPC and SMPS Spectrometers App Note (CPC-003) A4*. TSI. Retrieved 7 May from
UN. (2019). *World Urbanization Prospects: The 2018 Revision.* .
USEPA. (2019). Integrated Science Assessment (ISA) for Particulate Matter (Final Report, Dec 2019). *U.S. Environmental Protection Agency, Washington, DC*, *EPA/600/R-19/188, 2019*.
Valavanidis, A., Fiotakis, K., & Vlachogianni, T. (2008). Airborne Particulate Matter and Human Health: Toxicological Assessment and Importance of Size and Composition of Particles for Oxidative Damage and Carcinogenic Mechanisms. *Journal of Environmental Science and Health Part C-Environmental Carcinogenesis & Ecotoxicology Reviews*, *26*(4), 339-362. https://doi.org/10.1080/10590500802494538
Van Ryswyk, K., Evans, G. J., Kulka, R., Sun, L., Sabaliauskas, K., Rouleau, M., Anastasopolos, A. T., Wallace, L., & Weichenthal, S. (2021). Personal exposures to

traffic-related air pollution in three Canadian bus transit systems: the Urban Transportation Exposure Study. *Journal of Exposure Science & Environmental Epidemiology*, *31*(4), 628-640. https://doi.org/10.1038/s41370-020-0242-2

Viana, M., Rivas, I., Reche, C., Fonseca, A. S., Pérez, N., Querol, X., Alastuey, A., Álvarez-Pedrerol, M., & Sunyer, J. (2015). Field comparison of portable and stationary instruments for outdoor urban air exposure assessments. *Atmospheric Environment*, *123*, 220-228. https://doi.org/https://doi.org/10.1016/j.atmosenv.2015.10.076

Vinzents, P. S., Møller, P., Sørensen, M., Knudsen, L. E., Hertel, O., Jensen, F. P., Schibye, B., & Loft, S. (2005). Personal Exposure to Ultrafine Particles and Oxidative DNA Damage. *Environmental Health Perspectives*, *113*(11), 1485-1490. https://doi.org/doi:10.1289/ehp.7562

von Schneidemesser, E., Monks, P. S., & Plass-Duelmer, C. (2010). Global comparison of VOC and CO observations in urban areas. *Atmospheric Environment*, *44*(39), 5053-5064. https://doi.org/10.1016/j.atmosenv.2010.09.010

Vora, R., Zareba, W., Utell, M. J., Pietropaoli, A. P., Chalupa, D., Little, E. L., Oakes, D., Bausch, J., Wiltshire, J., & Frampton, M. W. (2014). Inhalation of ultrafine carbon particles alters heart rate and heart rate variability in people with type 2 diabetes. *Particle and Fibre Toxicology*, *11*(1), 31. https://doi.org/10.1186/s12989-014-0031-y

Vos, T., Lim, S. S., Abbafati, C., Abbas, K. M., Abbasi, M., Abbasifard, M., Abbasi-Kangevari, M., Abbastabar, H., Abd-Allah, F., Abdelalim, A., Abdollahi, M., Abdollahpour, I., Abolhassani, H., Aboyans, V., Abrams, E. M., Abreu, L. G., Abrigo, M. R. M., Abu-Raddad, L. J., Abushouk, A. I., . . . Murray, C. J. L. (2020). Global burden of 369 diseases and injuries in 204 countries and territories, 1990–2019: a systematic analysis for the Global Burden of Disease Study 2019. *The Lancet*, *396*(10258), 1204-1222. https://doi.org/10.1016/S0140-6736(20)30925-9

Vu, T. V., Delgado-Saborit, J. M., & Harrison, R. M. (2015). Review: Particle number size distributions from seven major sources and implications for source apportionment studies. *Atmospheric Environment*, *122*, 114-132. https://doi.org/10.1016/j.atmosenv.2015.09.027

Wallace, L. (2006). Indoor Sources of Ultrafine and Accumulation Mode Particles: Size Distributions, Size-Resolved Concentrations, and Source Strengths. *Aerosol Science and Technology*, *40*(5), 348-360. https://doi.org/10.1080/02786820600612250

Wang, A., Mora, S., Machida, Y., deSouza, P., Paul, S., Oyinlola, O., Duarte, F., & Ratti, C. (2023). Hyperlocal environmental data with a mobile platform in urban environments. *Scientific Data*, *10*(1), 524. https://doi.org/10.1038/s41597-023-02425-3

Wang, A., Paul, S., deSouza, P., Machida, Y., Mora, S., Duarte, F., & Ratti, C. (2023). Key Themes, Trends, and Drivers of Mobile Ambient Air Quality Monitoring: A Systematic Review and Meta-Analysis. *Environmental Science & Technology*, *57*. https://doi.org/10.1021/acs.est.2c06310

Wang, W., Liu, X., Xiao, Y., Han, S., Liu, S., Wang, B., & Wang, H. (2024). Real-time evolution characteristics and potential reactions of contaminants in commuter bus cabin air. *Science of The Total Environment*, *946*, 174440. https://doi.org/https://doi.org/10.1016/j.scitotenv.2024.174440

Wang, Z. B., Hu, M., Yue, D. L., Zheng, J., Zhang, R. Y., Wiedensohler, A., Wu, Z. J., Nieminen, T., & Boy, M. (2011). Evaluation on the role of sulfuric acid in the mechanisms of new particle formation for Beijing case. *Atmos. Chem. Phys.*, *11*(24), 12663-12671. https://doi.org/10.5194/acp-11-12663-2011

Watson, A., Bates, R., & Kennedy, D. (1988). *Assessment of Human Exposure to Air Pollution: Methods, Measurements, and Models.* . Retrieved 24 april from

Weichenthal, S., Dufresne, A., Infante-Rivard, C., & Joseph, L. (2008). Determinants of ultrafine particle exposures in transportation environments: findings of an 8-month survey conducted in Montréal, Canada. *Journal of Exposure Science & Environmental Epidemiology*, *18*(6), 551-563. https://doi.org/10.1038/sj.jes.7500644

WHO. (2021a). *WHO Global Air Quality Guidelines: Particulate Matter (PM2.5 and PM10), Ozone, Nitrogen Dioxide, Sulfur Dioxide and Carbon Monoxide*.

WHO. (2021b). WHO Global Air Quality Guidelines: particulate matter (PM2.5 and PM10), ozone, nitrogen dioxide, sulfur dioxide and carbon monoxide. . *World Health Organization*.

WHO. (2024). *Ambient (outdoor) air pollution*. WHO.

Williamson, C. J., Kupc, A., Axisa, D., Bilsback, K. R., Bui, T., Campuzano-Jost, P., Dollner, M., Froyd, K. D., Hodshire, A. L., Jimenez, J. L., Kodros, J. K., Luo, G., Murphy, D. M., Nault, B. A., Ray, E. A., Weinzierl, B., Wilson, J. C., Yu, F., Yu, P., . . . Brock, C. A. (2019). A large source of cloud condensation nuclei from new particle formation in the tropics. *Nature*, *574*(7778), 399-403. https://doi.org/10.1038/s41586-019-1638-9

Wu, H., Reis, S., Lin, C., Beverland, I. J., & Heal, M. R. (2015). Identifying drivers for the intra-urban spatial variability of airborne particulate matter components and their interrelationships. *Atmospheric Environment*, *112*, 306-316. https://doi.org/https://doi.org/10.1016/j.atmosenv.2015.04.059

Xiao, M., Hoyle, C. R., Dada, L., Stolzenburg, D., Kürten, A., Wang, M., Lamkaddam, H., Garmash, O., Mentler, B., Molteni, U., Baccarini, A., Simon, M., He, X. C., Lehtipalo, K., Ahonen, L. R., Baalbaki, R., Bauer, P. S., Beck, L., Bell, D., . . . Dommen, J. (2021). The driving factors of new particle formation and growth in the polluted boundary layer. *Atmos. Chem. Phys.*, *21*(18), 14275-14291. https://doi.org/10.5194/acp-21-14275-2021

Yang, L., Nie, W., Liu, Y., Xu, Z., Xiao, M., Qi, X., Li, Y., Wang, R., Zou, J., Paasonen, P., Yan, C., Xu, Z., Wang, J., Zhou, C., Yuan, J., Sun, J., Chi, X., Kerminen, V.-M., Kulmala, M., & Ding, A. (2021). Toward Building a Physical Proxy for Gas-Phase Sulfuric Acid Concentration Based on Its Budget Analysis in Polluted Yangtze River Delta, East China. *Environmental Science & Technology*, *55*(10), 6665-6676. https://doi.org/10.1021/acs.est.1c00738

Yang, S., Yuan, B., Peng, Y., Huang, S., Chen, W., Hu, W., Pei, C., Zhou, J., Parrish, D. D., Wang, W., He, X., Cheng, C., Li, X. B., Yang, X., Song, Y., Wang, H., Qi, J., Wang, B., Wang, C., . . . Shao, M. (2022). The formation and mitigation of nitrate pollution: comparison between urban and suburban environments. *Atmos. Chem. Phys.*, *22*(7), 4539-4556. https://doi.org/10.5194/acp-22-4539-2022

Yao, L., Garmash, O., Bianchi, F., Zheng, J., Yan, C., Kontkanen, J., Junninen, H., Mazon, S. B., Ehn, M., Paasonen, P., Sipilä, M., Wang, M., Wang, X., Xiao, S., Chen, H., Lu, Y., Zhang, B., Wang, D., Fu, Q., . . . Wang, L. (2018). Atmospheric new particle formation from sulfuric acid and amines in a Chinese megacity. *Science*, *361*(6399), 278-281. https://doi.org/doi:10.1126/science.aao4839

Ye, Q., Li, H. Z., Gu, P., Robinson, E. S., Apte, J. S., Sullivan, R. C., Robinson, A. L., Donahue, N. M., & Presto, A. A. (2020a). Moving beyond Fine Particle Mass: High-Spatial Resolution Exposure to Source-Resolved Atmospheric Particle Number and Chemical Mixing State. *Environmental Health Perspectives*, *128*.

Ye, Q., Li, H. Z., Gu, P., Robinson, E. S., Apte, J. S., Sullivan, R. C., Robinson, A. L., Donahue, N. M., & Presto, A. A. (2020b). Moving beyond Fine Particle Mass: High-Spatial Resolution Exposure to Source-Resolved Atmospheric Particle Number and Chemical Mixing State. *Environmental Health Perspectives*, *128*(1), 017009. https://doi.org/doi:10.1289/EHP5311

Yu, H., John, O., N., S. J., B., G. A., P., K. V., Yi, Y., Yiying, L., Kevin, H., Thomas, K., Roger, S., Chris, G., G., P. S., Lianhong, G., Jyri, M., & and Lee, S.-H. (2014). New Particle Formation and Growth in an Isoprene-Dominated Ozark Forest: From Sub-5 nm to CCN-Active Sizes. *Aerosol Science and Technology*, *48*(12), 1285-1298. https://doi.org/10.1080/02786826.2014.984801

Yu, H., Zhou, L., Dai, L., Shen, W., Dai, W., Zheng, J., Ma, Y., & Chen, M. (2016). Nucleation and growth of sub-3 nm particles in the polluted urban atmosphere of a megacity in China. *Atmos. Chem. Phys.*, *16*(4), 2641-2657. https://doi.org/10.5194/acp-16-2641-2016

Zang, H., Luo, Z., Li, C., Li, Z., Huang, D., & Zhao, Y. (2024). Nocturnal atmospheric synergistic oxidation reduces the formation of low-volatility organic compounds from biogenic emissions. *Atmos. Chem. Phys.*, *24*(20), 11701-11716. https://doi.org/10.5194/acp-24-11701-2024

Zeng, Y. Y., Cao, Y. F., Qiao, X., Seyler, B. C., & Tang, Y. (2019). Air pollution reduction in China: Recent success but great challenge for the future [Article]. *Science of the Total Environment*, *663*, 329-337. https://doi.org/10.1016/j.scitotenv.2019.01.262

Zhang, C. Y., & Stevenson, D. (2022). Characteristic changes of ozone and its precursors in London during COVID-19 lockdown and the ozone surge reason analysis. *Atmospheric Environment*, *273*, Article 118980. https://doi.org/10.1016/j.atmosenv.2022.118980

Zhang, Q., Fischer, H. J., Weiss, R. E., & Zhu, Y. (2013). Ultrafine particle concentrations in and around idling school buses. *Atmospheric Environment*, *69*, 65-75. https://doi.org/https://doi.org/10.1016/j.atmosenv.2012.12.015

Zhang, R., Suh, I., Zhao, J., Zhang, D., Fortner, E. C., Tie, X., Molina, L. T., & Molina, M. J. (2004). Atmospheric New Particle Formation Enhanced by Organic Acids. *Science*, *304*(5676), 1487-1490. https://doi.org/doi:10.1126/science.1095139

Zhang, Y., Li, D. Z. T., He, X. C., Nie, W., Deng, C. J., Cai, R. L., Liu, Y. L., Guo, Y. S., Liu, C., Li, Y. R., Chen, L. D., Li, Y. Y., Hua, C. J., Liu, T. Y., Wang, Z. C., Xie, J. L., Wang, L., Petaejae, T., Bianchi, F., . . . Kulmala, M. (2024). Iodine oxoacids and their roles in sub-3 nm particle growth in polluted urban environments. *Atmospheric Chemistry and Physics*, *24*(3), 1873-1893. https://doi.org/10.5194/acp-24-1873-2024

Zhang, Y., Liu, R., Yang, D., Guo, Y., Li, M., & Hou, K. (2023). Chemical ionization mass spectrometry: Developments and applications for on-line characterization of atmospheric aerosols and trace gases. *TrAC Trends in Analytical Chemistry*, *168*, 117353. https://doi.org/https://doi.org/10.1016/j.trac.2023.117353

Zheng, H., Kong, S., Zhai, S., Sun, X., Cheng, Y., Yao, L., Song, C., Zheng, Z., Shi, Z., & Harrison, R. M. (2023). An intercomparison of weather normalization of PM2.5 concentration using traditional statistical methods, machine learning, and chemistry transport models. *npj Climate and Atmospheric Science*, *6*(1), 214. https://doi.org/10.1038/s41612-023-00536-7

Zhu, W. B., Hu, B., Liu, Z. R., Pan, Y. P., Han, J. X., Li, C. H., Xu, M., Yang, S. H., Yin, Y. N., Zhou, J. X., Ji, D. S., & Wang, Y. S. (2023). Reduction of anthropogenic emissions enhanced atmospheric new particle formation: Observational evidence

during the Beijing 2022 Winter Olympics. *Atmospheric Environment*, *314*, Article 120094. https://doi.org/10.1016/j.atmosenv.2023.120094